Degradation and Degeneration: Synergistic impact of autophagy and mitochondrial dysfunction in Parkinson's Disease

Eve Simcox

BSc (hons) MRes

November 2013

Author's Declaration

This thesis is submitted for the degree of Doctor of Philosophy at Newcastle University. The research was conducted in the Wellcome Trust Centre for Mitochondrial Research, Institute for Ageing and Health, Newcastle University under the supervision of Prof D M Turnbull, Prof R N Lightowlers and Dr A K Reeve and all work is my own unless otherwise stated.

I certify that none of the material offered in this thesis has been previously submitted by me for a degree or qualification at this or any other university.

Abstract

The single greatest risk factor for the development of idiopathic Parkinson's Disease is advancing age. The differences at the cellular level that cause some individuals to develop this highly debilitating disease over healthy ageing are not fully understood. Mitochondrial dysfunction has been implicated in the pathogenesis of Parkinson's disease (PD) since the drug MPTP, known to cause Parkinson's like symptoms, was shown to invoke its deleterious effect through inhibition of Complex I (CI) of the mitochondrial electron transport chain. Since this discovery in the 1980s, several causative genes in the much rarer familial forms of PD have been shown to encode proteins which function within, or in association with mitochondria. Through inherited cases of the disorder the process through which mitochondria are removed, mitophagy, a specialized form of autophagy has also been associated with the pathogenesis that leads to en masse cell death in this disorder.

This work explores the interplay between mitochondrial deficiencies, through complex I dysfunction, and changes to autophagic processes. The methodologies to enable these observations are also described in detail with the development of novel and specialized techniques necessary to answer many of the specific research questions. The mechanisms behind complex I deficiency's impact upon cellular processes is also explored as part of this thesis. Mitochondria and autophagy are irrevocably linked through mitochondrial dynamics, to this end an exploration of the greater impact complex I dysfunction has upon mitochondrial motility, fission and fusion was investigated.

As the most prevalent neurodegenerative movement disorder of old age, understanding the molecular changes that result in Parkinson's Disease is vital to increase knowledge and offer novel therapeutic targets. Parallel studies in human upper midbrain tissue and cybrid cell lines within this work have revealed significant changes to both autophagy and mitochondrial dynamics in response to complex I deficiency. Given that mitochondrial 'health' and autophagic regulation directly impact upon one another identifying how exactly these may contribute to neuronal loss will hopefully allow therapeutic modulation at a point of PD pathogenesis where cells can still be retained.

For Gran and Grandad, Edna and Cliff x

Acknowledgments

There are so many people who have helped me over the past four years and made it possible for me to complete this thesis, for which I will be eternally grateful. First and foremost I would like to thank Prof Doug Turnbull, for giving me the opportunity to work within such a fantastic group and for all his support and guidance through the highs and lows of this project, I couldn't ask for a better PI! Also Prof Bob Lightowlers who's encyclopaedic knowledge was greatly appreciated whilst constructing the introduction to this thesis.

Secondly, I will be forever indebted to the Bunsen to my beaker, Dr Amy Reeve. Unquestionably one of the most wonderful people I have had the pleasure to meet. Her patience and support have been invaluable throughout this project. When I look back to when I joined the lab I realise I knew nothing and everything I am now capable of is down to the expert teaching skills of Dr Reeve. You have gone above and beyond the role of lab supervisor to the much more demanding role of 'Eve's Life coach'. Thank you for being an excellent teacher and becoming my best friend.

My wonderful family have been a constant source of support over the last 28 years but I have leant on them even more heavily over the course of this PhD, despite which their love and support has not faulted. Mum, I would hope it's unnecessary to put down here just how much you mean to me, you are my absolute rock. Thank you for always providing the haven to which I can return when times get tough, not to mention dietary support! Dad, I know you were hoping for a swimming pool by now, I imagine this large book is comparable right? Seriously though, thank you for all that you've allowed for me and ensuring I and Stavros/Tony/Frank and Norman (my cars throughout the years) made it back to Newcastle in one piece.

My beautiful, talented and generally wonderful older sister Faye has always been, and remains, my hero. Thank you for your fantastic (albeit unique) sense of humour which makes me laugh so much it hurts, your randomness brightens up my days in the lab. Finally, mini Mew, my adorable niece. You're only three as I write this but I imagine

you will understand most of this thesis. Thank you for always offering to 'help Auntie Eve' and 'come up to Noocastle to work with me and drink coffee'??! Your understanding of my day job is terrifying! Barry, thank you for your love and support through this final year. If any of this thesis comes up on pointless, it will all have been worthwhile! Seriously though….me and you against the world.

To Amber and Mel, who even from Derby have always been there to turn to. Mel, you carried me when I twisted my leg in primary school and have been supporting me ever since and Amber who somehow always knows the right thing to say. Without you guys I would have never made it this far, arguably I would never have survived school! In the wise words of the darkness-

<div align="center">

Hey you!

Do you remember me

I used to sit next to you at school

We indulged in all the extra-curricular activities

We weren't particularly cool

</div>

Finally, my acknowledgements would not be complete without mentioning the wonderful research group I work within. I have made some fantastic friends and had some of my most memorable times with you all. Special thanks to Ollie, Georgia, John Y, John G, Casey and Adya who had to deal with the bulk of my frustrations and thesis woes, remember guys, if experiments aren't going the way you want, don't stop believin'.

Table of Contents

CHAPTER ONE

CHAPTER TWO

CHAPTER THREE

CHAPTER FOUR

CHAPTER FIVE

CHAPTER SIX

CHAPTER SEVEN

CHAPTER EIGHT

CHAPTER NINE

List of Figures

xvii

List of Tables

List of Equations

Abbreviations (and chemical symbols).

3-MA	3-methyladenine.
8-OHG	8-hydroxy guanosine.
A	Adenine.
AD	Alzheimer's disease.
ADP	Adenosine diphosphate.
AMP	Ampicillin.
AMPS	Ammonium persulphate.
ANT	Adenine nucleotide translocator.
Asp	Aspartate.
Atg	Autophagy related gene.
ATP	Adenosine triphosphate.
BER	Base excision repair.
bp	Base pairs.
BrdU	Bromo-2-deoxy-Uridine.
BSA	Bovine serum albumin.
C	Cytosine.
Ca^{2+}	Calcium.
CAPS	3- [cyclohexylamino]-1-propanesulphonic acid.
Caspases	Cysteinyl aspartate specific proteinases.
CN	Copy number.
CO_2	Carbon dioxide.
COX	Cytochrome *c* oxidase.
CPEO	Chronic progressive external opthalmoplegia.
CSB	Conserved sequence blocks.
Cu	Copper.
D-loop	Displacement loop.
DA	Dopamine.
DAB	3. 3'Diaminobenzidine.
dATP	2'-deoxyadenosine 5'-triphosphate.
dCTP	2'-deoxycytidine 5'-triphosphate.
dGTP	2'-deoxyguanosine 5'-triphosphate.
dH_2O	Deionised water.
DMEM	Dulbecco's modified eagles' medium.

DMSO	Dimethyl sulfoxide.
DNA	Deoxyribonucleic acid.
DSBs	Double strand breaks.
DTT	Dithiothreitol.
dTTP	2'-deoxythymidine 5'-triphosphate.
e^-	electron
EDTA	Ethylenediaminetetreacetic acid.
EtOH	Ethanol.
g	grams
G	Guanine.
GMEM	Glasgow modified eagles' medium
GFP	Green fluorescent protein.
Gln	Glutamine.
H^+	hydrogen ion (proton)
H_2O_2	Hydrogen peroxide.
H-strand	Heavy strand.
HCl	Hydrochloric acid.
HEK 293	Human embryonic kidney cells.
h-mtTF	Human mitochondrial transcription factor.
HRP	Horseradish peroxidase.
HSP	Heavy strand promoter.
K^+	Potassium.
Kb	Kilobases.
KSS	Kearn's Sayre Syndrome.
L	litre
L-strand	Light strand.
LB	Lewy body.
LC	Locus coeruleus.
LHON	Leber's hereditary optic neuropathy.
LSP	Light strand promoter.
LV	Left ventricle.
MELAS	Mitochondrial encephalomyopathy with lactic acidosis.
Met	Methionine.
MERRF	Myoclonus epilepsy with ragged red fibres.
Mfn	Mitofusin.

$MgCl_2$	Magnesium chloride.
Ml	millilitre
MMR	Mismatch repair.
MPP^+	1-methyl-4-phenylpyridinium.
MPTP	1-methyl 4-phenyl 1,2,3,6-tetrahydropyridine.
mRNA	Messenger ribonucleic acid.
MRI	Magnetic resonance imaging.
mtDNA	Mitochondrial DNA.
mtEF	Mitochondrial elongation factor.
mtIF	Mitochondrial initiation factor.
mtRF	Mitochondrial release factor
mtSSB	Mitochondrial single strand binding protein.
MTTs	Mitochondrial tRNA genes
Mt-tRNA	Mitochondrial transfer ribonucleic acid
Na^+	Sodium.
NaCl	Sodium chloride.
NADH	Reduced form of nicotinamide adenine dinucleotide.
NaOH	Sodium hydroxide.
nDNA	Nuclear DNA
nm	nanometer
ng	nanogram
$O_2^-\cdot$	Superoxide ion.
$\cdot OH$	Hydroxyl radical.
O_H	Origin of heavy strand replication.
O_L	Origin of light strand replication.
OPA1	Optic Atrophy 1
OXPHOS	Oxidative phosphorylation.
PBS	Phosphate buffered saline.
PCR	Polymerase chain reaction.
PD	Parkinson's disease.
Pi	Inorganic phosphate.
POLG	Polymerase gamma.
POLRMT	Mitochondrial RNA polymerase.
PMS	Phenazine methosulphate.
Q	Ubiquinone

QH$_2$	Ubiquinol
rCRS	Cambridge reference sequence.
RNA	Ribonucleic acid.
rRNA	Ribosomal ribonucleic acid.
ROS	Reactive oxygen species.
Rpm	Revolutions per minute.
SDH	Succinate dehydrogenase.
SDS	Sodium dodecyl sulphate.
SN	Substantia nigra.
SNc	Substantia nigra pars compacta.
SNr	Substantia nigra pars reticulata.
SOD	Superoxide dismutase.
STN	Subthalamic nucleus.
T	Thymine.
TAE	Tris acetate EDTA.
TBS	Tris buffered saline.
TEMED	N,N,N'N'-tetramethylenediamine.
tRNA	Transfer ribonucleic acid.
TTBS	Tris buffered saline plus Tween 20.
U	Uracil.
UV	Ultraviolet.
URF	Unidentified reading frame.
VDAC	Voltage dependant anion channel (Porin).
v/v	volume per volume
w/v	weight per volume
μm	micrometer
μl	microlitre

Chapter One

Introduction

Chapter 1. Introduction

1.1   MITOCHONDRIA

1.1.1   Origins and endosymbiosis

It is widely accepted that mitochondria evolved through an endosymbiotic relationship between a primitive eukaryotic cell and eubacterium (Sagan, 1993). Unlike other organelles, mitochondria share distinct characteristics with bacteria, such as a double membrane and their own circular DNA molecules, separate to the nuclear genome. Alongside these observations, the mitochondrion's independent transcriptional and translational machinery coupled with the ability to replicate through binary fission, indicate a bacterial origin.

The endosymbiotic theory championed in 1971 by Lynn Margulis states that a prokaryotic organism capable of aerobic respiration entered into the cytoplasm of another cell which relied on an inefficient means of energy production such as glycolysis (Margulis, 1971a; Margulis, 1971b). Surviving endocytosis, a symbiotic relationship ensued which afforded the prokaryotic organism protection and metabolisable substrates, and the host cell a major evolutionary advantage through the provision of adenosine triphosphate (ATP) (Scheffler, 1999). The primitive eukaryote that benefitted from the introduction of oxidative respiration is of archaebacterial descent sharing common ancestry with the group *Crenarchaeota* (Embley and Martin, 2006; Foster *et al.*, 2009). The bacterial endosymbiont is generally thought to be an α-proteobacterium (Yang *et al.*, 1985). Following full genome sequencing of *Rickettsia prowazekii* it was shown this α-proteobacterium contains phylogenetically related respiratory chain complex enzymes and a complete set of tricarboxylic enzymes (Andersson and Kurland, 1998; Dyall and Johnson, 2000), strengthening the argument for their role in the endosymbiotic story.

The assimilation of these two is thought to have occurred around 1.5 billion years ago (Gray, 1992). Initially independent, over a large period of reductive evolution the invading prokaryote has become highly dependent on the host cell. A reduction in protein encoding genes within the mitochondrial genome and an on-going transfer to the

nuclear genome have rendered mitochondria incapable of independent functioning (Burger *et al.*, 1996; Andersson and Kurland, 1998). The reason for the continued presence of mitochondrially encoded genes is unclear but may represent an irreconcilable difference in the genetic code translation. Alternatively or possibly in conjunction, certain internal components of the mitochondrion are hydrophobic which may pose a challenge for transportation after translation (Claros *et al.*, 1995).

1.1.2   **Structure**

As independent organelles, mitochondria are typically 2µm in length and 0.5µm in diameter, although their form can range from extended reticular networks through to the more typically described rod structures. The structure of the mitochondrion is dictated by its role, with every aspect of its form contributing to a highly specialised function. A simplified schematic of the mitochondrion structure can be seen in Figure 1.1 showing the double plasma membrane and convoluted internal architecture. The first membrane, the outer membrane, forms the boundary between the organelle and surrounding cytosol. Its composition is similar to that of the cell membrane and as such allows the diffusion of lipid soluble molecules into the intermembrane space. Transportation of small proteins (<5000Da) and hydrophilic proteins is also made possible through porin, the voltage-dependent anion channel (VDAC) which is expressed in abundance within this outer membrane.

The internal mitochondrial membrane surrounds the central matrix of the mitochondrion and is impermeable to polar molecules and ions. This membrane is far richer in proteins than the outer membrane containing elevated levels of cardiolipin and polypeptides, required for a multitude of biochemical pathways within the organelle including electron transport. The restrictive nature of this membrane ensures efficient functioning of oxidative phosphorylation can proceed due to tight control of the proteins and molecules able to enter the surrounding space. The impermeability of this membrane coupled with the far more permeable nature of the outer membrane results in the inter-membrane space, an environment similar to that of the cytosol but with strict specificity for larger proteins that have a mitochondrial role. In order for larger proteins to gain access to the mitochondrion they require specific mitochondrial targeting sequences. These facilitate interaction with either the Transporter Outer Mitochondrial Membrane

complex (TOMM) or Transporter Inner Mitochondrial Membrane complex (TIMM); translocases that import proteins to compartments or membranes of the organelle (Herrmann and Neupert, 2000; Rehling *et al.*, 2004).
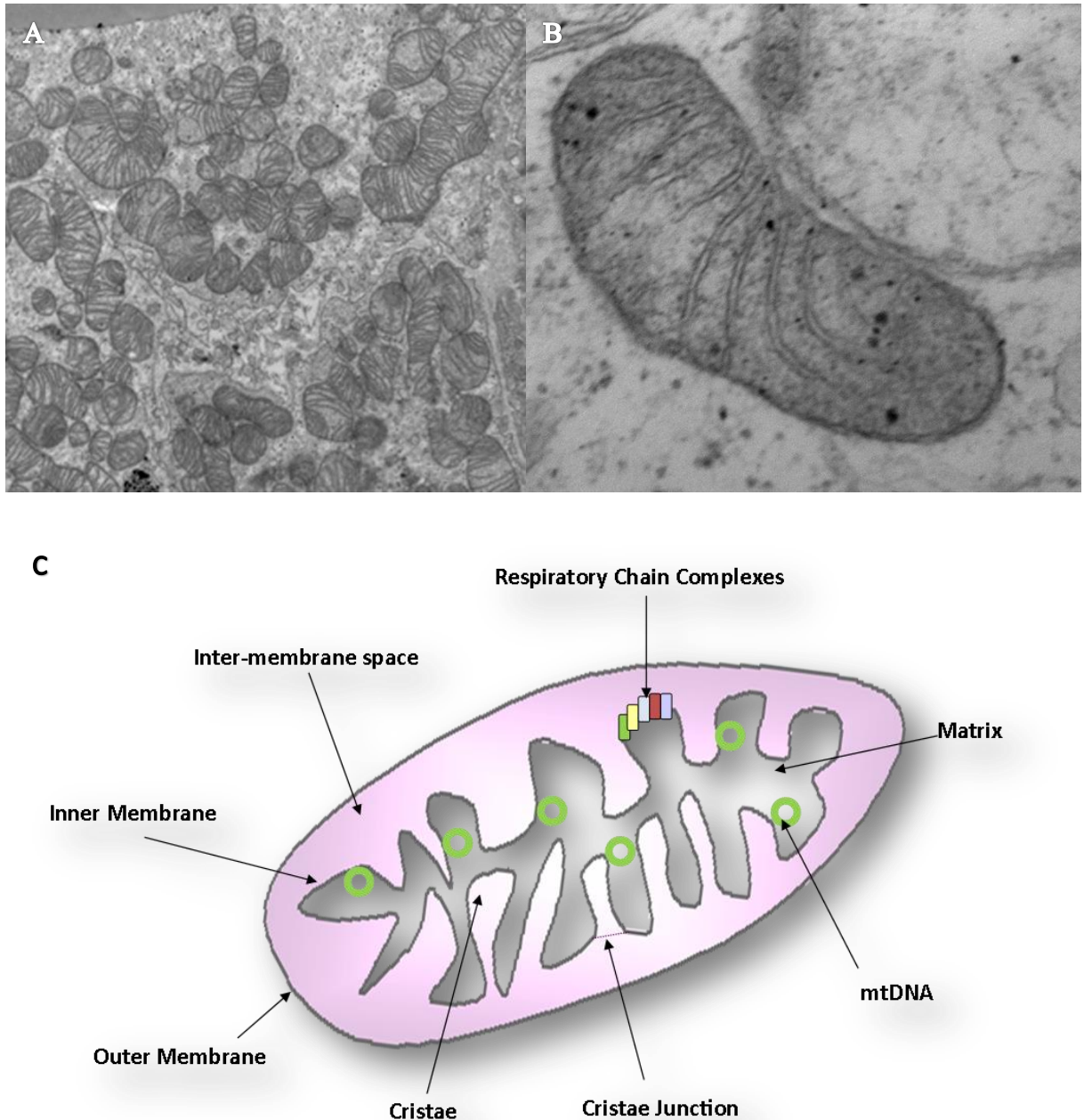
Figure 1.1. Schematic representation of a mitochondrion

EM image of multiple mitochondria within tissue (A). EM image of a single mitochondrion (B). Simplified mitochondrial structure showing the key components (C).

4

The invagination of the inner mitochondrial membrane was long believed to give rise to the internal folds that project into the matrix, called *cristae mitochondriales*, or cristae. This was first proposed in the 1950s and termed the 'baffle model' (Palade, 1953). Electron tomography analysis however, has now shown that this model is inaccurate with cristae actually arising from a distinct membrane connected to the inter membrane space through tubular inner membrane junctions (Frey and Mannella, 2000). Illustrative of the highly adapted form mitochondria have for their function, the cristae of the inner membrane provide a vastly enlarged surface area over which OXPHOS and maintenance of the H+ gradient can occur. Encapsulated by the inner membrane, the mitochondrial matrix houses multiple copies of mitochondrial DNA (mtDNA), machinery for its expression, alongside enzymes of the TCA cycle. Functionally within the matrix, iron-sulphur (Fe-S) cluster production occurs and the Krebs cycle generates precursors for oxidative phosphorylation.

1.2   MITOCHONDRIAL FUNCTIONS

Mitochondria are required for a plethora of functions, illustrated by their ubiquitous presence in nearly every eukaryotic cell. Although mitochondria are often simplified to 'powerhouses' of the cell due to their pinnacle and most well described role in ATP production via OXPHOS, their contribution and impact upon diverse cellular processes affects all aspects of cell homeostasis and functioning. The most well conserved mitochondrial function is that of iron sulphur cluster formation and as such this introduction will begin here. Aside from this, mitochondria are also responsible for calcium handling, apoptosis, cell signalling and ROS production.

1.2.1   Iron-sulphur cluster formation

Iron sulphur clusters are crucial inorganic cofactors for numerous biological processes including regulation of gene expression, enzyme catalysis and DNA repair. Within mitochondria themselves, Fe-S clusters function within complexes I, II and III due to their capacity as electron donors and acceptors. Dependent on function, the number of iron and sulphur atoms can vary within clusters and the maturation of these structures has been shown to be a vital function of mitochondria. Through studies within

S.cerevisiae two stages of Fe-S assembly have been elucidated-formation and conversion to holoenzymes. Over 20 proteins have been shown to be involved in these processes (Lill, 2009). The first stage briefly consists of the conversion of cysteine to alanine, releasing sulphur by the cystenine desulpharase complex Nfs1-Isd11 (Adam *et al.*, 2006) and then reduction to sulphide by electrons from NADH via ferredoxin reductase (Lange *et al.*, 2000).

To enter mitochondria, iron is transported through a member of the mitochondrial solute carrier family- mitoferrin (Paradkar *et al.*, 2009). Once within the inner membrane scaffold proteins including the highly conserved IscU and Nfu ((Tong and Rouault, 2000; Tong *et al.*, 2003) are employed to assemble Fe-S clusters. The Fe required for the construction of these clusters is provided through frataxin. Following synthesis of the Fe-S cluster it is released from the scaffold proteins and incorporated in apoproteins.

1.2.2   Oxidative Phosphorylation

Mitochondria house the biochemical machinery required for oxidative phosphorylation and subsequently the production of ATP molecules, the source of energy behind cellular functioning. Although oxidative phosphorylation itself occurs within the mitochondria the preceding stages of aerobic respiration begin in the cytoplasm with the anaerobic process of glycolysis. The glycolytic reaction can be seen below in Equation 1.1 but broadly speaking it converts one glucose molecule into two pyruvate molecules.

$$Glucose + 2(NAD^+) + 2(ADP) + 2(P_i)$$
$$\rightarrow 2(Pyruvate) + 2(NADH) + 2(H^+) + +2(ATP) + 2(H_2O)$$
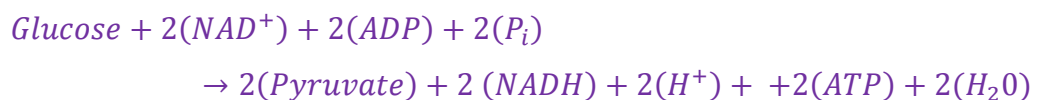
Equation 1.1. Glycolysis

The overall glycolytic reaction.

The next stage occurs within the mitochondria, where the aforementioned pyruvate, generated through glycolysis, is imported through specific carriers into the mitochondrial matrix to be utilised in the Krebs cycle. For this to occur pyruvate must be converted into acetyl CoA. This is achieved using the pyruvate dehydrogenase

complex (PDC) shown below in Equation 1.2. Alternatively acetyl coA can be generated through the β oxidation of fatty acids which are transported into the mitochondria in the form of fatty acyl CoA before undergoing oxidations, hydration and thiolysis which function to remove two carbons resulting in acetyl coA.

$$Pyruvate + CoA + NAD^+ \rightarrow AcetylCoA + NADH + H^+ + CO_2$$

Equation 1.2. Convertion of Pyruvate to AcetylCoA

Pyruvate dehydrogenase catalyses the conversion of pyruvate to acetyl CoA.

Acetyl CoA enters the tricarboxylic acid (TCA)/Krebs cycle (Krebs and Johnson 1937) through transfer of the acetyl group to oxaloacetate. This is followed by a series of chemical reactions that generate ATP, CO_2 and large amounts of the reduced electron carriers NADH and FADH2, ultimately leading to the regeneration of oxaloacetate, and allowing the cycle to continue (Figure 1.2).

Through the processes of glycolysis and the TCA cycle, a total of 2FADH2 and 10NADH electron carrying molecules are provided/glucose molecule. Importantly the 2 NADH molecules that are provided through glycolysis, are not able to pass through the inner mitochondrial membrane. Subsequently the transferal of electrons must occur through a different method than those derived within the matrix employing a process known as the 'glycerol 3-phosphate shuffle'. Here, the $2e^-$ carried by NADH are transferred within the cytosol to dihydroxyacetone, releasing NAD+ and glycerol 3-phosphate. The latter is then reoxidised to dihydroxyacetone by its dehydrogenase with the resulting $2e^-$ transferred to FAD generating FADH2. A final step enabling the electrons to enter the respiratory chain comes from the reduction of ubiquinone (Q) to ubiquinol (QH_2).

Ultimately, the process of aerobic respiration concludes through the process of OXPHOS (Figure 1.3). Here through the use of prosthetic groups, Q and cytochrome c, electrons are transported from both complex I and II to complex III then IV, along a redox potential. This series of reactions releases free energy which is used to pump

hydrogen ions across the inner membrane into the inner membrane space creating an electrochemical proton gradient across the inner membrane. It is this gradient which drives complex V's uptake of H+ and the subsequent transport of H+ back into the matrix a process which is coupled with the production of ATP from ADP and inorganic phosphate (Pi). The production of ATP through the coupling of the electron and proton transfer was first described in 1961 by biochemist Peter Mitchell who coined the term 'chemiosmotic theory' (Mitchell, 1961).

$$AcetylCoA + 3(NAD^+) + FAD + ADP + P_i + 2(H_2O)$$
$$\rightarrow CoA + 3(NADH) + 2(H^+) + FADH_2 + ATP + 2(CO_2)$$
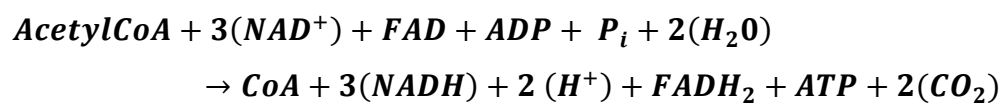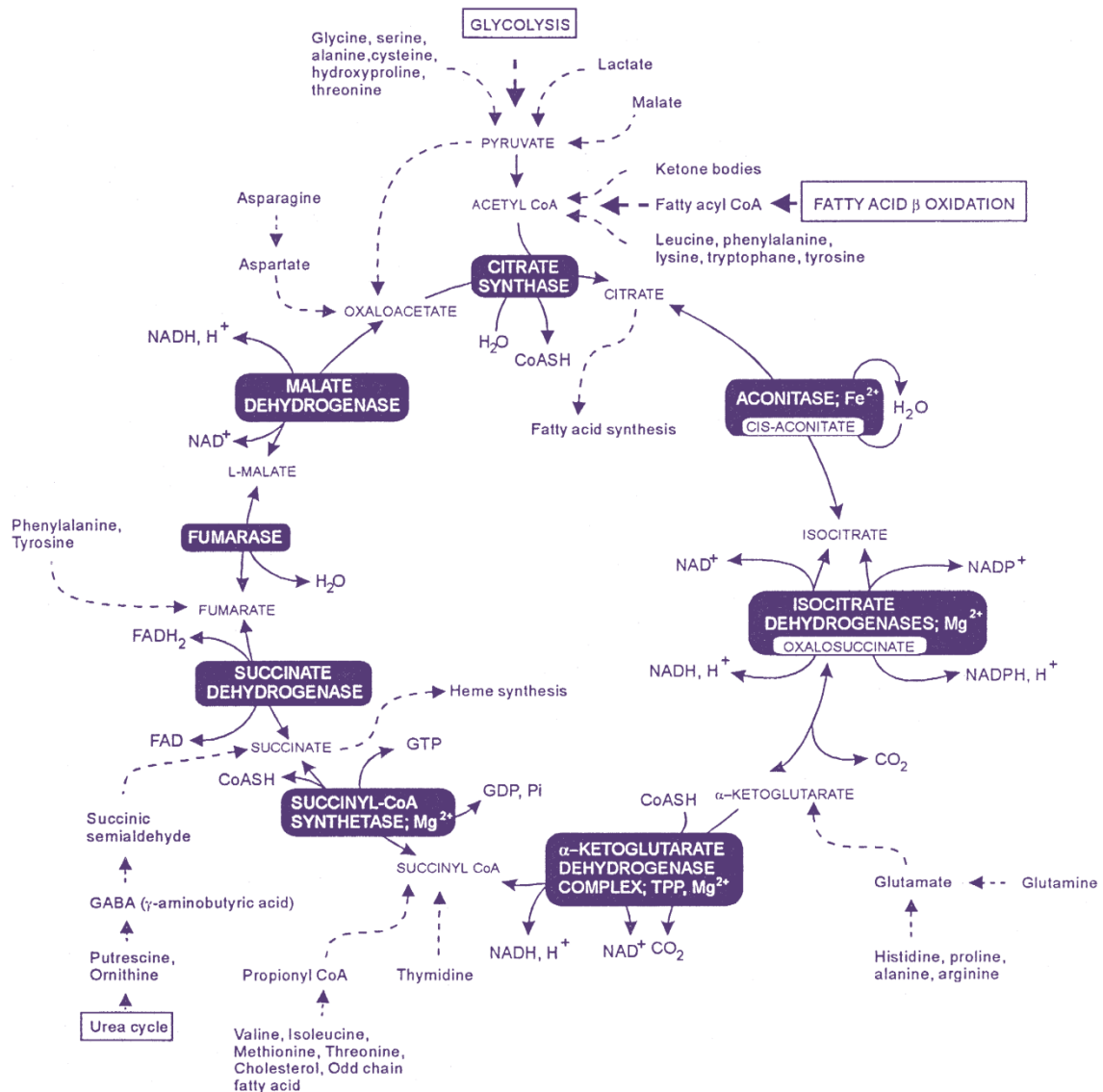
Figure 1.2 The Krebs Cycle

A schematic of the Krebs/TCA cycle (modified from (Rustin et al., 1997) and the overall TCA reaction.

Figure 1.3. Oxidative Phosphorylation

The diagram shows the main components and functioning of the respiratory system. Electrons (red dashed lines) move along the four components of the electron transport chain. Through the oxidation of NADH complex I catalyses the reduction of ubiquinone (Q) to ubiquinol (QH_2). Complex II functions within the Krebs cycle oxidising succinate to fumarate and transfers electrons to Q. In complex III OH_2 is re-oxidised to Q and electrons passed to cytochrome c. The reduction of O_2 to H_2O completes the electron transport chain in complex IV. The electrochemical gradient generated by H^+ pumping drives H^+ import through complex V to generate ATP.
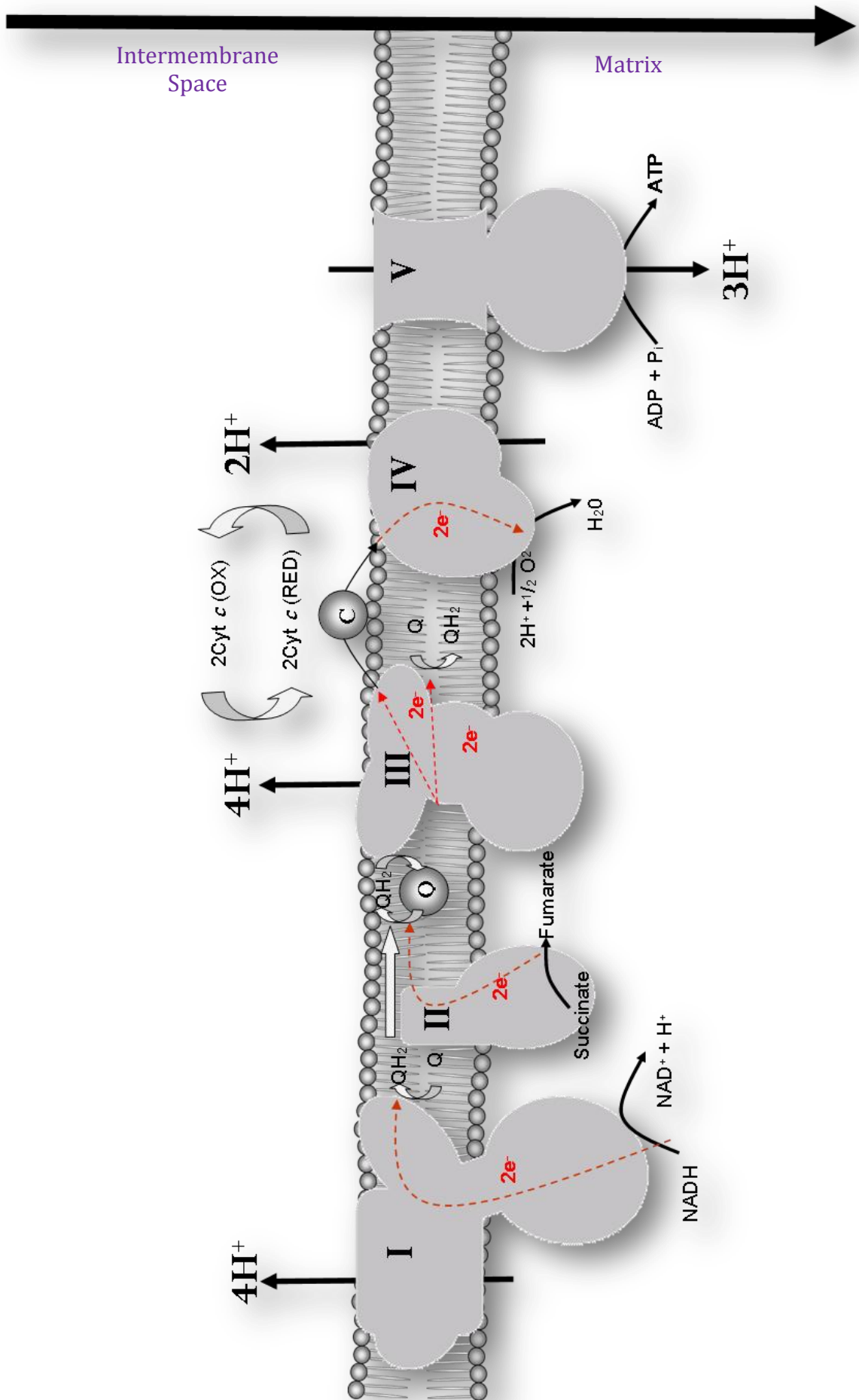
1.2.2.1 *Electron Transport Chain (ETC)*

The oxidative phosphorylation machinery consists of the four complexes of the electron transport chain (I-IV) and ATP synthase (complex V). A combination of nuclear and mitochondrial encoded subunits make up the five complexes; with the notable exception of complex II, a feature that allows for experimental manipulation and observation. The composition of each complex, along with its contribution to the proton gradient can be seen in Table 1.1.

Respiratory Components	Composition and Contribution		
	Nuclear Subunits	Mt Subunits	H^+ pumped
Complex I	39	7	4
Complex II	4	0	0
Complex III	10	1	4
Complex IV	10	3	2
Complex V	14	2	

Table 1.1. Composition and contribution of respiratory complexes

All complexes with the exception of complex II have both nuclear and mitochondrial encoded subunits. Complex II does not pump H^+ ions and subsequently does not add to the electron gradient.

1.2.2.2 *Complex I- NADH:ubiquinone oxidoreductase*

Complex I, (NADH ubquinone oxidoreductase) is the entry point to the electron transport chain and the largest of all the respiratory complexes with a molecular mass of 980 kDa (Hirst *et al.*, 2003). The protein has three distinct functional regions, module Q, N and P (Brandt, 2006) collectively composed of around 46 different proteins, the majority of which (39) are nuclear encoded (Hirst *et al.*, 2003). The fourteen core units shown to have prokaryotic homologues are made up from seven nuclear encoded genes and the seven mitochondrially subunits, encoded by ND1 to 6 and ND4L. This first step of the respiratory chain serves to catalyse the oxidation of NADH and reduce ubiquinone to ubiquinol (Equation 1.3).

The complex has a distinctive 'L'shape (Figure 1.4) with one arm located within the lipid bilayer containing all of the highly hydrophobic mitochondrially encoded subunits (Zickermann et al., 2009), and the other (more hydrophilic in nature) protruding into the

matrix (Hofhaus et al., 1991; Grigorieff, 1999). The peripheral arm of complex I contains module Q and N. The oxidation of NADH begins in module N where NADH is releases its $2e^-$ to the primary electron acceptor –flavin mononucleotide (FMN)(Walker *et al.*, 1992) generating FMNH2. These electrons are transferred through a series of seven Fe-S clusters to the Q module, the site of ubiquinone reduction. Ubiquinol is then released into the intermembrane space.

$$NADH + Q + 5(H^+)_{matrix} \rightarrow NAD^+ + QH_2 + 4(H^+)_{cytoplasm}$$

Equation 1.3. Complex I Reaction

The reaction catalysed by complex I

The lipid bilayer embedded arm is home to module P and is responsible for proton pumping. Following the transfer of electrons in the peripheral arm conformational changes occur which in turn cause physical changes to the membrane arm. This causes channels within the P module to open resulting in the translocation of four protons from the matrix for every two electrons donated by NADH. The mechanism and order of assembly of complex I is not fully elucidated although it appears that anchoring via the membrane bound P module may occur first allowing the peripheral arm to form later. Experimental evidence exists to suggest a sequential construction of subcomplexes that eventually come together to form the final complex.
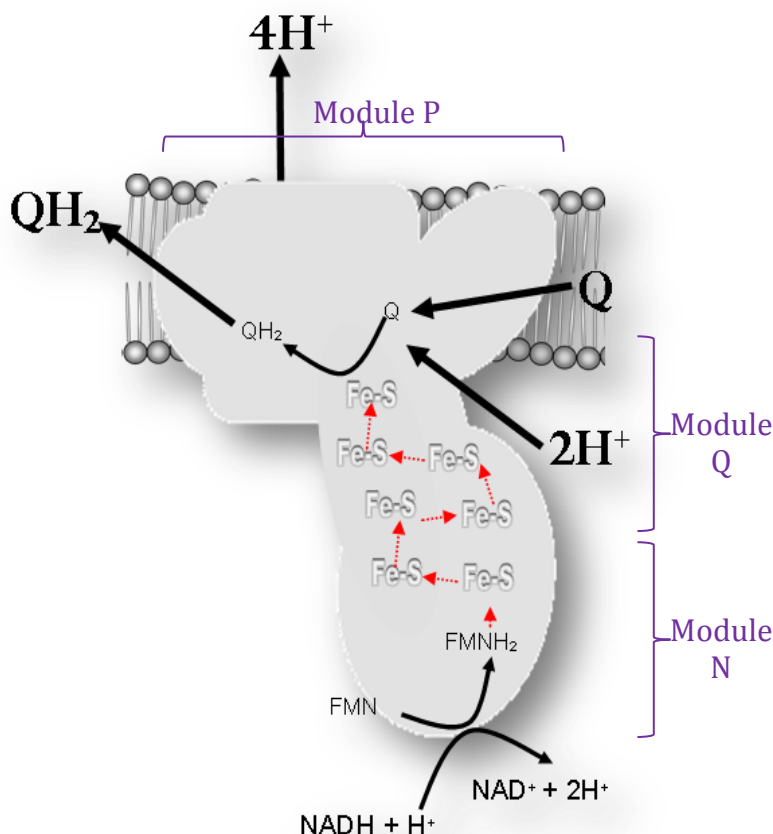
Figure 1.4. Complex I

The structure of complex I is a characteristic L shape composed of 3 modules. Module N transfers electrons from NADH to iron sulphur clusters. In module Q electrons from the iron sulphur clusters are transferred to Q. Module P is responsible for the export of H^+.

11

1.2.2.3   *Complex II- Succinate ubiquinone oxidoreductase*

Complex II (succinate ubiquinone oxidoreducatase) is unique amongst the OXPHOS complexes, in being solely encoded by nuclear genes. Consisting of just four proteins, complex II is also the smallest member of the electron transport chain (Figure 1.5). As with complex I, a portion of complex II, the hydrophobic SDHC and SDHD subunits exist within the membrane and act as an anchor for the two hydrophilic subunits, SDHA and SDHB. Together these matrix dwelling components make up the catalytic core of the enzyme succinate dehydrogenase (SDH) (Sun et al., 2005). Within SDHB exists three iron sulphur clusters that act as an electron transport link between the covalently bound FAD cofactor found within SDHA and the ubiquinone binding site at the membrane interface. A haem prosthetic group of unknown function also exists within complex II which may have a role in preventing ROS formation by the semiquinone intermediate or be responsible for assembly and stability of the complex (Hagerhall, 1997).
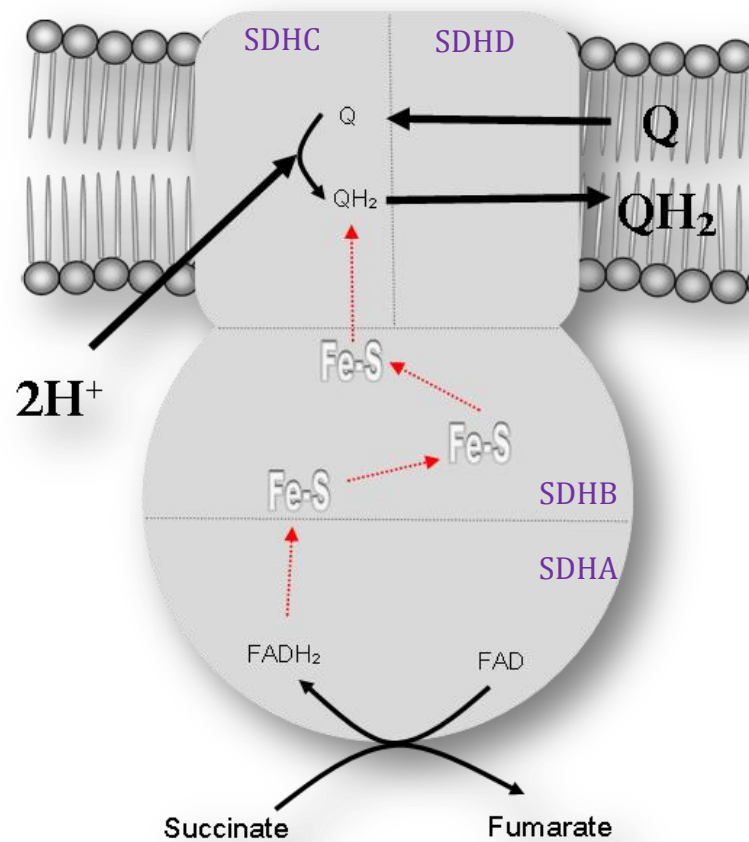
Figure 1.5. Complex II

Complex II is the smallest subunit of the respiratory chain containing only four subunits, SDHA, SDHB, SDHC and SDHD. Complex II does not export any H^+ ions.

Unlike all other complexes of the ETC, complex II does not translocate protons across the inner membrane, but acts as an enzyme of the TCA cycle, oxidising succinate to fumarate whilst reducing FAD to FADH2 (Equation 1.4). The reoxidation of FADH2 through a series of electron transfers along the three Fe-S clusters, results in the reduction of ubiquinone in two sequential single electron reactions within a 'hydrophobic pocket' formed by SDHB, SDHC and SDHD (Hagerhall, 1997; Sun *et al.*, 2005).

$$Succinate + FAD + 2(H^+) + Q \;\rightarrow Fumarate + FADH + Q$$
$$\rightarrow Fumarate + FAD + QH_2$$
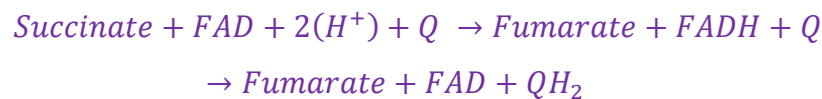
Equation 1.4. Complex II reaction

The reaction catalysed by complex II

1.2.2.4   *Ubiquinone (Coenzyme Q)*

Ubiquinone (Figure 1.6), often referred to as coenzyme Q, is a lipid soluble quinone and as such is able to move freely within the lipid bilayer. It functions as an electron carrier, shuttling electrons from complexes I and II to complex III. Within complex II the reduction of ubiquinone (Q) occurs in two single electron transfer steps, with reduction by a single electron first forming ubisemiquinone (Q-) before complete reduction generates ubiquinol (QH_2).
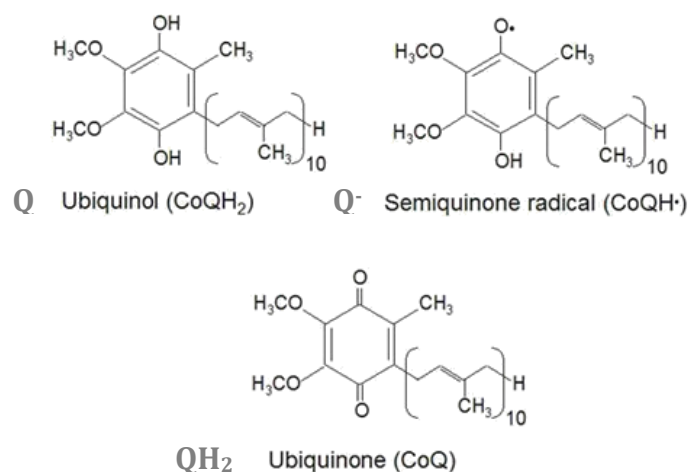
Figure 1.6. Ubiquinone forms

Diagram showing the electron acceptor molecule ubiquinone, in its reduced form- Ubiquinol (Q), oxidized form- ubiquinone (QH_2) and the intermediate- ubisemiquinone (Q^-). (adapted from biochemistrydictionary.org)

1.2.2.5   *Complex III- Ubiquinol cytochrome c oxidoreductase*

Complex III (Cytochrome *c* oxidoreductase) consists of 11 subunits forming a membrane spanning homodimer of 248kDa. This third complex is responsible for catalysing the transfer of 2 electrons within QH_2 to an individual cytochrome *c* molecule. Only one subunit of complex III is mitochondrially encoded (cytochrome b) (Sen and Beattie, 1986). The complex contains 5 key redox components, two b type hemes, a single c-type heme, the Rieske center (an Fe-S cluster) and ubiquinone (Figure 1.7).
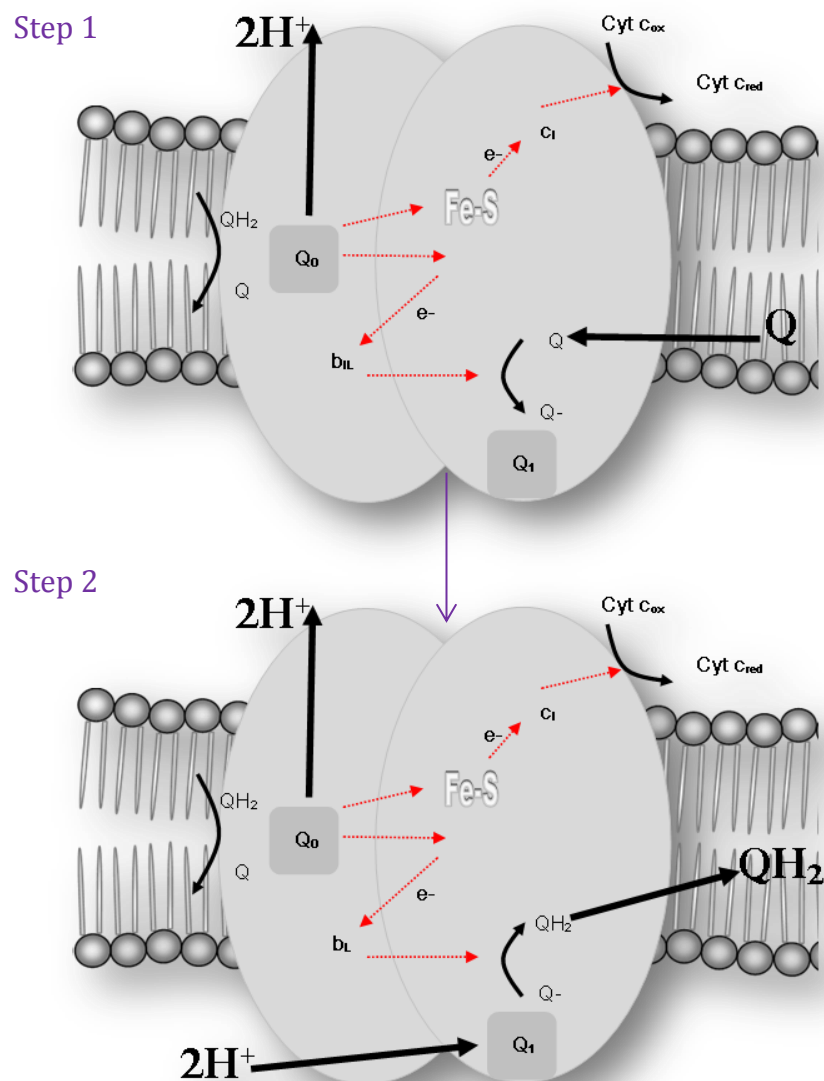
Figure 1.7. Complex III and the Q Cycle

Schematic of complex III structure and pathways of the Q cycle, for details see text.

The electron transfer from ubiquinol to cytochrome *c* occurs through a process known as the Q cycle (Mitchell, 1976) which couples the 2e$^-$ oxidation of ubiquinol to the release of two protons into the intermembrane space. This two-step process begins with the transferal of one electron from ubiquinol (forming semiubiquinone) first to the Rieske center where it is passed to cytochrome c1 and subsequently cytochrome *c* (within the Q0 site). The second electron is transferred within the Q1 site to cytochrome b where it first binds with low affinity to haem b_1 followed by haem b_h with higher affinity. The redox component ubiquinone is then reduced to form the semiquinone intermediate (Q-). A second Q cycle must then commence with QH_2 binding the Q0 site and the above process is repeated with the exception that haem b_h now fully reduces the Q- from the first cycle. Two OH_2 molecules therefore are consecutively processed within complex III for one complete Q cycle. The 2 electron oxidation of ubiquinol is accompanied by release of two protons into the intermembrane space.

1.2.2.6   *Cytochrome c*

Cytochrome *c* is a small haem protein (13kDa) that is a critical component of the ETC. The nuclear encoded highly soluble protein acts as a mobile carrier that shuttles electrons from complex III, through the haem group and transfers them to complex IV. Release of cytochrome *c* into the cytosol also initiates apoptosis through its binding with Apaf-1.

1.2.2.7   *Complex IV- Cytochrome c oxidase*

Complex IV (Cytochrome *c* oxidase) is the final enzyme of the electron transport chain. The protein consists of 13 subunits of which 3 (COX I-III) are mitochondrially encoded (Tsukihara *et al.*, 1996). Majority of the complex exists within the membrane, with COX I and II making up the majority of the catalytic core. The complex also consists of two iron sites, two copper sites and others for zinc and magnesium. Its role is the reduction of the terminal electron acceptor- oxygen and the formation of water. To achieve this four electrons are required with cytochrome c oxidase undergoing four sequential states (Figure 1.8).

Figure 1.8. Complex IV

Complex IV catalyses the reduction of O_2 to H_2O through the transfer of electrons from cytochrome c along a chain of haem and copper centres in a cyclic manner.
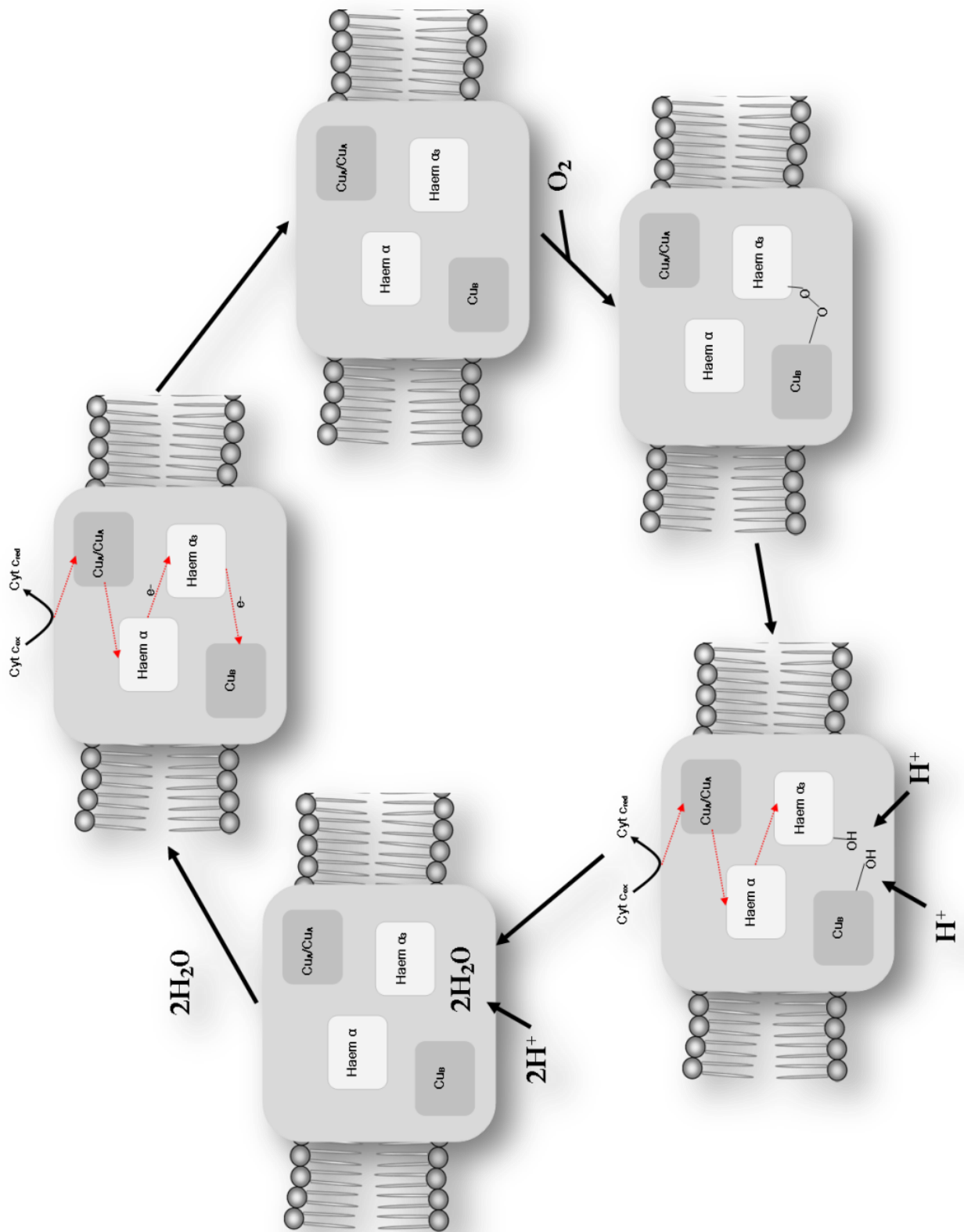
Cytochrome *c* binds complex IV at the intermembrane space side of the membrane where the first electron passes to a double copper centre (Cu_A) where Cu^{2+} is reduced to Cu. The electron is then passed to haem *a* and then to the catalytic site, haem a_3 and Cu_B. This pathway is repeated by the second electron but terminates by reducing haem a_3, producing an 'active centre'. At this point both Cu_B and haem a_3 are reduced enabling O_2 to bind generating a peroxide bridge termed the 'peroxy' state. The final two electrons repeat this process but bring about the conclusion of the peroxy state and commencement of the 'ferryl' state through binding of 2H+ causing cleavage of the peroxide bridge. Finally cytochrome *c* enters the 'oxidised' state with a further 2H+ molecules completing the reduction of O_2 to H_2O (Faxen *et al.*, 2005). The overall reaction can be seen below in Equation 1.5.

$$4\,(Cyt_c)_{red} + 8(H^+)_{matrix} + O_2 \rightarrow 4(Cyt_c)_{ox} + 2H_2O + 4(H^+)_{cytoplasm}$$

Equation 1.5. Complex IV reaction

The reaction catalysed by complex IV

1.2.2.8 *Complex V- ATP synthase*

The concluding step in the respiratory chain is the production of ATP from ADP and Pi via Complex V (ATP synthase). This final complex is around 500kDa consisting of 16 subunits with ATP 6 and 8 encoded by the mtDNA. Its structure is divided into two structural fractions termed FO and F1 (Figure 1.9). FO module is embedded in the mitochondrial inner membrane and contains a rotary ring of 8 hydrophobic c subunits that form the proton channel of the complex and subunits involved in the peripheral stalk responsible for stabilising the position of F1 (a,b,d,F6 and OSCP) and accessory units e, f, g and A6L.

F1 exists in the matrix side of the membrane as a water soluble, globular domain containing the catalytic binding sites of ADP and Pi. It is composed of five distinct subunits, α, β, ε, γ and δ. The γ and ε subunit form the central stalk of F1 that interacts with F0. Surrounding the coiled coil of the γ subunit are 3 α and 3 β subunits arranged one after the other forming a cylindrical shape.

Both fractions are rotary motors capable of bimodal functioning to either produce or hydrolyse ATP. Protons pass through the 8 c subunits of F0, where a glutamate molecule within each subunit of the c-ring undergoes protonation and deprotonation, as such for a single 360^0 rotation 8 protons are transferred. The electrochemical gradient generated by F0 is then used to generate rotary torque in F1 to drive ATP synthesis through the attachment of the F1 central stalk to the c ring. Synthesis of ATP from ADP and Pi is then driven at catalytic sites of the beta subunits of F1. These beta subunits consecutively exist in three different conformations, open, loose or tight. When loose ADP and Pi bind loosely, following rotation of F1 the conformation of these catalytic sites changes allowing ADP and Pi to bind to the catalytic site. Upon further rotation the beta conformation becomes tight enabling enough energy to produce ATP. The final rotation releases ATP as the beta subunits become open.

A complete 360^0 rotation of complex V therefore produces three ATP molecules (Jonckheere *et al.*, 2012) following the translocation of 8 protons. The cost of each ATP molecule therefore is 2.7 H+ (Watt *et al.*, 2010). The adenine nucleotide transporter (ANT) is then responsible for the export of ATP into the cytoplasm which occurs in parallel to the import of ADP into the mitochondrion via a conformational change of the ANT antiporter.
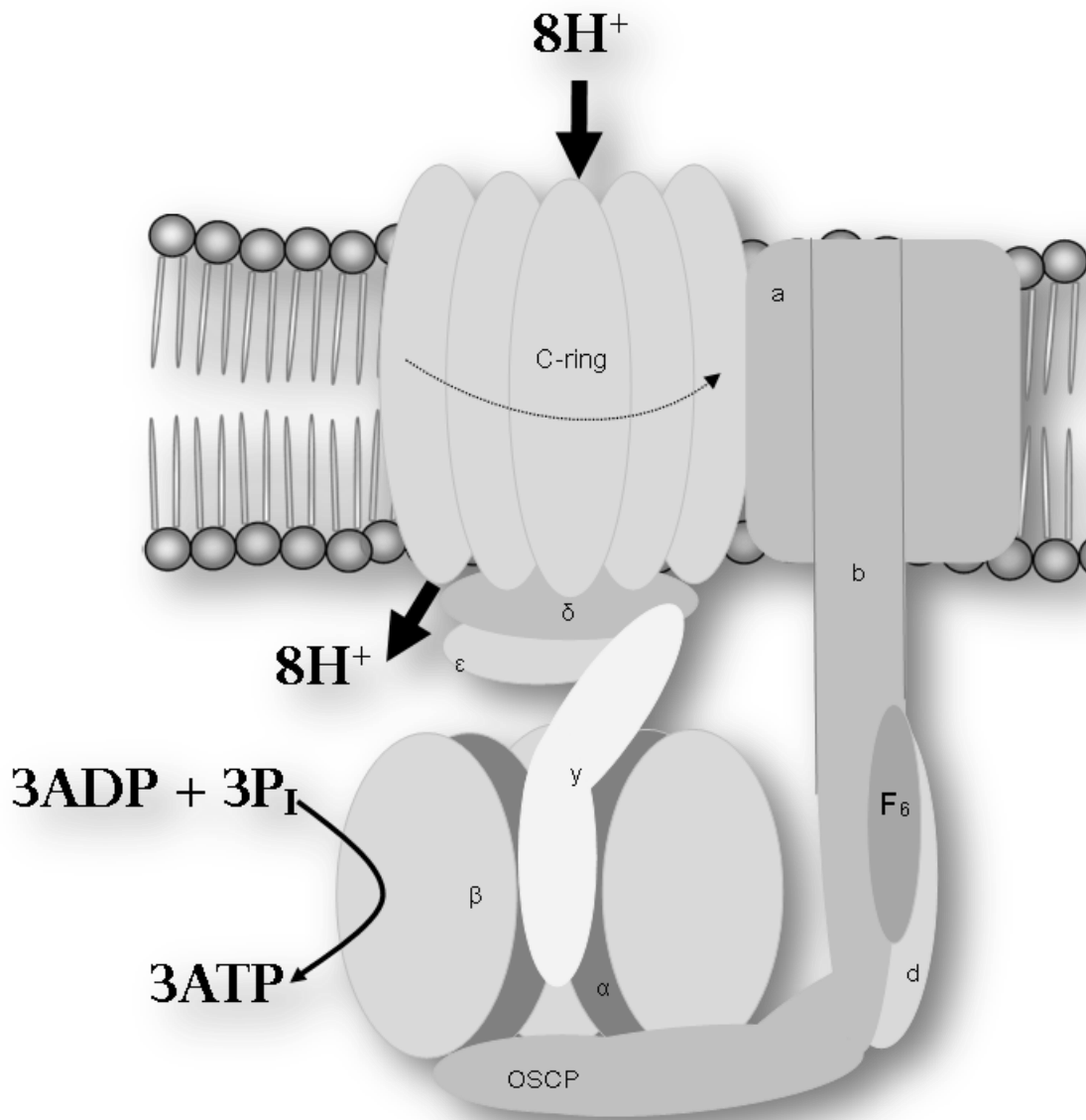
Figure 1.9. Complex V

Structural schematic of complex V comprising of the F_0 module with can be further divided into the c-ring and peripheral stalk and the F_1 module containing the central stalk and $\alpha_3\beta_3$ catalytic ring.

1.2.2.9 *Supercomplexes*

The complexes of oxidative phosphorylation are commonly thought of as independent sequential structures linked purely by the mobile carriers cytochrome *c* and ubiquinone. Conversely to the archetypal chain organisation however it is now understood that multiple complexes are able to physically interact with each other. The first evidence for the existence of these 'supercomplexes' in mammalian mitochondria was published in 2000 (Schagger, 2000). Since then structural (Dudkina *et al.*, 2005) and functional (Acin-Perez *et al.*, 2004) observations of supercomplexes have been shown.

The supercomplexes comprising complexes I, II, and IV are termed respirasomes, representing the basic unit of respiration within the mitochondrion. Such supercomplexes are thought to convey a clear biochemical advantage by increasing electron transfer efficiency by maximising the proximity of key ETC complexes and enabling substrate channelling. Existing alongside respirasomes however are partial complexes often missing Complex IV, the role of these incomplete units is less clear, although the interaction between Complex I and III may serve to stabilise the proteins (Acin-Perez *et al.*, 2004).

Importantly, supercomplex formation may have implications with relation to human pathogenesis. Recent understanding shows that respirasomes, other supercomplexes and the assembly of individual complexes are all linked, with intermediates of complex I preceding assembly of subunits of complexes III and IV which then precedes final formation of complex I through incorporation of its catalytic domain. The coordinated construction of complexes and their conglomerates goes some way to explaining how mutations within a certain complex can result in combined respiratory defects through compromised assembly and impacts within supercomplexes.

1.2.3 Reactive Oxygen Species (ROS)

Reactive Oxygen Species (ROS) are highly reactive molecules formed through the incomplete reduction of molecular oxygen. As such, mitochondria represent an important source of ROS. Examples of mitochondrially derived ROS include superoxide anion O_2-, hydrogen peroxide (H_2O_2) and the hydroxyl radical (OH).

Superoxide is generated when electrons leak from the ETC directly to O_2. This molecule is highly reactive and as such is converted to a less reactive H_2O_2 molecule through superoxide dismutase. H_2O_2 is still toxic and requires further enzymes such as catalase for its removal. The proximity of the ROS producing ETC to mtDNA means that the mitochondrial genome and mitochondrion themselves are particularly susceptible to ROS induced damage (oxidative stress). Externally ROS can damage all components of cells with numerous diverse implications ranging from reduced telomerase activity to affecting the self-renewal capacity of stem cells. For this reason, alongside antioxidants, dedicated DNA repair mechanisms exist to limit the impact of ROS damage.

In the 1950s Denham Harman proposed the free radical theory of ageing (Harman, 1956; Harman, 1981). The theory suggests that the accumulation of damage resulting from free radicals and the balance of the cells ability to compensate for such damage are pinnacle to the ageing process. Increased ROS and increased mtDNA mutations are commonly observed in aged tissue supporting the free radical theory. Exceptions to the rule however exist and show other factors are at play. For example the naked mole rat shows an elevated level of ROS but an extended life span.

The free radical theory was later expanded to the mitochondrial theory of ageing taking into account mitochondria as producers of ROS and the proximity of mtDNA to this production putting the organelle itself at the precipice of the ageing process (Miquel *et al.*, 1980), Harman, 1981). Indeed age associated accumulation of mtDNA mutations has been observed in human colon (Greaves *et al.*, 2006), skeletal muscle (Bua *et al.*, 2006) and the brain (Bender *et al.*, 2006). The age associated accumulation of dysfunctional mitochondria would subsequently bring about the gradual deterioration of organism functioning. Whether this is alone or more likely in contribution with an observed reduction in mtDNA abundance remains debated (Welle *et al.*, 2003).

Although deleterious through many routes, ROS may represent a necessary evil within the cell with key roles in intracellular cell signalling that are just beginning to be elucidated. By means of example superoxide has been shown to leave through VDAC where it signals hypoxia induced transcription and signals to autophagic processes

which are likely to be key to signalling the health of the mitochondrion and metabolic state.

1.2.4   Calcium Handling

Mitochondria play a pivotal role in the buffering and maintenance of calcium homeostasis. Calcium ions are secondary messengers in many cellular signalling pathways including energy transduction where increased Ca^{2+} uptake has been shown to activate the Krebs cycle through activation of pyruvate isocitrate and oxoglutarate dehydrogenase and increase ATP production (McCormack *et al.*, 1990; Jouaville *et al.*, 1999). Calcium in also intrinsically linked to apoptosis and necrosis via the mitochondrial permeability transition pore (MPT). Ca^{2+} overloading is sufficient to induce opening of this pore through which cytochrome *c* can release and bind apoptotic factors in the cytosol. Calcium release from the ER has also been shown to be coupled to the exodus of cytochrome *c* from the mitochondrion (Mattson and Chan, 2003). Subsequently, the buffering capacity of mitochondria is crucial for cell homeostasis ensuring intracellular calcium signals are equilibrated to alterations in extracellular calcium levels.

Found within the inner membrane, the Ca^{2+} uniporter is responsible for the uptake of calcium to mitochondria. Here, at high calcium concentrations, calcium binds to the cytosolic side of this uniporter causing its activation and is transported across the electrochemical gradient. Conversely, the efflux of calcium from the mitochondrion is facilitated through Na/Ca^{2+} exchange, although the molecular identity and complete functionality of this channel remains unknown. The process of Ca^{2+} efflux ensures equilibrium is never reached meaning, in theory, mitochondria are an unlimited calcium sink.

Calcium homeostasis is of particular importance in neurons where the ions are involved within signalling of presynaptic terminals. Following stimulation mitochondria are able to buffer, generating a Ca^{2+} 'plateau' that allows for rapid proceeding stimulations and subsequently enhanced responses. Within dopaminergic neurons of the substantia nigra Ca^{2+} is known to confer unique pacemaking abilities which may render this cellular population particularly vulnerable to dysfunctional mitochondria which are unable to

fully buffer calcium. This offers tempting links between mitochondrial functioning, calcium and Parkinson's disease as it is these dopaminergic neurons which suffer most dramatic reduction in this condition.

1.2.5   **Apoptosis**

Apoptosis is the highly regulated process of programmed cell death, in stark contrast to necrosis, an uncontrolled abrupt cell death caused by trauma or acute cellular injury. Apoptosis functions in important developmental stages and displays a distinct pathway, including condensation of the nucleus and cytoplasm, or 'blebbing' before phagocytosis and degradation by other cells (Kerr *et al.*, 1972). Although initially thought to be under nuclear control it is clear mitochondria play a huge role in the apoptotic process, not least through the nuclear encoded electron carrying molecule- cytochrome *c*. Despite being the most potent signalling molecule of apoptosis it was not identified as a factor until 1996 (Liu *et al.*, 1996). The mitochondrion's role was suggested prior to this through BCL-2 protein which is located primarily on the outer membrane. BCl-2 family of proteins are known to be crucial regulators of the apoptosis process through their interaction with proapoptotic members, Bax and Bak. These proapoptotic proteins are known to oligomerize in the outer mitochondrial membrane causing its permeabilisation and release of cytochrome *c*. Once in the cytosol, cytochrome *c* can interact with caspase 9 and APAF1 forming a heptameric protein ring, the apoptosome. The apoptosome is necessary for induction of preceding molecular changes required for the caspase cascade. Mitochondria are also responsible for the release of inhibitors of apoptosis including Smac/DIABLO which prevent the activity of the apoptosome. Alongside this, mitochondria release apoptosis inducing factor (AIF), which assists apoptosis through the degradation of nuclear DNA (Ye *et al.*, 2002).

1.3   **THE MITOCHONDRIAL GENOME**

The mitochondrial genome is a 16,569 base pair, closed, circular, double stranded DNA molecule. Located within the mitochondrial matrix, mtDNA exists in multiple copies that are freely dispersed but packaged into protein-DNA complexes known as nucleoids, which associate with the inner membrane (Albring *et al.*, 1977). Within each nucleoid, it was thought multiple copies of the genome could exist alongside the protein machinery required for transcription, replication and maintenance of the mtDNA (Holt *et al.*, 2007). Advances in imaging techniques, notably super resolution microscopy have shown most nucleoids actually only contain one molecule of mtDNA (Kukat *et al.*, 2011). It has also been suggested that complex assembly may take place in the peripheral region (Bogenhagen *et al.*, 2008).

1.3.1   **Genome organization**

The mitochondrial genome was first sequenced in 1981 (Anderson *et al.*, 1981) and following revision in 1999 (Andrews e*t al* 1999) has become commonly known as the revised Cambridge Reference Sequence (rCRS). The genome encodes for a total of 37 polypeptides (including 13 proteins essential to OXPHOS), 22 transfer RNAs (tRNA) and two ribosomal RNAs (rRNA) (Anderson et al., 1981) (Figure 1.10). These 13 proteins can further be divided into 7 subunits of complex I, a single subunit of complex III, three subunits of complex IV and 2 of complex V. Why these 37 genes were retained by the mitochondrial genome when around 1500 relocated to the nuclear genome is unclear but may be due to the hydrophobicity of these particular subunits which would pose challenging for transport into the organelle after translation. Alternatively, the retention of these genes has been proposed to enable rapid adaption of the OXPHOS system if necessitated by environmental changes (Wallace, 2007).

The mitochondrial genome is composed of two strands, named heavy and light reflecting their purine to pyrimidine ratio. The heavy chain contains more guanine residues in contrast to the abundance of cytosine residues of the light chain. Only ND6 and 8 of the mitochondrial tRNA genes (MTTs) are transcribed from the light strand, the remaining 12 protein encoding genes, 14 MTTs and the two mt-rRNAs are transcribed from the heavy chain. The compact mtDNA molecules differ from the nuclear genome containing no introns with the only extended non coding region being

found within the displacement loop, an area that controls transcription and replication of the genome (Clayton, 1982; Clayton, 2003).
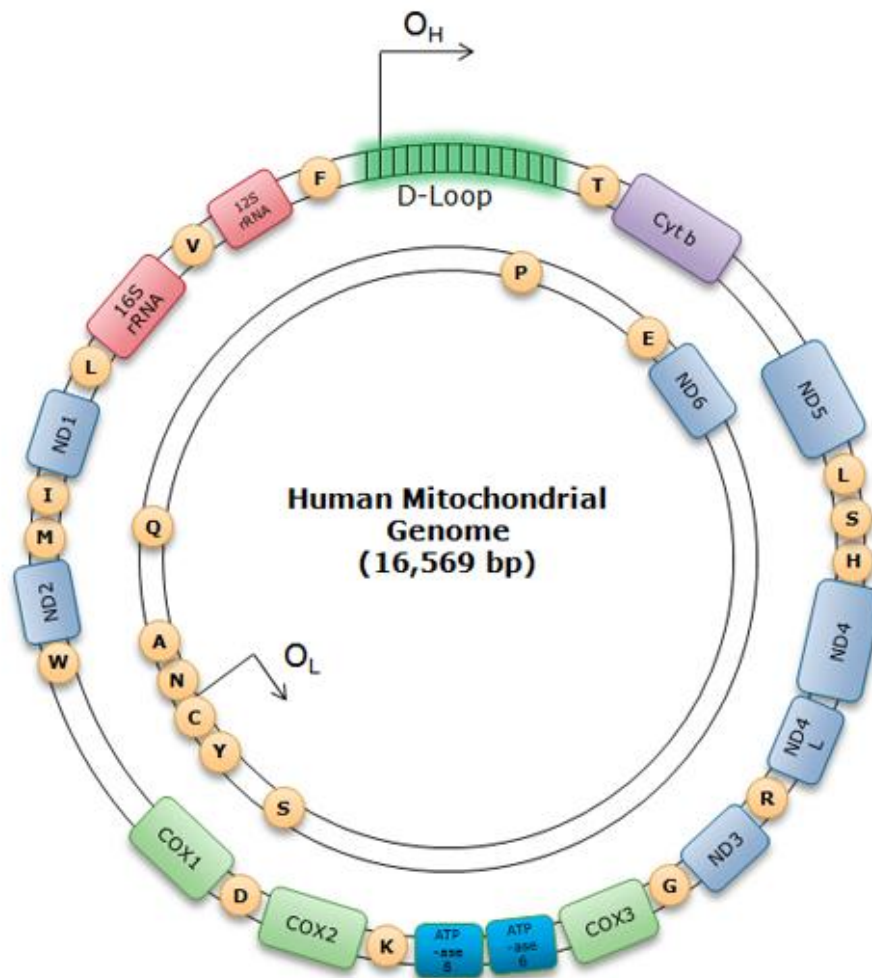
Figure 1.10. The Mitochondrial Genome.

The mtDNA molecule encodes 13 proteins, 7 subunits of complex I (blue), 1 subunit of complex III (purple), 3 subunits of complex IV (green) and 2 subunits of complex V (turquoise) . Alongside this it encodes 2 mRNAs (red) all of which are punctuated by 22 tRNA (orange letters). Both origins of transcription (O_H and O_L) are labelled, areas without labels represent non coding regions. (Figure reproduced with permission from Mr Casey Wilson)

1.3.2   **Transcription**

A promoter region for transcriptional initiation is found on both the heavy and light strands of the mitochondrial genome- the light-strand promoter (LSP) and the heavy-strand promoter (HSP). As such mtDNA transcription occurs bi-directionally. HSP transcription is initiated from one of two heavy strand promoters (H1 or H2) with H1 producing a short transcript encompassing the two rRNAs whilst H2 covers the entire length of the genome (Zollo *et al.*, 2012). Transcription initiation of the light chain conversely occurs from a single promoter site (L1) but also produces long polycistronic molecules corresponding to nearly the entire length of the genome (Montoya *et al.*, 1982; Chang and Clayton, 1984; Hixson *et al.*, 1986; Taanman, 1999).

1.3.2.1   *Protein machinery of transcription*

Three key components for mitochondrial transcription have been described, mitochondrial DNA-directed RNA polymerase (POLRMT), mitochondrial transcription factor B1 and B2 (TFB1M/TFB2M) and mitochondrial transcription factor A (TFAM).

TFAM was the first transcription factor to be identified in humans in 1988 (Fisher and Clayton, 1988). Structurally TFAM consists of two tandem domains separated by a 27 amino acid linker region and a 25 residue C-terminal tail important for DNA recognition (Dairaghi *et al.*, 1995). TFAM is able to unwind and bind DNA which may be crucial to exposing the promoter regions for accessibility of other transcriptional factors. Its binding has also been shown to induce conformational changes upstream of the transcriptional start sites (Fisher *et al.*, 1992). Although once thought to be a critical component of transcription it has recently been shown that overexpression of TFAM can actually inhibit transcription (Rebelo *et al.*, 2009). Within yeast, the TFAM homologue Abf2 is not required for transcription (Xu and Clayton, 1992) as such the only indispensable components of transcription are POLMRT and TFB1M or TFB2M, with the use of TFB2M shown to have tenfold efficiency for reasons currently unclear (Falkenberg *et al.*, 2002).

POLRMT itself is known to contain promoter recognition regions although its function requires the assistance of a mitochondrial transcription factor with which it forms a

heterodimer. Together these activate transcription through binding with TFAM at specific sites in proximity to the promoter regions (Bonawitz *et al.*, 2006). Although transcription can occur in the absence of TFAM it is thought that it plays a regulatory role in directing transcription initiation (Falkenberg *et al.*, 2007).

TFB1M and TFB2M represent two functional homologues of transcription factor B first identified in 2002 (Falkenberg *et al.*, 2002). Although both are known to independently support initiation of transcription it would appear TFB2M may show greater efficiency due to its ability to directly contact DNA at the transcription start site where it may assist in promoter melting (Sologub *et al.*, 2009) and/or stabilise single stranded DNA following unwinding by TFAM (Falkenberg *et al.*, 2007). TFB1 is more important in methylation role of the diadenine bases in 12S rRNA.

1.3.3   Termination of transcription

Crucial for the termination of transcription from all three promoters is the family of regulators known as mitochondrial transcriptional termination factors (mTERF) of which 4 have been identified. With regards to mechanism of termination the H1 promoter is most well characterized. mTERF1 has been shown to bind the termination site of H1- a 28bp region immediately downstream of RNA1(Kruse *et al.*, 1989) but also contradictorily the H1 promoter site. It is thought that the resulting rDNA loop structure that contains both rRNA genes resulting from this binding, serves to rapidly recycle the transcription machinery (Rebelo *et al.*, 2011).

The three homologues of mTERF1 are less well understood. mTERF2 and 3 have been shown to be important for mitochondrial transcription through their binding with mtDNA promoter region. Interestingly mTERF3 has been shown to be a negative regulator of transcription, whereby its depletion causes increased mitochondrial transcription (Park *et al.*, 2007). Conversely, mTERF2 decrease in mice is linked to decreased mitochondrial transcription implying it has the reverse effect of mTERF3. The role of mTERF4 was until recently relatively unclear although it has now been demonstrated to have a role in the regulation of mitochondrial translation through the

recruitment of rRNA methyltransferase (NSUN4) to the large ribosomal subunit
(Camara *et al.*, 2011) this undoubtedly requires further investigation.

1.3.4   **Replication of mitochondrial DNA**

Mitochondrial DNA has an autonomous mechanism of replication (Figure 1.11).
Independent of nuclear DNA replication, mtDNA replication can occur throughout the
cell cycle (Bogenhagen and Clayton, 1977) and within post mitotic cells where nuclear
replication has halted. Interestingly, despite this independent nature, the machinery for
replication is entirely encoded by the nuclear genome. Although mechanistically more
simple than nDNA replication, requiring far fewer proteins, the exact mechanism of
replication remains debated with two models being proposed.
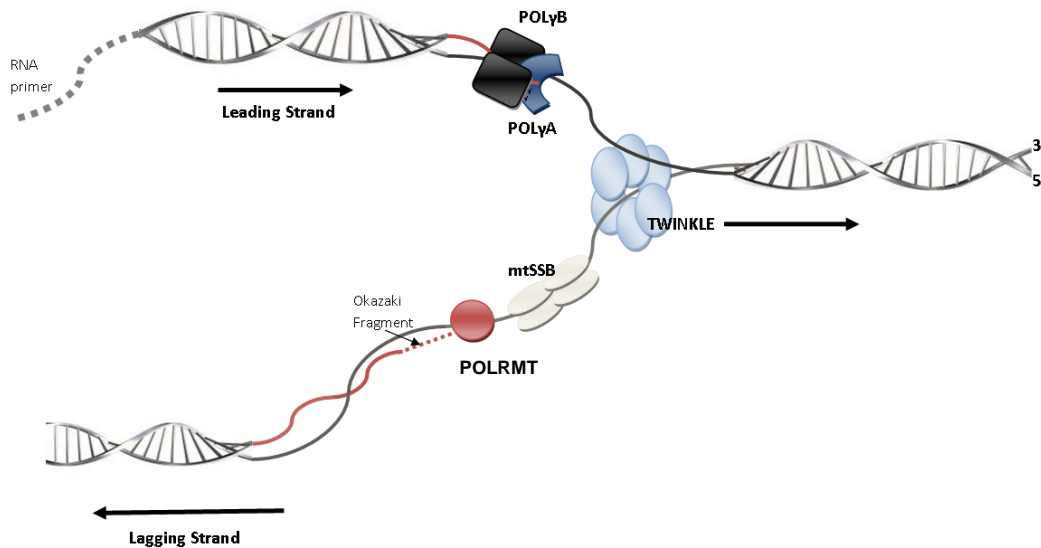
Figure 1.11. Replication of mtDNA

*The autonomous mechanism of mtDNA replication requires the co-ordinated functioning of TWINKLE,
mtSSB, POLRMT and POLγ. For details see text.*

1.3.4.1 *Replication machinery*

The mitochondrial minimal replisome consists of three proteins. The mitochondrial DNA helicase TWINKLE is responsible for unwinding mtDNA in the 5' to 3' direction in an ATP dependent manner (Korhonen *et al.*, 2003). To achieve this, a fork like structure with 5' and 3' single stranded stretches of DNA is required (replication fork). Mitochondrial single stranded binding proteins (mtSSB) maintain the integrity of DNA and prevent ssDNA forming secondary stable structures that would impair the functioning of mitochondrial polymerase gamma (POLγ), a 190kDa protein (Gray and Wong, 1992) required for replication of the mtDNA. Leading strand synthesis is performed by the catalytic subunit of POLGγ- POLγA which forms a complex with two subunits of POLγB (Yakubovskaya et al., 2006). The final contributor is POLRMT previously described for its role in transcription.

1.3.4.2 *Initiation of replication*

Transcription and replication of mtDNA are intrinsically linked. In order for replication to begin, premature termination of transcription from the LSP is required (Bonawitz *et al.*, 2006). Critical to this process are three conserved sequence blocks (CSBs) located downstream of OH and termed CSBI, CBII and CSBIII. Premature termination occurs in around 60% of cases but always at CSBII, leading to a short RNA primer which then generates an RNA-DNA hybrid (Xu and Clayton, 1995). Termination is then thought to occur through cleavage of the transcript by the RNase mitochondrial processing enzyme (RNase MRP) (Lee and Clayton, 1997) or through CSBIIs inherent transcription termination qualities (Pham *et al.*, 2006).

The minimal replisome is able to begin DNA synthesis from the origin of heavy chain replication (O_H) (Wanrooij and Falkenberg, 2010). A triple stranded structure (7S DNA) of unknown function is produced when synthesis terminates at the termination associated sequence (TAS) (Clayton, 1982). Leading strand synthesis proceeds in a 3' to 5' direction, whereby the DNA helicase TWINKLE forming a hexameric structure unwinds DNA in the 5' to 3' direction, revealing the replication fork (Korhonen *et al.*, 2003).

1.3.5   **Models of replication**

Two models of mitochondrial replication have been proposed, the synchronous (Holt *et al.*, 2000) and asynchronous (Robberson and Clayton, 1972) models. In the original asynchronous model replication begins at OH and proceeds around the mtDNA until the origin of light strand (OL) is exposed by TWINKLE (Clayton, 1991). This then forms a single stranded stem-loop structure which in turn initiates formation of a primer by POLRMT and triggers lagging strand replication in the opposite direction (Tapper and Clayton, 1981). This first model therefore produces two distinct molecules, one consisting of the parental H-strand and a partially synthesised L-strand. MtDNA molecules are converted into their closed spherical form once L-strand synthesis is complete.

The synchronous model of replication proposed by Holt in 2000 suggests bidirectional replication whereby leading strand synthesis is coupled to short stretches of lagging strand synthesis from initiation sites revealed as the DNA unwinds. The activation of these initiation sites is postulated to occur through binding of Okazaki fragments (although unobserved in mitochondria) which act as primers (Wanrooij and Falkenberg, 2010). Initiation of this model was initially thought to occur at OH although research now shows initiation occurs at multiple sites within a broad zone (OriZ) and that OH actually acts as a termination point through stalling of the replication fork (Bowmaker *et al.*, 2003). A final model, a variation on the synchronous theory is the Ribonucleotide Incorporation Throughout Lagging Strand (RITOLS). In this, leading strand replication occurs in parallel to synthesis of the lagging strand as RNA which following exposure of OL, is replaced with DNA (Yasukawa *et al.*, 2006).

1.3.6   **Mitochondrial translation**

Mitochondrial translation is a highly complex process that follows transcription and post transcriptional RNA modification. The process can be separated into four major stages, initiation, elongation and termination and recycling, all of which occur within the mitochondrial matrix and require the importation of many nuclear encoded proteins (Figure 1.12). Essential to mitochondrial translation are the mitochondrial transfer RNAs (mt-tRNAs). The 22 mitochondrial tRNAs are all encoded by the mitochondrial genome, subsequently mutations of these genes are common causes of mitochondrial disease. All but two mt-tRNAs show the classical cloverleaf form consisting of 4 stems and 3 loops. tRNAs function to recognise the 3-base codon sequences of the mRNA bringing the appropriate cognate amino acid to the growing polypeptide.

1.3.6.1   *Initiation*

Two essential initiation factors have been identified in mitochondria mtIF2 and mtIF3. These function to bring together the initiator tRNA and ribosome. The mitochondrial ribosome is surprisingly different in composition to its bacterial counterpart despite having a similar mass, mitoribosomes contain over twice as much protein but half the quantity of RNA, with many of the bacterial RNA structural components replaced with protein. The mitoribosome contains 2 subunits, the large (39S) subunit, which contains approximately 48 proteins and the 16S RNA and the small subunit (28S) containing approximately 29 proteins and the 12S RNA. Both RNAs are mitochondrially encoded. Binding of the mtIF3 to the small ribosomal subunit (SSU) causes dissociation of the large and small subunits. MRNA is then able to bind in a manner that locates the methionine initiation codon at the peptidyl site (P site) (Smits *et al.*, 2010). The tRNA for methionine (tRNAMet) has functions within both initiation and elongation. Distinction between its two roles is made possible through modification to a formylated version (mt-tRNAfMet). This mt-tRNAMet has reinforced binding with mt IF2 which subsequently prevents its binding to elongation factor Tu (Mikelsaar, 1983; Janiak *et al.*, 1990). Human mitochondria do not possess two separately encoded mt-tRNAMets for the two roles and as such tight regulation of availability of both forms is necessary (Takeuchi *et al.*, 2001). Binding of tRNAfMet to the small ribosomal subunit at the Psite is the final, GTP dependent step of initiation and requires the presence of mtIF2.

Initiation is complete when mtIF3 and mtIF2 are released and the LSU and SSU are re-associated.

1.3.6.2 *Elongation*

The peptide chain is elongated through step wise addition of aminoacylated mt-tRNAs upon presentation of their associated codons at the acceptor (A) site of the mitoribosome. For this to occur mitochondrial elongation factor Tu (meFTu) forms a complex with GTP and each of the mt-tRNAs. MtEFTu plays a vital role in carrying the mt-tRNA to the ribosomal complex alongside protecting it from degradation. Following codon recognition GTP hydrolysis occurs releasing GDP bound mtEFTu. The elongation factor Tu is recycled by mtEFTs reducing its affinity for GDP allowing its replacement and subsequent reactivation with GTP. At this point the amino acid bound to the mt-tRNA in the A site forms a peptide bond with the nascent peptide chain which is bound to mt-tRNA at the Psite. Mitochondrial elongation factor (mtEFG1) bound to GTP then causes a conformational change in the mitoribosome allowing the mRNA to shift by 3 nucleotides so that the A site is once again empty as the A site bound mt tRNA moves to the evacuated P site. The P site bound mt tRNA is thought to move to the exit site (E site) although there is speculation as to whether this site exists in mammalian mitochondria (Mears *et al.*, 2006), this in turn would enable easier frame shifting for human ribosomes as only a single anticodon/codon pairing would need to be broken. This entire process is repeated enabling the polypeptide to extend through the polypeptide exit tunnel before emerging into the matrix where it folds (Sharma *et al.*, 2003).

1.3.6.3 *Termination*

In order for the growth of the polypeptide to be terminated a STOP codon must appear at the A site which mt-tRNAs are unable to bind. Instead mitochondrial release factor 1a (mtRF1a) recognises the codon which catalyses the hydrolysis of the ester bond holding the polypeptide to the mt-tRNA at the P site. Dissociation of the entire mitoribosome complex and release of the mRNA and tRNA are achieved through the joint binding of mitochondrial ribosomal recycling factor (mtRRF) and mitochondrial elongation factor G2 (mtEFG2) at the LSU. Here the final step requires hydrolysis of the mtEFG2 bound GTP releasing the LSU allowing the process of translation to begin again.

1.3.6.4 *Hungry Codons*

The use of specific stop codons in mitochondrial translation differs from other systems. Importantly although there were originally thought to be four separate STOP codons in mtDNA, namely UAA, UAG,AGA and AGG, the single release factor mtRF1a was shown to be unable to interact with either AGA or AGG despite the open reading frames for MTCO1 and MTND6 being terminated by AGA and AGG respectively. It is now understood that either of these codons within the A site of the ribosome is not recognised by mtRF1a or any mt-tRNA. This codon is therefore referred to as a 'hungry' codon. causing a pause in the translation process. Strong secondary structure in the respective mt-mRNAs immediately downstream of the hungry codons helps to facilitate a single reverse nucleotide frameshift by the mitoribosome aligning a UAG in the mitoribosomal A site from immediately upstream of either AGA or AGG codons in their respective mt-mRNAs (Temperley *et al.*, 2010). This UAG is recognised by mtRF1a, leading to standard termination. The relatively small number of mt-tRNAs (Dittmar *et al.*, 2006) also means codon reading must be more flexible in mitochondrial translation. Variability is enabled through post transcriptional modification and a process known as the 'wobble hypothesis' whereby the first base of the anticodon is less spatially confined and subsequently able to bind non Watson-Crick pairs.
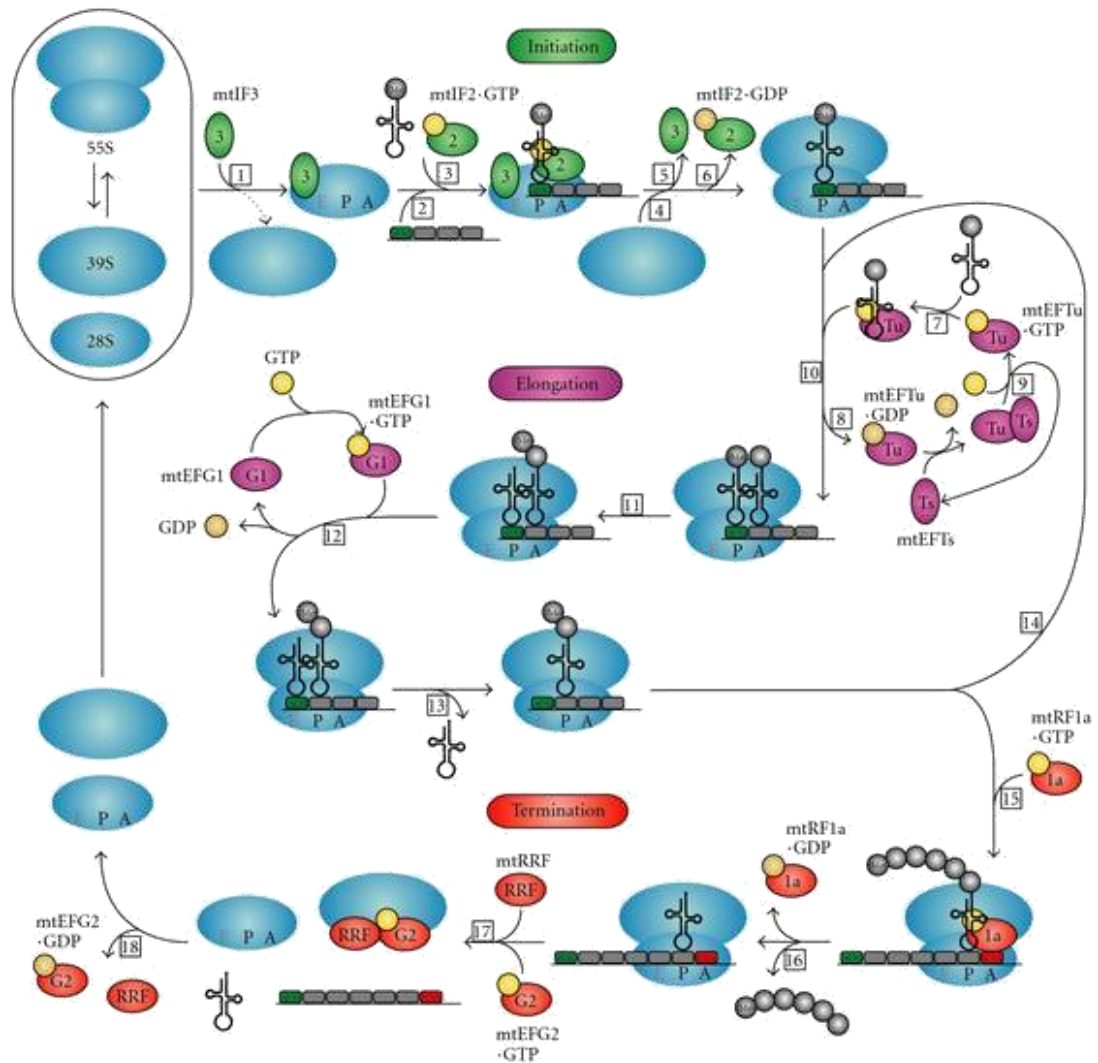
Figure 1.12. Mitochondrial translation

The schematic highlights the three stages of mitochondrial translation, Initiation, Elongation and Termination are shown alongside the required protein machinery. (Figure was taken with permission from (Smits et al., 2010)

1.4   MITOCHONDRIAL GENETICS

1.4.1   Mutations of the mitochondrial genome

Mutations of the mitochondrial genome can exist as point mutations, deletions, insertions and large scale deletions. These are all known to occur at a higher rate than those of the nuclear genome. This is likely a result of a combination of factors. Firstly the close proximity of the mtDNA to the ETC and subsequently free radical production means it is exposed to a high level of oxidative damage. Secondly, the lack of non-coding DNA coupled with an absence of protective histones mean deleterious mutations are far more likely to occur. Finally, mitochondria lack the same level of DNA repair mechanisms observed within the nuclear genome.

1.4.1.1   *mtDNA repair mechanisms*

It is now clear that there are many DNA repair mechanisms within the mitochondrion, despite lack of such processes potentially underlying the high mtDNA mutation rate. Indeed, there are many forms of DNA repair in mitochondria, but they do lack the major nucleotide excision pathways found in the nucleus. To date the most well studied repair mechanism is short base excision repair (sBER). In this mechanism mutated bases are removed by a DNA glycosylase leaving an abasic site (apurinic/apyrimidinic) which is then processed by an AP endonuclease (APE1) leaving a 3'-hydroxyl and 5'deoxyribose-5-phosphate residue. This is then filled in by polG activity   and the nick sealed by DNA ligase (Bohr *et al.*, 2002). Less well understood and currently incomplete pathways exist in the form of long patch base excision repair (which functions as short BER but for multiple nucleotides), direct repair of damaged nucleotides (Satoh *et al.*, 1988) and mismatch repair (MMR; Mason et al. 2004). Research has shown mitochondrial MMR functions independently from nuclear MMR (de Souza-Pinto *et al.*, 2009). Crucially, mitochondria lack nucleotide-excision repair, evidenced by the observation that UV-induced pyrimidine dimers were not removed from mtDNA (Clayton *et al.*, 1974).

1.4.2   **Homoplasmy and heteroplasmy**

Mitochondrial DNA molecules exist in multiple copies within each cell. A cell whose mtDNA molecules are all wildtype or mutant is said to be homoplasmic. However a situation can arise whereby wild type molecules can co-exist with mutated molecules giving rise to a heteroplasmic situation. This phenomenon has profound implications for mitochondrial disease. It is worth noting that although healthy cells are said to be homoplasmic it is likely that even these have a clinically insignificant percentage of mutated mtDNA molecules (<1%) (Lightowlers *et al.*, 1997; He *et al.*, 2010).

1.4.3   **The threshold effect**

Owing to the existence of heteroplasmy within cells, a situation exists whereby the ratio of mutated to wildtype molecules can dictate the clinical presentation of a deleterious mutation (Figure 1.13). Although some pathogenic homoplasmic mutations have been characterized, heteroplasmic mutants are, by far, more common. The threshold level for expression of a biochemical defect varies dramatically for mutation type, individual, and tissue, with reports as low as 8% in a very unusual case of a dominant mutation (Sacconi *et al.*, 2008). Typically however mutational thresholds and subsequent phenotypic expression occur at around 70-90% heteroplasmy, evidencing the recessive nature of almost all mutations. One of the complexities of mitochondrial disease therefore is the variability in expression between patients dictated by the mutational load as well as the mtDNA locus (McFarland *et al.*, 2004; Elson *et al.*, 2009). Further variation occurs when considering inheritance of the mutational level whereby factors including the mitochondrial bottleneck and other (as yet poorly understood) mechanisms can dramatically alter the heteroplasmy level within the offspring.

1.4.4   **Clonal Expansion**

It has been demonstrated that accumulation of mtDNA mutations occurs over time and that the pattern of this accumulation is focal (Muller-Hocker *et al.*, 1993; Schwarze *et al.*, 1995). This process is known as clonal expansion and has been confirmed in a variety of tissues. Although it is known that a single mutational event (be it deletion or point mutation) has the capacity to begin in a single mtDNA molecule and eventually express in an entire cell or tissue, the mechanism by which it does so is not clear. This is

made more complicated by the pattern of clonal expansion differing in tissue type (Liu *et al.*, 1998). Several models have been proposed, as yet no definite hypothesis can be proven (Elson *et al.*, 2001).
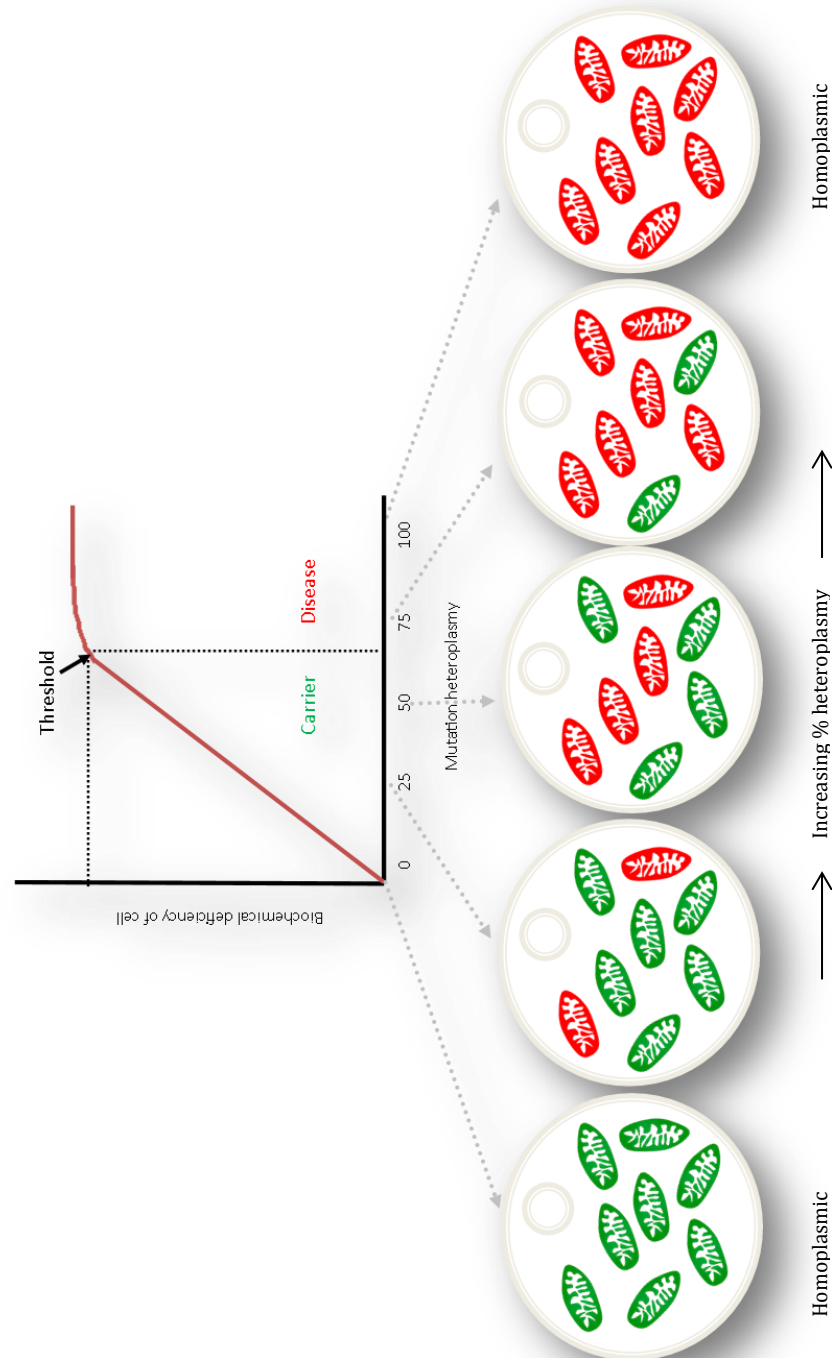
Figure 1.13. Threshold and heteroplasmy

Mitochondrial heteroplasmy means a mixture of wildtype and mutated mitochondria can reside within the same cell. When the number of mutant mitochondria reach a level where clinical presentation is observed it is termed the 'threshold'.

1.4.5   **Proposed mechanisms of clonal expansion**

Survival of the fastest proposed by Wallace in 1992, suggests large scale deletions may have a replicative advantage over the larger non mutated mtDNA molecules. This mechanism however comes under contention when we consider the entire mtDNA molecule is capable of replication in less than 90 minutes. This may not entirely dismiss the proposed mechanism if we factor in mitochondrial fusion events which would render division rates irrelevant. It is also very difficult to explain how single point mutations would be able to expand if this hypothesis was correct.

Survival of the slowest put forward by Aubrey de Grey in 1997 suggests that a decrease in respiration observed within mitochondria with mutant mtDNA molecules offers them selective advantage through decreased ROS production and subsequent low level oxidative damage (de Grey, 1997). Less damage would mean reduced degradation of mitochondria containing these molecules. This theory again comes under contention when considered under the light of fission and fusion events. The sharing of mtDNA molecules and subsequent buffering of respiratory challenge would arguable render this method implausible.

Random genetic drift unlike the preceding theories negates the requirement of a selective advantage. Data based on simulations within post mitotic tissues suggest that random genetic drift alone is capable of causing clonal expansion, made possible by the relaxed replication of mtDNA (Birky, 1994; Elson *et al.*, 2001). In this mechanism relaxed replication therefore means there is an equal chance of molecules being lost as replicated. This model is dependent on knowing the replication rate of mtDNA in these tissues.

1.4.6   **Inheritance**

MtDNA is strictly inherited down the maternal lineage (Giles *et al.*, 1980; Birky, 1994). Following fertilisation maternal mtDNA molecules vastly outnumber the paternal contingent and any remaining paternal molecules are actively degraded through ubiquitination (Cummins *et al.*, 1997). Only one exception to the rule has ever been

reported, a process known as paternal leakage (Schwartz and Vissing, 2002). The maternal inheritance is exploited for phylogenetic analysis as mtDNA inheritance is devoid of complicating bi-parental recombination (Pakendorf and Stoneking, 2005). Evolution of mtDNA can therefore be characterised by the emergence of lineages resulting from an extent of mtDNA recombination known as haplogroups. The most variable region of the mtDNA is the D-loop (non coding region) and as such much phylogenetic analysis is focussed here (Ingman, 2006). Importantly haplogrouping has valuable applications with regards to human disease, enabling the rejection of benign polymorphisms which would be expected within set groups.

1.4.7   **Mitochondrial bottleneck**

Coupled with a high mutation level, in the absence of recombination, the mitochondrial genome should undergo mutational meltdown as predicted by Muller's ratchet (Muller, 1964). This is however not the case as evidenced in Holstein cattle where the predominant mtDNA variant was shown to be capable of switching within just a couple of generations (Hauswirth and Laipis, 1982). How this is so with such a high mitochondrial copy number and limited recombination was explained through the presence of a mitochondrial bottleneck (Figure 1.14). Multiple studies have now shown that mtDNA is not replicated in the early stages of development lowering the number of mtDNA molecules/cell. Both mature mouse and bovine oocytes have been shown to have dramatically increased mtDNA compared to somatic controls. It is postulated therefore, that the amplification of these uses limited templates and as such few mtDNA molecules will predominate in the cell. What's more, if the templates happen to have a certain level of heteroplasmy this could explain the rapid genotypic shifts observed in the Holstein cattle reported above and explain why mitochondria escape the fate predicted by Muller's ratchet.
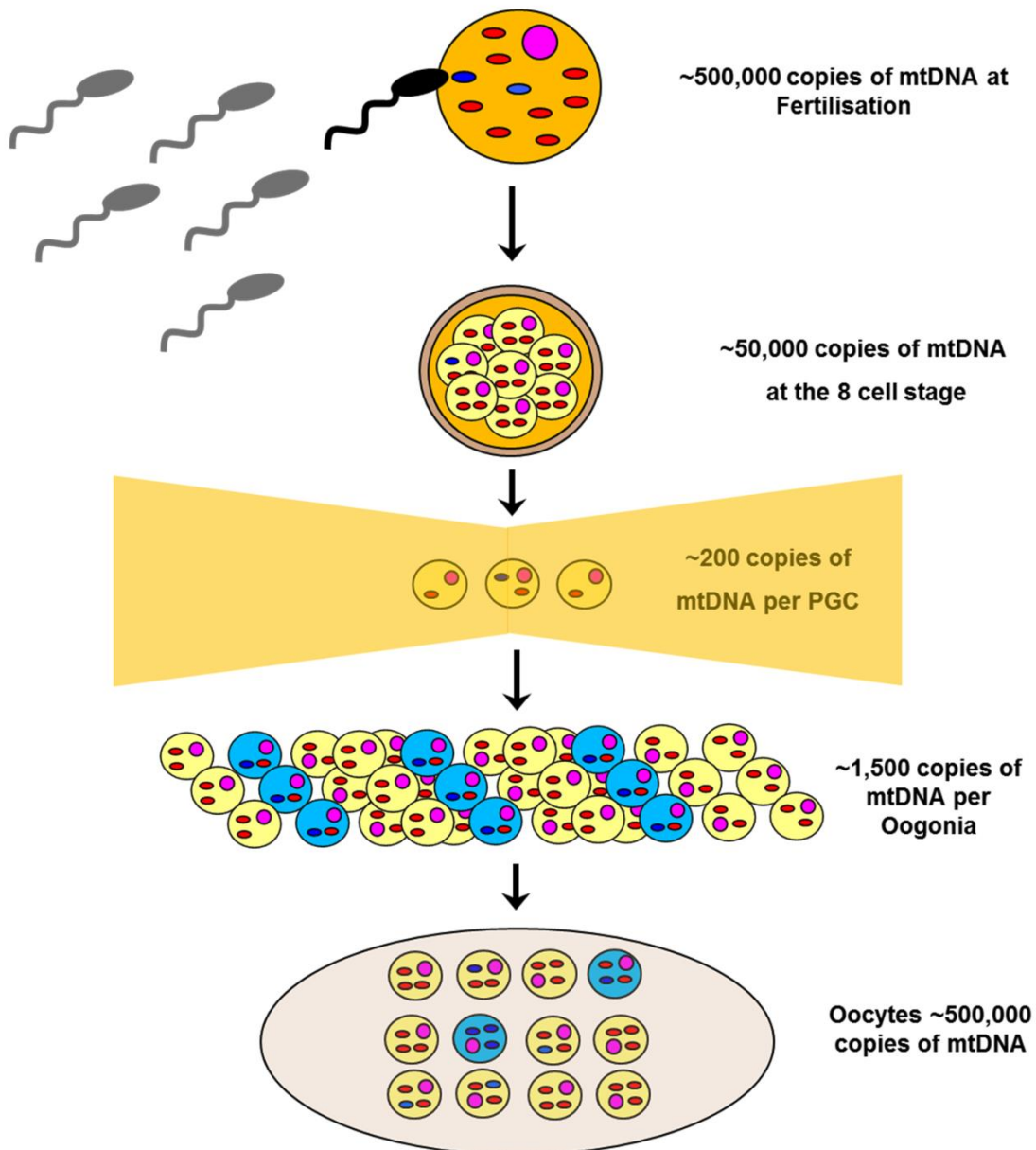
Figure 1.14. The mitochondrial bottleneck

Diagram shows fertilization of a heteroplasmic oocyte and proceeding embryo development. It is postulated that a limited number of primordial germ cells (PGCs) provide the templates for amplification and as such few mtDNA molecules will eventually predominate in the cell (Reproduced with permission from Dr John Yarham).

1.5   MITOCHONDRIAL DYNAMICS

1.5.1   Fission and fusion

The notion of mitochondria as lone ellipsoid organelles has long past. Mitochondria can exist in a multitude of forms, shown to be dynamic, and dependent on numerous factors. The transition between elongated reticular networks and punctate structures is dependent on two antagonistic processes - fission and fusion, both of which are vital for cell survival as they directly affect organelle number/shape and location. The interaction between individual organelles is vital for maintaining respiratory function mixing mitochondrial contents which benefits mitochondrial DNA stability and is capable of rescuing damaged phenotypes. Changes in both these processes have been shown to cause certain neurodegenerative conditions and are implicated in the pathogenic pathway of many others.

1.5.1.1   *Fusion machinery*

Fusion events are mediated through the mitofusins of the outer mitochondrial membrane and OPA1 of the inner membrane (Figure 1.15). The Mitofusins in mammals consist of the two homologues- Mfn1 and Mfn2, both are large GTPases containing hydrophobic heptad repeats, with long transmembrane repeats that contain charged residues. The N and C terminal of both protrude into the cytosol (Rojo *et al.*, 2002). The ability to form a U shape within the membrane is thought possible through the unusually long transmembrane domain and the charged residues within it. Ablation of either Mfn1 or Mfn2 in cells causes greatly reduced levels of fusion, removing both, halts all mitochondrial fusion. The two mitofusions display similar biochemical roles, with cells lacking either protein capable of rescue through overexpression of the other. This said, certain cell types appear to rely more heavily on one than the other, for example fibroblasts devoid of Mfn1 display a more severe phenotype than those lacking Mfn2 (Chen *et al.*, 2005). This may be reflective of differing expression levels in different tissues or may highlight slight differences in their function, for example OPA1 (discussed below) seems to be reliant on Mfn1 functioning and not Mfn2 (Cipolat *et al.*, 2004)

OPA1 is situated in the inner membrane and functions within the intermembrane space (Griparic *et al.*, 2004). It is a dynamin family GTPase and was first identified through its mutation in optic atrophy. Eight protein isoforms are generated through mRNA splicing and possibly more through postranslational processing. Removal of OPA1 causes loss of mitochondrial fusion as with the mitofusins, but also causes severe modification in mitochondrial cristae (Griparic *et al.*, 2004).

1.5.1.2   *Mechanism of fusion*

Their positioning in the outer membrane mean the mitofusins play a key role in initiating the interaction between two mitochondria. Both organelles require mitofusin expression to fuse together, suggesting that they form complexes between the two organelles. Mixing of the mitochondrial matrix requires fusion of both the inner and outer membranes. These two processes are tightly co-ordinated but mechanistically distinct, shown by the fact the two events can be experimentally uncoupled.
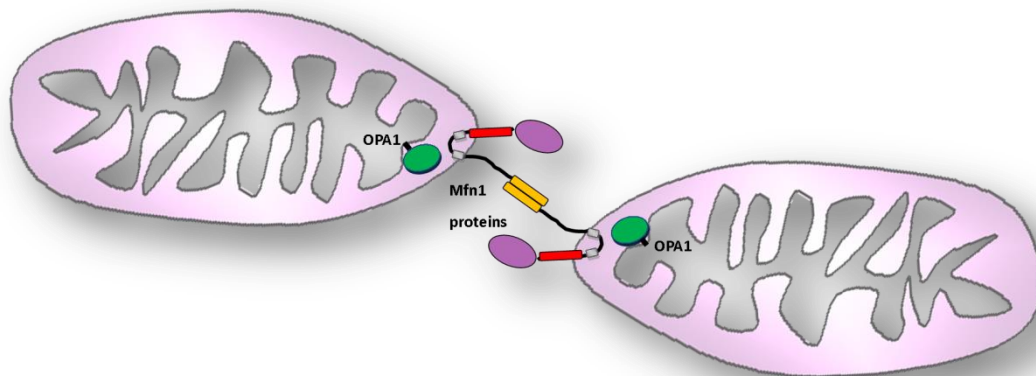
Figure 1.15. Fusion mechanism

The mitofusins serve to tether two mitochondria together. Hydrophobic heptad repeats mediate homotypic interactions between the two organelles MFN1s. OPA1, located in the inner membrane is thought to be involved in controlling tabulation and curvature of the inner membrane although its function is also required for outer membrane fusion.

1.5.1.3   *Fission machinery*

Fission generates individual smaller organelles that are necessary for transportation purposes as well as selecting unwanted mitochondria for programmed removal (Figure 1.16). FIS1 and DRP1 are heavily involved in fission events. Dynamin-related protein 1 (Drp1) is predominantly found within the cytosol although a subset has been shown to localize to mitochondrial tubules. Furthermore, a proportion of these puncta have gone on to be fission sites. As a dynamin family GTPase Drp1 contains a characteristic GTPase domain, a central domain and a GTPase effector domain. Its removal increases mitochondrial length and tubule complexity (Smirnova *et al.*, 2001). FIS1 is a small outer membrane protein that contains a single C-terminal transmembrane domain and within the cytosolic domain a helical bundle (Dohm *et al.*, 2004). Knockdown as with DRP1 causes elongation of mitochondria, whilst overexpression causes fragmentation of the mitochondrial network (Lee *et al.*, 2004).

1.5.1.4   *Mechanism of fission*

Initially mitochondrial constriction occurs independently of DRP1 as evidenced in yeast whereby transient constrictions occur frequently without expression of Dnm1 (Drp1 yeast homolog). In some cases this stage also coincides with recruitment of Drp1 to the mitochondrion although the two events are mechanistically independent, shown by the fact that knockdown of FIS1 does not affect DRP1s recruitment (Lee *et al.*, 2004). Importantly, the mechanism by which this recruitment occurs is unclear. Once localized to the mitochondria Drp1 then functions to further constrict the organelle, most likely through hydrolysis of GTP, acting as a mechanochemical enzyme. Following a completed fission the Drp1 complex formed during constriction remains on one of the two daughter organelles and is subsequently disassembled. Nucleoid positioning is thought to occur in parallel to fission events giving rise to daughter mitochondria that always contain at least one mtDNA molecule (Legros *et al.*, 2004).
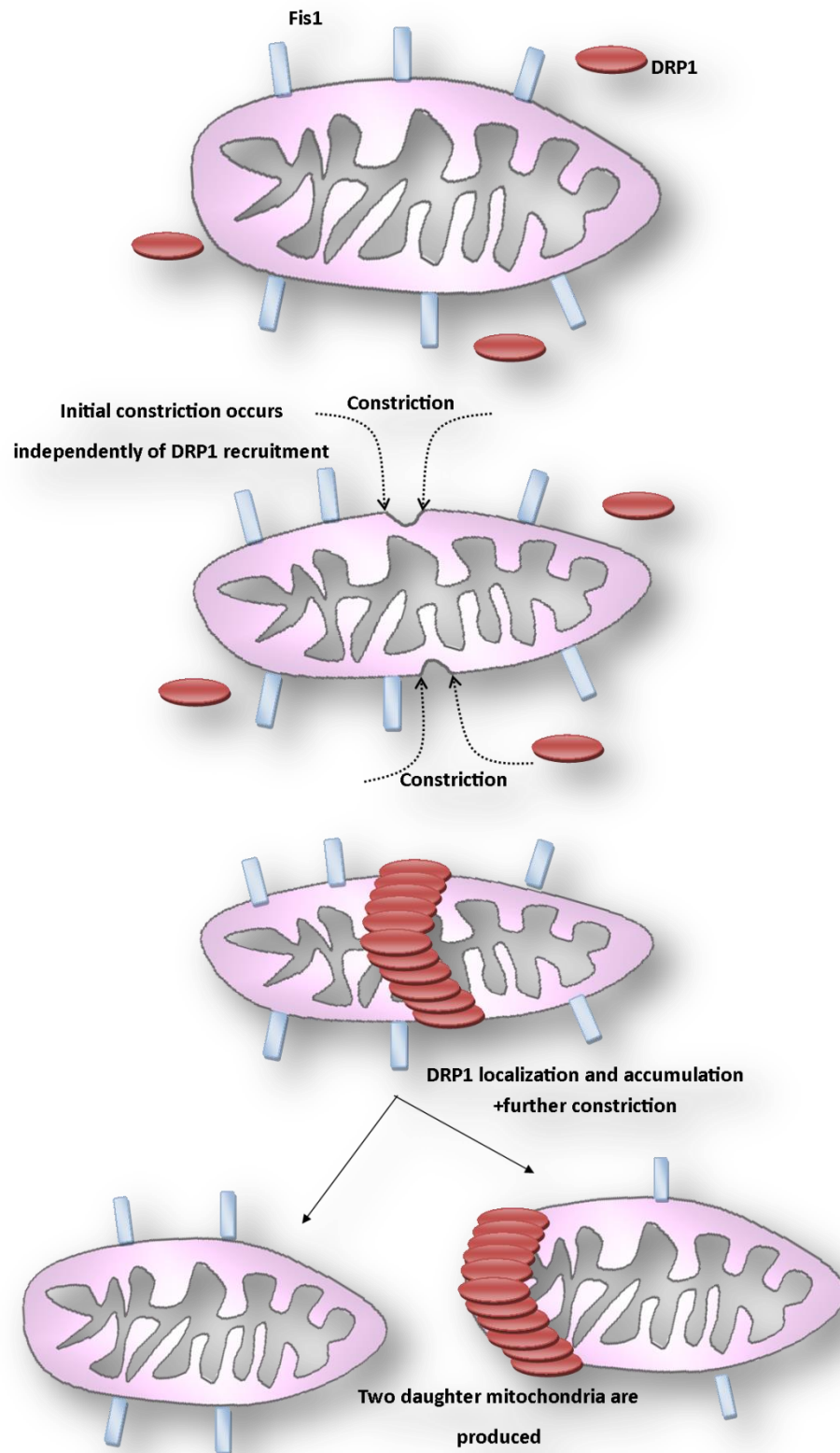
Figure 1.16. Fission mechanism

Several parameters of mitochondrial fission remain unclear. The proteins FIS1 and DRP1 are critical as revealed by the lack of fission following their removal. Constriction of individual mitochondria is able to occur independently of Drp1 recruitment, the mechanism of which remains unclear. Once localised to the mitochondria a subset of Drp1 puncta go on to form sites of active fission, most likely mediated by assembly and activation of Drp1. Further constriction occurs eventually resulting in two daughter mitochondria.

1.5.2   **Mitophagy**

If mitochondrial damage is irrecoverable through fusion, the option to remove individual organelles through fission and subsequent mitophagy exists. Removal of damaged or unnecessary mitochondria is a highly regulated event, with current understanding highlighting PINK1 and PARKIN as key to facilitating this process (Figure 1.17). It is worth noting however that several factors in this relatively recent discovery remain unclear and it is likely that other components of the pathway or indeed novel pathways are yet to be uncovered. To highlight just one example, recent work has shown that Fbxo7 (MIM 605648) participates in mitochondrial maintenance through direct interaction with PINK1 and Parkin and acts in Parkin-mediated mitophagy. Mutations in Fbxo7 (encoded by PARK15) also cause early-onset autosomal recessive Parkinson's disease (Burchell *et al.*, 2013). PINK1 and PARKIN therefore likely function alongside, and dependent on, various factors yet to be revealed.

*PINK1 (*MIM 608309) encodes a serine threonine kinase with a mitochondrial targeting sequence and localises to either the outer or inner membrane depending on membrane potential (Jin *et al.*, 2010), *PARKIN* encodes an E3 ubiquitin ligase (MIM 602544). Parkin has been identified as having a role in tagging mitochondria with reduced membrane potential and in doing so selecting them for autophagy. Narenda *et al* demonstrated that Parkin is directly recruited to damaged mitochondria followed by a subsequent up regulation of mitophagy (Narendra *et al.*, 2008). Upon depolarization of mitochondria following damage/uncoupling, PINK1 accumulates on the outer mitochondrial membrane recruiting PARKIN which ubiquitinates numerous outer mitochondrial membrane proteins including VDAC1 and MFN that signal autophagic factors and seal the organelles fate for degradation (Okatsu *et al.*, 2012). Fission is known to occur prior to mitophagy in both yeast and mammalian cells (Nowikovsky *et al.*, 2007) (Twig *et al.*, 2008), this allows 'individual' mitochondria to be easily engulfed by the autophagosome and more importantly sections off damaged mitochondria for their selective removal.

Any inhibition of this pathway can easily lead to accumulation of mitochondria that can then harm other cellular components. Useful components that would ordinarily be recycled are confined in these accumulations and the control of apoptotic signals is lost.

Parkin translocation has been shown to be highly selective, with accumulation occurring on damaged mitochondria but not healthy organelles within the same cell (Narendra *et al.*, 2008). Complementing this data, it has been shown that mitochondria containing mutations in cytochrome *c* oxidase subunit 1 are removed selectively when parkin is over expressed in cybrid osteosarcoma cells (Suen *et al.*, 2010). In doing so the population of wildtype mtDNA molecules in the cell is increased and COX function rescued.
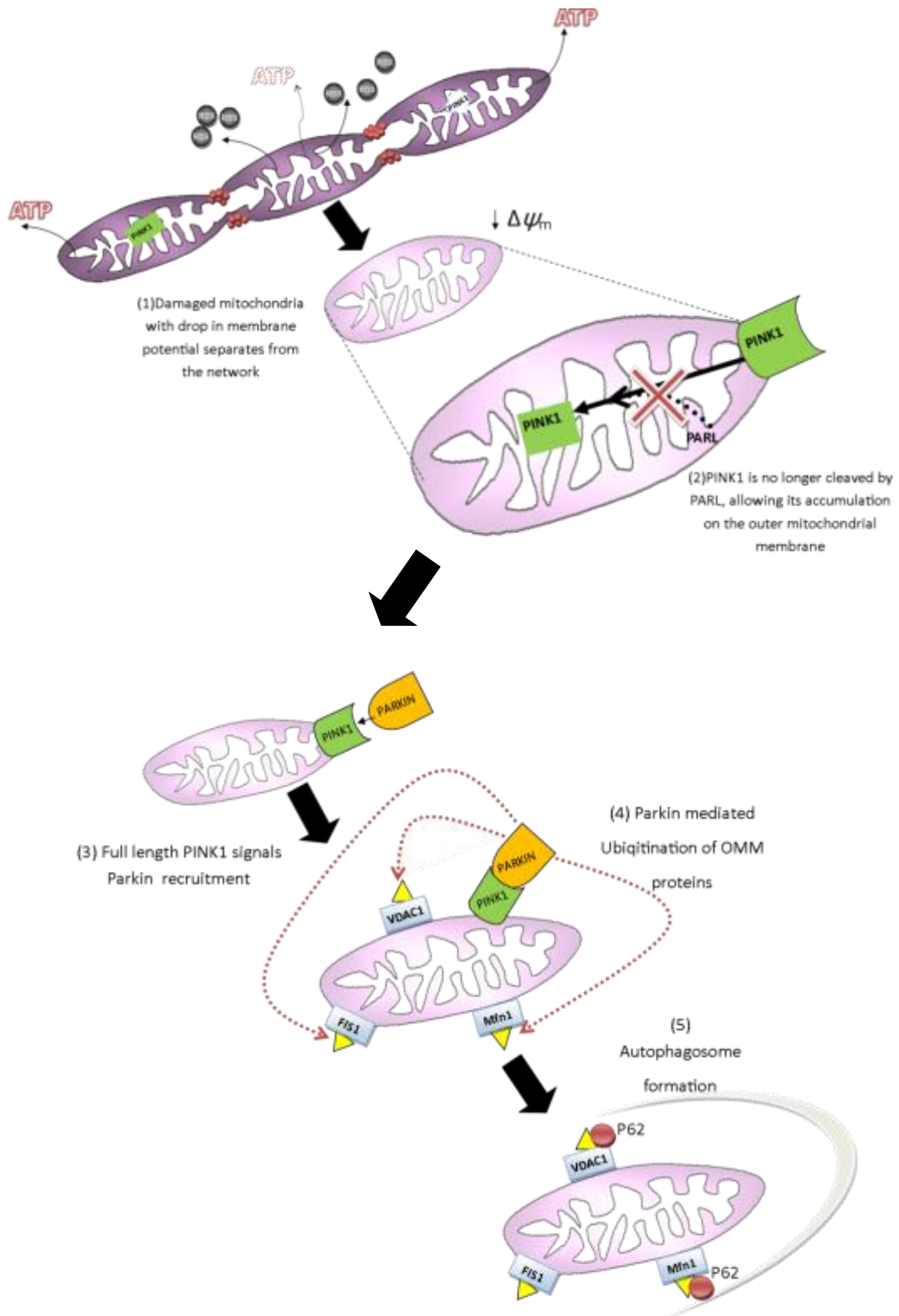
Figure 1.17. PINK1/Parkin mechanism of mitophagy

Selective degradation of mitochondria occurs through mitophagy. Current understanding of the process relies heavily on the involvement of PARKIN and PINK1. Following a drop in membrane potential individual mitochondria separate from the mt-network (1). In healthy mitochondria PINK1 is cleaved by PARL. Following damage however this no longer occurs, allowing full length PINK1 to accumulate at the OMM (2). This accumulation signals for PARKIN recruitment (3). PARKIN ubiquitinates a multitude of OMM proteins (4) and subsequently signals for autophagosome formation and encapsulation.

1.5.3 **Motility**

Mitochondria not only show dynamic movement within the network but also show motility throughout cells. For example, around 35% of neuronal mitochondria estimated to be moving at any given time (Overly *et al.*, 1996; Waters and Smith, 2003; Chen *et al.*, 2007b). Sophisticated trafficking machinery exists to enable mitochondria to be readily transported to areas of increased energy demand or returned for degradation. Mitochondria typically have set styles of movement. These can be fairly uniform over long distances or show more 'stop-start-reconsider' characteristics, where movements are shorter and often punctuated with a pause that can precede a change in direction.

Within neurons mitochondria are largely moved along microtubules, although movement using actin filaments has been reported for smaller distances and within dendritic spines and growth cones (Saxton and Hollenbeck, 2012) (Figure 1.18). The 'docking' and 'shipping' of mitochondria onto these cellular tracks is facilitated through motor proteins and a plethora of adaptor proteins such as Milton, Miro, Myosin and Dynactin. Microtubules display uniform polarity in axons with all positive poles aligning at the axonal terminal, the tracking of mitochondria along these is mediated via different motors dependant on direction. For anterograde movement (towards the axon terminal) kinesin motors are employed, conversely, retrograde movement utilises dynamin motors (Baas *et al.*, 1989).
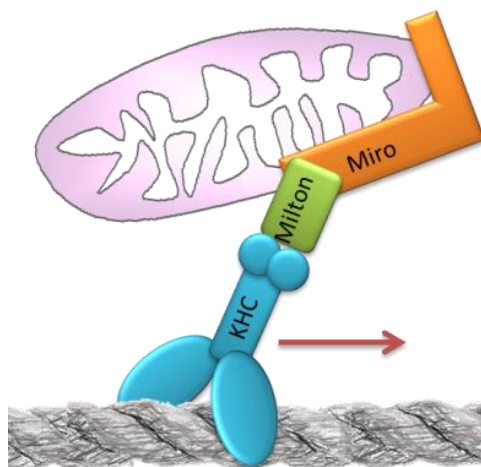
Figure 1.18. Basic machinery of mitochondrial movement in neurons

Within neurons mitochondria are primarily transported along microtubules, the transportation is facilitated through the KHC-Milton-Miro complex.

1.6   DEGRADATIVE PROCESSES IN EUKARYOTIC CELLS

Maintenance of homeostasis is vital for cellular survival. A key aspect for conserving this steady state is the ability to balance biosynthesis with the removal of unnecessary or harmful cellular components. As such, dedicated degradative mechanisms are essential. Within eukaryotic cells large scale degradation is carried out by two distinct processes, the ubiquitin proteasome system (UPS), and autophagy. Although a degree of similarity both in functionality and specifics of action exists, several distinctions can be made as summarised in Table 1.2.

Degradation in Eukaryotic Cells	Process	
	Autophagy	UPS
Products Degraded	Long lived proteins Protein aggregates Damaged/redundant organelles	Short-lived, mis-folded proteins
Mechanism	Degradation that ultimately occurs within lysosomes	Requires ubiquitin Tags and the proteasome (an ATP-dependant protease complex)
Specificity	Variable depending on subtype of autophagy	Highly specific both for substrate and timing.
Redundancy	Can compensate for UPS dysfunction	Cannot compensate for autophagy dysfunction

Table 1.2 Degradative processes in eukaryotic cells.

Autophagy and the ubiquitin proteasome system (UPS) represent two distinct processes that serve to degrade intracellular components.

A degree of convergence between the two proteolytic pathways has been observed. In a form of autophagy known as chaperone mediated autophagy (CMA), protein tags mark cellular components for degradation in the lysosomes. Ubiquitin has been shown to function as such a tag in the autophagic system as well as in UPS (Korolchuk *et al.*, 2009a). Similarly, it has been shown that cargo recognition molecules associated with autophagy, such as p62, are utilised in both pathways (Lamark *et al.*, 2009). Although the remainder of this discussion will focus on autophagy and its role in homeostatic control it is worth noting at this point that crosstalk does exist between the two systems

and as such may be relevant to disease pathology (Korolchuk *et al.*, 2009b; Korolchuk *et al.*, 2009c).

1.6.1 **Autophagy**

Autophagy- literally 'self-eating' is the process by which large cytoplasmic constituents and longer lived proteins are degraded; including entire organelles such as mitochondria. This then makes constituent amino acids accessible to the cell for more urgent purposes, for example, maintaining the metabolite pool particularly during starvation. Three principle forms exist, macroautophagy, microautophagy and chaperone mediated autophagy (CMA). All modes of autophagy share a common end point, degradation via the lysosomes (Figure 1.19). These single membrane organelles contain a wealth of hydrolase enzymes, all of which are functionally more active at around pH 4.5. To allow for maximal enzymatic activity, the lysosomes create a low interior pH via an ATP-dependent proton pump located on the lysosomal membrane. Although united in a common endpoint, the mode of cargo recognition, sequestration and delivery differ across autophagy subtypes. Furthermore the substrates degraded and the levels of specificity in each system vary. The main characteristics of each are described below-

Macroautophagy- Often referred to in the literature simply as 'autophagy', macroautophagy represents the most extensively studied form to date. Here, cytosolic components are engulfed along with large areas of the surrounding cytosol in a double membrane vesicle. Fusion of this vesicle with endosomes or lysosomes completes the degradative process. Large scale degradation of organelles and longer lived proteins are achieved by this means.

Microautophagy- In this, the formation of the intermediate double membrane vesicle is not required. Instead extrusions of the lysosomal membrane itself protrude and engulf smaller cytosolic regions. These are then internalised as single membrane vesicles and subsequently degraded.

Chaperone-Mediated Autophagy (CMA) - In CMA single proteins are degraded individually. Whole organelles therefore cannot be removed by this method. Similar to

UPS, proteins are tagged for degradation via a specific motif (KFERQ-like) which signals for their degradation in lysosomes (Massey *et al.*, 2006). The consensus peptide sequence is recognized by a cytosolic chaperone complex. The chaperone is then recognized by Lysosomal Associated Membrane Protein (LAMP2A). Next, the protein is unfolded and, assisted by a luminal chaperone, translocated to the lysosomal lumen where degradation occurs.
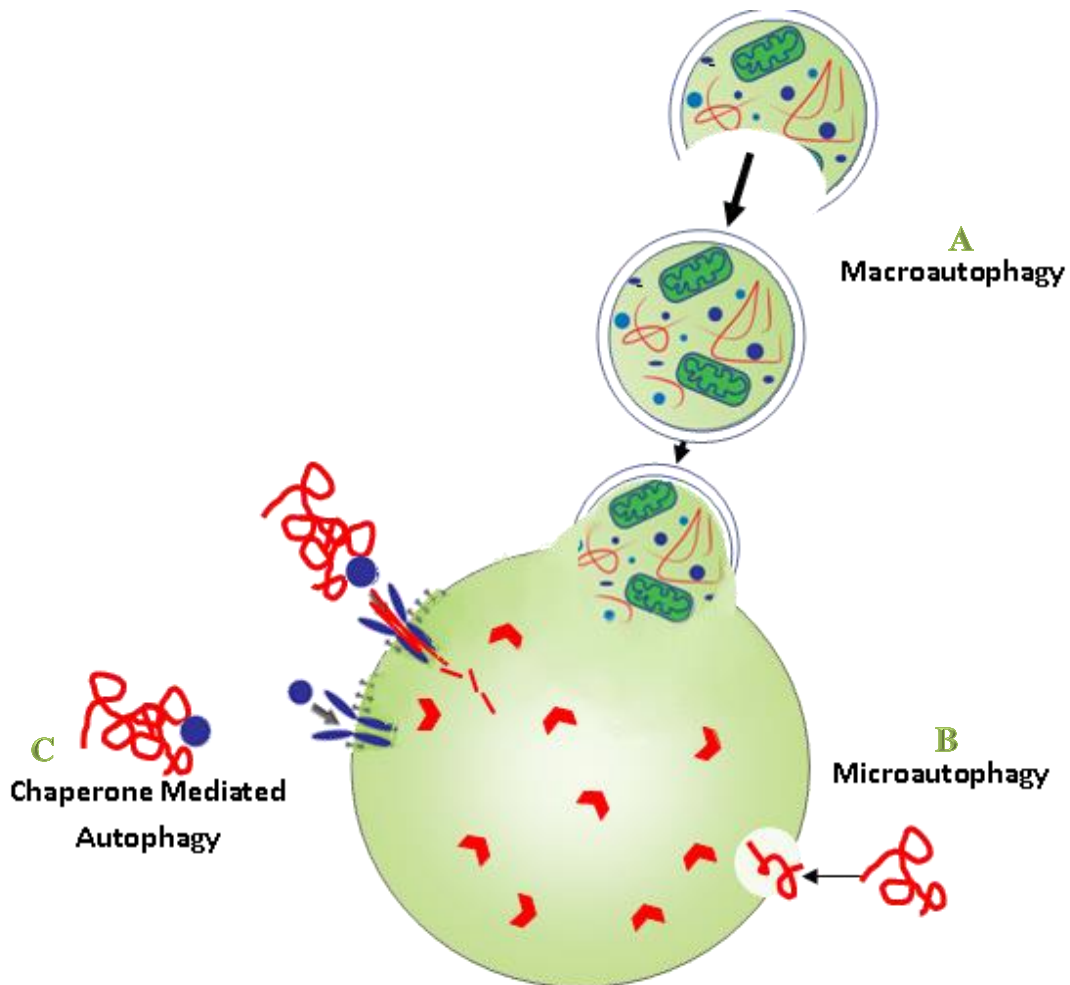
Figure 1.19 Types of Autophagy.

Three main forms of autophagy exist, all of which ultimately result in degradation of cytosolic components in the lysosome. The precluding steps to delivery in the lysosome vary for each subtype. In macroautophagy (A) a double membrane vesicle forms, expands and eventually encapsulates a whole region of cytoplasm before fusing and releasing its contents into the lysosome. In microautophagy (B) the lysosome itself sequesters smaller regions of the cytoplasm. Chaperone mediated autophagy (C) (CMA) requires recognition of a targeting motif by chaperones that then mediate its delivery to the lysosome. Here it is recognised by a receptor and forms a translocation complex. The substrate protein is then translocated to the lumen by a luminal chaperone.

1.6.2   **The macroautophagy pathway**

Macroautophagy, hence forth autophagy, proceeds in a stepwise manner and relies on numerous interactions. Understanding of autophagy has been vastly improved by the characterization of several key components in yeast, mammalian homologs of many of which have now been identified.

1.6.2.1   *Initiation*

Upon **induction** (Figure 1.20(1)), via appropriate external or internal stimuli a series of sequential events initiate autophagy. The process begins with **nucleation** (Figure 1.20(2)) whereby a double membrane crescent known as the isolation membrane or phagophore is formed.
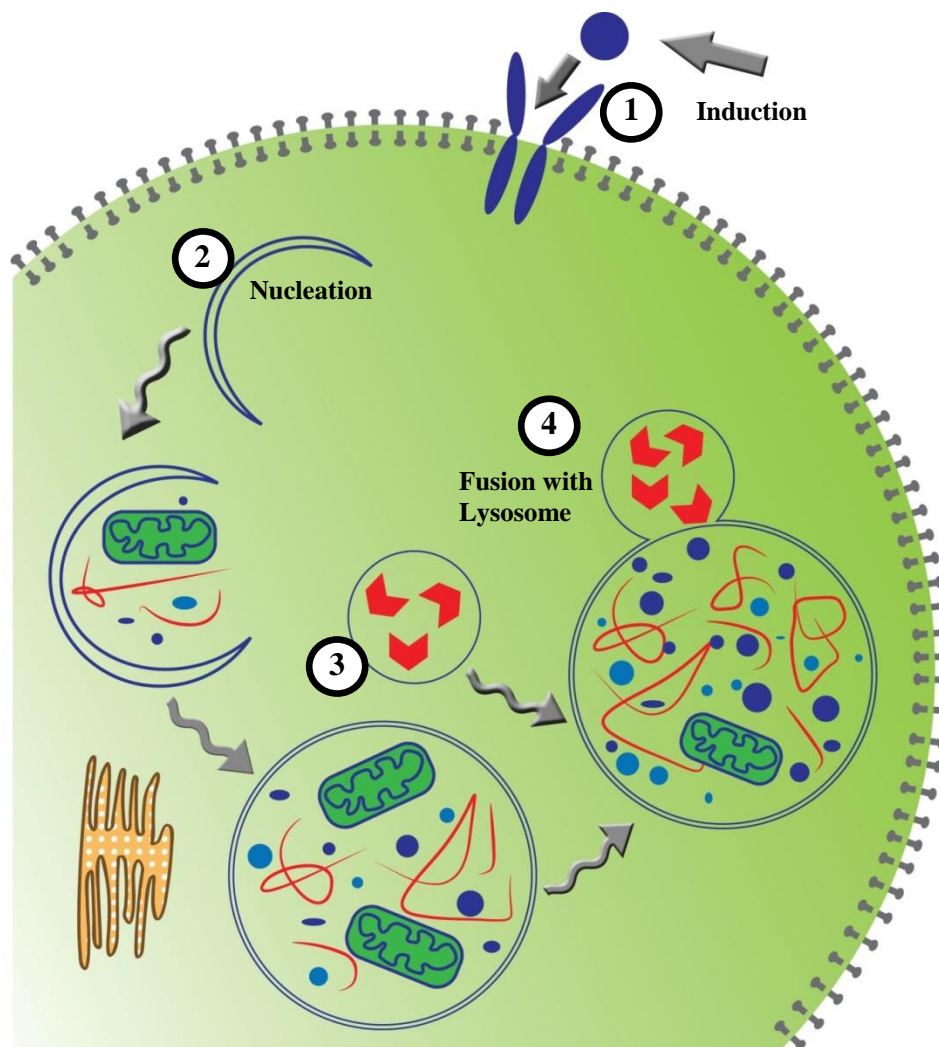
Figure 1.20. The Autophagy Pathway.

Sequential events occur to sequester and deliver a region of the cytoplasm for degradation in the lysosome. (1) Induction, (2) nucleation, (3) membrane expansion and (4) fusion with the lysosome. For details see text.

1.6.2.2   *Membrane Expansion*

This initial expansion step requires several autophagy (ATG) proteins and their interacting factors (Figure 1.21). Phosphatidylinositol (PI) phosphorylation is crucial for the process to progress. Phosphatidylionsitol-3-Phosphate (PtdIns3P) is generated by Vps34, a class III phosphatidylinositol 3-Kinase. Activation of Vps34 requires formation of the Beclin 1-class III phosphatidylinositol 3-kinase (PI3K)/Vps34 lipid kinase signalling complex, the activity of which is modified by several factors in response to environmental changes, including Ambra1, UVRAG, Bif-1 and Bcl (Fimia *et al.*, 2011).
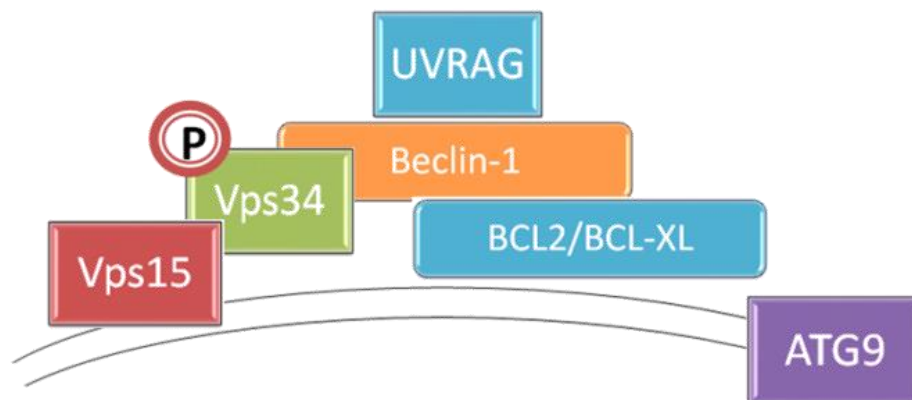
Figure 1.21. Nucleation Complex.

Nucleation requires activation of Vps34, a class III phosphatidylinositol 3-kinase (PI3K). This activation is dependent on the formation of a complex containing beclin-1 (the mammalian orthologue of ATG6), UVRAG (UV irradiation resistance-associated tumour suppressor gene) and a kinase such as Vps15.

Following intiation a region of the cytoplasm is encapsulated and **membrane expansion** (Figure 1.20(3)) occurs. The sequestration of cargo and eventual closure of the phagophore relies on the formation of two conjugation systems containing the ubiquitin like molecule LC3 (the human homologue of yeast ATG8) and ATG12 (Figure 1.22).

(1) ATG12-ATG5 conjugation requires E1 like enzyme-ATG7 and E2 like enzyme-ATG10 (ubiquitin activating enzymes). E1 enzymes bind ubiquitin along with ATP and pass the ubiquitin protein to E2, an ubiquitin carrier protein (Hanada *et al.*, 2007). The

ATG12-5 complex then goes on to non-covalently interact with ATG16, resulting in oligomerisation and the formation of the ATG16 complex (Geng *et al.*, 2008).
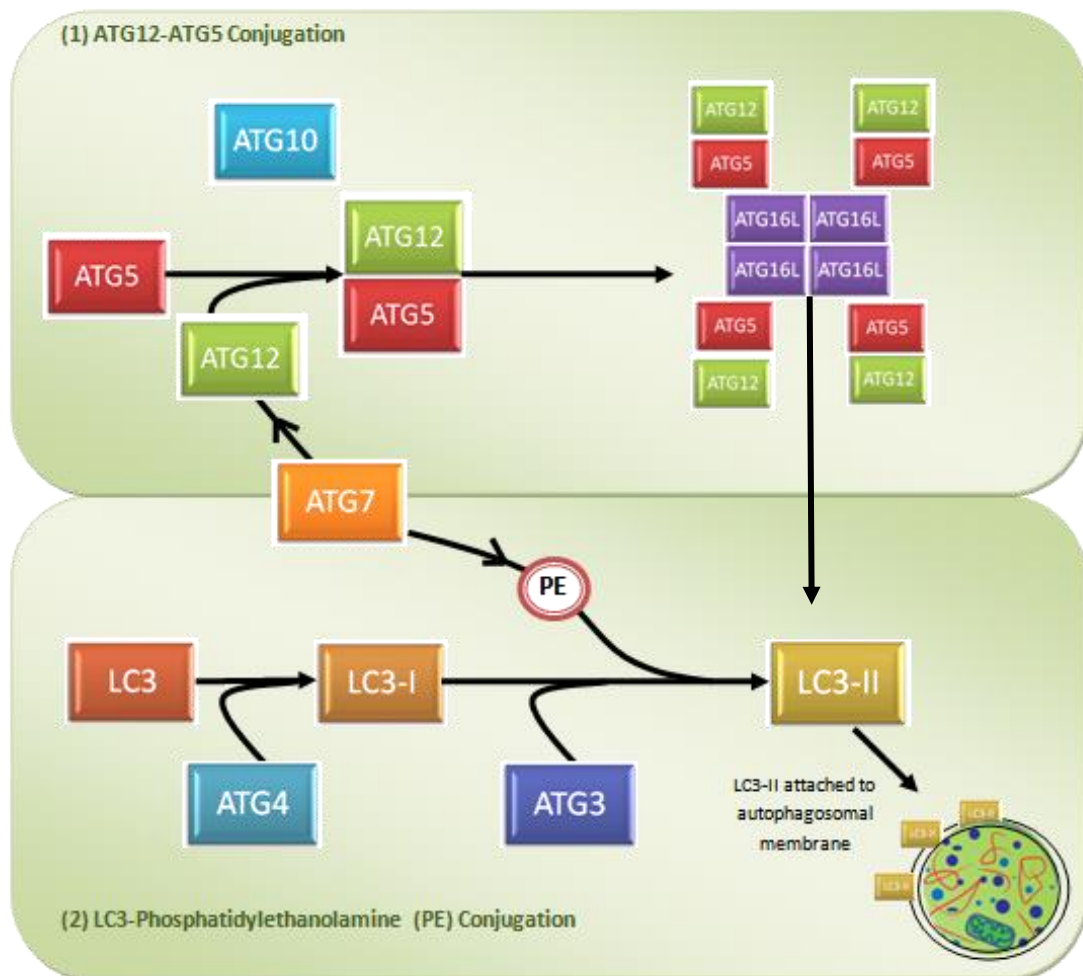
Figure 1.22. Two ubiquitin like conjugation systems.

(1) ATG12-ATG5 conjugation and (2) LC3- PE conjugation act sequentially to bring about membrane expansion.

(2) LC3-phosphatidylethanolamine (PE) conjugation - Newly synthesised LC3 is cleaved at its C terminus by ATG4 (a protease) to generate cytosolic LC3- termed LC3-I. This can then be conjugated to PE, a process that requires ATG7 and ATG3 (E1 and E2 like respectively).

These two conjugations act sequentially with ATG12-ATG5 conjugation occurring first which then promotes conjugation of LC3 and PE. This then results in formation of the autophagic membrane lipidated form of LC3-referred to as LC3-II. The final stage of vesicle expansion requires deconjugation of LC3-II from the outer membrane by ATG4

and recycling of the ATG5-12-16 complex. The final retrieval process is not fully understood, but recycling of ATG proteins from and to the autophagosomal membrane is thought to involve the transmembrane proteins ATG9 and ATG1.

1.6.2.3   *Completion and lysosomal degradation*

The resulting vesicle- the autophagosome- is now a sealed double membrane 'transient organelle' containing cytoplasmic material indistinguishable from the surrounding cytosol. Finally and completing the degradative process, fusion with the lysosome (Figure 1.20(4)) occurs creating the autolysosome. Here, the inner vesicle of the autophagosome is released allowing its contents to be degraded by lysosomal hydrolytic enzymes such as lysosomal cysteine and aspartyl proteases, and cathepsins B and D. Following lysosomal degradation, macromolecules are released for reutilization through the action of ATG22 a vacuolar integral membrane protein (Yang *et al.*, 2006).

1.6.3   **Regulation of autophagy**

A range of environmental stresses such as-nutrient depletion, pathogen infection and hypoxia can initiate an up regulation of the autophagy system. Similarly, internal stimuli such as an increase in protein aggregates can invoke the same response (He and Klionsky, 2009). During periods of nutrient starvation autophagy is up regulated and conversely in nutrient rich conditions inhibited. Such dynamic fluctuations are made possible by the co-ordination of several signaling pathways. Negative regulation of the process occurs primarily through the mammalian target of rapamycin (mTOR). TOR is a serine threonine protein kinase well known for its central role in sensing and regulating energy status within the cell. TOR exists in two complexes TORC1 and TORC2 (Bhaskar and Hay, 2007), TORC2 has been shown to function as an important regulator of the cytoskeleton whereas TORC1 is involved directly with autophagy regulation.

In all eukaryotic cells, autophagy is activated when mTOR is inhibited (Codogno and Meijer, 2005). In yeast TOR impacts on autophagy through its effect on the ATG1-ATG13-ATG17 complex. This complex is involved in several steps of autophagosome

formation including initiation, nucleation and expansion of the membrane. During nutrient rich conditions upstream signals activate TOR and autophagy is suppressed. This is achieved through phosphorylation of ATG13 and ATG1 in a TOR dependent manner. Once hyperphosphorylated, the complex dissociates. In doing so ATG1 protein kinase activity is reduced and subsequently autophagy levels fall (Kamada *et al.*, 2000). In the reverse situation, through nutrient depletion or rapamycin treatment, TOR is inactivated. This leads to dephosphorylation of ATG13 and increased complex formation, which in turn up regulates ATG1 activity and autophagy. As such it is the ATG1 complex that integrates the signal from TOR. The human homologues of ATG1 are ULK1 and ULK2 (UNC51-like kinase). As in yeast and other eukaryotic models, protein kinase activity of ULK proteins have been shown as essential for autophagy (Scott *et al.*, 2007). It is worth noting that the target of ATG1 has not yet been identified (Nair and Klionsky, 2005). Mammalian TOR is by no means the only regulator of autophagy. Indeed, numerous mTOR independent regulatory pathways exist. For example amino acids and insulin control, as well as inositol and IP3 can modulate autophagy in pathways parallel to, or beneath mTOR (Sarkar and Rubinsztein, 2006).

1.6.4   Autophagy in the Healthy State

A low level of autophagy is occurring in most tissues at all times. This constitutive level exists to maintain homeostasis through the elimination of damaged or unnecessary organelles and removal of cellular 'clutter' in the form of aggregations (Mizushima, 2005). The importance of this steady state level of autophagy for cellular homeostasis has been demonstrated in various tissues in ATG knock out mouse models, with loss or reduction of autophagy leading to rapid loss of function and cell death (Komatsu *et al.*, 2005; Hara *et al.*, 2006). In times of starvation and experimentally with chemical interference (i.e. through the addition of rapamycin) these basal autophagy levels can be rapidly up-regulated.

Initially believed to function solely as a means of recycling intracellular components, a multitude of cellular processes are now understood to be reliant upon autophagy. These include defense against external pathogens, having a role in both the innate immune response (Levine, 2005) and antigen presentation (Munz, 2006; Crotzer and Blum, 2009). Autophagy also plays a role in programmed cell death, contributing apoptotic

signals (Shimizu *et al.*, 2004) and having the capacity to cause cell death independent of apoptosis (Clarke, 1990). Its ability to govern survival and selective death of cells means it plays a pivotal role in development and tissue remodeling in various organisms (Levine and Klionsky, 2004). Of particular importance to neuronal functioning is axonal differentiation and maintenance mediated by autophagy (Zeng and Zhou, 2008). Finally, it has been shown that autophagy plays a prominent role in ageing (Terman *et al.*, 2007) and the progression of numerous diseases as discussed below.

1.6.5   **Implications of impaired autophagy**

Dysfunction of the autophagy system can have a myriad of negative implications. Firstly, an inability to clear damaged material increases the amount of damage they themselves are able to cause. In the case of compromised mitochondria an increase in free radical production may harm many other cellular constituents (discussed in detail in 1.2.3). Secondly, unwanted material can function as a cellular 'road block', hindering normal cellular functions. The accumulation of protein aggregates is a hallmark of numerous neurodegenerative conditions, including α-synuclein in Parkinson's Disease, amyloid β in Alzheimer's Disease and huntingtin in Huntington's. These inclusions can be toxic to the cellular environment and further block degradative pathways. It has been demonstrated that autophagy plays a role in prevention of aggregate formation in mouse models (Klionsky *et al* 2006). Furthermore, these collections of 'cellular junk' contain useful components which the cell is unable to retrieve. This becomes of particular importance during times of starvation when the ability to recycle products into more urgently needed molecules is vital. An example of this is provision of substrates for ATP production from oxidative phosphorylation within the mitochondria during times of high bioenergetic demand (Mizushima, 2005).

Inhibition of autophagy has been shown to result in apoptotic cell death (Boya *et al.*, 2005). In this sense autophagy can be considered a mediator of cell survival, crucially, offering an alternative to apoptosis. If this clearance process is damaged or inhibited for some reason the only option open to the cell is apoptotic cell death. If autophagy is inhibited in numerous cells the result will be *en masse* cell death. The constitutive level of autophagy ensures that only the most efficient organelles remain, and as such, even slight perturbations are dealt with early on. It is easy to see that any problems in the

system can quickly become self-perpetuating, with more damaged components circulating, which are themselves able to cause damage. Dysfunction and deregulation of the lysosomal degradative pathway has been implicated in a broad range of disorders including the development of some cancers, immunological disorders, heart disease, lysosomal disorders and neurodegeneration (Martinet *et al.*, 2009).

When we consider the multistep nature of autophagy, several areas may become dysfunctional. Depending on their point of action, dysfunction can have a range of consequences. Errors in initiation from upstream signalling caused by defects in any number of the autophagy related genes lead to a debilitated autophagy response. This ultimately leads to an accumulation of damaged organelles and aggregates which may have a role in the progression of tissue degeneration. Alternatively, the completion steps of the autophagy pathway may be contravened in some way. The implication of this is observed in several neurodegenerative disorders such as Alzheimer's disease where accumulation of autophagic material is observed in post-mortem tissue (Boland *et al.*, 2008). Non-completion of the pathway leads to an accumulation of autophagosomes alongside the associated problems of a non-functional degradative pathway. Lysosomal abnormalities can also occur such as failure of the lysosomal hydrolases and an inability of autophagosomes to fuse to lysosomes, resulting, for example, from mutations in LAMP2A (Tanaka *et al.*, 2000; Malicdan *et al.*, 2008). Finally more exterior complications can impact upon the autophagy system. Autophagosome trafficking for example may be hindered by mutations in dynactin, a dynein receptor (Yamamoto *et al.*, 2010)

An overall decrease in the activity of autophagy is seen across all cell types with age (Yen *et al.*, 2008). Parallel to this a decline in function and an accumulation of damage are characteristics of tissues in the ageing phenotype. The role alterations in autophagy play in this decline are not fully understood but work into genetic modulations of key autophagy genes and a greater understanding of the features of autophagy on the whole suggest it plays a substantial role.

1.6.6   **Monitoring Autophagy**

Observing and quantifying autophagy is difficult because, by definition, it is a dynamic process. Given the increasing evidence of its pivotal role in health and disease, research into the field is increasing exponentially and alongside this, methodologies are advancing. Traditionally, a morphological approach has been taken to monitor autophagy, indeed the process was first identified by electron microscopy (EM) by Clark in 1957 and the model was further established by Ashford and Porter in 1962. By calculating the volume of autophagic vacuoles (AVs) and expressing them as a ratio of the total cytoplasmic area, crude quantifications of activity of the process can be made. This particular methodology is not without its draw backs. Identifying autophagic vacuoles from EM images is a time consuming and labour intensive method requiring specific skills. Defining specific stages of autophagy is also extremely difficult by EM alone, hence autophagosomes and autolysosomes often being collectively referred to as autophagic vacuoles. The utilisation of antibodies as markers of autophagosomes in EM is commonly used to assist in the definition and quantification of autophagy.

A somewhat more specific analytical tool is that of autophagy markers, the most widely used being LC3. As discussed previously two conjugation systems are required for autophagosome formation. ATG12-ATG5 and LC3/ATG8 conjugated to PE. In its conjugated, non-soluble form LC3-II stably associates with the autophagosomal membrane. As such detection of LC3-II serves as a marker of these structures and can be assessed both by microscopy and biochemically, looking at conversion of LC3-I to LC3-II. Differentiation between the two is possible via immunoblotting, since LC3-I= 18kDa and LC3-II=16Kda, the ratio between the two then serves as an estimation of the number of autophagosomes. One concern with this method is that LC3-II may be more sensitive to the process than LC3-I, and as such may be overestimated. The production of chimeric LC3 fused with green fluorescent proteins allows visualisation of the location of LC3. Furthermore the fluorescent signal is weaker from autolysosomes due to the fact that less LC3-II is membrane bound in autolysosomes, thus distinction between the two can be made. Finally, assessing the bulk degradation of long lived products may serve as a measurement of autophagic activity. This does not however allow for the differentiation of macroautophagy from micro or indeed chaperone mediated forms of the process.

The effect of dysfunctional autophagy can be observed by experimentally modulating the process. Knock down of different autophagy related genes not only help in elucidating their physiological role but also allows an insight into the consequences of dysfunction at various points. Alongside this, autophagy can be induced or inhibited through pharmacological intervention. MTOR functioning as mTORC1 can be inhibited by rapamycin treatment and subsequently, autophagy is up regulated. Conversely, inhibition of autophagy can be achieved by targeting fusion of the autophagosomes with lysosomes by bafilomycin treatment, which inhibits the lysosomal proton pump (Rubinsztein *et al.*, 2007). The current methods for studying autophagy all come with limitations. Using an array of approaches therefore allows greater confidence in results produced. The main drawback of traditional approaches is they are very static in their observations. Quantification of autophagic flux is not possible in such techniques which measure activity at any given moment. Future approaches may well look at the process 'in action' making use of advances in live cell imaging or taking several measurements of factors along the autophagy pathway.

1.7   **SYNUCLEINOPATHIES**

1.7.1   **Definition of Synucleinopathies**

Idiopathic Parkinson's disease (iPD) and dementia with Lewy Bodies (DLB) are prevalent neurodegenerative disorders with overlapping pathological and clinical traits. In the UK, Parkinson's disease alone affects one person in every 500 (~127,000 people in the UK). The pathological hallmarks of these disorders include cell loss in pigmented brain stem nuclei, gliosis and formation of fibrillar intraneuronal inclusions known as Lewy Bodies (LBs). Collectively these disorders are termed synucleinopathies, the predominant components of Lewy bodies being insoluble alpha synuclein. Along with Parkinson's disease with Dementia (PDD), PD and DLB represent three main clinical phenotypes, which can be regarded as points on a gamut of pathological and clinical traits (Figure 1.23).

PD   PDD   DLB

Bradykinesia, tremor, muscle rigidity   Dementia
Cognitive Impairment seen later   Movement disorders seen later
Greater *Substantia pars compacta* (SNc) neuronal Loss   Earlier involvement of Limbic Lobe?
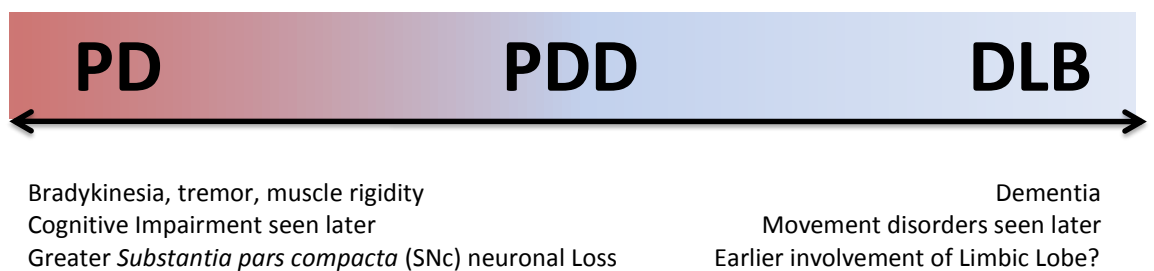
Figure 1.23. The spectrum of Synucleinopathies.

Synucleinopathies present with various clinical and pathological characteristics which define the disorders ranging from Parkinson's disease with greater SNc loss and dementia with Lewy bodies (DLB) where movement disorders are seen later in progression of the disease.

PD and DLB differ in age of onset as well as degree and type of pathology. In PD the initial loss of midbrain dopaminergic neurons (responsible for motor symptoms associated with PD) is rapid but occurs after pathology appears in other brain regions whilst Lewy body formation/ infiltration is slower. Conversely, DLB has a rapid onset with denser and more widespread Lewy body distribution (Jellinger, 2009). Clinically this presents as predominant cognitive symptoms in DLB and motor symptoms in PD. The exact cause of these disorders remain unclear although several pathogenic mechanisms have been proposed, including mitochondrial dysfunction and perturbations in cellular events.

1.7.2 **Symptoms and Pathology**

Majority of PD cases arise without known cause and occur sporadically. Roughly 5% however are familial and to date several PD related genes have been identified. The characteristic symptoms associated with Parkinson's disease are movement disturbances such as bradykinesia, muscle rigidity and tremor. These stem from neurodegeneration within the basal ganglia, a collection of structures responsible for the control of movement. Structures within the basal ganglia include the striatum, globus pallidus, substantia nigra and the subthalamic nucleus (Figure 1.24a). Communication between these areas is complex and tightly regulated by both inhibitory and excitatory synapses (Figure 1.24b). In PD a severe loss of dopaminergic neurons within the substantia nigra pars compacta (SNc) results in a deficiency of dopamine which then affects the basal ganglia circuitry. Primarily, reduced dopaminergic impulses restrict communication between the substantia nigra and the striatum. This results in increased excitation of the subthalamic nucleus and globus pallidus internus. An increased inhibition of the thalamus is also observed, inhibiting the motor cortex which gives rise to the loss of smooth controlled movement. Several non-motor symptoms are also associated with PD. These symptoms likely arise from changes outside of the pathways described above within both dopaminergic and non-dopaminergic neurotransmitter systems.
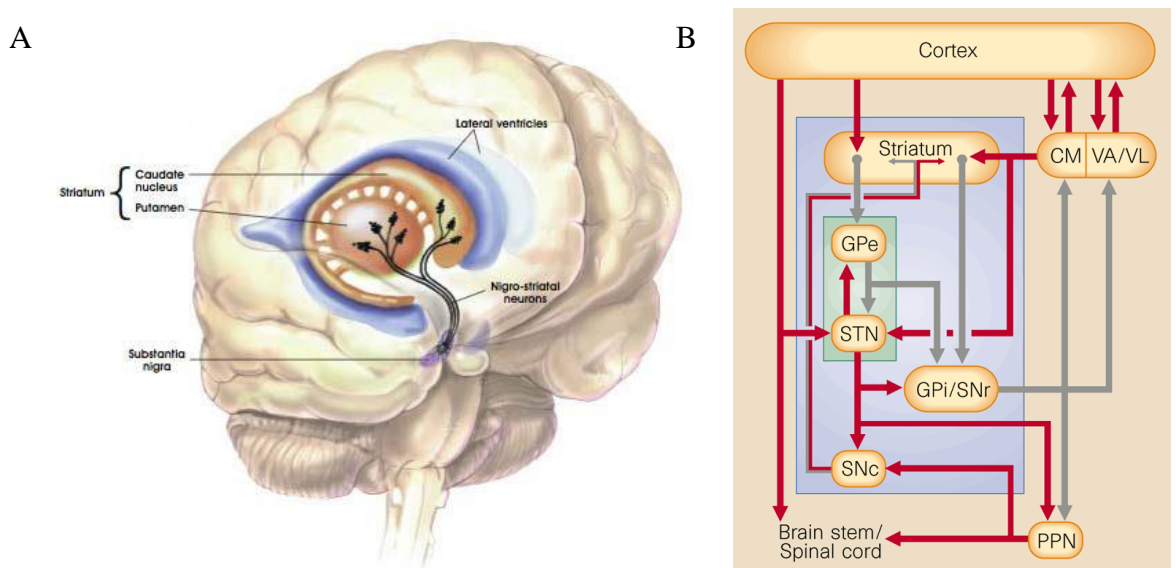
Figure 1.24. Location and Circuitry of the Basal Ganglia network.

(A) Location of the substantia nigra and striatum. (B) Inhibitory (grey) and excitatory (red) communication between structures in the basal ganglia (Image adapted from brainmaps.com).

1.7.3   **Mitochondrial Dysfunction in Synucleinopathies**

Mitochondrial dysfunction had been implicated in the pathogenesis of PD since the environmental toxin MPTP was found to result in a parkinsonian syndrome. Specifically the active metabolite MPP+ was found to inhibit complex I of the electron transport chain (Langston *et al.*, 1983). Since this discovery in 1983 further evidence for complex I dysfunction in PD has been put forward. In the substantia nigra of PD patient's complex I activity has been shown to be decreased (Schapira *et al.*, 1990). Increased levels of carbonyls- caused by the oxidation of amino acid residues on proteins, have also been demonstrated in several catalytic subunits of complex I in PD brains suggesting excessive oxidative damage of subunits resulting in misassembly and subsequent dysfunction (Keeney *et al.*, 2006b). High levels of somatic deletions in mitochondrial DNA have been seen within the substantia nigra neurons in aged individuals and PD patients (Bender *et al.*, 2006; Kraytsberg *et al.*, 2006). Furthermore this can be directly linked to decreased respiratory activity when mtDNA deletions are correlated with cytochrome-c-oxidase (COX) activity, increased levels of mtDNA deletions correspond with COX deficiency. As a number of complex I subunits are encoded by the mtDNA, these deletions will directly affect this complex. Alongside this, deletions may cause disruption in protein translation through removal of tRNAs.

Adding to the case for mitochondrial involvement in PD is the discovery that several of the gene mutations linked with inherited forms of PD have been shown to encode proteins which carry out important functions within mitochondria and/or act to reduce oxidative stress. *PARK 2* (Parkin) is a cytosolic E3 ubiquitin ligase and has been shown to function as a potent mitochondrial protection factor. Parkin over expression prevents mitochondrial swelling and cytochrome *c* release; enhanced expression of complex I subunits and reduced accumulation of ROS (Darios *et al.*, 2003). Parkin is also selectively recruited to dysfunctional mitochondria expressing PINK1 with low membrane potential, which in turn promotes engulfment and destruction in autophagosomes (covered in section 1.4.3) (Narendra *et al.*, 2008).

PINK1 (PTEN induced putative kinase 1) is a serine threonine kinase imported into the mitochondria via an N-Terminal target sequence (Lin and Kang, 2010). Familial PINK1 mutations impair the ability of PINK1 to phosphorylate TNF receptor-associated protein

1(TRAP1) (Pridgeon *et al.*, 2007). TRAP1 functions as a chaperone and its phosphorylation is required to prevent oxidative stress-induced release of cytochrome c (Wood-Kaczmar *et al.*, 2008). In human dopaminergic neurons loss of PINK1 leads to abnormal mitochondria and reduced viability (Wood-Kaczmar *et al.*, 2008). In SH-SY5Y cells PINK1 knockdown increases accumulation of mitochondrially targeted autophagosomes (Dagda *et al.*, 2009).

PARK 7 (DJ1) is also thought to play a part in protecting the cell from oxidative stress (Mitsumoto and Nakagawa, 2001). Under stress the predominantly cytosolic protein moves to the mitochondria and later the nucleus suggesting a neuroprotective function. It has been proposed that DJ1 may function as a chaperone preventing mis-folding and aggregation of proteins under stress (Shendelman *et al.*, 2004).

One of the challenges with regards to studying the impact of mitochondrial dysfunction in Parkinson's Disease is the lack of an appropriate model. Animals treated with MPTP are often used as a proxy for PD but do not recapitulate all PD symptoms. This is the case for the MitoPark mouse which uses the selective knockout of the mitochondrial transcription factor, TFAM in SN neurons to generate mice with progressive parkinsonism and intraneuronal inclusions (which do not contain α-synuclein). Within these mice the mitochondrial dysfunction is far more severe than the decline we see in ageing and develops at 6 weeks in the mice (Ekstrand *et al.*, 2007). In order to fully understand how the progressive nature of the mitochondrial defect affects the SN neurons of these patients much more subtle models need to be employed.

1.7.4   Autophagy in Neurodegenerative conditions

The critical role of autophagy as a mediator of neuronal survival has been extensively demonstrated. Increasingly, factors associated with the progression of neurodegenerative disorders are emerging as factors that impact upon the autophagy process or are themselves affected by autophagic dysfunction. A key aspect of neurodegenerative disorders is the accumulation of intracytoplasmic aggregates. Ordinarily components of these aggregates are removed by the UPS system. This system however, can become overwhelmed in neurodegenerative disorders as a result of

misfolded proteins blocking the proteasome or the sheer quantity of 'junk' overwhelming the system. In such conditions it turns to autophagy to compensate. The simple fact these inclusions are able to form would suggest a failing of both degradation processes. Initial, UPS failure followed by retarded autophagy unable to compensate (due to inherent problems, overwhelming or damage to the system) = less clearance of aggregated proteins = increased toxicity. Furthermore, mutated forms of proteins that aggregate in common neurodegenerative disorders seem to be preferentially degraded by autophagy compared to wild type. This may be due to this inability for the mutated forms to enter the narrow entrance of the proteasome. Interestingly in the case of alpha synuclein in Parkinson's Disease clearance of both wildtype and mutant forms is increased by up regulated autophagy (Webb *et al.*, 2003).

Several autophagy related proteins have been shown to be affected in various neurodegenerative disorders. Beclin1, for example, has been shown to be markedly reduced in Alzheimer's (Pickford *et al.*, 2008). Conversely, mTOR, the main inhibitory regulator of autophagy has been shown to dramatically increase in conjunction with Tau pathology in Alzheimer's disease (Caccamo *et al.*, 2010). Recent genetic studies have highlighted the importance of constitutive autophagy in neurons. Mouse ATG5 or ATG7 knockout studies demonstrate the importance of basal autophagy, the result of such ablation causing severe neurodegeneration (Hara *et al.*, 2006). In both *drosophila* and murine models of Huntington's disease the protein aggregations themselves have been shown to suppress mTOR activity and in doing so up regulate autophagy (Ravikumar *et al.*, 2004). This could be considered an intrinsic response by the cell to clear aggregations. The point of autophagic dysfunction may vary across different neurological disorders. In Alzheimer's disease an accumulation of autophagosomes has been observed implying that autophagy is functional to a point, but that the dysfunction occurs in the lysosomes or fusion processes. These differences may become critical when modulating autophagy for neurodegeneration therapeutics.

1.7.5   **Autophagy and Synucleinopathies**

A link between autophagy dysfunction and the pathology of Parkinson's disease has been drawn previously. Several proteins known to be involved in the autophagy pathway are mutated in inherited forms of PD. Mutations in Parkin for example are

known to result in recessive cases of PD. Parkin's physiological role is clearly important, demonstrated by its expression in many tissue types and its role in mitophagy discussed above.

In *drosophila* models, parkin has been shown to function in the same pathway as PINK1 (PARK6)(Clark *et al.*, 2006). Furthermore PINK1 activity is necessary for the translocation of parkin from the cytosol (Matsuda *et al.*, 2010). How exactly PINK1 signals dysfunctional mitochondria's removal is not fully understood. It may be that proteolysis of PINK1 is inhibited within damaged mitochondria leading to its accumulation and a subsequent recruitment of parkin (Narendra *et al.*, 2010). Ordinarily, proteolysis maintains very low levels of PINK1 in healthy mitochondria meaning they avoid parkin mediated mitophagy. Mutated forms of the PINK1 protein have been shown to cause Parkinson's disease (Hardy *et al.*, 2009), it may be its crucial role in mitophagy is compromised in these cases (Geisler *et al.*, 2010).

Further PD associated genes can also be linked with autophagy. DJ-1 (PARK7) is also thought to play a role in protecting the cell from oxidative stress (Mitsumoto and Nakagawa, 2001). Lack of function of DJ1 has been shown to impair the autophagic response to hypoxia (Vasseur *et al.*, 2009). Research carried out by Irrcher *et al* showed DJ1 altered autophagy in murine and human cells (Irrcher *et al.*, 2010). Furthermore, specific Leucine-rich repeat kinase 2 (LRRK2) mutations have been shown to cause a dramatic increase in autophagic vacuoles (Alegre-Abarrategui *et al.*, 2009).

Blocking mTOR via over expression of the translation inhibitor THOR can reduce PD associated pathology, in *drosophila* for example, a reduction in degeneration of dopaminergic neurons is seen. *In vivo* rapamycin activates this translation inhibitor. Recent work by Crews *et al* showed that in the brains of DLB patients there was an increase in mTOR levels and a decrease in ATG7 given by immunoblot and immunolabelling (Crews *et al.*, 2010). Furthermore, activating autophagy by rapamycin treatment in transgenic mice ameliorated neurodegeneration and reduced accumulation of alpha synuclein.

Many aetiological factors associated with PD reduce autophagic activity. Alpha synuclein, proposed to have a role in synaptic plasticity and the main component of intracellular inclusions in PD has been shown to induce cell toxicity at high levels. It has been shown that alpha synuclein may interfere with autophagy mechanisms (Meredith *et al.*, 2002) and that it can be degraded by lysosomes (Cuervo *et al.*, 2004). Normal degradation of wildtype alpha synuclein occurs via the UPS or chaperone mediated autophagy (CMA). Mutant forms of the protein have been shown to bind LAMP2 with higher affinity than its wildtype counterpart causing a blockage of their own and other substrates degradation by this method. Work by Spencer *et al* showed that over expression of alpha synuclein in both neuronal cultures and transgenic mice led to dysfunctional autophagy and subsequent neurodegeneration. The consequence of this is a disruption in transportation to the lysosomal lumen and consequently a block in chaperone mediated autophagy. Interestingly, this could be reversed by Beclin1 (Spencer *et al.*, 2009b). The role of alpha synuclein may extend beyond that of its effect on CMA as the clearance of the protein has been shown to be mediated by macro as well as chaperone mediated autophagy (Webb *et al.*, 2003).Furthermore, mTOR was more abundant in neurons displaying alpha synuclein accumulation in DLB brains (Crews *et al.*, 2010) and ultra-structural analysis went on to show abnormal and increased autophagosomes.

Further evidence showing a role for autophagy in PD stem from the affect certain neurotoxins, shown to invoke PD like symptoms in models of the disease, have upon the process. When animals are exposed to MPTP autophagic dysfunction is observed, associated with alterations in signal transduction pathways (Zhu *et al.*, 2007). Finally, lysosome dysfunction may play a key role in Parkinson's development as indicated by a susceptibility to alpha synuclein aggregation and parkinsonism in some lysosomal storage disorders (Raja *et al.*, 2007).

1.8   INTERACTIONS

1.8.1   Interaction between autophagy and mitochondria

Mitochondria have been associated with the process of autophagy since they were first observed within lysosomes and autophagosomes via electron microscopy in the 1950s, reviewed in (De Duve and Wattiaux, 1966). Since then a host of biochemical and ultra-structural studies have confirmed the removal of these whole organelles via autophagy. Although mitophagy, as the main process of mitochondrial quality control has been known for some time, questions regarding the specificity of the process remained. Once thought to be nonselective, more recent evidence points to a highly regulated and specific method in place, with mitochondria selectively targeted for degradation. Studies in yeast show regulation of mitophagy is distinct from general autophagy (Kanki *et al.*, 2008) and whole mitochondria with reduced membrane potential have been shown to be selectively removed via autophagy (Twig *et al.*, 2008). When neurons are cultured with caspase inhibitors, apoptosis induction results in complete removal of mitochondria by mitophagy (Tolkovsky *et al.*, 2002). During apoptosis outer mitochondrial membrane (OMM) permeabilization occurs prior to caspase activation and as such these results add to the idea that mitochondrial damage can induce mitophagy (Tolkovsky *et al.*, 2002).

Mitochondria are the main source of cellular reactive oxygen species (ROS), a by-product of oxidative phosphorylation. In a controlled state ROS are known to function as signalling molecules within numerous signalling pathways, including autophagy (Scherz-Shouval *et al.*, 2007c). A crucial step in the initiation of autophagy is conjugation of LC3 to phosphoethanolamine (PE), when complete a deconjugation reaction occurs mediated by the protease ATG4. Recycling of ATG4 is regulated by ROS (Scherz-Shouval *et al.*, 2007c). Furthermore ATG4 has been shown as a direct target for oxidation by H_2O_2 during starvation (Scherz-Shouval *et al.*, 2007c; Chen *et al.*, 2009). The production of ROS is essential for stress induced autophagy. Indeed, amino acid restriction has been shown to trigger mitochondrial ROS production (Azad *et al.*, 2009) and oxidised proteins are taken up more efficiently by lysosomes (Scherz-Shouval *et al.*, 2007a). Taken together these findings indicate ROS, increase autophagy, which then serves as a defence mechanism against oxidative stress.

As mitophagy serves as the main quality control process for removal of defective mitochondria it is easy to understand how the maintenance of healthy mitochondrial populations and subsequently cellular homeostasis, crucially depend upon this process. An inability to remove damaged mitochondria has two major implications. Firstly, damaged mitochondria may produce an increased amount of ROS. ROS mediated damage affects various cellular components. Furthermore if damaged mitochondria are not removed efficiently, damage builds rapidly which can affect other mitochondria. This vicious circle hypothesis of mitochondrial damage has been hypothesised as the main driving force behind ageing (Harman, 1972) and thought to occur within numerous disease states.

High levels of oxidative stress within a cell cause an accumulation of oxidised proteins that can quite conceivably overwhelm the autophagic response, leading to aggregations. Furthermore, the lysosomal machinery itself is not immune from ROS related damage and as such damage can occur to lysosomal membranes and affect membrane permeability (Hwang *et al.*, 2008). Alongside removal of damaged mitochondria, mitophagy serves to remove superfluous mitochondria. In maintaining only the essential numbers of mitochondria the cell ensures the level of ROS production is as low as functionally possible. Aside from ROS production, damage to the outer mitochondrial membrane causes a release of Cytochrome *c* which triggers caspase activity and eventually apoptosis.

A lack of functional mitochondria also has profound effects on cellular energetics. Specifically, with regards to autophagy, the break down products created upon starvation via autophagy need to be reconstructed, a process which is reliant on ATP and thus functional mitochondria. Nutrient mobilization is a key role of autophagy but without sufficient energy production at every stage of the process, necessary molecules fail to be successfully retrieved or incorporated into new components.

Although still heavily debated, mitochondria have been proposed as contributing to the autophagosomal membrane. The origin of which is not fully understood (Overbye *et al.*, 2007). Work by Hailey and colleagues explored the role of mitochondria in formation of the autophagosomal membrane in times of starvation (Hailey *et al.*, 2010). It has

been demonstrated that the outer membrane of mitochondria participates in autophagosomal biogenesis. The autophagy marker ATG5 was found to localize to puncta on the outer mitochondrial membrane which co-localised with LC3. Furthermore photo bleaching revealed that membranes of mitochondria and autophagosomes are transiently shared. Although previous studies have interpreted this membrane sharing as mitophagy, Hailey and colleagues demonstrated a diffusion barrier actually prevents delivery of mitochondrial proteins but NOT lipids, suggesting this is not mitophagy but mitochondria contributing membranes to autophagosomes (Hailey *et al.*, 2010).

Alterations in mitophagy have massive implications for cells and as a result several changes in the process have been observed within different pathologies. Disruption in autophagic processes has been postulated to result in neurodegeneration in mouse and human models (Komatsu *et al.*, 2006; Jellinger, 2009). Neurons are heavily energy dependant post mitotic cells and as such are especially vulnerable to disruptions in autophagy. As long lived cells they rely on efficient quality control mechanisms to ensure cellular homeostasis and specifically mitophagy for the removal of damaged mitochondria. Previous work has shown that deletion of autophagy genes in the CNS can result in neurodegeneration (Komatsu *et al.*, 2006).

1.8.2   **Interactions between mitochondrial dynamics and PD**

Integral changes in mitochondria have long been implicated in the pathogenesis of Parkinson's Disease (PD), notably in relation to Complex I (CI) of the electron chain reviewed in (Papa and De Rasmo, 2013). Mitochondrial bioenergetics, transmembrane potential, dynamics and trafficking are interrelated. Complex I dysfunction can affect mitochondrial morphology and morphological changes can modulate complex I activity. The combined dysfunction of these two is likely to be key to the understanding of the development of PD (Figure 1.25).

It is vital for cells to regulate mitochondrial integrity, number and location, to balance energy needs, buffer calcium and modulate various signalling pathways. The distinctive characteristics of dopaminergic neurons within the substantia nigra, known to undergo profound degeneration in Parkinson's disease, may render this population uniquely

susceptible to perturbations in mitochondrial motility. The increased oxidative burden placed on dopaminergic neurons through the metabolism of dopamine, alongside their unique calcium maintained pacemaking activity are just two individualities that may render this population vulnerable to mitochondrial dysfunction. Furthermore, this organelles pivotal role in energy provision, ROS production and calcium buffering highlights its contribution to neuronal survival in this brain region.

Fission, fusion and motility are intertwined and work shows that the likeliness of one event is tied into others. Alterations in these processes are therefore rarely independent and subsequently affect many factors controlling mitochondrial stability. Some OPA1 patients, for example, actually show increased numbers of mtDNA mutations adding to the argument that fusion is necessary for maintenance of mtDNA integrity (Amati-Bonneau *et al.*, 2008). In addition, neurons expressing mutant huntingtin (Htt) or tau show impaired mitochondrial movement, specifically suppression of mitochondrial fusion with mitochondrial shortening (Schulz *et al.*, 2012). With relation to PD, a loss of MFN2 in the nigrostriatal neurons of mice causes retrograde degeneration of dopaminergic neurons, indicating alterations in mitochondrial dynamics can independently cause PD like nigrostriatal defects (Pham *et al.*, 2012). These data highlight the impact of perturbed mitochondrial dynamics on the survival of neurons.

Figure 1.25 Implications of CI induced morphological differences in neurons.

Complex I dysfunction may bring about changes in mitochondrial structure and dynamics. The implications of these changes may be felt most prominently in neurons due to their reliance on mitochondrial trafficking and their post mitotic, restrictive, extended nature. If complex I dysfunction causes fragmentation and/or swelling of the mitochondrial network in neurons this may cause a blockage of axons or dendrites. Alternatively, fragmentation may lead to uncontrolled apoptotic signalling or instability of the mtDNA due to limited rescue through mitochondrial fusions. Conversely, if elongation of the network occurs mitochondria may be unable to escape the cell body and travel along processes. Their motility will be restricted due to their size and they may form physical barriers to the trafficking of other cellular components. Finally a hyperfused network may be compromised in its ability to segregate and degrade damaged mitochondria.
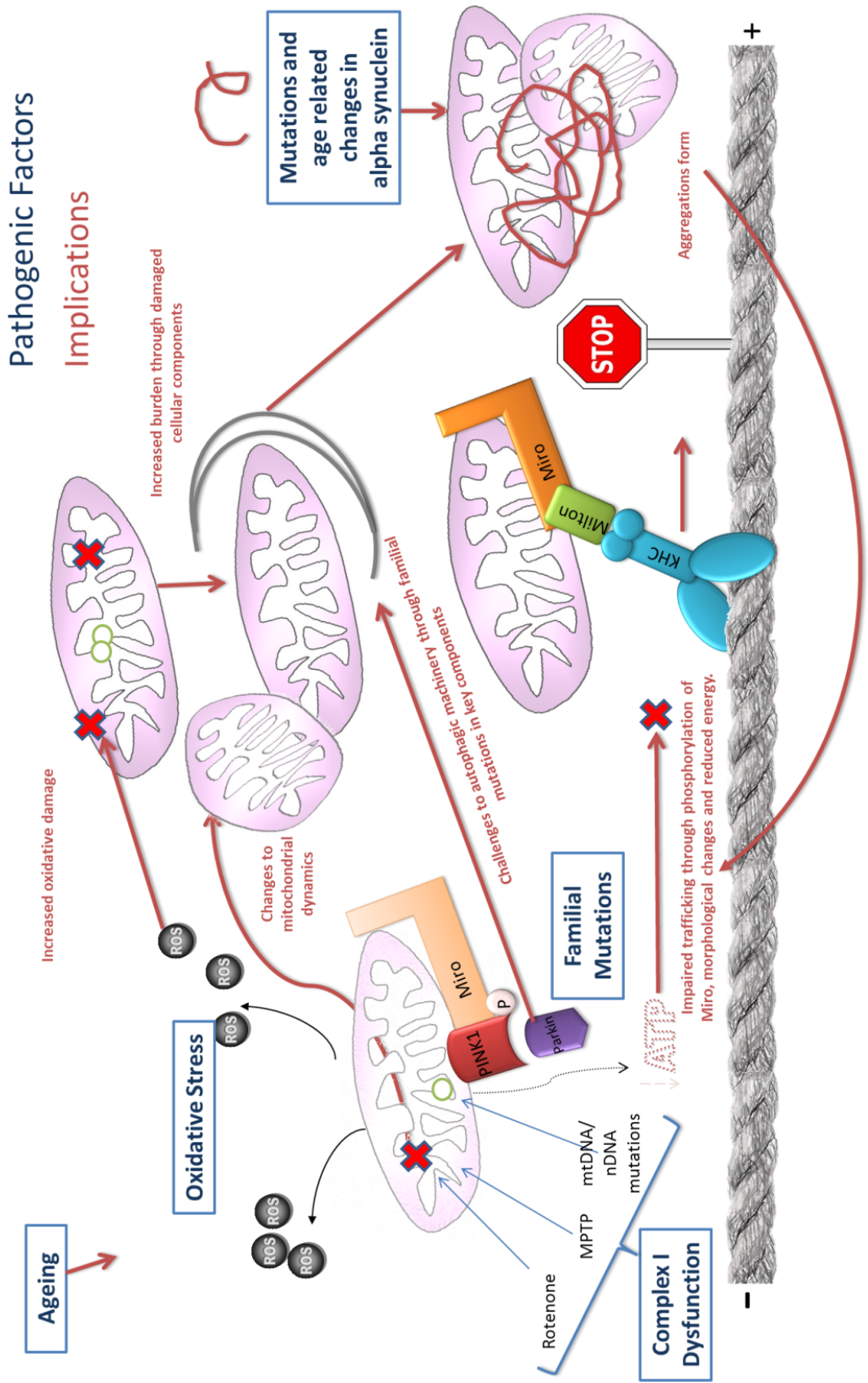
1.8.2.1   *Mitochondrial morphological changes in the pathogenesis of Parkinson's disease*

Changes to the ultrastructure of mitochondria have been observed in many relevant PD models. In fibroblasts derived from patients with *PINK1* mutations fragmented mitochondria have been observed (Exner *et al.*, 2007). This phenotype can also be seen in *PINK1* knockdowns in human neuronal SH-SY5Y cells (Dagda *et al.*, 2009). This phenomenon however does not appear universal for all cell types, for example in COS7 cells, elongation of mitochondrial networks have been observed following *PINK1* knockdown (Yang *et al.*, 2008). Discrepancies in findings amongst and within different model systems add complexity to understanding the role of mitochondrial dynamics in PD but could equally reflect the multicomponent nature of the disease and highlight that the pathways are far from fully elucidated. This variation could also explain how it takes a unique cellular environment and chain of events to bring about cell death following deficiency, as highlighted by the preferential loss of SN neurons.

Pharmacological modulation, for example through toxins that inhibit complex I, are used to create PD animal models and links between complex I and mitochondrial morphology are tantalizing linked through PINK1, but as yet not fully understood. In *drosophila* for example, no obvious morphological differences have been observed in *PINK1* mutants, despite this, synaptic dysfunction occurs. Interestingly *PINK1* KO cells isolated from mouse liver revealed a dramatic decrease in enzymatic activity and complex I driven respiration, importantly this finding was unique for complex I. The authors therefore conclude that ablation of PINK1 results in a primary functional defect in the catalytic activity of complex I. This is made relevant to the human condition using human cells expressing *PINK1* carrying mutations, which display a severe complex I dysfunction similar to that observed in mouse *PINK1* knockout cells. Furthermore rescue experiments using human wild type *PINK1* expression affects complex I, but not other electron transport chain complexes (Morais *et al.*, 2009).

Knock-out of both *PARKIN* and *PINK1* show varying levels of oxidative stress and changes in respiration in a number of mouse models (Gautier *et al.*, 2008; Mortiboys *et al.*, 2008; Gispert *et al.*, 2009). PINK1 null mice, for example, display impaired dopamine release, deficient respiration and increased response to oxidative stress (Kitada *et al.*, 2007; Gautier *et al.*, 2008). This phenotype increases in severity and

distribution in *drosophila* (Greene *et al.*, 2003), while the modulation of PINK1 and PARKIN in this model have elegantly displayed that they function in the same pathway (Clark *et al.*, 2006). Loss of PINK1 has also been shown to alter mitochondrial morphology to differing degrees dependant on cell type, for example a loss of PINK1 in dopaminergic neurons leads to a swollen abnormal mitochondrial phenotype in conjunction with reduction in viability (Wood-Kaczmar *et al.*, 2008). These experiments further highlight the debilitating impact of changes in this pathway and further reiterate the links between neuronal survival, mitochondrial fission, fusion and mitophagy.

1.8.2.2 *Mitochondrial motility in Parkinson's Disease*

The efficient movement of mitochondria has previously been shown to be compromised in numerous neurodegenerative disorders. The role of mitochondrial motility in PD is arguably one of the strongest cases for interplay between movement and neurodegeneration, strengthened by the discovery of *PINK1* and *PARKIN*, familial gene mutations in autosomal recessive cases of PD. Alongside their role in degradation discussed above, these two proteins are known to interact with Mitochondrial RHO GTPase (MIRO), an adaptor protein that links a kinesin motor to mitochondria (Wang *et al.*, 2011; Liu *et al.*, 2012). Upon damage and the subsequent decrease in membrane potential both PINK1 and PARKIN have been shown to show stronger physical interaction with Miro. PINK1 can phosphorylate Miro which marks it for degradation and in turn arrests mitochondrial movement in all directions. A second role for PINK1/PARKIN may therefore be with regards to confining unwanted mitochondria, limiting any harm the damaged organelle can do, avoiding its transportation to critical areas and enabling its subsequent encapsulation via autophagosomes. Alterations through mutations in these genes may explain why trafficking is altered in PD and why ultimately neurodegeneration occurs. It is important to also consider that trafficking pathways are not solely dedicated to mitochondria but serve as transport links for a plethora of cellular components. Mitochondrial 'swellers' such as valinomycin have been shown to lead to fast inhibition of organelle movement suggesting steric hindrance of mitochondria (Kaasik *et al.*, 2007). This block prevents not only their own, but other organelles movement, which in part may explain how simple deviations from normal trafficking can quickly bring about collapse of the cellular environment.

 Impaired mitochondrial transport is implicated in numerous neurodegenerative disorders. Elucidating whether dynamic alterations are primary factors or result from other compounding mitochondrial issues remains difficult. The role of mitochondrial dynamics in apoptosis must also not be overlooked. Morphology is tightly linked to apoptosis demonstrated by the fact MFN2 GTPase activity relies on Bcl2 family members (Karbowski *et al.*, 2004) and OPA1 affects apoptosis through availability of cytochrome *c* release (Frezza *et al.*, 2006). Decreased membrane potential may lead to increased susceptibility to apoptosis, a process which is modulated through different pathways including changes in the morphology of mitochondria (Morais *et al.*, 2009). Calcium also serves an apoptotic stimuli (Scorrano *et al.*, 2002), one may postulate that areas of increased calcium such as dopaminergic neurons may be quicker to react to mitochondrial changes which diminish their calcium sink capabilities and leave apoptotic cascades unchecked.

1.9   AIMS OF THIS RESEARCH

This project aims to assess the correlation between mitochondrial dysfunction and changes to the autophagy process in the context of Parkinson's disease pathogenesis.

Both mitochondrial dysfucntion and autophagy have been implicated in the progression of PD through various different experimental models, and increasing evidence points to the two processes synergistically having a role in PD development, notably through mitophagy. Crucial to mitophagy and overall mitochondrial function are mitochondrial dynamics, encompassing motility, fission and fusion. As such, these processes will also be analysed in relation to mitochondrial dysfunction and autophagy.

Given the relevance of complex I in PD pathogenesis, deficiency of this complex will serve as the mitochondrial dysfunction analysed in these studies. To enable assessment of pathogenic alterations in mitochondria and autophagy in conjunction with elucidating possible modes of action, tissue and cell culture based assays will be employed.

Cell Model

1. Characterise bioenergetics and protein expression of cybrid ES cell lines containing differing severities of mtDNA mutations.

2. Assess markers of autophagy in fixed ES cells and newly differentiated neurons.

3. Analyse morphology of mitochondria within cybrid cell lines.

4. Analyse motility of organelles in newly differentiated neurons.

5. Look for further correlation between morphology and autophagy in complex I deficient patient fibroblasts.

Tissue model

1. Optimize dual immunohistochemical fluorescence assay in upper mid brain sections, including means to quench autofluorescence and normalise quantification.

2. Assess expression of C120, a marker of complex I assembly, in individual substantia nigra neurons in PD and control tissue sections.

3. Assess expression of autophagy markers in individual substantia nigra neurons in PD and control tissue sections.

4. Analyse relationship between C120 expression and expression of autophagy markers.

5. Assess SNc density in PD vs. control tissue, look for correlation with age and autophagy marker expression.

Chapter Two

Materials and Methods

Chapter 2. Materials and Methods

2.1   MATERIALS

2.1.1   Equipment

ABI 3130cl genetic Analyser	Applied Biosystems.
ABI Gene Amp 9700 Thermal Cycler	Applied Biosystems.
ABI Prism 7000 sequence detection system	Applied Biosystems.
AURA PCR UV Cabinet	Bio Air Instruments
Autoclave	Astell
Automated plate reader EIx800	Bio-Tek
Balance: Adventurer OHAUS	Jencons-PLS
Balance: EK-120A	Salter
Bench-top Microcentrifuge	Sigma
Bench-top Centrifuge 3-15	Sigma
Bench-top Centrifuge 5417 R (refrigerated)	Eppendorf
Binder General Purpose Incubator	Philip Harris
ChemiDoc MP Imaging System	Bio-Rad
Countess® Automated Cell Counter	Life technologies
Dry Heat Block (DB.3.A)	Techne
Electrophoresis power supply model 250EX	Life Technologies
ErgoOne® Single & Multi-Channel Pipettes (P20, P200, P1000)	Starlab
Grant JB Series Water bath	Grant Instruments
Horizontal Agarose Gel Electrophoresis Systems	Sci-plas
InCu SafeTM CO2 Incubator	Sanyo
Laminar Flow hood	Jencons-PLS
Light Microscope	Leica
Microflow Biological Safety Cabinet	Bioquell
Nanodrop ND-1000 Spectrophotometer	Labtech International
ND-1000 Software	Labtech International
NANOpureII Water Purification System	Barnstead
Neubauer Improved haemocytometer	Millipore

Nikon Imaging system (used for live cell imaging)

    Nikon BioStation CT   Nikon

    Nikon A1R (Invert)   Nikon

    Nikon TIRF / Spinning Disk   Nikon

pH Meter (3510)   Jenway

PhosphorImager, Storm 860   Molecular Dynamics

Rotating hybridisation oven   Hybaid

Seahorse Extracellular Flux Analyser XF24   Seahorse Bioscience

UV Gel Documentation System   Alpha Innotech

AlphaImage series 2200 Software   Flowgen

Vortex Genie 1 Touch Mixer   Wolf Laboratories

Vortex Genie   Scientific Industries

Zeiss Imaging System (used for tissue sections).

    Zeiss Axio Imager 2 (with Apotome)   Zeiss

    Axioplan 2iE Light Microscope   Zeiss

    AxioCam HRc digital camera   Zeiss

    AxioVision imagecapture software   Zeiss

Zeiss Imaging system (used for tissue culture)

    Axiovert 200M fluorescence microscope   Zeiss

    AxioCam MR3 digital black and white camera.   Zeiss

    AxioVision image capture software (Ver 4.6.3.0).   Zeiss

Image Analysis Software

    ImageJ   NIH

    Volocity 6.2   Perkin Elmer

    IMARIS 7.2   Bitplane

2.1.2 Consumables

0.2ml Thin-Walled PCR tubes   Biogene

0.5ml Thin-Walled PCR tubes   Biogene

1.5ml Eppendorf tubes   Biogene

2.0ml Eppendorf tubes   Biogene

96 well optical bottom plates   Nunc

Aerosol resistant Pipette tips   Starlabs

Coverslips (22x22mm, 22x40mm, 22x50mm)   VWR International

Cellstar® Disposable Pipettes   Greiner

(5ml, 10ml, 25ml)

Cellstar® Tissue Culture flasks	Greiner
($25cm^3$, $75cm^3$, $225cm^3$)	
Countess® Cell Counting Chamber Slides	Life technologies
Cryotube Vials	NUNC
Culture Slides	BD Falcon
Falcon tubes (15ml and 50ml)	BD Biosciences
Gel Extraction Kit	Qiagen
Gilson Pipetteman (P2, P10, P20, P200, P1000)	Anachem
Immobilon Transfer Membranes PVDF	Millipore
Microscope Slides (76x26x1.0-1.2mm)	Merck
MILLEX Syringe-Driven Filters (0.22um)	Milipore
Pasteur Pipettes (glass)	VWR International
Pipette Tips (Including filter tips)	Starlab
Polyethylenenaphthalate (PEN) membrane slides	Leica
QIAamp DNA micro Kit	Qiagen
Seahorse XF24 Cell Culture Microplates	Seahorse Bioscience
SlideRite 5 mailerTM	CellPath
SuperFrost plus Glass Microscope Slides	VWR International
Syringes	BD Plastipak
Whatman Grade I Filter paper	Merck

2.1.3 **Solutions**

Unless specified otherwise, all solutions listed and others mentioned in the text were prepared in nanopure (18 Mega Ohms activity) water.

Coomassie Blue	0.1% (w/v) Coomassie Brilliant Blue Reagent
	7% (v/v) acetic acid
	50% methanol
Destain Solution	100ml Methanol
	80ml dH_2O
	20ml Acetic Acid

DNA Loading buffer   0.25% (w/v) Bromophenol Blue

0.25% (w/v) Xylene Cyanol

30% (v/v) Glycerol

Electrophoresis Buffer   100ml 10x TAE

900ml NANOpure water

80µl ethidium bromide

Lysis buffer   100µl 0.5M Tris/HCl + 52µl 2.5M

NaCl + 4µl 0.5M MgCl2

150µl of 7x Roche Protease

inhibitors

20µl Nonidet P-40

674µl ddH$_2$O

5% Milk solution in TTBS   5g Skimmed Milk powder

100ml TTBS

4% Paraformaldehyde   20g paraformaldehyde in 250ml

nanopure water

250ml 0.2M phosphate buffer

Phosphate Buffer (pH 7.4)   200ml 0.2M di-sodium hydrogen

phosphate

50ml 0.2M Sodium dihydrogen

phosphate

Phosphate Buffered Saline   Prepared from tablets; 1 Tablet in

100ml water

Running Buffer (Westerns) 5x   15g Trisma base

72g Glycine

5g SDS

Sample Buffer (Westerns)   10ml Stacking buffer

4ml Glycerol

	4ml 20% SDS
	0.02g Bromophenol blue
	2ml dH$_2$O
10x Tris-Acetate EDTA (TAE)	24.2g Trisma Base
	5.71ml Glacial Acetic Acid
	10ml 0.5M EDTA (pH 8.0)
	DEPC water to 500ml
1M Tris-HCl pH 8.8 (Separating Buffer) dH$_2$O.	60.55g Trisma base in 500ml
0.5M Tris-HCl pH 6.8 (Stacking buffer) dH$_2$O	30.275g Trisma base in 500ml
Tris EDTA (TE)	10mM Tris-HCL
	1mM EDTA
TTBS pH7.6	2.42g Trisma base
	8g NaCl
	Made up to 1L with dH$_2$O
	0.1% Tween 20

2.1.4 Chemicals and Reagents

100% Ethanol and 100% Methanol Analar	Fisher Chemical
Liquid nitrogen	BOC
Normal Goat Serum	Sigma
Nonidet P40	BDH
β-mercaptoethanol	Sigma

2.1.4.1   *Histological and Histochemical Reagent.*

3.3'Diaminobenzidine Tetrahydrochloride (DAB)	Sigma
ATG5 Rabbit pAB	Abcam
ATG7 Rabbit mAB	Millipore
ATG12 Mouse AB	Cell Signalling
Avidin/ Biotin Blocking Kit	Vector
Beta-tubulin Rabbit pAB	Covance
Beclin1 pAB	Millipore
Cy5 Conjugated Mouse secondary	Abcam
DPXTM Mountant	Merck
Ethanol Analar	Merck
Fluorescien Isothiocyanate (FITC) Fluro Antibody	Jackson ImmunoResearch
FITC conjugated GP secondary	Abcam
Formaldehyde	Merck
Goat Serum	Sigma
Haematoxylin	Merck
HistoclearTM	National Diagnostics
Hoechst 33342 Fluorescent Antibody	Invitrogen
Hydrogen Peroxide	BDH
LAMP2A Mouse mAB	Abcam
LC3 Rabbit mAB	Cell Signalling
Methanol Analar	Merck
Nestin Mouse mAB	Abcam
OXPHOS Antibodies	Abcam (formally Mitosciences)
P62 Guinea Pig pAB	Progen
Paraformaldehyde	Sigma
Peroxidase Substrate kit	Vector
Rhodamine Red Fluorescent Antibody	Jackson Immunoresearch
Sodium Azide	Sigma
Sodium dihydrogen phosphate	Sigma
Triton X-100	Sigma
VDAC1 pAB	ProteinTech
WDFY3 Rabbit pAB	Abcam

2.1.4.2   *DNA extraction, precipitation and purification reagent.*

Ethylenediaminetetreacetic acid (EDTA)	Sigma
Glacial Acetic acid	BDH
3M Sodium Acetate pH 5.2	Sigma

2.1.4.3   *Polymerase chain reaction and Sequencing reagents*

Ampitaq Gold DNA polymerase	Applied Biosystems
10x PCR Buffer	
BigDye Terminator v3.1 cycle sequencing kit	Applied Biosystems
Biotin labelled Primers	IDT
Bovine Serum Albumine	New England Biolabs
Deoxynucleotide Triphosphates	Roche
Dimethyl sulfoxide DMSO	
(molecular biology grade)	Sigma
EDTA (125mM)	Sigma
ExoSAP-IT	GE Healthcare
HiDi	Applied Biosystems
Proteinase K Solution	Invitrogen
Taqman mastermix	Applied Biosystems
Sodium Acetate (3M)	Sigma
Tween-20	Sigma

2.1.4.4   *Gel electrophoresis reagents*

Agarose MP	Roche
Ammonium Persulphate (AMPS)	Sigma
Bis:Acrylamide 29:1 30%	Sigma
Bromophenol Blue	Sigma
Butanol	AnalaR
1Kb DNA ladder	Gibco BRL
Ethidium Bromide	Merck
Gel Red Nucleic Acid Stain	Biotium
Glycerol	Sigma

Hyperladder IV	Bioline
Tetramethylenediamine (TEMED)	Sigma
Sodium Dodecyl Sulphate (SDS)	BDH
Tris acetate EDTA (TAE:10x)	Sigma
Urea	Sigma
Xylene Cyanol	Sigma

2.1.4.5   *Tissue Culture Reagents*

2-mercaptoethanol	Sigma
B27 Supplement	Gibco
Cyto-ID® Autophagy detection kit	Enzo Life Sciences
Dimethyl sulfoxide (DMSO)	Sigma
Dulbecco's modified Eagle Medium (DMEM)	Gibco
DMEM/F12	Gibco
Foetal Calf Serum	Gibco
Galactose	Sigma
Glasgow modified Eagle Medium (GMEM)	Gibco
JC1 mitochondrial Potential Sensor	Invitrogen
L-Glutamine (100mM)	Gibco
Leukocyte Inhibitory Factor (LIF)	Millipore
N2 Supplement	Gibco
Non-essential amino acids (NEAA)	Sigma
Mitotracker red	Invitrogen
Mitotracker deepred	Invitrogen
Mitotracker Green	Invitrogen
Modified Eagle Medium (MEM)	Gibco
MEM Vitamins	Gibco
Penicillin and Streptomycin solution (Pen-Strep)	Gibco
Protease Inhibitor tablets	Roche
Rapamycin	LC laboratories/
(20µg/ml stock diluted in DMSO)	Enzo life sciences
Sodium Pyruvate (100mM)	Sigma
Trypsin	Gibco
Uridine	Sigma

2.1.4.6   *Western reagents*

Bradford Assay Kit	Biorad
Coomassie Brilliant Blue R	Sigma
ECL-Plus Western Detection Kit	Amersham
ECL-Prime Western Detection Kit	Amersham
Immobilon-P transfer membrane	Millipore
Kaleidoscope Pre-stained standards	Bio-Rad
Mouse anti-Porin	Molecular Probes
Mouse anti-β-Actin	Sigma
Polyoxyethylenesorbitan monolaurate (Tween 20)	Sigma
Rabbit anti-Mouse HRP conjugated	DakoCytomation
Skimmed milk Powder	Marvel
Trizma base	Sigma

2.1.4.7   *Seahorse reagents.*

Antimycin	Sigma
Trifluorocarbonylcyanide Phenylhydrazone (FCCP)	Sigma
Oligomycin	Sigma
Rotenone	Sigma

2.1.4.8   *Functional and Molecular Studies*

1M Dithiohreitol (DTT)	Sigma
Acetic Acid	Sigma
Ampicillin	Sigma
B-Mercaptoethanol	Sigma
Bacto Agar	Sigma
Bacto-Tryptone	Sigma
Bacto Yeast Extract	Sigma
Bovine Serum Albumin	New England Biolabs
Bradford Reagent	Sigma
Coomassie Dye	Fisher
Glycine	Sigma

NP-40   Sigma

Protease inhibitor Mini tablets   Roche

Spectra Multicolour Broad Range Protein Ladder   Fermentas

XL10_Gold Kan UltraCompetent Cells   Fisher

2.2   METHODS

2.2.1   Standard polymerase chain reaction.

2.2.1.1   *Polymerase chain reaction.*

All standard polymerase chain reactions (PCRs) were set up on ice on the bench and were performed in a 25µl volume containing: 16.87µl nanopure water, 2.5µl 10x PCR buffer (10mM Tris-HCl pH 8.3, 1.5mM MgCl2, 50mM KCl, 0.001% wt/vol gelatine), 2.5µl 10x dNTPs, 0.13µl Ampitaq Gold DNA polymerase, 2µl primers (forward and reverse), and 1µl of DNA. 1µl of wild type murine DNA extract was used as positive control. Standard PCR reactions were carried out on a thermal cycler (GeneAmp® PCR System 9600) under the following conditions: 95ºC for 10 minutes then 30 cycles of 94ºC for 45 seconds, 58°C for 45 seconds and 72°C for 1 minute. The final extension was at 72ºC for 8 minutes.

2.2.1.2   *Primer Design*

Primer pairs for mouse mtDNA were designed to incorporate each of the mutations in cybrid cell lines. Wherever possible oligonucleotides with comparable melting temperatures (Tm) were used. All primers were obtained from Eurofins UK or Integrated DNA Technologies and are listed below.

G3739A   F- acgcttccgttacgatcaac   480bp fragment

                  R- atgatggcaagggtgatagg

Nd5 G12273A F- tatcctcacctcagccaaca   360bp fragment

              R- gaggccaaattgtgctgatt

Nd6 iC13887 F- aaacctctataatcaccccaat   360bp fragment

              R- gtcgcagttgaatgctgtgt

COI C6247T   F- atcctcccaggatttggaat   420bp fragment

              R- ctccgtgtagggttgcaagt

COI T6589C   F- tgggagcagtgtttgctatc   420bp fragment

              R- ggcagccatgaagtcattcta

A8414G   F- ccttccacaaggaactccaa   369bp fragment

              R- ggctgaaaaggctccagtta

All primers were resuspended in sterile NANOpure water to a concentration of 100μM
and stored in 5μl aliquots at -20°C.

2.2.1.3   *Gel electrophoresis*

Following amplification, products were ran through a 1.5% agarose gel (1.5g agarose in
100ml TAE). The agarose was heated in a microwave, following which, 2μl of ethidium
bromide was added and the gel was cast and allowed to cool. 2μl of each sample was
then loaded into each well with the addition of 0.5μl loading buffer (0.25% (w/v)
bromophenol blue, 0.25% (w/v) glycerol). To verify fragment size 2μl of 1Kb DNA
ladder was loaded alongside the samples. The gel was run in TAE buffer at 75V to
separate products. Visualisation of the bands was possible using the UV gel
documentation system following intercalation of ethidium bromide into the DNA.

2.2.2 **Sequencing**

2.2.2.1 *Purification of PCR Products*

Once the correct PCR products had been generated they were sequenced using the Applied Biosystems 3130 Genetic Analyser. Prior to sequencing 5μl of each PCR product was transferred to a 96 well plate on ice where 2μl of ExoSap (Amersham Biosciences) was added, mixed and briefly pulse spun down. The plate was then placed in a Geneamp PCR System 9700 where digestion at 37°C was undertaken for 15mins. Following this, samples were incubated at 80°C for a further 15mins to ensure enzyme denaturation.

2.2.2.2 *Sequencing Protocol*

A master mix is added to each sample consisting of 7μl dH_2O, 3μl 5X sequencing buffer, 1μl 3.2μM dilution of primers, and 2μl of Big Dye v3.1. The plate is then capped and returned to the 9700 thermocycler through 1 cycle of 96°C for 1 minute, 25cycles of 96°C for 10 seconds, 50°C for 5 seconds and 60°C for 4mins.

2.2.2.3 *DNA precipitation*

2μl 125mM EDTA is added to each well and the plate gently tapped to ensure delivery of the EDTA to the sample. Following this 2μl of 3M sodium acetate is added to each sample followed by a brief pulse spin. 50μl of 100% EtOH is then added to each well and mixed through inversion 4 times before being left to stand at room temperature for 15mins. After this, the plate is spun at 2090g for 30mins, the caps are removed and the plate inverted onto paper towel before spinning again at 100g to remove supernatants. 70μl 70% EtOH (Analar) is added to wash samples and spun at 1650g for 8mins. Once again the plate is inverted and briefly spun to remove supernatants. The plate is then left to dry in the dark for 20mins at room temperature. After this, 10μl of HiDi formamide is added to each well of the 96well plate which is then returned to the 9700 for 2mins at 95°C. After completion the plate is placed in the ABI 3100 automated DNA sequencer. Outputs are then compared to reference sequences and analysed through Seqscape software (ABI).

2.3   BIOENERGETIC ANALYSIS

2.3.1   Oxygraph

2.3.1.1   *Oxygraph Preparation*

The Oxygraph (Oroboros Instruments) was turned on and the temperature set to 37°C. Stoppers, and the 70% ethanol in which the chambers were stored are removed. The chambers were then filled with 100% ethanol and stirred for 3mins. Following this, a further wash in 70% ethanol was carried out for 10mins. The stoppers and washers were then washed at least three times in dH$_2$O. 2.5ml of ES Growth medium (see Table 2.2) was added to each chamber, the stoppers screwed fully down, the chambers fully sealed and stirrers turned on. To allow equilibration with atmospheric oxygen, the stoppers were then opened half way to allow oxygen to enter the chambers, this was allowed to proceed for 20mins, during which time the cells for experimentation were harvested. After 20mins, and when both trace lines (oxygen concentration and oxygen consumption) were stable, calibration of the machine was performed for each chamber based on oxygen solubility (as per the manufacturer's instructions).

2.3.1.2   *Oxygraph Measurements*

The cell pellet was resuspended in 150μl of ES Growth media to create a single cell suspension. Stoppers were removed and 75μl of cells added to each chamber. The cells were allowed to disperse for 5mins with the stirrers on. 10μl of the cells were then taken from each chamber and a cell count performed. Next, stoppers were closed slowly to seal the chambers and using the cell count the number of cells/ml was calculated and inputted into the software. Sequential addition of reagents allowed for measurement of basic mitochondrial parameters. Firstly, 1μl of Oligomycin (2μg/ml-final concentration) to inhibit ATP synthase was added. Once the oxygen consumption trace on the software had stabilised 1μl of FCCP (0.5μM) was added to uncouple the mitochondria, this was repeated until the oxygen concentration trace no longer increased (13μl for ES cells). 2μl of rotenone (0.5μM) to inhibit complex I was then added, followed by 3μl of Antimycin A (2.5μM) to inhibit complex III once the trace had stabilised. Data was then analysed by inputting the figures into template excel sheets provided by Oroboros.

2.3.2   **Seahorse**

2.3.2.1   *Seahorse Preparation*

Cells were seeded at a predefined optimal density of 50,000 cells/well (see methods development) 24hrs prior to experimentation in 20 of 24 wells of a seahorse experimentation plate. Four wells were left as background controls for each run. Each well contained 100μl of normal growth media for the culture being investigated. For semi adhesive cell lines (for example the ES cell cybrids), 100μl of 0.1% gelatine was used to line the bottom of each well. To allow cells to form a monolayer and avoid growth on the sides of wells, cells were allowed to settle in 100μl growth media for at least three hours prior to topping up media to 250μl/well. The plate is then left overnight in the $37^{o}C$ incubator with 5% CO_2. During this time the cartridge was rehydrated in rehydration buffer (Seahorse Biosciences) at $37^{o}C$ without CO_2.

On day of run, experimentation media was prepared supplemented with 5% FBS, 10mM pyruvate, 2mM L-Glutamine and 1mg/ml glucose and warmed to $37^{o}C$. The media in the experimentation plate was replaced for this media gradually, removing and replacing 200μl at a time to ensure cells were always covered. This was repeated three times with the final change topping each well to 500μl. The plate was then left for an hour in $37^{o}C$ incubator without CO_2 to equilibrate. In this time injections are prepared. A total of 4 compounds (Table 2.1) are injected sequentially, from ports A,B,C,D, appropriate final concentrations were achieved by adjusting the volumes injected as so:

Port	Solution	Inhibits	Concentration	Amount
A	Oligomycin	ATP Synthase	1μg/ml	50μl
B	FCCP	Resp. Chain Uncoupler	2μM	55μl
C	Rotenone	Complex I	0.5μM	60μl
D	Antimycin	Complex III	2.5μM	65μl

Table 2.1. OXPHOS inhibitors used in Seahorse Bioenergetic Analyser

To assess different parameters of mitochondrial function sequential injections of oxidative phosphorylation inhibitors were used at a pre-optimized concentration.

After incubation the injection cartridge was then removed from the incubator and each OXPHOS inhibitor was added in the following volumes, 50μl A, 55μl B, 60μl C and 65μl D. This was then placed within the seahorse extracellular flux analyser to calibrate. Upon completion of calibration (~15mins) the cells were added and the selected protocol was run.

2.3.2.2   *Normalization*

To control for variations in cell growth over 24hrs, following each Seahorse run the plates were washed in PBS and fixed in 4% PFA for 10mins, then stored in PBS at 4°C. Visualisation of cell nuclei is achieved through Hoechst staining (30mins 1:200 dilution in dH$_2$O) and imaging at 10x magnification using the Axiovert 200M (Zeiss). Four images from each well were taken. These images are then run through quantification software (Matlab) and all Seahorse measurements are normalised to cell number.

2.3.3   **Tissue Culture protocols**

2.3.3.1   *Basic Media Formulations.*

ES Complete Media	4:1 Media	Fibroblast growth media
500mls Glasgow Modified 50mls FCS	80mls Neurobasal media	433mls MEM
5mls NEAA	20mls DMEM/F12	50mls FCS
5mls Sodium pyruvate	1600μl B27 supplement?	5mls Mem-Vits
5mls Glutamine	200μl N2 supplement	5mls NEAA
1ml 2-mercaptoethanol	1ml pyruvate	5mls L-glutamine
56μl LIF	1ml glutamate	5mls pen/strep
	1ml NEAA	5mls pyruvate
	1μg BFGF	1ml uridine

Table 2.2. Basic Media Formulations

Growth and differentiation medias were made up in 500ml volumes and filter sterilised prior to use.

2.3.3.2   *Initiating cell growth.*

The cells to be grown are removed from the -80ºC freezer or liquid nitrogen stores and thawed through tituration with 1ml of prewarmed growth media (Table 2.2). The cell aliquot is then added to 10ml of growth media and the cells resuspended. The cells are spun at 1100rpm for 4 minutes; this releases the DMSO from the cells into the supernatant where it can be removed. The supernatant is discarded and the cells are resuspended in 7-10mls of medium (depending on the number of flasks to be seeded and the number of cells required). An appropriate volume of medium is added to flasks (precoated with 0.1% gelatine for non-adherent lines) to be seeded and then the cells are added. The flasks are gently agitated and placed in an incubator at 37ºC with 5% CO_2 until confluent.

2.3.3.3   *Harvesting cells.*

When the cells are confluent the medium is aspirated, the cells are then gently washed in 10mls Phosphate Buffered Saline (PBS), removing all traces of foetal calf serum which inhibits trypsin. The PBS is then drained and 1ml of trypsin is added, the trypsin is rinsed around the flask ensuring coverage of the entire cell surface. The flask is returned to the incubator for 1 minute, and then gently tapped to check that the cells have lifted off from the growing surface. 9mls of growth medium (containing FCS) is added to the flask, this neutralises the trypsin. The cells are fully resuspended and then divided amongst an appropriate number of flasks before being returned to the incubator at 37ºC until confluent.

2.3.3.4   *Freezing cells.*

The cells to be frozen are harvested as above and the 10mls of cells are added to a universal, the cells are then spun at 1200rpm for 4 minutes. The freezing mixture is made up, which is composed of 90% complete growth medium and 10% DMSO. This freezing mix is then syringe filtered. When the spin is complete, the supernatant is removed and an appropriate volume of the freezing mix is added depending on pellet size. Cells are resuspended in the freezing mix and aliquoted into cryotubes (500μl/vial), tubes are sealed and frozen at -80ºC for 24hrs, if longer storage is required the cells are moved to liquid nitrogen.

2.3.3.5 *Neuronal Differentiation*

Both control and cybrid cell lines were initially differentiated following the 4+/4-protocol (Bain *et al.*, 1995). This method (outlined in Figure 2.1) requires the formation of embryoid bodies (EBs) in suspension. To achieve this, cells at around 80% confluency were dissociated, resuspended in GMEM (without LIF) and transferred to non-tissue culture treated petri dishes to minimize adhesion. The cells were then allowed to form aggregates for four days with a medium change conducted on the second. On the fourth day 0.5µM retinoic acid (RA) is included with the medium change and subsequently repeated on the sixth day. RA has been shown previously to have a fundamental role in development of the CNS and as such determines a neuronal fate for the ES cells. (Maden and Holder, 1992)(Maden and Holder, 1992)(Maden and Holder, 1992)(Maden and Holder, 1992)(Maden and Holder, 1992)

After 8days the Ebs are washed three times in PBS and disaggregated in 500µl of trypsin incubated at 37°C for four minutes. Following this the supernatant containing the digested cells was removed and centrifuged. The cells were resuspended in neurobasal medium (GIBCO, Invitrogen) to achieve a plating density of 5 x 10^{5} cells/500 µl. 500µl were then transferred to each well of 6 well plates on PDL/laminin coated coverslips with 2mls of 4:1 medium supplemented with 1µg BFGF. The plates were then incubated as before up to a maximum of eight days, during this time half the medium from each well was removed every other day and replaced with 4:1 medium without BFGF.

Figure 2.1. Neuronal differentiation through the Bains 4+/4- protocol.

The diagram shows the main steps for generating neurons from ES cells over a 2 week protocol .For details see text.
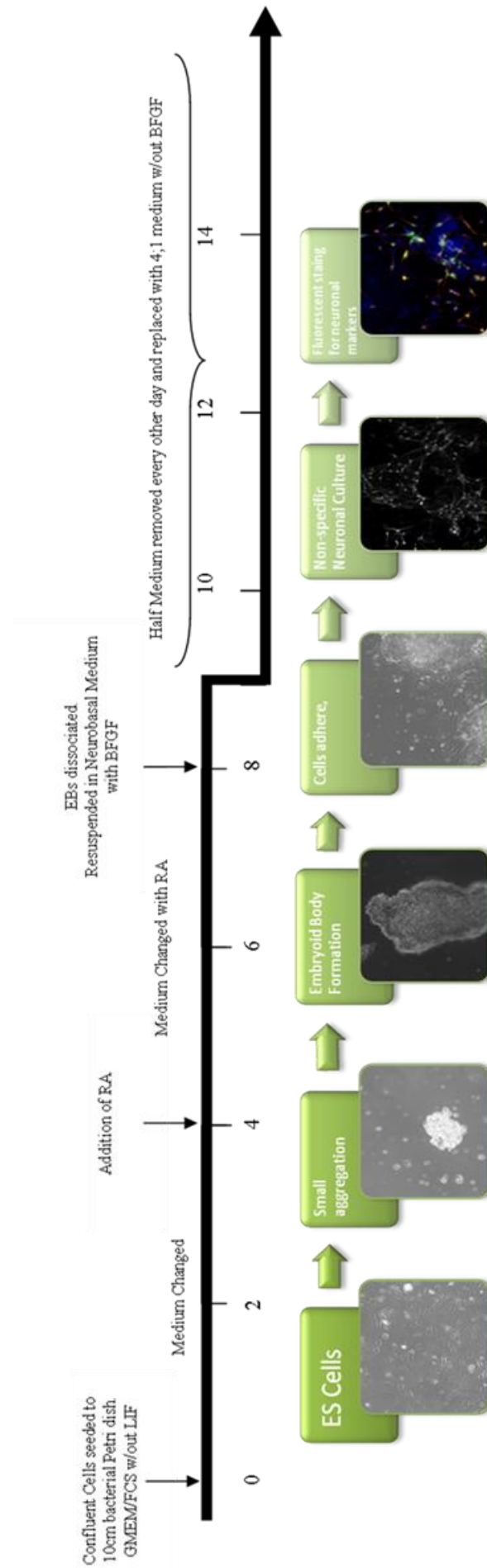
2.3.4 **Western Blot Protocol.**

2.3.4.1 *Whole cell lysis protocol.*

The lysis buffer is prepared from 170µl of 50mM Tris/HCl 150mM NaCl and 2mM MgCl$_2$, 28µl of protease inhibitors (Roche) and 2µl of Nonidet P-40 (NP-40). The cells to be lysed are harvested and pelleted and the pellet is then washed in 5ml PBS. The PBS is drained off and the pellet resuspended in an appropriate volume of lysis buffer dependant on the pellet volume (for a T25 this volume is ~100µl). The pellet is vortexed in the lysis buffer for 30 seconds and spun at 2300rpm (560g) for 2 minutes. The supernatant is transferred to a fresh 1.5ml centrifuge tube and diluted with an equal volume of 10mM Tris-HCL pH 7.5. The cell lysate is then aliquoted and stored at -80ºC until required.

2.3.4.2 *Bradford Assay.*

Bovine serum albumin (BSA) standards are made by diluting an appropriate volume of 1µg/µl BSA in water to give standards of 0µg, 2µg, 5µg, 10µg, 15µg and 20µg in 800µl dH$_2$O, to which is added 200µl of Bradford reagent (Biorad). The samples of unknown protein concentration (cell lysates, prepared as in 2.3.4.1) are then prepared, two mixes are prepared one containing 1µl of cell lysate (plus 799µl of water) with 200µl of Bradford reagent and the other containing 5µl of cell lysate (plus 795µl of water) with 200µl of Bradford reagent. The samples are then loaded on to an optical bottom plate, which is loaded on to the automated plate reader and a report and standard curve generated. The concentration of protein per µl can then be calculated using the standard curve.

2.3.4.3 *Sample preparation.*

The concentration of protein to be loaded is determined as above using the Bradford assay. Each sample is loaded in a final volume of 10µl. 5µl of sample buffer is added to 5µl of Kaleidoscope prestained standards. The samples and the ladder are then denatured at 37ºC for 30mins or 95ºC for 10mins depending on protein to be probed. Following denaturation, 10µl of each sample is loaded into each well and the gel is run at 75V until the dye enters the separating gel (75V, 17mA for ~15 minutes). When the

dye has entered the separating gel the running voltage is increased to 150V and the gel is then ran until the dye runs off the bottom (150V, 24-26mA for ~1hour 15 minutes). For precast gels (Biorad) the gel is ran for 1hour at 120V.

2.3.4.4 *Protein Transfer.*

When the proteins have been separated on the gel they are then transferred to a nitrocellulose PVDF membrane. To achieve this transfer the gel is separated from the gel running assembly and the bottom right hand corner of the gel is nicked to allow the membrane to be properly orientated. The gel is then soaked for 15 minutes in chilled transfer buffer on a shaking platform. During this time 4x filter papers (10x8cm) are cut as well as one piece of PVDF membrane (Millipore) (5x8cm). The bottom right hand corner of the membrane is nicked to allow gel and membrane to be correctly aligned and for orientation purposes. The membrane is activated in 100% methanol for 15 seconds, washed in 5x dH$_2$O and equilibrated in transfer buffer for 15mins, on the shaking platform with the gel.

The transfer apparatus is then assembled as follows, (all the components are pre-wet in transfer buffer); firstly the black side of the cassette is placed at the back, this is followed by a sponge, then 2x filter paper, then the gel, the membrane, 2x filter paper, a second sponge and the cassette is then closed. The assembled cassette is then placed into the transfer tank with the black side towards the back, closest to the negative electrode. The tank is then filled with cold transfer buffer. This is stirred during the transfer using a magnetic stirrer. The proteins are transferred by running this assembly at 300mA for 3 hours (300mA, 65V).

2.3.4.5 *Coomassie Blue staining.*

Following transfer of the proteins the gel is placed in Coomassie blue stain and left for 30mins-1hour on the shaker at room temperature. The stain is poured off and the gel is rinsed in dH$_2$O. The gel is then incubated in de-stain overnight in the cold room. An image of the gel can then be captured using white light on the UV gel documentation system to check the transfer of proteins to the membrane.

2.3.4.6   *Immunoblotting of the PVDF membrane.*

Non-specific binding sites are blocked by incubating the membrane in 5% milk in TTBS overnight in the cold room on a shaking platform. The following morning the membrane is incubated with the primary antibodies (Table 2.3) diluted in 5% milk in TTBS for 60mins at room temperature on a shaking platform. The membrane is then washed in TTBS for 2x5mins and 1x10mins on the shaker at room temperature to remove excess primary antibody. The membrane is then incubated with the appropriate horseradish peroxidise conjugated secondary antibody for 60mins at room temperature on a shaking platform. Finally, the membrane is washed in TTBS on the shaker for 2x5mins and 1x15mins.

Antibody	Size of Antigen (KDa)	Dilution
Mouse β-Actin (Sigma)	42	1 in 30000
Rabbit TOM20 (Santa Cruz)	30	1 in 1000
Mouse anti-Porin (Abcam)	39	1 in 1000
Rabbit LC3 (Cell Signalling)	17/19	1 in 1000
Rabbit ATG12 (Cell Signalling)	16/55	1 in 1000
Guinea Pig p62 (Progen)	62	1 in 700
Mouse C120 (Abcam)	20	1 in 1000
Mouse COXI (Abcam)	37	1 in 1000

Table 2.3. Antibody concentrations for western blotting

Table shows manufacturer, size of antigen and optimized dilution.

2.3.4.7   *Signal development.*

To detect the secondary antibodies various methods were used. Firstly the Amersham Bioscience ECL Plus Western Blotting detection kit was used. 2ml of reagent A is mixed with 50µl of reagent B and this mix is then incubated with the membrane for 5 minutes. The membrane can then be scanned using the phosphor imager or exposed to photographic film. For film exposure the membrane is exposed to the photographic film in the dark in a cassette for an appropriate time period. The film is then developed in developer until bands are at appropriate strength, then washed in fixative and finally washed in water. The film is then allowed to dry before imaging. Later runs were developed using the Amersham Bioscience ECL prime Western Blotting detection kit. 1ml of reagent A is mixed with 1ml of reagent B in which the membrane is incubated

for 5mins. Bands are then visualised using the ChemiDoc System (Biorad) and analysed using Imagelab software (Biorad).

2.3.5 **Immunocytochemistry**

2.3.5.1 *Growing Cells*

Prior to growing cells for staining, 22mm glass coverslips were treated with 250µl of PDL (1µg/ml) for 30mins and following three washes in PBS, 25µl of laminin (2 µg/ml) for a further 30mins. Cells were seeded at an appropriate density from which they would reach ~70% confluency on day of imaging. When sufficient growth was achieved cells were washed once with PBS, fixed in 4% PFA for 10mins, washed three times in PBS, and left in the final wash at 4^oC in preparation for staining.

2.3.5.2 *Staining Cells*

On day of staining, coverslips are incubated in 100µl 5%NGS (made up in PBST) for 30mins. Primary antibodies (Table 2.4) are then incubated at room temperature for 90mins made up in 5%NGS. Following this coverslips are washed three times in PBST. Appropriate secondary's are used at preoptimised concentrations , again made up in 5%NGS, and incubated for 60mins at room temperature. For fluorophore conjugated secondary's, incubations were undertaken in the dark. After this time, the coverslips were once again washed three times in PBST, followed by two washes in PBS. Coverslips were inverted onto clean microscopy slides and mounted with Vectashield+Dapi (Vector Labs) or ProLong® Gold Antifade Reagent (Life Technologies). For long term storage coverslips were sealed with nail varnish and stored at -20^oC in the dark.

Antibody	Dilution
Rabbit Beclin 1 (Abcam)	1 in 200
Rabbit ATG5 (Abcam)	1 in 100
Rabbit LC3 (Cell Signalling)	1 in 200

Table 2.4. Antibody concentrations for ICC

Final working dilutions for ICC antibodies.

2.3.6   **Immunohistochemistry**

2.3.6.1   *Basic Dual Immunohistochemistry Protocol*

In order to study two proteins in the same section, a dual immunohistochemical assay was performed, staining firstly for a marker of interest followed by C120 to assess mitochondrial protein levels. The staining protocol can be seen in Figure 2.2 and briefly consisted of deparafinisation through two sequential histoclear incubations and rehydration through a series of graded alcohols to water. High temperature EDTA antigen retrieval at pressure was used for all antibodies to allow access to the antigen. Following a wash in distilled water endogenous peroxide activity was blocked using 30mins incubation in 3% hydrogen peroxide if the method for signal detection/ amplification required it. The sections were then washed in phosphate buffered saline at pH 7.4 (PBS) before being blocked in 1% normal goat serum (NGS) made up in PBS for 30mins. The blocking stage reduced background staining and nonspecific binding of proteins as all primary antibodies were produced in goat.

The protocol then requires two rounds of primary and secondary incubations. All primary antibodies were incubated for 90mins or overnight at $4^{o}C$ at predefined concentrations and following a PBS wash, appropriate secondary antibodies were added for 60mins at room temperature. Upon completion of both incubations and secondary detections, sections were counterstained with 1:200 Hoechst made up in dH_2O for 30mins at room temperature before sudan black in 70% ethanol treatment was applied to quench autofluorescence for 10mins. Following this 4 fast PBST washes and 3 PBS washes are completed over 10mins before mounting and fixation in ProLong® Gold Antifade Reagent (Life technologies).

Antibody	Dilution
Rabbit Beclin 1 (Abcam)	1 in 300
Rabbit ATG5 (Abcam)	1 in 400
Rabbit LC3 (Cell Signalling)	1 in 200
Guinea Pig p62 (Progen)	1 in 100
Mouse C120 (Abcam)	1 in 100
Mouse C119 (Abcam)	1 in 100

Table 2.5. Antibody concentrations for IHC

Final working dilutions for IHC antibodies.

Deparaffinising (25mins at 65 °C)

Rehydration through Histoclear and graded alcohols to water

40 minutes high temperature retrieval in 1mM EDTA, pH 8.0 at pressure

Washed in Distilled water (dH_2O) and endogenous peroxidase activity blocked in 3% H_2O_2 for 30mins

Washed in Phosphate buffered saline pH7.4 (PBS)

Blocked in 1% Normal Goat Serum (NGS)

Primary Antibody applied overnight

Washes in PBS

Fluoro conjugated secondary applied for 90mins

Washes in PBS

Primary autophagy antibody applied for 90 mins

PBS wash

Fluoro conjugated secondary applied for 90mins

PBS Wash

Hoechst nuclear dye applied for 30mins

PBS wash

Sudan black treatment for 10mins

Fast PBST and PBS washes

Mount and seal

Figure 2.2. Dual immunohistochemical protocol

Schematic outlines main stages of dual immunohistochemical assay for day one (pink) and day two (blue.) For details see text.

101

2.3.7 **Live Cell Imaging**

2.3.7.1 *Growing Cells*

Cells were seeded at a density of 30,000-100,000 cells (dependant on cell type) in iBIDI dishes (Thistle Scientific) or WillCo-dish® (WillCo Wells). For ES cells the surfaces were coated in 400µl of 0.1% gelatine to aid adhesion. All cell types were given 2mls normal growth media and allowed to settle for at least 24hrs. Imaging was performed when cells were between 50% and 80% confluent. On day of experimentation, cells were washed in appropriate assay buffers and all staining incubations carried out in a volume of 1ml unless otherwise stated.

2.3.7.2 *Live cell Dyes*

All dyes were tested for optimal working concentrations prior to experimentation. For Tetramethyl Rhodamine Methyl Ester (TMRM) (Invitrogen) staining, cells were washed in KRB buffer with 5.5mM glucose, 1.3mM Ca_2 and 5nM TMRM then incubated in 1µl 5nM TMRM in normal growth media for ten minutes and finally washed and left in growth media for imaging. For PicoGreen (Invitrogen) staining, 3µl was used in 1ml of media and added 45mins prior to imaging.

Mitotracker (Invitrogen) was routinely used at a concentration of 150nM (red/deep red) and 100nM (green) in normal growth medium and incubated for 20mins, the solution was then removed and replaced with prewarmed growth medium. For visualisation of mitochondrial membrane potential, JC1 (Invitrogen) was used at a concentration of 2µg/ml in warm growth media and incubated for 20mins. To image, cells were illuminated at 488nm and the emissions were collected between 515/545nm and 575/625nm.

For live autophagosome detection, CytoID Autophagy Detection Kit (Enzo Life Sciences) was used, briefly 500µl of assay buffer was diluted in 4.5mls deionized H_2O supplemented with 5% FBS, in which cells were washed twice. Dual detection reagents were prepared in assay buffer through addition of 2µl cytoID and 1µl Hoechst (optional) in 1ml. Cells were incubated in 400µl of dual detection reagent for 25mins

before a further wash with assay buffer. Cells were then imaged in assay buffer or normal growth media depending on cell type.

2.3.7.3   *Imaging (Confocal and TIRF)*

Majority of live cell imaging was undertaken on a Nikon A1R point scanning confocal microscope, housed in a 5% CO_2 $37^{o}C$ controlled chamber. The microscope employs hardware focal drift correction and is fully-enclosed in a darkened, heated environmental chamber with the ability to set, maintain and monitor temperature, humidity, CO_2 and O_2 levels as imaging conditions dictate. A 65x oil immersion lens was routinely used to monitor individual cells. For prolonged time course experiments resonant scanning was utilised to minimise cell exposure to lasers and subsequent photo bleaching. Temporal image capture was dictated by specific dyes; number of dyes used and z stacks captured as well as cell type (see methods development 3.3/3.4). For total internal inflection microscopy (TIRF) experiments, Nikon Eclipse Ti inverted microscope was used with images being taken every second, captured using a Photometrics Evolve 512 EM CCD camera for 20–30 minute periods and recorded using Nikon Elements software.

2.3.7.4   *Quantification and Analysis*

Analysis of live cell work was carried out on IMARIS software (Bitplane). For mitochondria tracking, mitochondria were first defined as surfaces and using a touching components algorithm tracked through multiple time points. For analysis of autophagosome formation images were captured in z stacks enabling 3D reconstruction in IMARIS. Autophagosome number and volume were then measured and compared for cell lines. From this, association between autophagosomes and mitochondrial structures was analysed.

2.3.8 **Cloning, transformation and transfection.**

2.3.8.1 *Growing up plasmid stocks*

GFP-tagged open reading frame clone of mouse MAPLC3b was obtained from Origene Bioscience. Stocks were grown up on agar plates (5g NaCl, 5g tryptone, 2.5g yeast extract, 10g agar) containing 100mg/ml ampicillin .

2.3.8.2 *Transformation*

An aliquot of SOC medium is removed from the freezer and put into a 42ºC water bath. The XL10-Gold Kan Ultra competent cells are thawed on ice. The cells are gently mixed by hand and 40µl of the cells are aliquoted into one 500µl eppendorf tube for each insert plus one negative control. To this is added 1.6µl of β-mercaptoethanol mix (provided with the cells) and the contents of the tube are gently swirled. The cells are incubated on ice for 10mins, swirling gently every two minutes. Following this incubation, 2µl of the ligated insert is added to the cells and swirled gently; this step is discarded for the negative control. The cells and the insert are incubated on ice for 30 minutes. When the 30 minute incubation has finished the tubes are heat pulsed at 42ºC for 30 seconds and incubated on ice for 2 minutes. 450µl of preheated SOC medium is added to each tube and this mix is then incubated at 37ºC for 1 hour with shaking at 225–250 rpm. During this time the required number of plates are removed from the cold room and allowed to warm to room temperature. After an hour's incubation the cells are spun at 1000rpm for 10 minutes. The supernatant is discarded and the cell pellet is resuspended in 150µl of fresh SOC medium at 42ºC. The 150µl of cells is pipetted onto the plate and spread out evenly using the aseptic technique. The plates are then incubated upside down overnight at 37ºC.

2.3.8.3 *Checking for inserts.*

The following morning the plates are removed from the incubator and the negative control is checked for an absence of colonies. Fresh plates are removed from the cold room and warmed to room temperature. From each plate 25-35 colonies are selected and grown in the 37ºC incubator for approximately four hours. During this time the tubes are prepared. 10µl of 10% triton-X is added to as many 200µl PCR tubes as colonies

picked. After the 4 hours, a small amount of the smeared colonies is picked and added to the triton. 1µl of this triton mix is then added to a standard PCR reaction to check the colonies for the required insert.

2.3.8.4 *Plasmid Purification*

Qiagen Miniprep was used to purify plasmid from bacterial pellets. To ascertain DNA quantity DNA elution was nanodropped before storage at -20^0C.

2.3.8.5 *Lipofectamine Transfection*

Lipid based transfections were carried out using Lipofectamine LTX with PLUS reagent (Invitrogen). Cells to be transfected were 70-90% confluent at time of experiment. Lipofectamine LTX reagent is diluted in serum-free medium such as Opti-MEM® Reduced Serum Medium. Plasmid DNA is then diluted in Opti-MEM® and plus reagent added. Diluted DNA is then added to diluted Lipofectamine (1:1 ratio). The DNA lipid complex is then added to cells and incubated for 1-3 days. Following transfection cells were returned to the 37^oC incubator and GFP expression was assayed for after 24hours. As per manufacturer's instructions a complexation plate was created to optimize the amount of plasmid DNA being used and the ratio of lipid to DNA. Although high numbers of transient transfects were achieved we were unable to attain stable transfected cells from this methodology and as such moved onto viral methods.

2.3.8.6 *Viral Transfections*

Viral particles for GFP-nuclear reporter tagged LC3 and GFP tagged LC3 were purchased from Millipore. The latter being LentiBrite ™ GFP-LC3 Control Mutant Lentiviral Biosensor, which importantly did not contain a selectable marker. The GFP-nuclear tagged LC3 served as a control for the other virus and the affect an additional GFP molecule had upon cellular trafficking and mitochondria morphology. All transfection work was carried out in Dr Chris Morris's lab with appropriate risk assessments in place. Cells were seeded to reach the optimal confluency of 40% on day of transfection. Media was replaced with pre-warmed media containing viral particles of MOI of 20. Alongside each transfection a non-viral control was included for each cell

line. For viral particles that contained a selectable marker the selection agent was applied after 48hrs. Those that were not selectable in such a way were analysed for GFP expression via microscopy, and to establish pure stable stocks subjected to FAC sorting.

Chapter
Three

Methods
Development

Chapter 3. Methods Development

Several aspects of this project required novel approaches to answer specific questions. As such, time was taken to develop experimental techniques and optimize pre-existing methodologies for use with the two main model systems in this work- the ES cybrid cell lines and human upper midbrain tissue. Specifically, areas that needed optimization were the bioenergetic assays for ES cells, the dual immunohistochemical assay and live cell assays including mitochondrial tracking in newly differentiated neurons alongside a method for concurrent mitochondria and autophagosome tracking.

3.1   BIOENERGETIC ASSAYS

3.1.1   Introduction

Mitochondrial bioenergetics are impacted on, and crucial for, cellular functioning and survival. Previous work has shown different mutations induce varying severity of respiratory dysfunction in the cybrid cell lines (Kirby *et al.*, 2009). To ascertain the extent to which the mutation affected oxidative phosphorylation in our cell lines, cellular bioenergetics were assayed. Results from these experiments would complement data previously generated on the enzymatic activity of respiratory complexes within these cells.

3.1.2   Aims of Study

To optimize a reliable method of assessing bioenergetics in the embryonic stem (ES) cells.

1. Optimize Oxygraph (Oroboros Instruments™) and Seahorse extracellular flux analyser (Seahorse Bioscience™) for use with ES cells.

2. Record bioenergetic differences between control and cybrid cells.

3. Assess parameters of mitochondrial functioning using OXPHOS inhibitors.

3.1.3 **Oxygraph**

Initially, bioenergetic analysis was undertaken using the Oxygraph (Oroboros Instruments). After multiple runs it was clear that the system would not enable the quantity of data required to be gathered, furthermore the background error was a concern (Figure 3.1-arrow). Although some differences were visible between complex I cybrids and controls (Figure 3.1 bottom graphs) it was deemed more subtle differences would not be picked up by this methodology. As such, bioenergetic assays were completed thence forth using the Seahorse extracellular flux analyser XF24 (Seahorse Biosciences, Massachusetts).
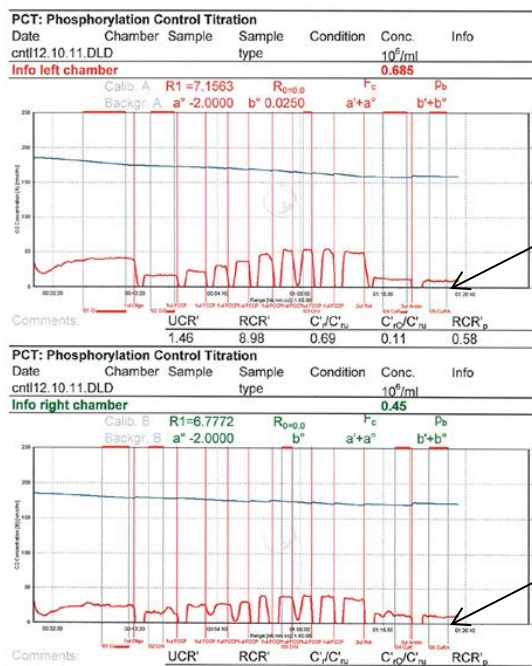
Figure 3.1. Oxygraph measurements.

Top graphs display traces from Oroboros Oxygraph for control and complex I cybrids. Arrows highlight background measurements that led to the rejection of this methodology. Bar charts display calculated parameters for the two Oxygraph chambers (top and bottom) again for control cells (left) and complex I cybrids (right). Cr- Routine resp, CrO-following oligomycin addition, Cru-Maximal after FCCP addition, CruRA- After antimycin addition and CrR- after rotenone admission.
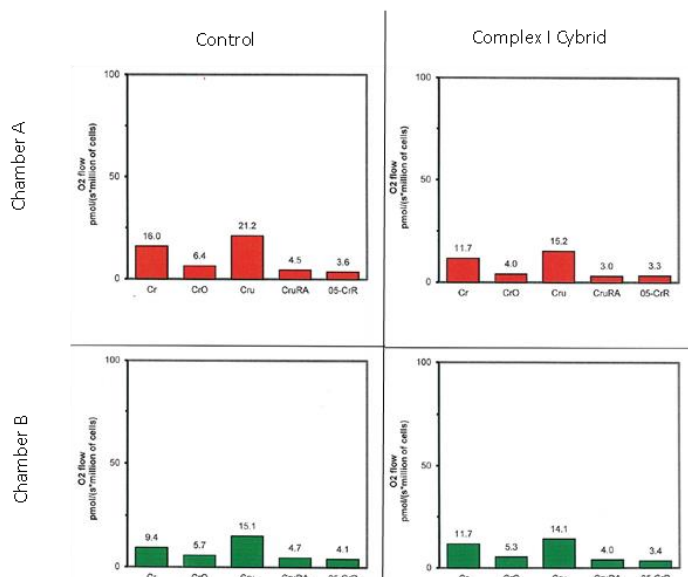
3.1.4   **Optimization of Seahorse extracellular flux analyser XF24**

Various stages of optimization were required as the embryonic stem (ES) cells had not previously been used in the seahorse bioanalyser. Initially, the cells ability to grow in the specialized seahorse plates (Seahorse Biosciences, Massachusetts) was assessed, noting the need for further plate coating. Appropriate cell numbers are also essential for the success of the seahorse run and value of the data collected. For the ES cells, seeding densities ranging from 25,000-100,000 cells/well were assessed (Figure 3.2). The composition of the experimental media is also assay dependent, with FBS supplementation and pyruvate concentration varying for cell type. As such, these were also optimized for the ES cells. Finally, OXPHOS inhibitors were optimized. This was especially important with FCCP, as the titration curve is known to be quite sharp, and too much FCCP has been shown to diminish responses in Oxygen Consumption Rate (OCR), a balance was therefore needed between a concentration capable of achieving maximal respiratory capacity without inhibiting OCR.

3.1.5   **Results**

3.1.5.1   *Cell Number and plate coating*

Although ES cells initially adhered to the uncoated seahorse plates, after several hours, 'clumping' was observed, and a number of cells detached from the surface of the plates (Figure 3.2). Given the number of washes involved in the seahorse protocol, 100µl of 0.1% gelatine was used to ensure adherence throughout experimentation in all future runs. The amount of media used throughout the run was also tested (Figure 3.3.A). Both 250µl and 500µl showed comparable results. Cell densities of 25,000, 50,000, 75,000 and 100,000 were assessed. Densities of 50,000-100,000 cells/well were seen to provide the desired OCR (~400-800pmoles/min). Future runs were carried out at 75,000 cells/well.

3.1.5.2   *Pyruvate and FBS concentrations*

10mM pyruvate and 2% FBS were added to experimental runs. Serum is ordinarily omitted from the final media formulation as it may affect the buffer capacity of the

media, however, in the case of the ES cells, it was deemed necessary for maintaining

cell viability. Experimental media therefore contained 2% FBS compared to 5% in

normal growth media. Cell viability was maintained at this level and the addition of

FBS was not seen to impact on buffering capacity (Figure 3.3.B).
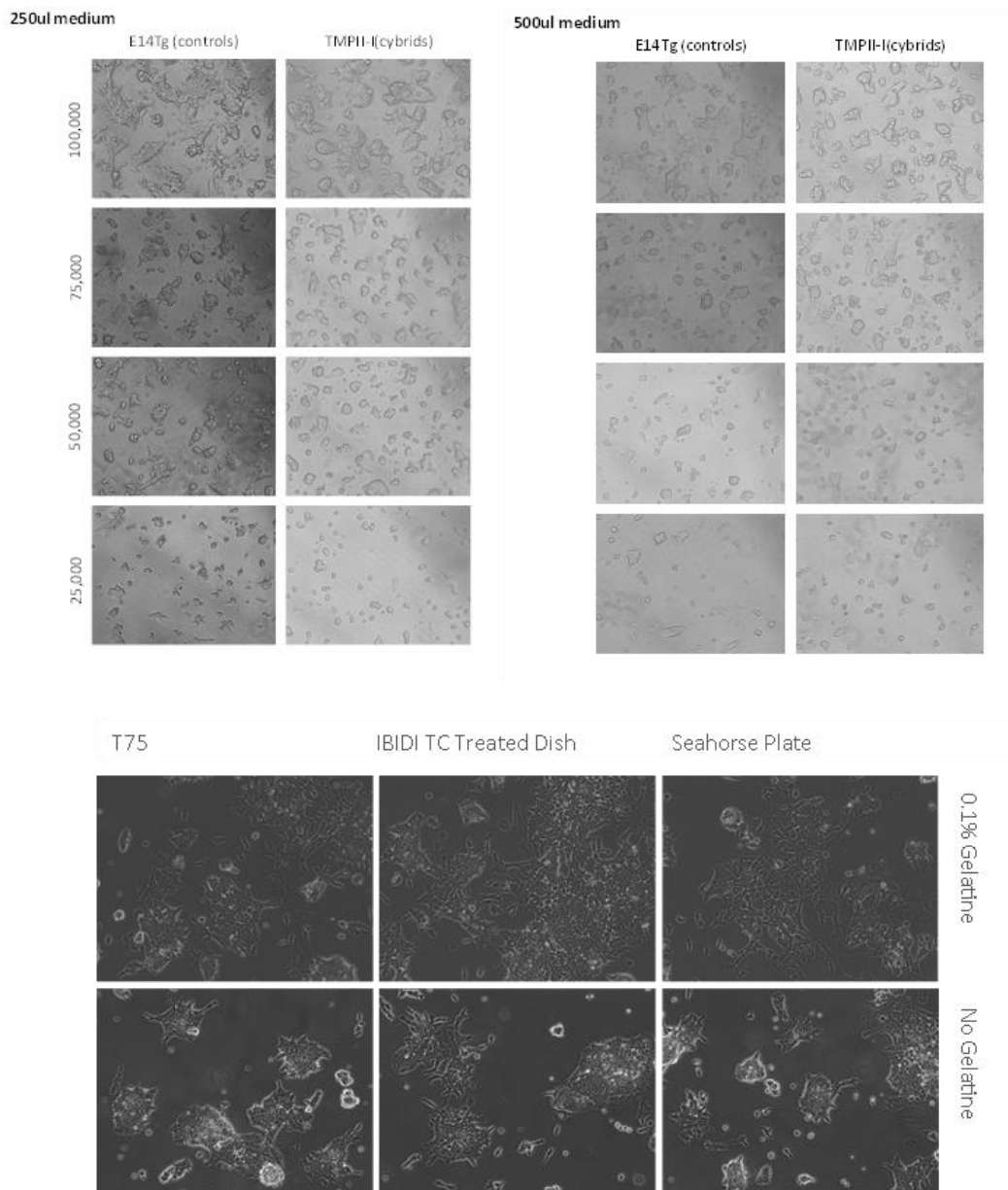
Figure 3.2. Optimization of seahorse extracellular flux plates

Prior to bioenergetic assays being performed on the Seahorse Extracellular flux analyser Xf24, conditions specific to ES cell growth had to be optimized. This included, growth media volume and cell density (top panel). The coating of different plates was also assessed for its effect on cellular morphology and viability (lower panel).

Concentrations of 1-10 mM pyruvate were tested to understand the optimal
concentration of pyruvate to obtain maximal respiration (Figure 3.3.C). The presence
and concentration of pyruvate has been shown especially important in obtaining the
maximal respiratory capacity due to FCCP. Seahorse Bioscience have previously
reported a number of cells lines in which the omission of pyruvate abrogates the ability
of cells to respond maximally (above baseline) to FCCP. ES cells were able to respond
maximally through all concentrations tested. 10mM was selected to ensure pyruvate
availability could not be a limiting factor in OXPHOS.

Figure 3.3. Optimization of conditions for seahorse run

*A. Cell numbers, B. Addition of FBS and C. Concentration of pyruvate were all assessed for seahorse
runs utilising the ES cells (N=20wells/experiment).*
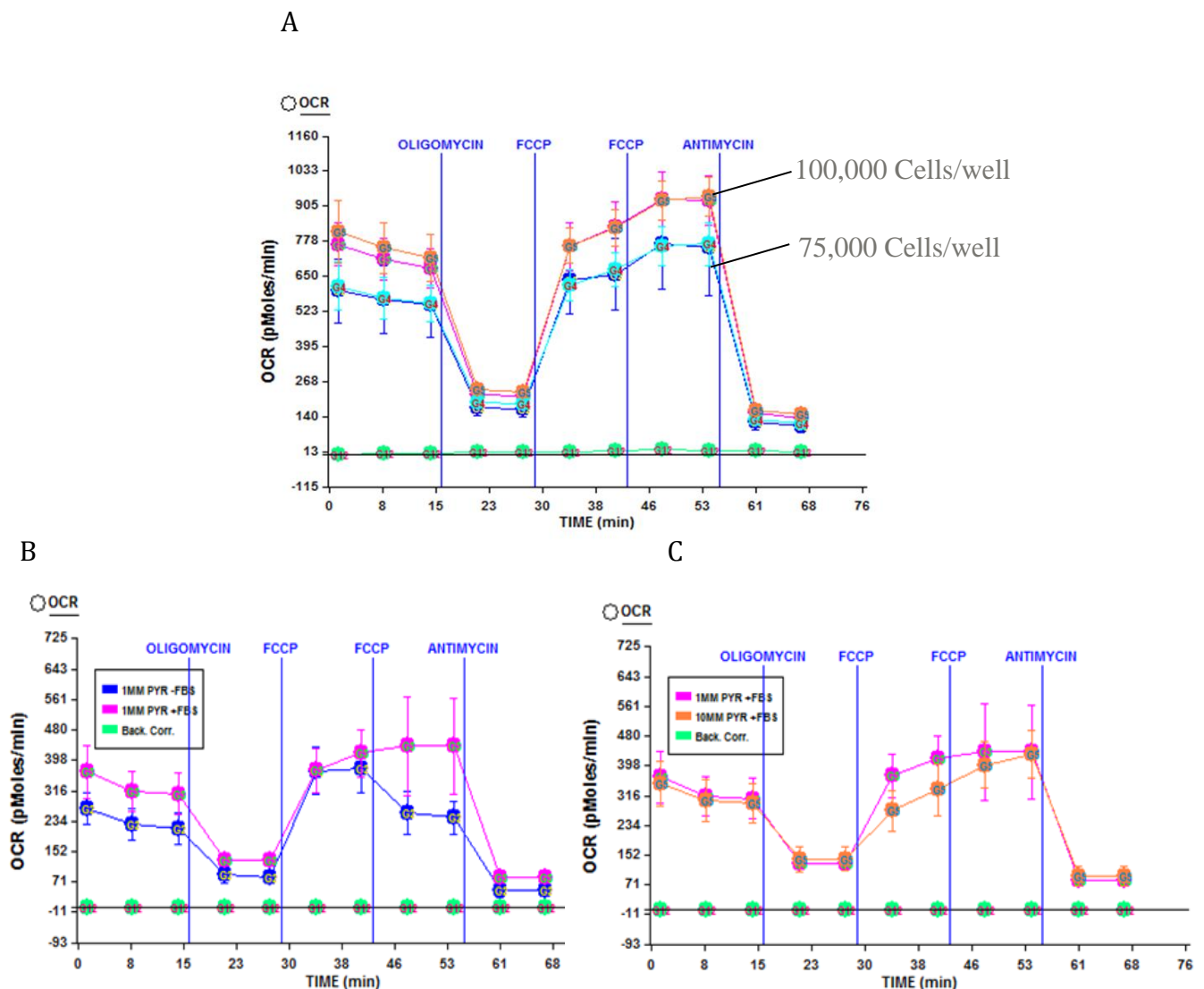
3.1.5.3 *Injection Titration*

OXPHOS inhibitors were tested as per manufacturer's instructions (Table 3.1). Final concentrations were:

Compound	Experimental Range	Working Concentration
Oligomycin	0.1 – 1.0 µg/ml	1ug/ml
FCCP	0.1 – 5.0 µM	2uM
Rotenone	0.1 – 1.0 µM	0.5uM
Antimycin	NA	2.5uM

Table 3.1. Tested and working concentrations of OXPHOS inhibitors

Commonly used OXPHOS inhibitors were used at pre-optimized concentrations specific for the ES cell bioenergetic assays. These values were often lower than those routinely used with other cell lines such as fibroblasts.

3.1.6 **Conclusions**

The seahorse extracellular flux analyser (Seahorse Biosciences) provided the most robust assay for analyzing the ES cell lines bioenergetic capacity. The multi-plate, automated interface enabled several cell lines to be ran in parallel controlling for experimental variation. The ES cells morphology and growth rates were not altered by the conditions within the seahorse plate, although supplementation with FBS and pyruvate was deemed necessary to ensure cell viability. Cell concentration did not exceed 100,000 cells/well of the seahorse plate.

3.2   IMMUNOHISTOCHEMICAL OPTIMISATIONS

3.2.1   Introduction

To enable observation of mitochondrial dysfunction and autophagy in human tissue, time was spent optimizing a dual immunohistochemical protocol. Several issues had to be overcome to establish this methodology. Firstly, the upper midbrain sections being used in this study express high levels of autofluorescence; as such a method for quenching this signal was required. Autofluorescence in this region is caused by various factors; the accumulation of age related inclusions, the naturally occurring neuromelanin pigment in substantia nigra neurons and the paraffin fixation process. The process of paraffin fixation can result in the production of fluorescent products through Schiff-acid base reactions causing high background fluorescence and unspecific reactions with antibodies (Beisker *et al.*, 1987). Importantly, the chosen quenching process needed to sufficiently remove the background without diminishing the signal of the markers to be studied.

In order to gain the best possible results from the immunohistochemistry, time was also spent selecting the most appropriate antibodies and furthermore, the optimal working conditions for each of these. Antibody selection was based on a screen of prior peer reviewed literature with emphasis on antibodies which had been utilised in the same or similar protocol as this study's. To ensure high sensitivity and specificity, the optimal working concentration of each antibody needed to be established. A balance was required between maximal signal strength and minimal background noise and/or nonspecific staining

3.2.2   Aims of Study

To optimize dual immunohistochemical assay

1. Optimize antibody concentrations and incubation conditions

2. Develop a method of quenching autofluorecence.

3.2.3   **Methodological Approach**

To assess two markers in parallel two immunohistochemical methodologies were initially trialed. Firstly, chromagen staining followed by signal separation through nuance imaging software (Perkin Elmer). With this method certain antibodies required further amplification of signal, for which, various methods were trialed (3.2.3.1). The second method employed fluorescent staining whereby signals of multiple markers could be separated on the basis of their different excitation spectra.

As many antibodies were novel to this methodology they were initially optimized independently with chromagen staining in human colon to ensure the antibodies were working (Figure 3.4). The decision on which concentrations to test were based on a combination of the manufacturers' recommended dilutions (if given), and assessments of the literature. For antibodies that had not previously been used in this experimental setting the search parameters were widened and a greater number of concentrations were tested. When antibodies were shown to be effective, they were then optimized fluorescently, again singularly in colon followed by upper midbrain sections. All antibody concentrations were then checked following sudan black treatment to ensure the signal and specificity remained. Finally, for dual staining, antibodies were once again checked to ensure signal was retained. Throughout optimization, the inclusion of a 'no primary control' was used where the omission of the primary antibody ensures against nonspecific binding.
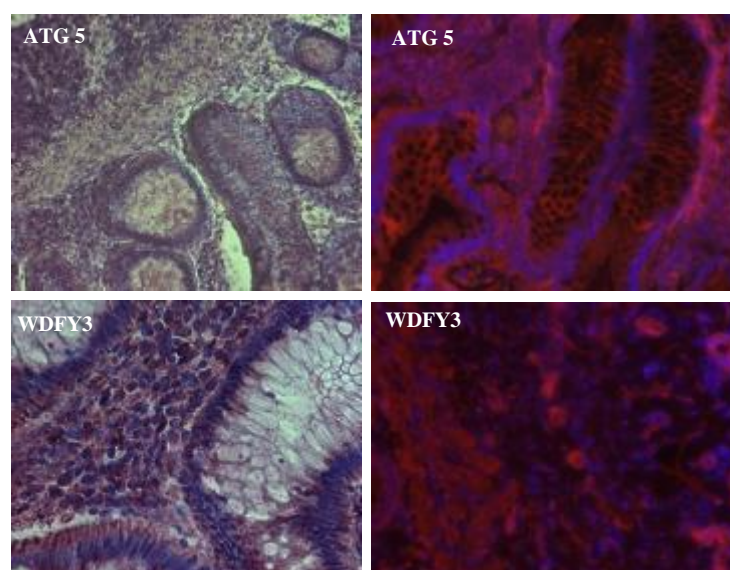
Figure 3.4. Initial trials of autophagy antibodies.

Preliminary antibody tests were undertaken in control colon tissue and optimized for chromagens (left) and fluorescent secondary's (right).

3.2.3.1   *Signal Amplification*

To increase weak chromagen staining, various different signal amplification methods were trialed.

3.2.3.1.1   Avidin Biotin Complex Kit

Avidin is a glycoprotein that possesses four binding sites for biotin. Biotin is a small vitamin that has a single binding site for avidin. The avidin biotin complex (ABC) (Vector Laboratories) takes advantage of the high affinity of avidin for biotin (Figure 3.5). The ABC method utilizes a biotinylated secondary antibody which targets the unlabeled primary antibody bound to tissue antigen. The third reagent is a large complex of avidin mixed with biotin which has been labeled for example with peroxidase. This is mixed prior to application so that proportions of avidin and biotin in the complex are adjusted to give just enough free binding sites to bind the biotinylated secondary antibody. Detection in this method is achieved through a label conjugated to the biotin molecules of the ABC which is then visualized using a chromagen. As many biotin molecules are bound in complex there is an increased amount of label at the site of reaction, and so amplification of the signal is greater. Certain considerations with this technique are that the ABC may become too large and be hindered by steric effects while trying to access the bound primary antibody.

3.2.3.1.2   Polymer Kit (Chromagen Staining)

Following deparaffination, rehydration, antigen retrieval and endogenous peroxidase blocking, the primary antibody was incubated for 90mins. Following a TBST wash a universal probe (Menapath Kit, A. Menarini Diagnostics), which recognizes the mouse epitope of the primary antibody, was applied to the section for 30mins at room temperature. Following this incubation the sections were once again washed in TBST and incubated with a horse-radish peroxidase (HRP)-polymer (Menapath kit, A. Menarini Diagnostics) for a further 30mins at room temperature. This recognizes and binds the universal probe. Finally, visualization of the marker was achieved through incubation for 5mins with chromagen. Sections are then washed well in distilled water for 5 mins to remove unbound chromagen.
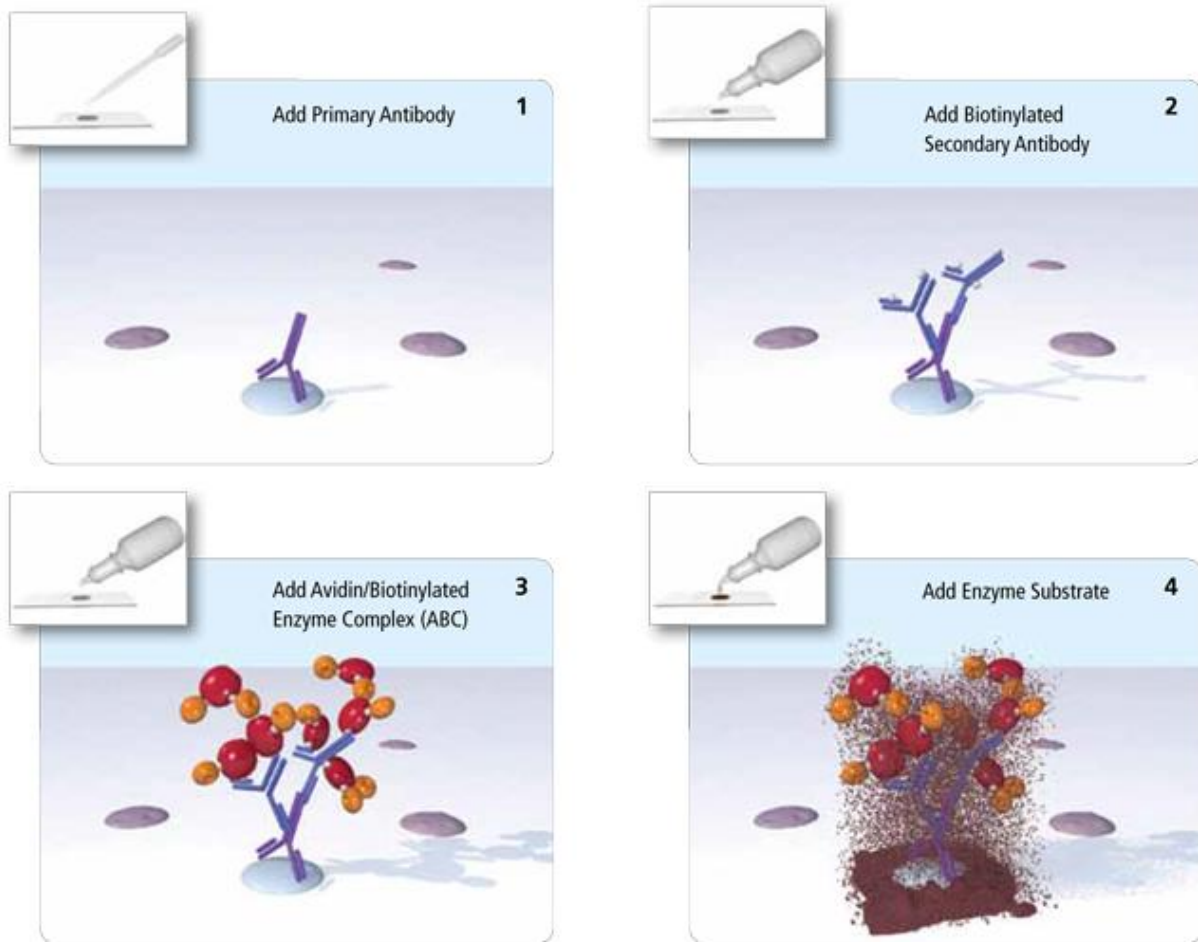
Figure 3.5. ABC signal amplification method

In the ABC method binding of the primary antibody to antigen is recognised by a biotinylated secondary. The Avidin/Biotinylated enzyme complex then associates, the addition of the enzyme substrate allows for visualisation of the marker of interest (taken from Vectorlabs.com).

3.2.3.1.3   Tyramide Amplification Kit (fluorescent staining)

Due to variance in the quality of mitochondrial staining, a new method for amplification was trailed. Tyramide Signal Amplification (TSA) (Invitrogen) is an enzyme based detection method (Figure 3.6). Incubation with primary antibodies occurs as per normal IHC protocol. Secondary detection is achieved through HRP conjugated secondaries. HRP converts the TSA reagent to a highly reactive free radical that binds covalently to electron-rich amino acids like tyrosine and tryptophan immediately proximal to the target resulting in minimal loss of signal localization. The TSA reagent is labelled with a fluorophore (alexa fluor 488/ alexa fluor 566) which can then be detected through fluorescent microscopy.

117
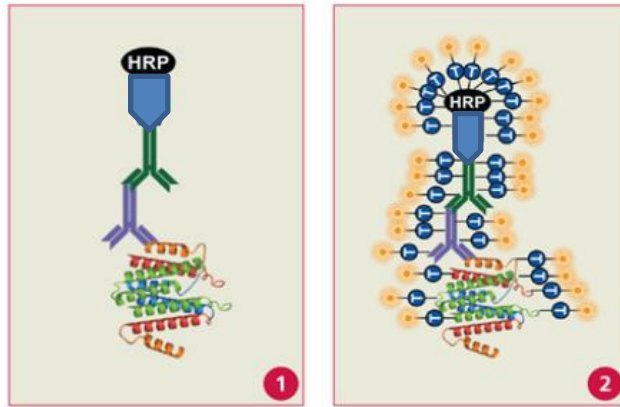
Figure 3.6. TSA Amplification method

HRP conjugated secondary's are used to identify primary antibodies (1). HRP then converts the TSA reagent to a highly reactive radical that binds electron rich amino acids close to the primary antibody. The TSA reagent is labelled with a fluorophore to enable visualisation (2). Modified from PerkinElmer.com

3.2.3.2   *Autofluorescence treatment*

Several methods of autofluorescence quenching were trailed, including irradiation, spectral unmixing and chemical treatments. Photobleaching through UV irradiation has previously been shown as an effective method for reducing autofluorescence signal (Billinton and Knight, 2001). This is achieved through altering the molecular structure of a fluorophore to the point whereby it loses its ability to fluoresce. UV exposure was carried out before removal of paraffin, tissue sections were irradiated with UV light at room temperature for two hours, after which they were transferred to PBS. A notable decrease in some but not all sections was observed, specifically substantia nigra neurons still showed high residual levels of autofluorescence. Next Sudan Black was assessed as a means for addressing autofluorescence. Chemical removal, specifically with Sudan Black has previously been used successfully to quench autofluorescence signal in multiple tissue types (Cowen *et al.*, 1985; Mosiman *et al.*, 1997; Clancy and Cauller, 1998). All experiments used 0.3% Sudan black made up in 70% EtOH, filtered through 0.2µm syringe tip filters. A range of incubation periods and washing protocols were tested as shown below in

Finally, spectral unmixing was employed to separate signals based on parameters predefined by measuring the background fluorescence on unstained sections. Due to the sheer level of autofluorescence in these samples and the variance between different tissue cases, this method was unable to distinguish actual signal from background without prior treatment with UV irradiation or sudan black treatment.

Table 3.2 and visualised in Figure 3.7. The method was also tested in combination with TSA amplification (Figure 3.8).

Finally, spectral unmixing was employed to separate signals based on parameters predefined by measuring the background fluorescence on unstained sections. Due to the sheer level of autofluorescence in these samples and the variance between different tissue cases, this method was unable to distinguish actual signal from background without prior treatment with UV irradiation or sudan black treatment.

Incubation Periods	Washes
10min	x3PBST x3PBS over 10mins
	x3PBST x3PBS over 5mins
	10washes with PBST LEFT IN PBS
20min	x3PBST x3PBS over 10mins
	x3PBST x3PBS over 5mins
	10washes with PBST LEFT IN PBS
30min	x3PBST x3PBS over 10mins
	x3PBST x3PBS over 5mins
	10washes with PBST LEFT IN PBS

Table 3.2. Sudan black incubation and wash optimization

Different lengths of incubation with sudan black and washing protocols were trialled to achieve the necessary level of autofluorescence quenching without seeing a marked reduction in signal or accumulation of SB precipitates.
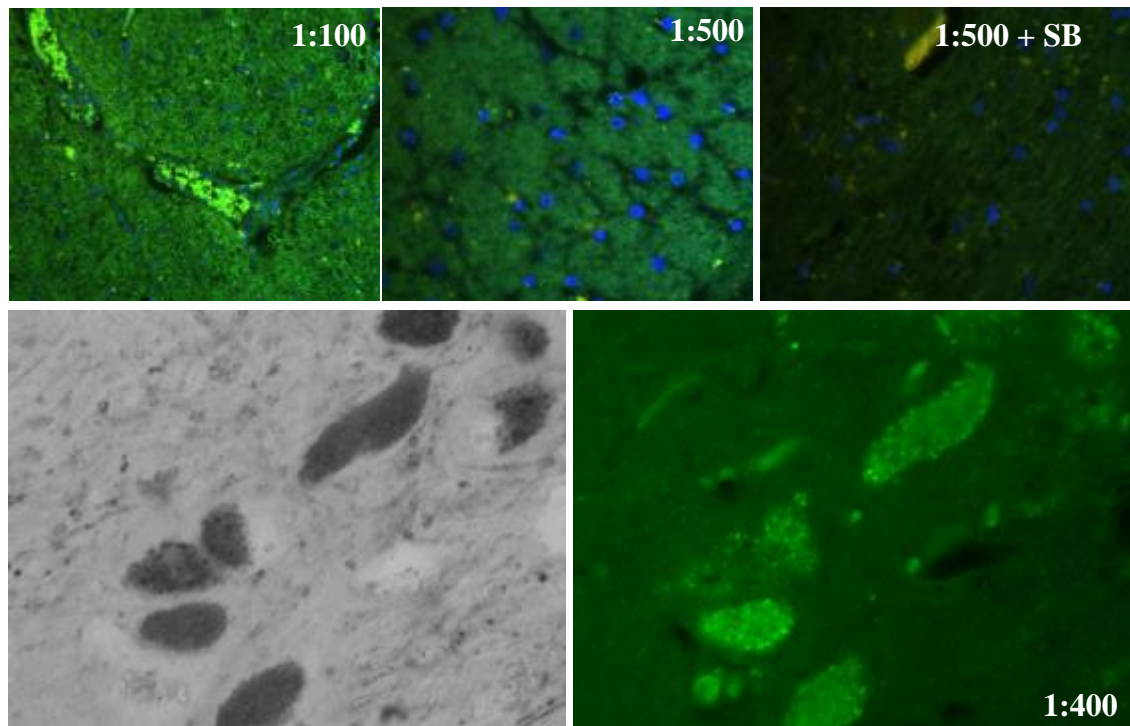
Figure 3.7. ATG5 optimization with sudan black treatment

Representative images of ATG5 immunofluorescent staining in upper midbrain sections. Top panel shows various concentrations and sudan black treatment (x20). Lower panel shows x40 mag images of SNc neurons showing desired pattern of ATG5 staining at 1:400 and following sudan black treatment.

Figure 3.8. Sudan black treatment and TSA.

Sudan black treatment worked alongside tyramide signalling amplification methods. Figure shows upper midbrain sections with SNc neurons. Sudan black effectively removed autofluorecence on unstained FITC and TRITC channels (top panel). Middle panel shows TSA amplification of autophagy marker (green) and mitochondrial marker (red) with optimal exposure. Bottom panel shows signal generated if TSA staining is baselined against non-stain controls.

Merge

FITC

TRITC

DAPI

Phase/DIC
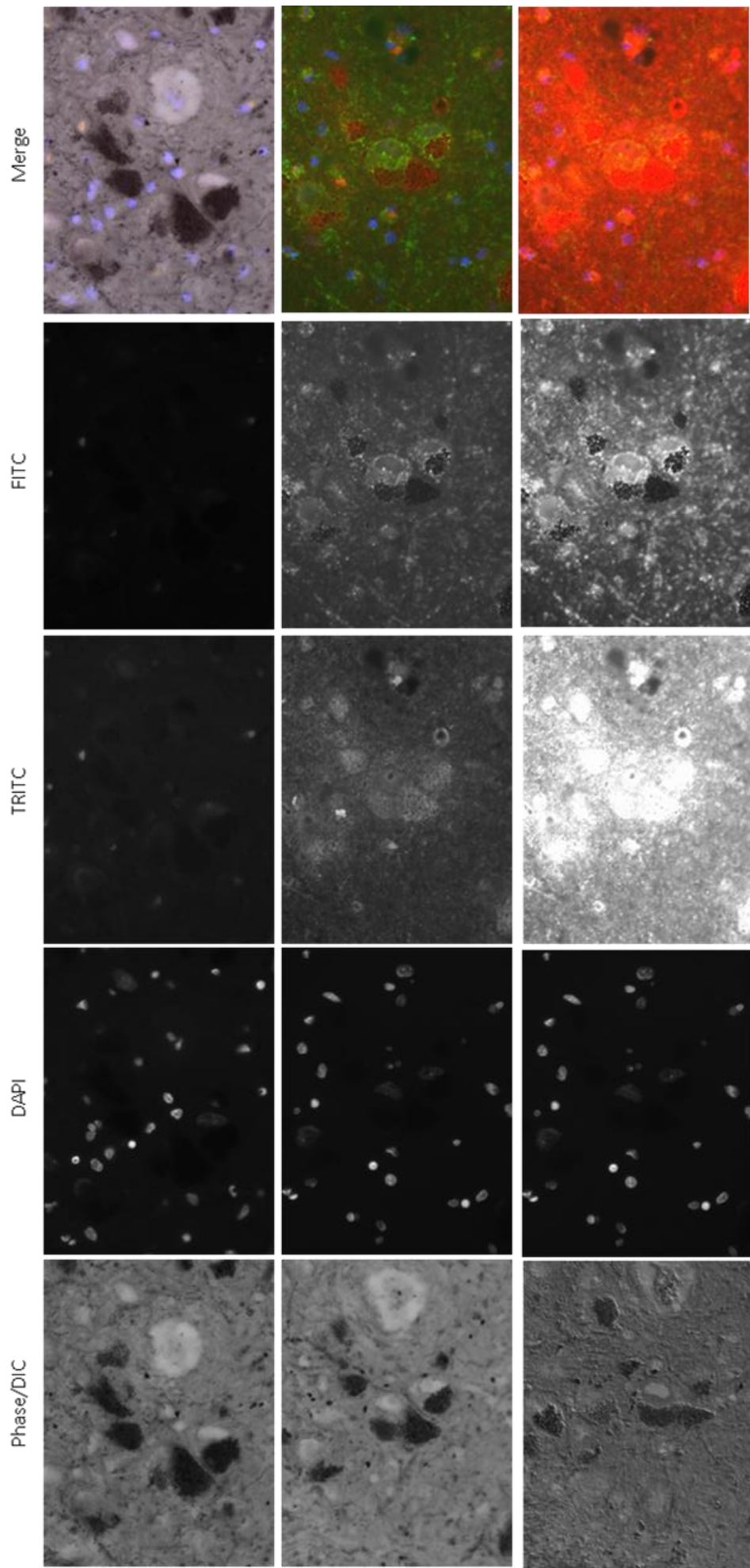
No Stain Control

Cl19 and Beclin1
Optimal exposure

Cl19 and Beclin1
Control exposure

120

3.2.4 **IHC Optimization Results**

To study two markers in parallel within the same neurons, different staining methodologies were tested. Due to the proximity of many of the markers it was clear nuance separation would not suffice for this project, subsequent experiments were therefore carried out fluorescently. Throughout the optimization of this project certain experimental hurdles had to be overcome. Sensitivity of antibodies, notably the complex I markers went through extremely variable phases. As such it was necessary to amplify signals using TSA kits described above. Despite successful amplification in some sections, variability remained and subsequent investigations established the antigen retrieval stage was where this variability was introduced. Upon replacement of the decloaker unit, amplification was no longer required and variability in sections was no longer an issue. Once this issue had been addressed the antibodies could be re-optimized. The following antibodies were selected for their specificity and reproducibility.

3.2.4.1 *Autophagy Antibodies*

3.2.4.1.1 Beclin1

Beclin1 is the mammalian ortholog of ATG6 in yeast and has a crucial role in the initiation of autophagosome formation. Human Beclin 1 is 450 amino acids in length with a molecular weight of 60kDa and forms part of a lipid-kinase complex, through its interaction with UVRAG and class III phosphoinositide 3-kinase (PI3K). The anti-Beclin 1 antibody (Millipore) recognises the C-terminus of the human beclin 1 protein. Concentrations were tested in the range of 1:100-1:2000. Antigen retrieval in the Decloaker (A Menrani, UK) immersed in 1mmol EDTA at pH8 was deemed an effective method for accessing Beclin 1 antigens along with a final working concentration of 1:300 with no further amplification.

3.2.4.1.2 LC3

Microtubule-associated protein 1A/1B-light chain 3 (LC3) is a ubiquitously expressed soluble protein with a molecular mass of ~16-18kDa. A homologue of yeast ATG8, LC3 is essential for autophagosome formation and subsequently macroautophagy. Post

translational modifications results in two distinct forms of LC3. Immediately following synthesis, cleavage of a C-terminal fragment of LC3 occurs to yield the cytosolic form- LC3-I (18 kDa). A subpopulation of LC3-I is further converted to a membrane bound form- LC3-II (16 kDa). LC3-II is formed through conjugation with phosphatidylethanolamine (PE) and subsequent recruitment to autophagosomal membranes upon initiation of autophagy. *De novo* autophagosomes form to engulf cytosolic components, including proteins and whole organelles. Once encapsulation has occurred the sealed autophagosome fuses with a lysosome where its contents are degraded by lysosomal hydrolases. Due to its specific association with autophagosome membranes, LC3-II is widely accepted as the most reliant marker of autophagosome formation.

The anti-LC3B antibody (Cell Signalling) detects endogenous levels of LC3B protein. Both LC3-I and LC3-II are recognised by this antibody although stronger reactivity is observed with LC3-II. Optimization of the primary LC3 antibody was performed as outlined in 3.2.3. Antigen retrieval in the Decloaker (A Menrani, UK) immersed in 1mmol EDTA pH8 was deemed an effective method for accessing LC3 antigens. A range of concentrations were applied, from 1:100-1:500, in addition to a no primary control. A working concentration of 1:200 was settled upon as this required no further amplification.

3.2.4.1.3   P62

P62 also known as sequestosome 1 (SQSTM1), is a ubiquitin-binding scaffold protein that colocalizes with ubiquitinated protein aggregates. P62 and LC3 have been shown to bind directly via a specific sequence motif. Accumulation of p62 shows indirect correlation with autophagy, with an increase observed when autophagy is inhibited and decreased expression when autophagy is upregulated. Furthermore, the protein itself is degraded via autophagy. As such autophagic flux can be inferred from p62 levels. The anti-P62 antibody (Progen Biotechnik) recognises the C-terminal domain of human p62. Optimization was achieved ia a similar methodology to LC3. Again, antigen retrieval was achieved through high pressure EDTA incubation. Dilutions in the range of 1:100- 1:200 were trialled. A working concentration of 1:100 was settled upon as this required no further amplification steps.

3.2.4.1.4   ATG5

ATG5 is an E3 ubiquitin ligase which associates with the isolation membrane and is necessary for elongation of the autophagosomal membrane and subsequent autophagy. It is activated by the ubiquitin E1-like enzyme ATG7 and the E2-like enzyme Atg10 forming a complex with ATG12 and ATG16L1. This complex supersedes, and is required for the formation of the LC3-PE conjugation. Heat mediated antigen retrieval in EDTA was once again used to gain access to the antigens. The anti-ATG5 antibody (Abcam) was tested at the dilution range 1:300-1:2000 with a final working concentration of 1:400 with no further amplification.
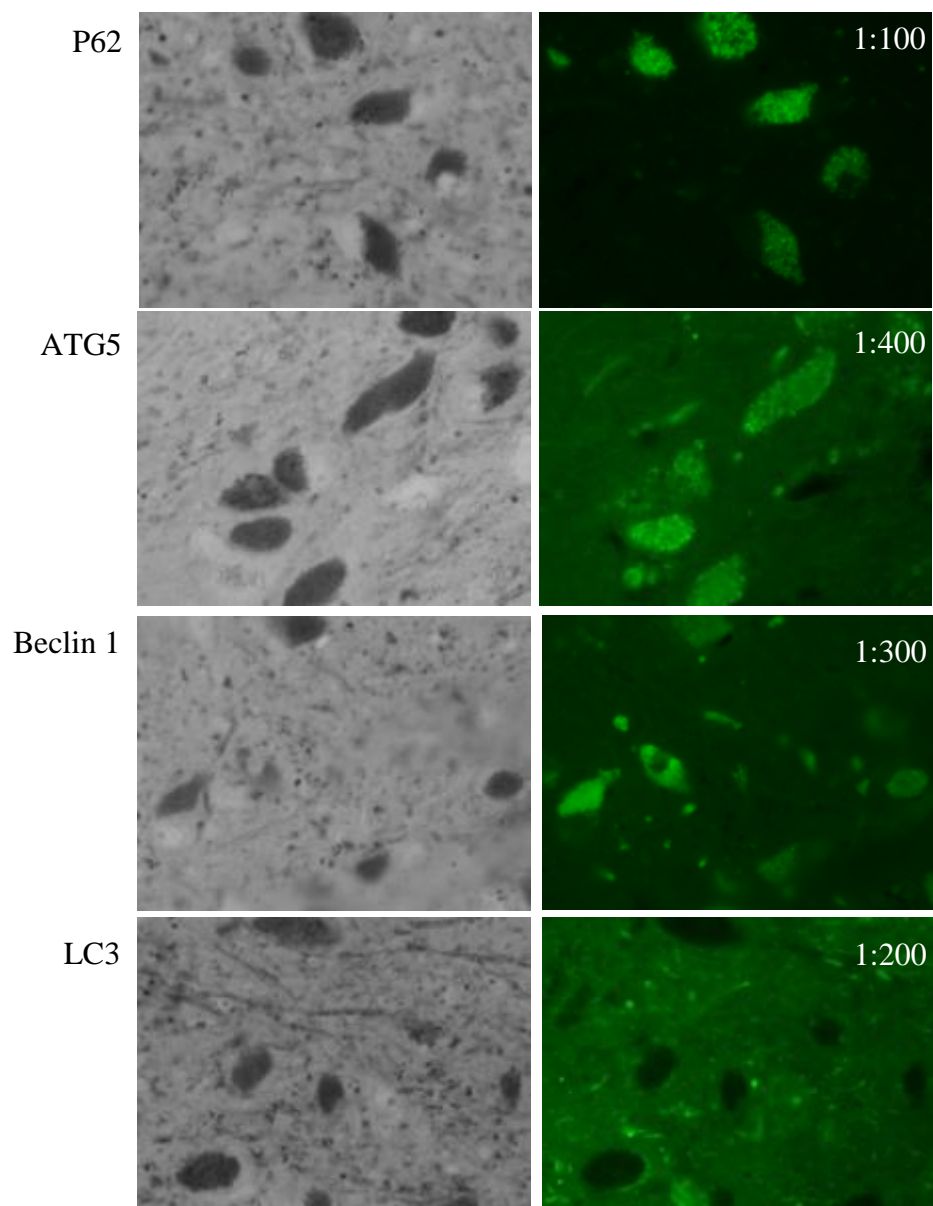
Figure 3.9. Final concentrations of autophagy markers

Following optimization final working concentrations were established for all autophagy markers as shown above.

3.2.4.2 *Mitochondrial markers*

3.2.4.2.1   CII9

CII9/GRIM19 (NDUFA13) is a subunit of the mitochondrial membrane respiratory chain NADH dehydrogenase (Complex I), which functions in the transfer of electrons from NADH to the respiratory chain. The protein is required for complex I assembly and electron transfer activity. Chromagen staining of the anti CII9 antibody (Abcam) revealed an effective working dilution of 1:300, however, when the protocol was moved to a dual fluorescent platform, sensitivity was severely diminished. To overcome this a higher concentration of 1:100 was used.

3.2.4.2.2   CI20

CI20 (NDUFB8) is an accessory subunit of the mitochondrial membrane respiratory chain NADH dehydrogenase (Complex I), that is believed not to be involved in catalysis. Importantly, CI20 has previously been associated with Complex I assembly (Triepels *et al.*, 2001a; Triepels *et al.*, 2001b; Lebon *et al.*, 2007). Similar weakening of the CI20 signal was observed in fluorescent staining compared to chromagen as described with CII9. As such, a working concentration of 1:100 was used. Importantly, when being used in conjunction with autophagy markers it was found that both mitochondrial markers signal diminished if stained for first. All experiments were therefore performed with autophagy markers being stained first followed by a mitochondria marker.
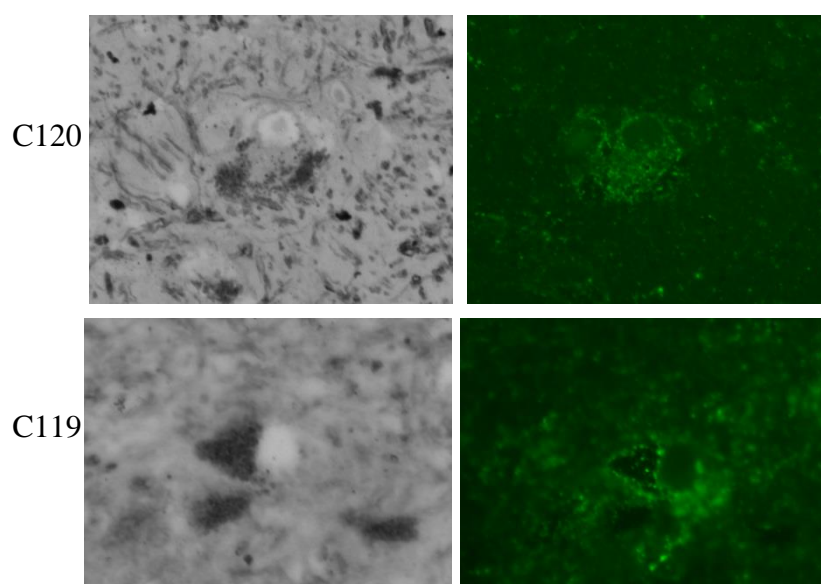
Figure 3.10. Final concentrations of OXPHOS antibodies
Both complex I subunit antibodies were used at a working concentration of 1:100

3.2.4.3 *Treatment of Autofluorecence*

UV treatment was ineffective in this experimental setting as a high level of autofluorecence was still observed following irradiation. Sudan black was chosen as the most effective method of autofluorecence quenching (Figure 3.11, Figure 3.12). Subsequent IHC was carried out to include a final 10 minute incubation with filtered 0.3% Sudan black made up in 70% ethanol, at room temperature. This was then removed with three fast washes in PBST followed by four PBS washes over 5mins to ensure no sudan black precipitates were left. These treatments did slightly reduce the intensity of immunofluorescent labelling; however, the reduction of these fluorophores was far less dramatic than that of the background fluorescence. Finally, for each experimental run a no stain sudan black control was incorporated into the protocol. This slide was not treated with either of the two primary antibodies but was counterstained with Hoechst to allow for correct focal positioning. Sudan black treatment was applied to this slide in parallel to the others. During image capture, this slide was used first to establish the level of background fluorescence (if any) that existed. The microscope settings required to generate a signal were recorded for this no stain control and subsequent images were kept below the exposure needed to generate signal on this slide.

Figure 3.11. Level of autofluorescence in unstained upper midbrain sections.

Human upper midbrain sections showed high levels of autofluorescence when excited by the three most commonly used wavelengths (Left hand graphs). Following sudan black treatment this signal was reduced to, or nearing zero (middle graphs). Representative images show signal without any staining.
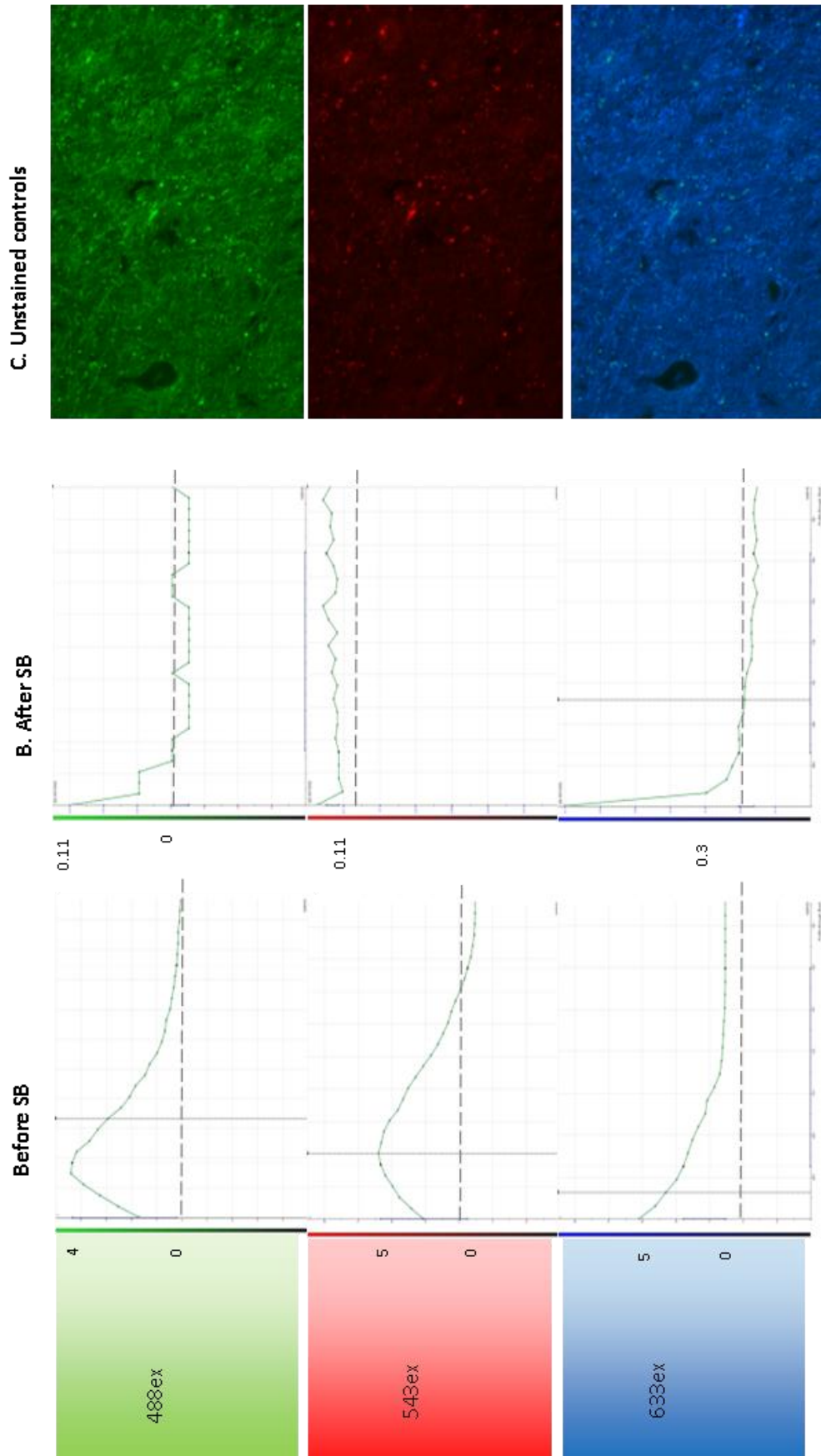
Figure 3.12. Optimization of sudan black treatment.

Figure shows no sudan black treatment (top row), 30mins SB treatment (second row), and 10mins SB treatment (third row). Ten minute incubations sufficiently quenched autofluorescence without diminishing signal. Bottom row show dual autophagy and mitochondrial stains with ten minutes sudan black treatment showing effective staining.
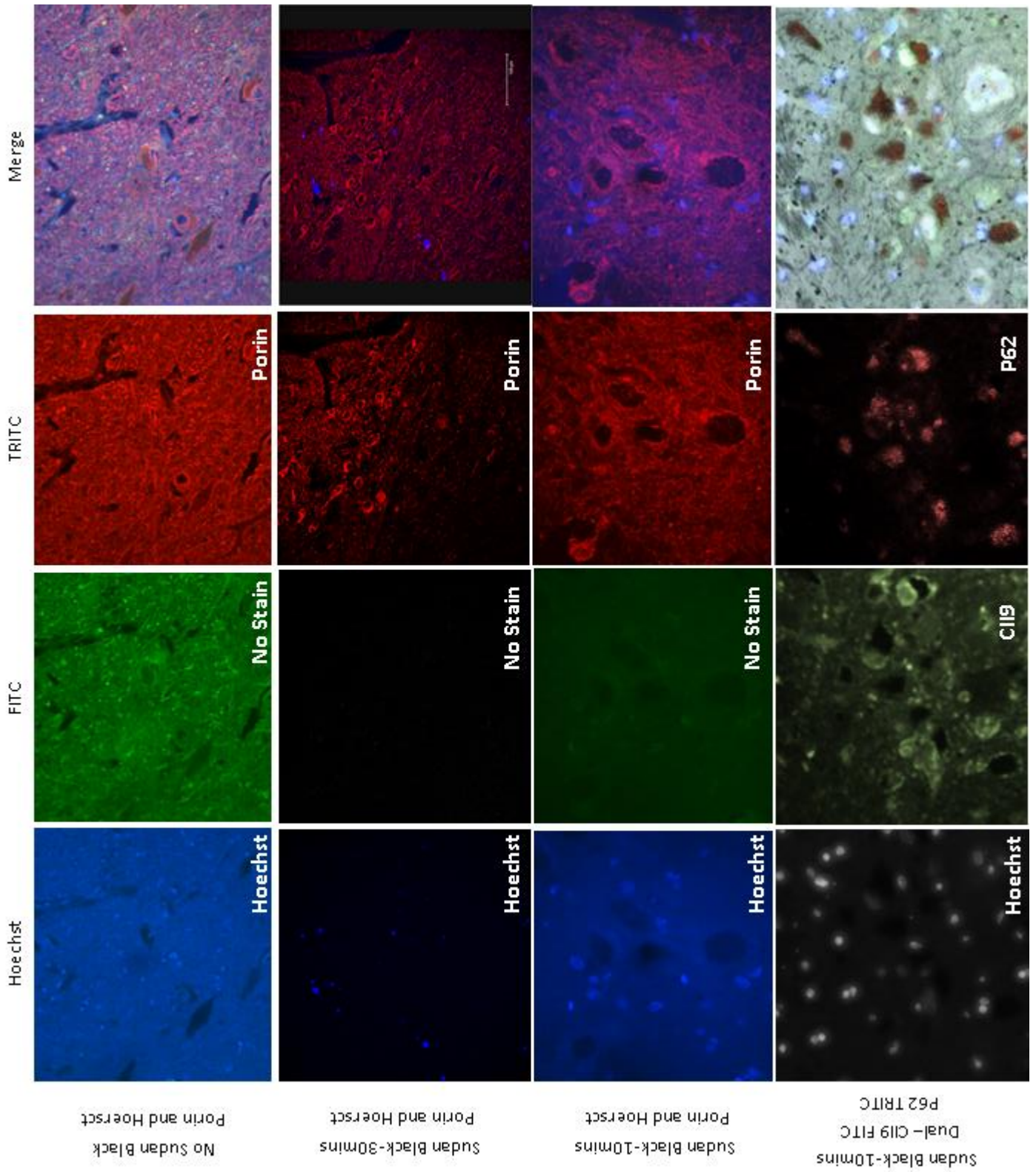
3.2.5   **Conclusions**

Careful optimization of antibodies is crucial for the reliability and interpretation of IHC results. The inclusion of no primary controls with each antibody optimization allows for confidence in the specificity of the antibody. Time was spent at this part of the project to ensure antibody concentrations were sufficient to pick up the marker of interest without causing unwanted background and/or unspecific staining. The final optimal antibody dilutions used for each marker are shown in chapter 2.3.6.1, table 2.5. Dealing with autofluorescence in the upper midbrain sections used in this study added an extra level of complexity to this study. Following rigorous testing, sudan black treatment in conjunction with spectral unmixing was capable of generating a reliable, repeatable method of quenching, without diminishing required signal.

3.3   **MITOCHONDRIAL TRACKING IN NEWLY DIFFERENTIATED NEURONS**

3.3.1   **Introduction**

Mitochondrial dynamics are essential for maintaining organelle stability and function. Through fission, fusion and mitophagic events, optimal populations of organelles are retained. Subsequently, alterations in such processes can have profound effects on the individual mitochondrion and the cell within which they reside. Neurons are post mitotic, energy dependent cells and as such are particularly vulnerable to alterations in cellular bioenergetics and increased stress that may occur as a direct or indirect result of mitochondrial dysfunction. The trafficking of mitochondria to areas of higher energy requirements, such as synapses, further highlights the importance of efficient mitochondrial dynamics in neurons.

As pluripotent cells, the ability to select cell fate in the cybrid cells is retained, for the purpose of these experiments a mixed neuronal lineage was created. Previous studies

had shown these cell lines to be compromised in their efficiency to generate neurons. Only 21% of complex I cybrid cells showed neuronal development, compared with 53% in the parental ES cell line (Kirby *et al* 2009 and discussed in chapter 4); the role of dynamics in this is yet to be investigated.

Previous limitations to observing mitochondria within these neurons include the delicate nature of the cell type, tendency to phototoxicity, and difficulties visualizing individual organelles due to the complex nature of the network in certain regions of the cell. To overcome this, Total Internal Reflection Microscopy (TIRF) was employed to limit the amount of light the cells were subjected to. Furthermore the enhanced resolution, albeit in a limited field, lends itself to imaging neuronal projections, as limiting the penetration of excitation ensures only individual organelles are imaged, reducing the complexity of the data collected. Independent neuronal projections were selected due to their thin structure which forces mitochondria to segregate to move within them.

3.3.2 **Aims of Study**

To develop a method of imaging and tracking mitochondria in newly differentiated neurons.

1. Maintaining neuron viability whilst using live mitochondrial markers.

2. Develop a methodology to track organelles along neuronal processes

3.3.3 **Imaging Methodology**

Cells were observed using a 60x objective (Nikon Plan Apo VC 1.49) on a on a Nikon Eclipse Ti inverted microscope A1R encased within a fully-enclosed environmental chamber. TIRF allows for selective excitation of fluorophores in a limited field, usually less than 100nm. This meant that only events at, or very close to the plasma membrane were captured. All images were captured using a Photometrcs Evolve 512 EM CCD camera for $5-20$ minute periods and recorded using Nikon Elements software.

3.3.3.1   *Optimization of TIRF Microscopy*

The successful analysis of live cell imaging is heavily reliant on high quality image capture. As such time was spent optimizing TIRF microscopy of the newly differentiated neurons. A balance was required between the speed of image acquisition and the overall length of imaging (Figure 3.13). As with all biologically active samples, increasing the amount of light the sample is exposed to can result in phototoxicity and photobleaching. As such efforts were made to limit the exposure wherever possible, however imaging needed to occur frequently enough that individual mitochondria could be tracked successfully by the IMARIS software.
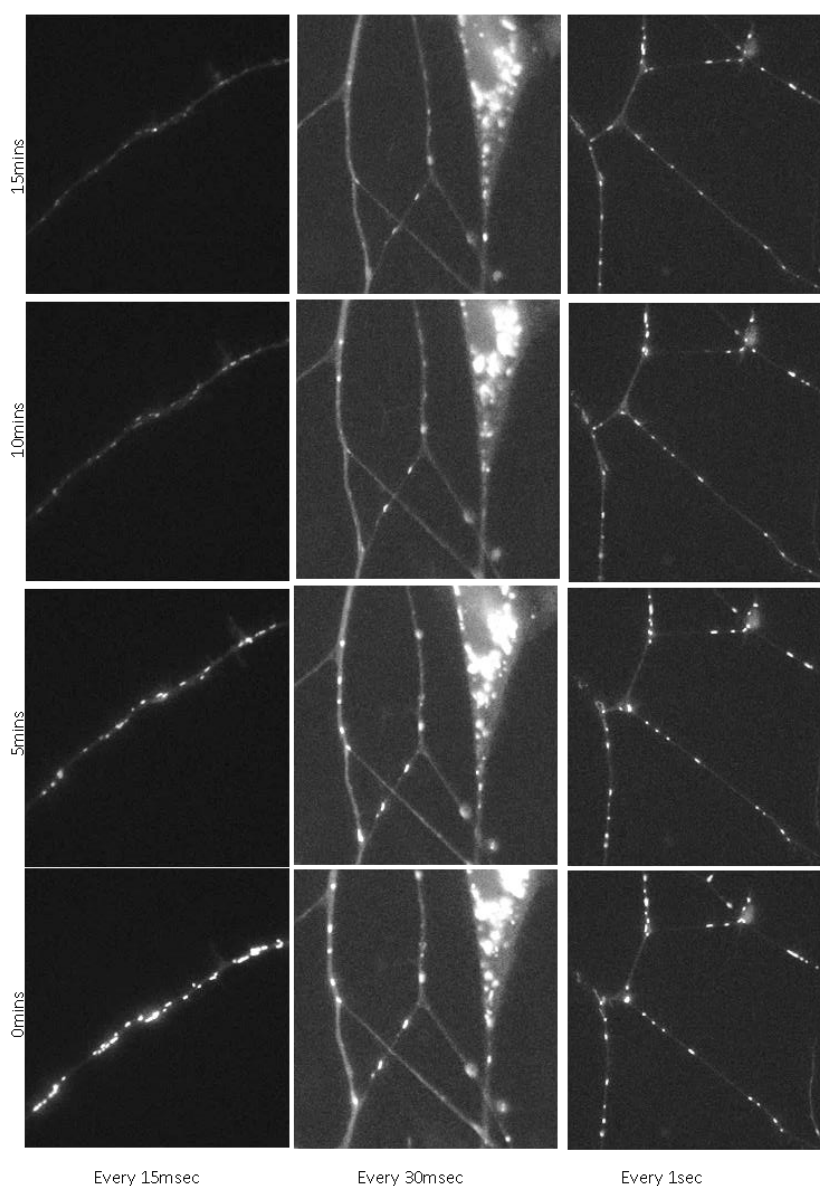
Figure 3.13. Photobleaching in TIRF microscopy

Increasing length and rate of imaging had inverse effects on image quality with higher exposure causing photobleaching. As such the optimal time (y axis) and rate (x axis) of imaging was established.

3.3.3.2 *Analysis*

Imaris 7.6 (Bitplane Scientific Software) was used for all live image analysis. Individual neuronal processes were selected on predefined criteria based on connections and excluding regions close to axons, neuronal boutons (excluding areas of increased energetic demand) or near neuronal growth cones (the process must not be an area of active growth). Regions of these processes were then defined as ROIs within the software (within which individual mitochondria did not leave). Mitochondria were then defined and tracked through entire image sequences utilizing the methodology shown in Figure 3.14. Briefly, Mitochondria were first identified as structures based on average mitochondrion size, once these structures were defined they were then tracked through each frame using the 'connected components' algorithm. Selecting this method enabled data to be generated on parameters of movement but also fusion events. The success of automated tracking was verified as tracks were routinely assessed for accuracy by eye and fusion events were compared from automated data and observed
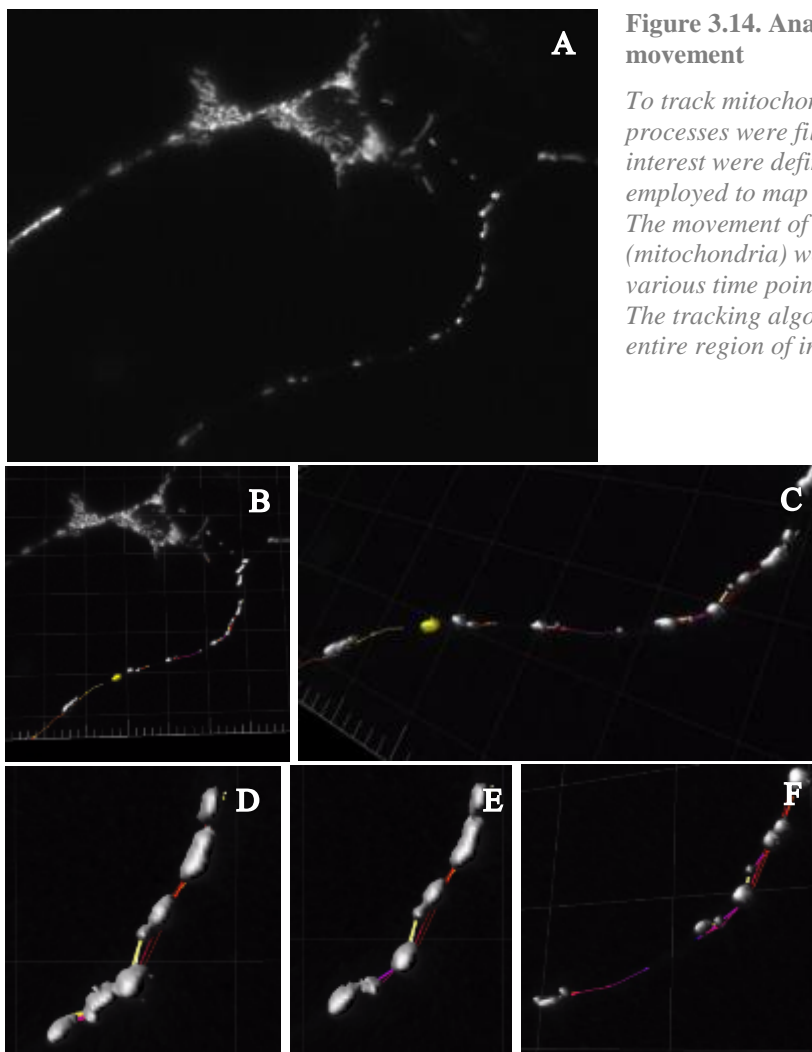
Figure 3.14. Analysis of mitochondrial movement

To track mitochondrial movements neuronal processes were filmed for 15mins (A). Regions of interest were defined (B-C) and Imaris software employed to map each organelles surface (D). The movement of each of these surfaces (mitochondria) were then followed through various time points to ensure correct tracking (E). The tracking algorithm was then applied to the entire region of interest (F).

3.3.4   **Results**

3.3.4.1   *Substantiation of Methodology*

It was deemed that imaging every second for 15 minutes was sufficient to track mitochondria effectively without causing undue stress to the cells and/or reducing fluorescent signal to a suboptimal level (Figure 3.13). Previous groups have tracked mitochondrial movements utilising different imaging software and filament tracer in IMARIS, we are however the first group we are aware of to utilise the automated tracking module for neuronal process mitochondria tracking. As such rigorous analysis of the methods was necessary. We found numbers of fusion events observed by eye and counted automatically through the software were comparable $P<0.0001$ (Figure 3.15).

Estimated	45s, 16µM	12.9s, 3.06µM
Automated	50.1s, 18.4µM	14.1s, 3.86µM
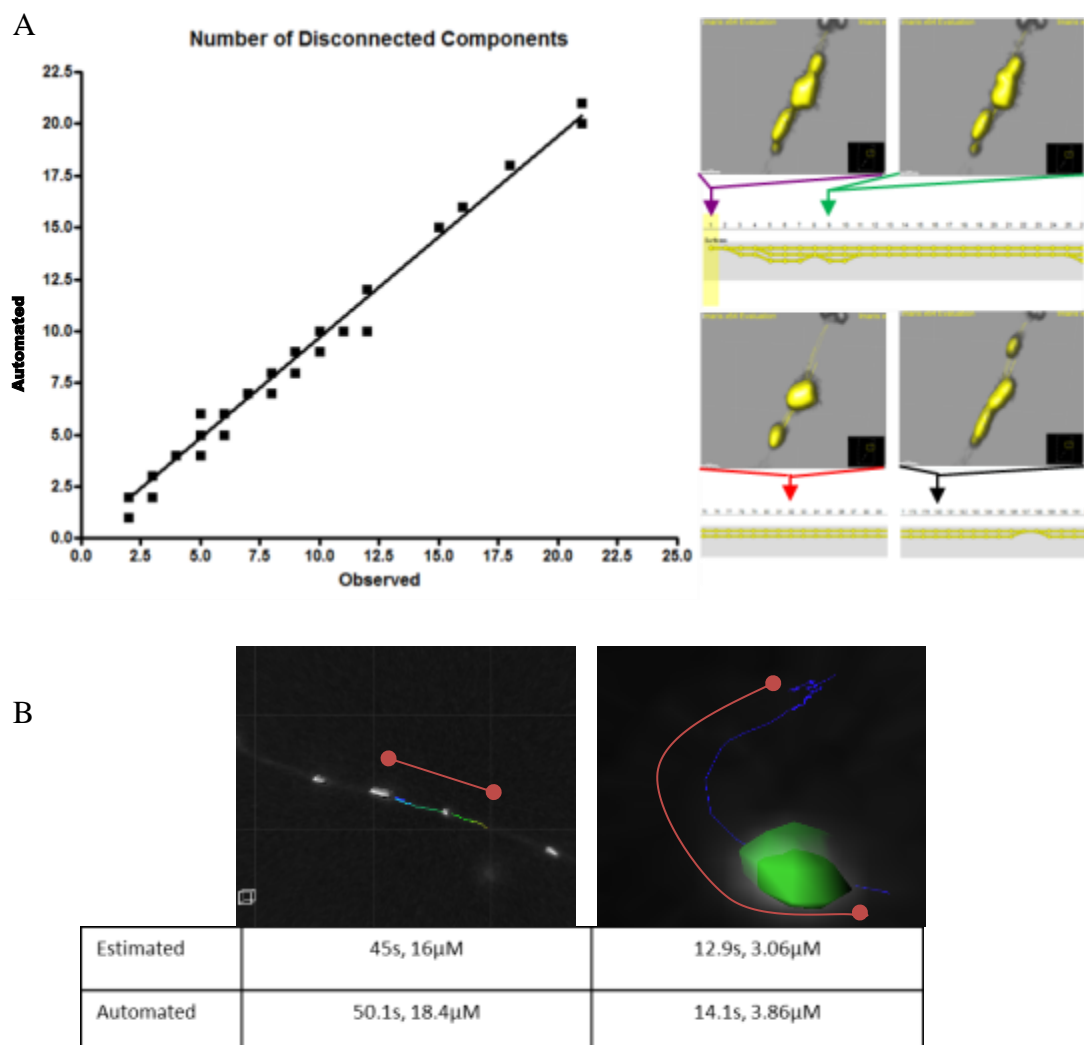
Figure 3.15. Observed vs. automated fusion events

Analysis of the number of observed fusion events (two surfaces becoming one) were compared with the number of structures calculated by Imaris at any given time (A). Track lengths were also routinely checked against automated calculations (B).

3.4   MITOPHAGY IN REAL TIME

3.4.1   Introduction

The removal of mitochondria through macroautophagy cannot be elucidated through fixed cell/tissue studies. Although certain things can be inferred from alterations in autophagy markers and mitochondrial numbers, to separate mitophagy from general autophagy a method of observing the process in 'real time' was needed.

To achieve this, live cell markers of both mitochondria and autophagosomes were used in conjunction, allowing for the observation of mitophagic events. Several obstacles in the development of this methodology needed to be addressed. Firstly, optimization of appropriate dyes was required. Next image capture, including, excitation, length of image capture and number of z stacks needed to be optimized for both fibroblasts and ES cells.

3.4.2   Aims of this study

To develop a method of imaging and tracking mitochondria and autophagosomes in fibroblasts and embryonic stem cells.

1.   Establish markers for autophagosomes and mitochondria that were well tolerated in fibroblasts and by the ES cells.

2.   Develop a methodology to track both structures in relation to one another in live cells.

3.4.3   Imaging Methodology

Cyto-ID (Enzo biosciences) was routinely used to stain for autophagosomes in fibroblasts as the dye was well tolerated. This was used in conjunction with mitotracker red. Analysis of the mitochondrial network and autophagosome number/volume was conducted on Imaris 7.6 (bitplane). Correlations between mitochondria and autophagosome characteristics were then analysed. To look more in depth at mitophagic events the proceeding step was to look at the two-mitochondria and autophagosomes in

parallel. As the cybrid ES cell lines were the most valuable for these experiments, time was spent establishing a mitophagy assay in these cells. Unfortunately the ES cells are particular sensitive to certain dyes, with methods that worked with minimal toxicity in fibroblasts causing noticeable morphological changes and in severe cases cell death. As such Cyto-ID proved ineffective for the ES cell lines. The decision was made to transfect these lines with GFP-tagged LC3. Firstly this was achieved through a lipid based transfection kit although no stable transfected lines were generated. The experiments then moved onto viral transfection, again with mixed results. Stable lines were generated for the complex IV cybrid line only, with complex I lines and controls failing to express GFP-LC3. Due to constraints of this project the mitophagy assay was developed in this cell line to be utilized with the other cell lines once stable transfections had been generated. The analysis described below therefore outlines a methodology for future mitophagic observations.

Following successful co-labeling of mitochondria with mitotracker and LC3 through GFP transfection, z stacks were generated for both channels. Two types of experiment were undertaken- short and long. For short experiments images were captured every 5 seconds for 15mins, allowing greater resolution of autophagosome number, volume and locale, relative to mitochondria. For long experiments, assays were run overnight, with image capture occurring every 5mins with reduced laser strength. Although this reduced resolution, it ensured photobleaching was not a limiting factor over these longer time periods which enabled the assessment of mitophagic events.

3.4.3.1 *Analysis*

Analysis was conducted using Imaris 7.6 (Bitplane). For identification of mitochondria, 'surfaces' were mapped (Figure 3.16.2). Autophagosomes were characterized as 'particles' within the software (Figure 3.16.3). Movements of both surfaces and particles were then tracked through each time frame with measurements of size, location and interaction recorded.
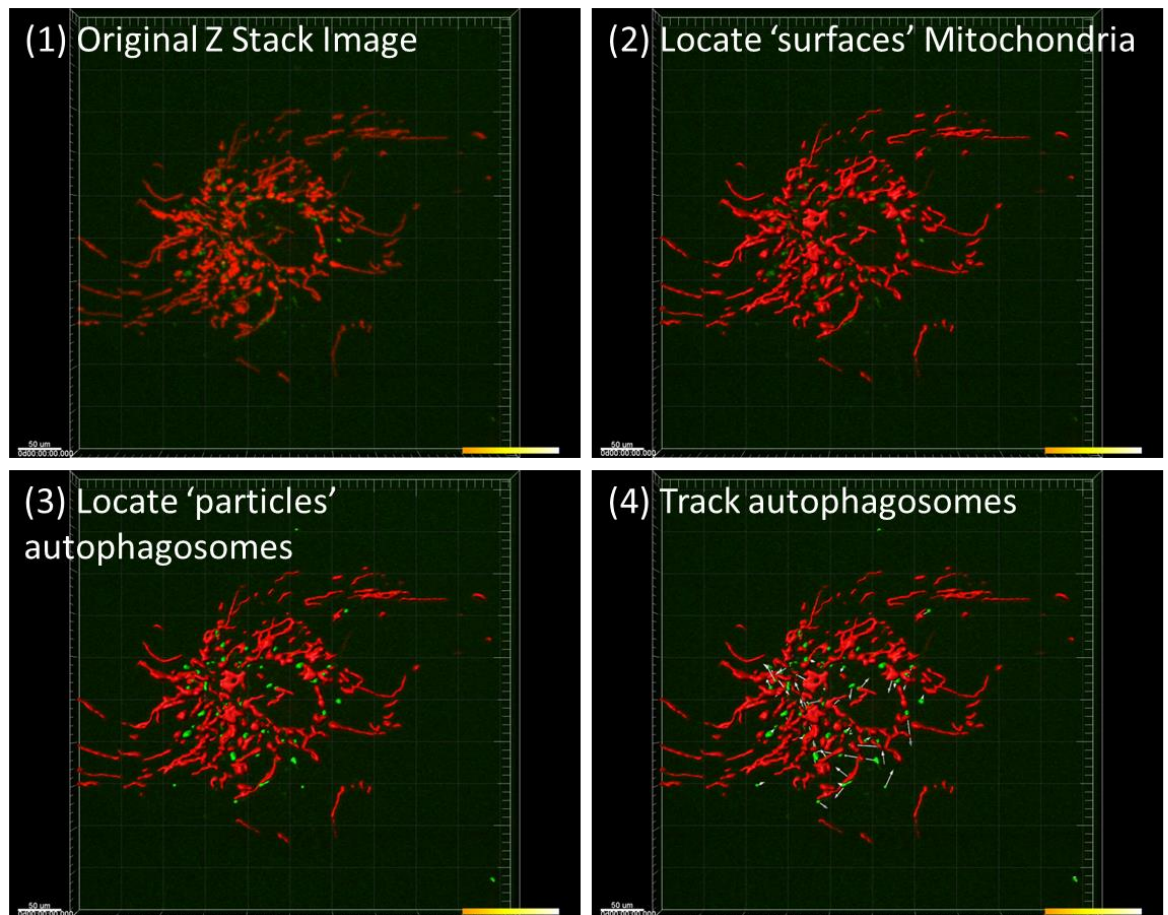
Figure 3.16. Autophagosome and Mitochondrial interactions

Analysis of mitochondria and autophagosomes was undertaken using Imaris 7.6. Through this software mitochondria were defined as surfaces and autophagosomes were identified as particles. Parameters of these two could then be assessed with regards to localization, size and number.

3.4.4   **Results**

Through transfection of GFP tagged LC3 and mitotracker dyes it was possible to develop a methodology that could assess mitochondria and autophagosomes in parallel. Characteristics that can now be assessed through this novel methodology are outlined in Figure 3.17.

Figure 3.17. Measurements achievable through novel mitophagy methodology

The figure shows example images taken from videos of autophagosomes and mitochondria in live cells. From these, measurements of different parameters can be achieved. GFP-LC3 transfected cells can be subjected to different treatments (A) and the intensity of autophagosome formations can be measured (B). Dual mitochondrial and LC3 staining (C) can reveal formation of characteristic autophagic rings (D), which can be assessed in different cell lines. Measurements of autophagosome localization, for example in relation to the nucleus, can be calculated (E) alongside total number of autophagosomes/cell (F). Finally observations of the interactions between mitochondria and autophagosomes can be made, looking firstly at the interactions between the two (G) and more specifically mitophagic events (H,I,J) through the measuring of mitochondria engulfed by LC3 (arrows) and colocalizaiton of the two markers (arrow heads).

Intensity of Vesicles

Formation of autophagosome 'rings'

Localization and number of autophagosomes

Interactions between mitochondria and autophagosomes (mitophagic events)
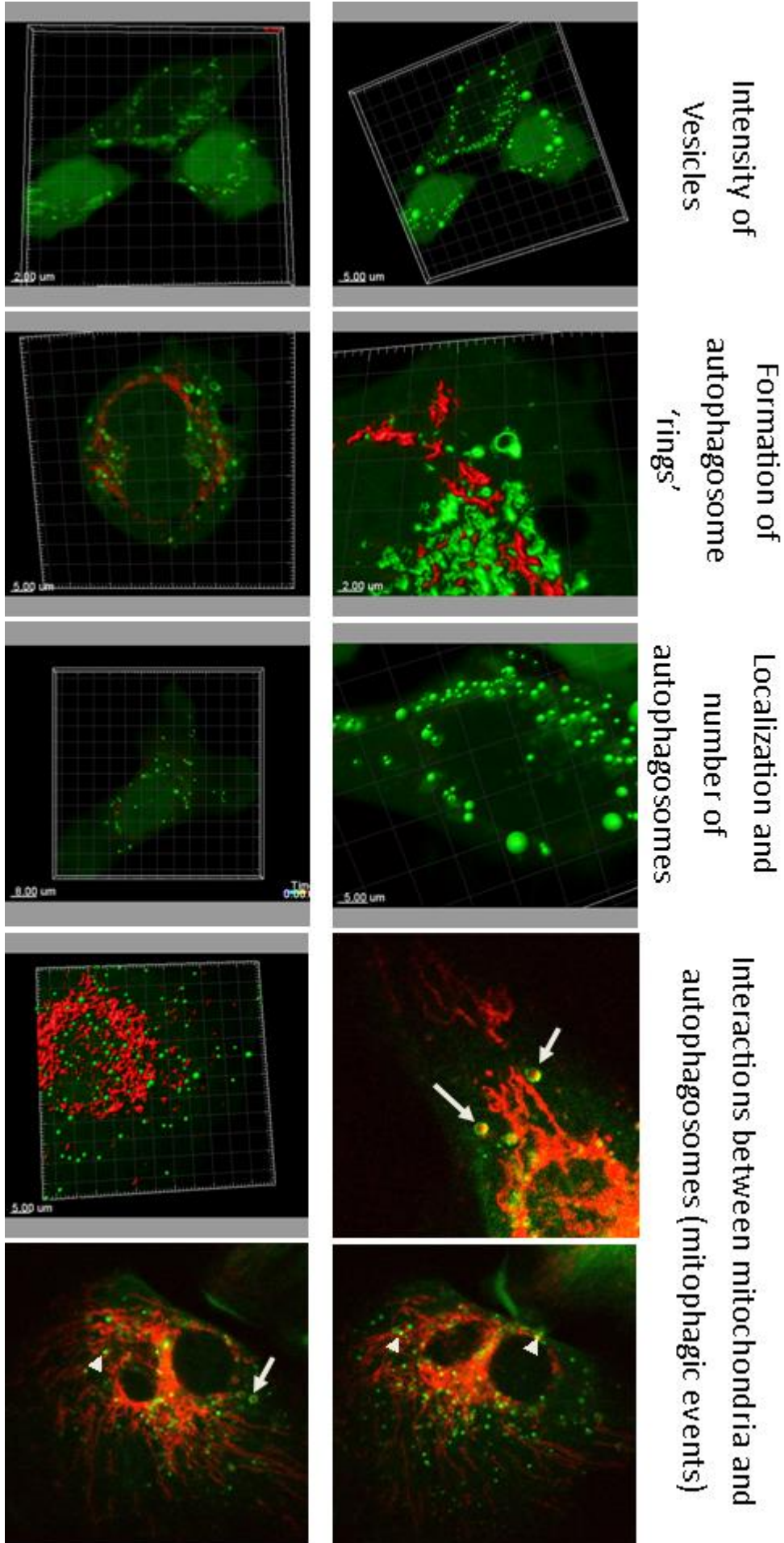
3.4.5   **Conclusions**

To observe dynamic events real time imaging is required, it is clear that static observations of mitochondria are no longer sufficient to deduce complex dynamic processes that may be key to pathogenic alterations in a range of common disorders. The methodology established as part of this project will be essential in assessing live mitophagic events and how these differ in cell lines harboring different mutations.

3.5   **DISCUSSION**

The techniques optimized as part of this chapter will serve as a tool set for experiments described in the subsequent chapters. Many of the techniques will be optimized futher as the project progresses and used in novel settings for this and other works within the group.

Chapter Four

Characterization of Cybrids

Chapter 4. Characterization of Cybrids

4.1   INTRODUCTION

4.1.1   Overview

Cybrids- 'Cytoplasmic Hybrids' allow the effects of specific mtDNA mutations to be studied by comparing them with control cells containing wild type mtDNA that are raised in the same nuclear DNA background. Transmitochondrial cybrids had previously been generated and the methods for this are outlined in (Kirby *et al.*, 2009). Briefly, the cell lines were generated by treating embryonic stem cells (CC9.3.1 cell line) with rhodamine 6G to remove endogenous mtDNA. These were then fused with cytoplasts from mouse fibroblasts (L929 cell line) carrying a range of mtDNA mutations that were fixed over long-term culture (Figure 4.1). Cell lines were a gift of Prof. Anne Voss (Walter and Eliza Hall Institute, Melbourne, Australia).
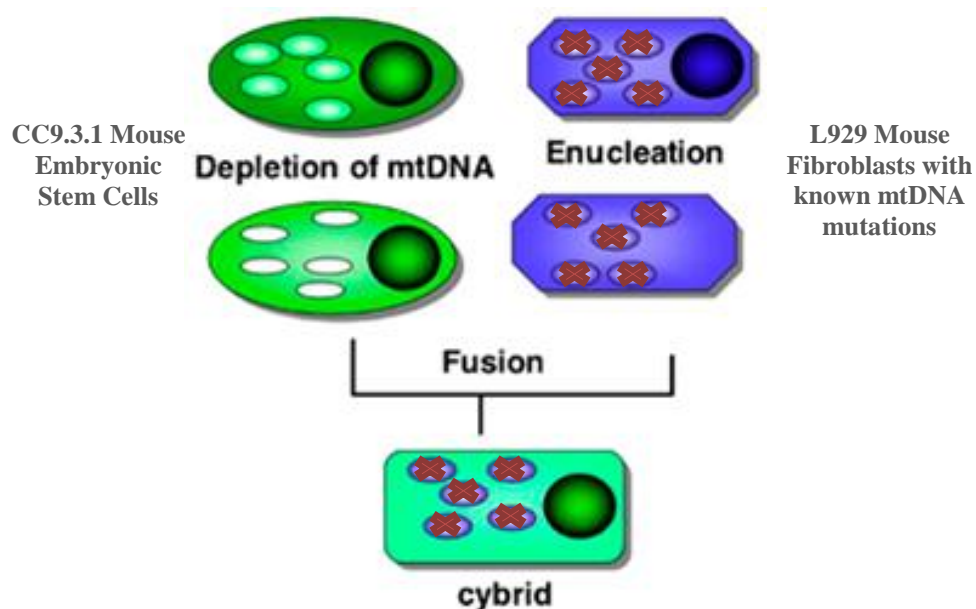
Figure 4.1. Cybridization process

Embryonic stem cells are depleted of mtDNA through Rhodamine 6G treatment. These are then fused with enucleated mouse fibroblasts containing known mtDNA mutations. (Modified from (Ohta, 2006)

4.1.2   **Cybrids used in this study**

The cybrids used for this study were mouse embryonic stem cells which contained mutations/polymorphic variants in different complexes of the respiratory chain as shown in Table 4.1. The presence of mtDNA mutations was established through polymerase chain reaction- restriction fragment length polymorphism (PCR-RFLP) at time of cybrid generation (Kirby *et al.*, 2009).

Collective Cybrid Cell Lines	Characteristics		
	Existing prefix	Mutation	Location
Controls	E14Tg/CC9.3.1	-	-
Complex I	CPC5.5/Cy3-I	ND6 iC13887 and ND5 G12273A	Complex I
Complex IV	ICP9.4/Cy2-I	COI T6589C	Complex IV
Complex IV hetero	C2C12	COI C6247T	Complex IV
Complex V	TMPII-I	A8414G ATPase 6 gene	Complex V
RNA polymorphism_R	ICP57.6/Cy1-I	MTTR Adel m9821	tRNA R
RNA polymorphism_I	mB77	tRNA Ile G3739A	tRNA I

Table 4.1. Cybrid Cell Lines

The cybrids available for use in this study are listed in the table above. Lines have previously been used in different experimental settings and therefore have been identified in different ways as shown in the existing prefix column.

Two control lines were initially used in the characterization step of this study the E14Tg line and CC9.3.1 (true nuclear control). For later experiments the CC9.3.1 cells were used independently. The controls alongside complex I, complex IV and tRNAR polymorphism mutants were sourced from stocks created within the mitochondrial research group, details of their generation can be found in Kirby *et al* 2009. Three novel lines, Complex V, complex IV heteros and RNAI polymorphisms were a gift from Professor Jose Antonio Enriquez (Centro Nacional de Investigaciónes Cardiovasculares Carlos III, Spain). Complex I and complex IV mutants have previously been classified based on severity of enzymatic activity deficiency compared to controls (see below in 4.1.3). The impact of a scale of bioenergetic dysfunction can therefore be assessed with complex I mutants showing a severe phenotype and complex IV a mild phenotype. The tRNA polymorphisms provide an important control for the cybrid derivation process, ensuring the effects of the mutation are assessed, and not any downstream impact of the cybrid construction process. All mutations were homoplasmic with the exception of the

complex IV C6247T mutation and the *mtND5* point mutation which was 90% heteroplasmic.

4.1.3   **Previous findings**

Previous studies using the complex I and complex IV cybrid cell lines have quantified the consequences of mtDNA variations by measuring respiratory chain enzyme activities using spectrophotometricity, measured relative to a matrix marker (citrate synthase-CS). The ratio enzymatic activities are displayed in Table 4.2. The results showed that the mtDNA mutations caused a spectrum of biochemical defects. No significant alterations in enzymatic activity were quantified for the polymorphic control, mild enzymatic decrease was seen in the complex IV cells and severe enzymatic activity loss was recorded in the complex I cybrid line.

Ratio enzymatic activity	*Trans*mitochondrial cybrid % ratio of parental ES cell line		
	CY1-I	CY2-I	CY3-I
Complex I/CS	74	71	7
Complex II/CS	56	64	83
Complex III/CS	83	114	89
Complex IV/CS	57	37	57

Table 4.2. Respiratory chain enzyme activities in undifferentiated cybrids.

The activities are expressed relative to the mitochondrial matrix enzyme citrate synthase (CS ratio), as percentages of the CS ratio in the parental embryonic stem (ES) cell line. CY-I/RNA polymorphic variant, CY2-I/Complex IV and CY3-I/ Complex I. (Modified from (Kirby et al., 2009).

4.1.3.1   *Neuronal Differentiation*

As pluripotent cells, the ability to select cell fate in these cells is retained, using a differentiation protocol as outlined in Bain's *et al,* a mixed neuronal lineage can be created (Bain *et al.*, 1995). Previous studies have shown that all the cell lines are capable of neuronal differentiation by this methodology, however the efficiency of the differentiation capabilities varies for different mtDNA mutations this was shown to associate with severity of mutations. β-tubulin expression (a microtubule element of the

tubulin family found almost exclusively in neurons) was used to indicate neuronal differentiation. Quantification of this staining revealed only 21% of complex I cybrid cells showed neuronal development, compared to 53% in the parental ES cell line (Abramov *et al.*, 2010). Interestingly the complex IV mutants did not show a significant reduction in differentiation capacity implying that this finding is either complex I or severity dependent. If the latter is true it would suggest a fairly high threshold for differentiation impairment (Figure 4.2). Further studies into the synaptic activity of these cell lines using patch clamp recordings revealed neurons with the highest level of respiratory deficiency had marked defects, with complex I mutant cells being completely devoid of all synaptic currents. In contrast control and mild mitochondrial mutants showed typical spontaneous currents around 2 weeks after plating (Abramov *et al.*, 2010).
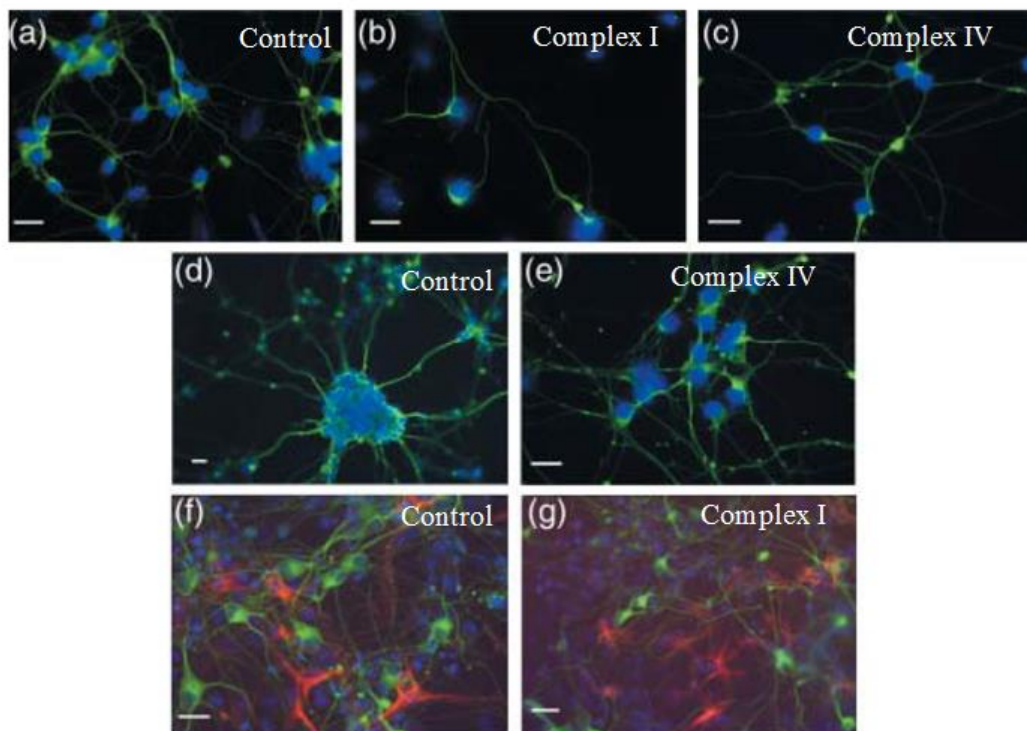
Figure 4.2. Differentiation into neurons and astrocytes

Control, complex I and complex IV cell lines were capable of differentiation into neurons and astrocytes as demonstrated by β-tubulin staining (green) and GFAP staining (red f and g). Complex I mutants showed a severe reduction in both stains showing diminished differentiation capacity complex IV cells were not significantly different. (modified from (Abramov et al., 2010).

142

4.1.3.2 *Reactive Oxygen Species (ROS) production*

Mitochondrially generated ROS were measured in cybrid cell lines using hydroethidium (cytosolic indicator) and signals from the mitochondrially targeted hydroethidine. ROS levels were increased in both complex I and complex IV lines. Oxidative stress measured by glutathione depletion suggested a significant increase in complex I but not complex IV cell lines. Furthermore this increased ROS was associated with neuronal death, highlighted by attenuation through administration of ROS scavengers (Abramov *et al.*, 2010).

4.1.3.3 *Calcium homeostasis*

Calcium is fundamental to neuronal functioning, transducing molecular from electrical signals, alongside universal roles in cell death pathways. As such, the regulation of calcium directly impacts on neuronal capabilities. To ascertain the impact the mitochondrial mutations had upon calcium homeostasis in the cells, membrane potential and calcium concentrations were measured simultaneously. It was revealed using Ca^{2+} agonists (ATP to stimulate and Potassium chloride -KCL to depolarize plasma membrane and subsequently open voltage gated Ca^{2+} channels) neither of the mutants induced pathogenic changes to Ca^{2+} signals. This is thought to be possible through a maintained membrane potential (Abramov *et al.*, 2010).

4.1.4 **Complex I focus**

Initial experiments were conducted using all available cybrid cell lines. However, early on in experimental design it was realised that maintaining and controlling variability in so many different cell lines was problematic and limited the amount of parallel repeats that were possible. For this reason and to use the most relevant model system for PD, in which complex I dysfunction has been extensively described, focus was shifted to looking at the severe complex I mutants in relation to their nuclear controls, the complex IV mild mutants and the cybridization controls. This allowed for tighter control of the variables and the opportunity for increased repeats, enabling greater confidence and consistency in any observations.

4.1.5   **Aims of this study**

This chapter aimed to define the nature and extent of dysfunction in cybrid cell lines, as well as optimizing growth conditions for future imaging assays. Construction of cybrids was accomplished prior to the start of this project and as such data already existed on certain parameters of mitochondrial and overall cellular functioning. This study therefore aimed to confirm previous findings using novel techniques and build on an existing knowledge base, looking at different aspects of mitochondrial function.

1. Confirm mutations in cell lines

2. Monitor growth and viability

3. Define bioenergetic alterations

4. Confirm decreased differentiation capacity of complex I cybrids

4.2   **METHODS**

4.2.1   **Sequencing**

Once the correct PCR products had been generated they were sequenced using the Applied Biosystems 3130 Genetic Analyzer (Life technologies). Briefly, sequencing of the DNA is achieved by the addition of fluorescently tagged dideoxynucleotides. When DNA polymerase generates a complementary DNA strand it incorporates both normal nucleotides but also fluorescently tagged dideoxynucleotides. When a dideoxynucleotide is added the reaction is terminated. As incorporation of the fluorescently tagged nucleotides is stochastic, strands are randomly terminated and as such a mixture of strands of varying lengths is generated. The mixture is then cleaned to remove any unwanted material and the samples are put in the genetic analyser for electrophoresis. The analyser injects DNA molecules into a capillary array which are separated according to size, smaller fragments moving more quickly than larger fragments. The fragments are detected via the fluorescent tag incorporated earlier on and appear as a coloured peak on the software. The raw data can then be converted into a complete DNA sequence using the sequencing program, Seqscape (Invitrogen).

4.2.2   **Optimization of growth conditions**

To ensure variability of growth conditions would not influence any results gathered from cell culture experiments, time was spent optimizing the exact growth conditions for the ES cells. Previous studies have successfully cultured these cells and as such these conditions were matched. All cells were grown in a humidified incubator at 37°C with 5% CO_2 in tissue culture flasks pre-coated in a 0.1% porcine skin gelatine (Sigma) solution. The cells were initially grown in Glasgow Modified Eagle's Medium (GMEM) with 10% foetal calf serum, supplemented with Non-essential Amino Acids (NEAA), Sodium Pyruvate and Glutamine (all GIBCO, Invitrogen). Leukocyte Inhibitory Factor (LIF, Millipore) alongside 2-mercaptoethanol (GIBCO, Invitrogen) were added to limit spontaneous differentiation of ES cells during propagation. For novel applications of these cells, i.e. growth in imaging dishes the application of different coatings was tested to achieve adherence for both undifferentiated and neuronal cells. The tolerance to different dyes at a range of concentrations was also established for the ES cells and newly derived neurons.

4.2.3   **Measurement of growth**

To further characterize the cybrids a method for monitoring their growth was developed. Initially, cell counts were taken every 24hrs, where the cells were dissociated, collected and counted using the Countess automated cell counter (Life Technologies). The Countess generates cell counts along with measurements of viability (live, dead and total cells) using imaging of trypan blue stained cells (Figure 4.3.A). Alongside this, a second assay was developed using the CT Biostation Live Cell imager (Nikon Instruments Inc.) This allowed visualization of the growth alongside assessment of morphology. To limit variation all cell lines were grown at the same time and seeded to six well plates at a density of 1x 10^5/500µl. Three wells were seeded for each cell line and the plates were loaded into the fully automated Biostation. The machine was programmed to take images at three points within each well at hourly intervals for a period of 72 hours. This generated videos of each cell line. Still images from 12hour intervals were then analysed using area calculations as shown in Figure 4.3.B.

A

B
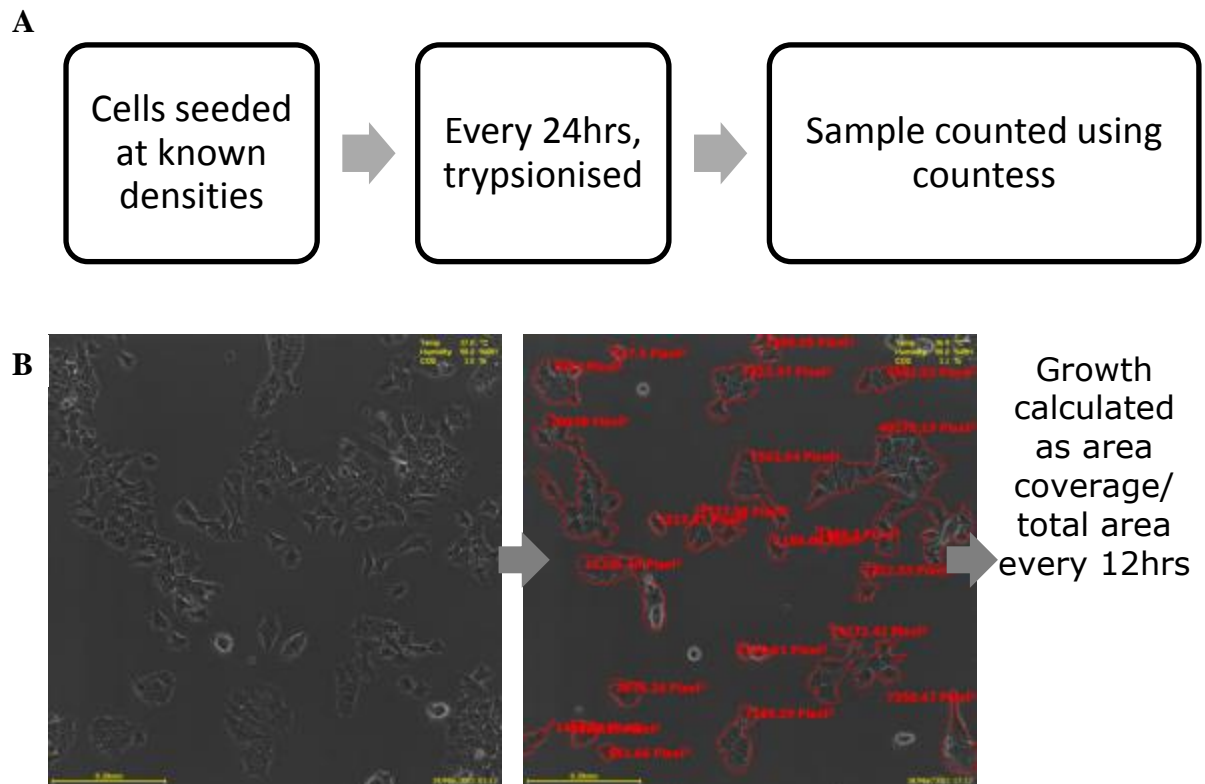
Figure 4.3. Growth Analysis

Two methods were employed to monitor growth. Firstly a standard growth curve was produced through Trypan Blue staining and cell counts (A). A second imaging method was used alongside computer analysis of overall growth areas every 12hrs.

4.2.4 **Measurement of steady state protein levels**

To assess if steady state levels of certain complex I and complex IV subunits of their associated cybrids were affected, immunoblotting was performed as outlined in chapter 2.3.4. Complex I cybrids were probed for NDUFB8, the 20kDa subunit of complex I (C120) which has been previously shown as a reliant marker of complex I assembly. Complex IV cells were probed for COXI in which the cybrid contains its mutation. All westerns were probed in parallel with housekeeping genes (β-actin and TOM20 respectively).

4.2.5 **Microoxygraphy**

Previous work has shown different mutations induce varying severity of respiratory dysfunction. To ascertain the extent to which the mutation affected oxidative phosphorylation in our cell lines, cellular bioenergetics were assayed using the Seahorse

146

extracellular flux analyser x24 (Seahorse Biosciences, Massachusetts). Briefly, cells were seeded to a Seahorse 24 well plate 24hrs before experimentation at a previously optimized density (chapter 3.1.5). Prior to running, growth media was replaced with experimental media (without pH buffering) and allowed to equilibrate in a CO_2 free incubator for 1hour. During experimentation, oxygen consumption rates (OCR) and extracellular acidification rates (ECAR) were monitored in parallel. Sequential injections of oligomycin, FCCP, rotenone and antimycin were added to allow different parameters of mitochondrial function to be measured.

Data were normalized by cell number calculated for Hoechst staining and automated nuclei counting post run. From this a number of parameters were assessed. Non-mitochondrial respiration (NMR) was subtracted from all values. Basal respiration was calculated from the average of the first three measurements for each run. Spare respiratory capacity was generated by subtracting basal respiration from maximal respiration (following FCCP treatment) for which the highest value was taken. Each cybrid cell line was run multiple times with a minimum n of 16wells. An unpaired, two-tailed Student's t test was performed to determine the significance of any differences between the data sets and p values were considered significant at the 95% confidence interval.

4.2.6   Determining differentiation capacity

Previous studies have highlighted the impaired differentiation capacity of complex I cybrid cells compared to complex IV mutants, nuclear controls and cybridization controls. All cell lines had undergone extensive cryostorage and/or transportation prior to this study and as such the decision was taken to regularly quantify neuronal differentiation for each cell line during the course of neuronal experiments. To this end, cells that were passage matched, equally seeded, differentiated and fixed on the same days were routinely imaged at x10 and x40 magnification. These images were then analysed for number of neurons/field of view and degree of arborisation (number of branches/cell body). These data were combined and plotted as a percentage of controls for the complex I cybrids.

4.3 RESULTS

4.3.1 Sequencing

To ensure cybrid cell lines contained the expected mutation, regions of the mtDNA known to contain the mutated site were amplified using primers detailed in section 2.2.1.2 and subsequently sequenced. Preliminary runs revealed two of the lines were lacking the mutations thought to be contained when frozen down. To overcome this, a series of earlier passage aliquots were sourced and sequenced until cells retaining the mutation were found (Figure 4.4). Stocks from these were then grown up and re-sequenced to ensure the mutation had not been lost again.
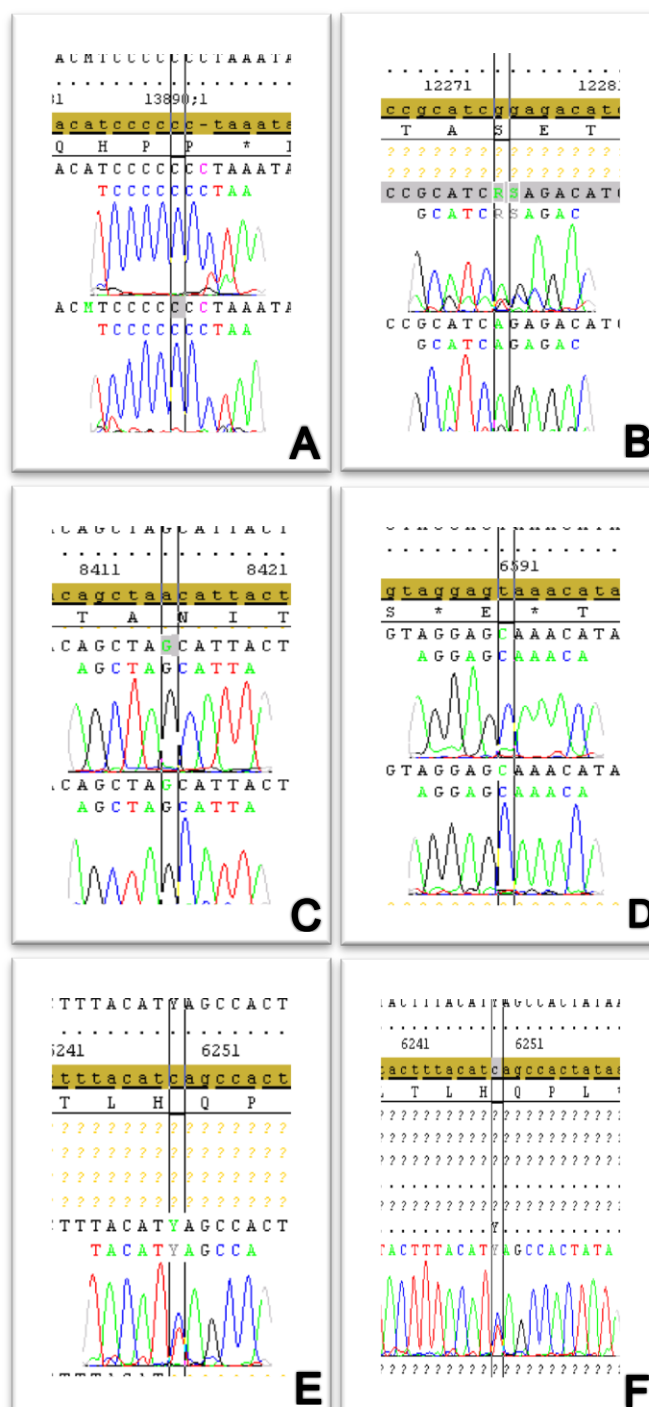
Figure 4.4 Sequencing Data from Cybrid Cell Lines.

a/ CPC5.5 Complex I mutant iC13887 b/ CPC5.5 Complex I mutant G12273A c/ TMPII-I CV Mutant A8414G d/ ICP9.4 CIV Mutant T6589C e/ C2C12 Complex IV mutant C6247T f/ Repeat of C2C12 showing heteroplasmic expression of C6247T mutation.

4.3.2   Steady state protein levels

To assess whether the mitochondrial mutations affected the steady state expression of their associated proteins, immunoblotting was performed. Both the complex I and complex IV cells showed a significant reduction in C120 and COXI respectively (Figure 4.5). The westerns were repeated a minimum of three times on lysates collected from different passage number cells, obtained on different days.

A
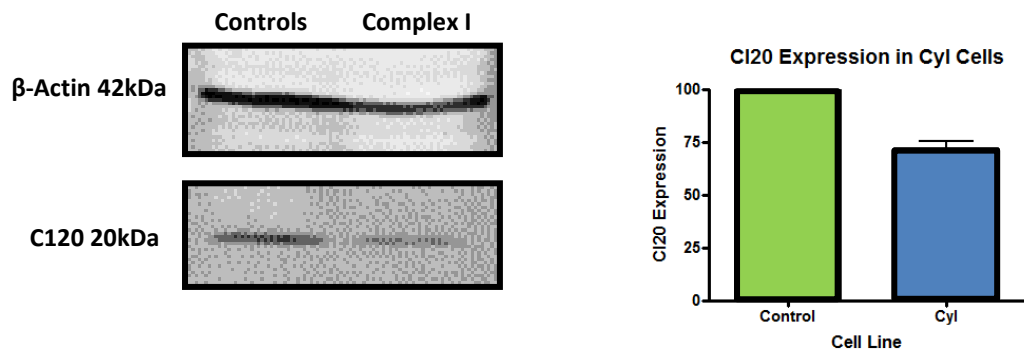
B
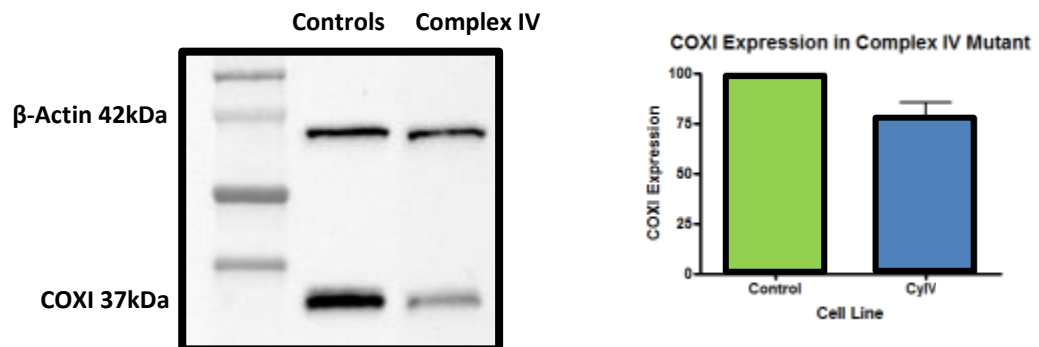
Figure 4.5. Western Blot Analysis of Steady State Complex Levels in Cybrid Cell Lines.

A/Control cells compared to complex I mutants for C120 levels showing a marked reduction in expression (P=0.0174). B/ Homoplasmic complex IV mutant showing reduced COXI expression when compared to control cells (P=0.0224). Quantification shows combined results of 3 blots.

4.3.3   Growth Conditions

Media constitution and growth conditions were kept the same as previous studies (Kirby *et al.*, 2009; Abramov *et al.*, 2010; Trevelyan *et al.*, 2010). Imaging at the resolution

required for this project had not been undertaken before on these cells. As such the ability to grow on different surfaces was assessed, including glass bottom imaging dishes. The cells were routinely grown on 0.1% gelatin to aid adherence to T75s. The imaging dishes to be used in this study come pretreated with ibiTreat-a physical surface modification. Despite initial settling and growth, all non-coated dishes began to show detachment and cell death after 48hrs (Figure 4.6). As such all plates were coated with 0.1% gelatin which was shown to not adversely affect imaging results.
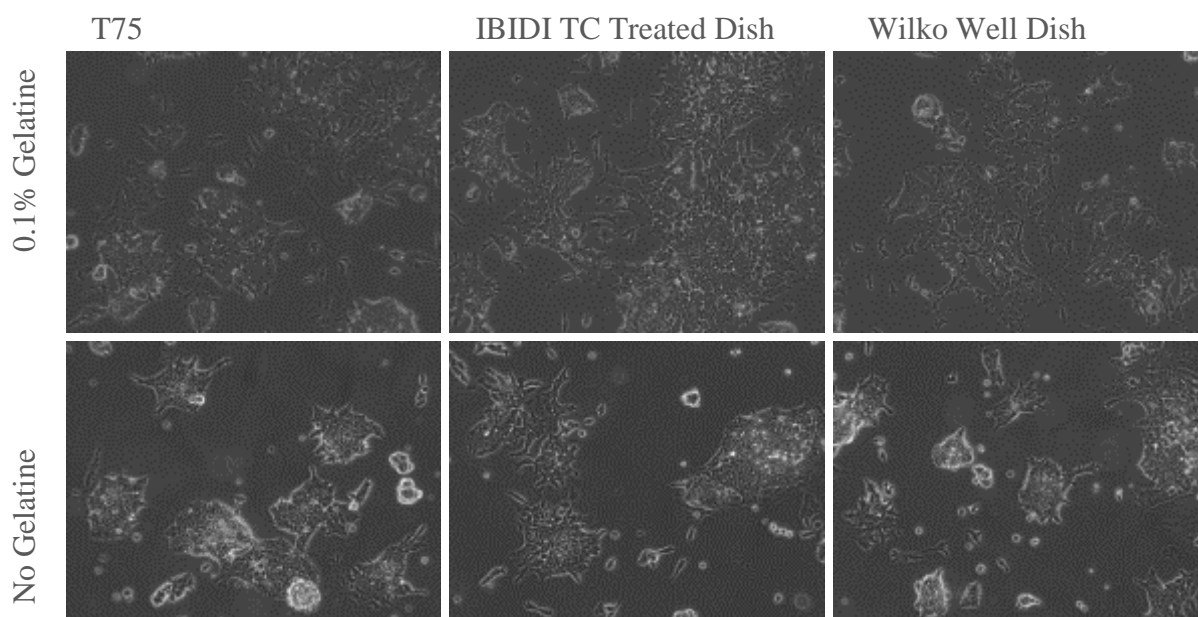
Figure 4.6 Coating of plates.

Representative images of cell stability in plates with and without gelatine coating.

4.3.4   **Growth**

Analysis of the growth of all cybrid lines was carried out through two parallel methodologies. Firstly growth curves were generated from cell counts (live, dead and total cell number) carried out in triplicate every 24hrs for 72 hrs. Interestingly no measurable differences were observed for cell viability between controls, complex I cybrids, complex IV cybrids and polymorphic controls (Figure 4.7.A/B). The rates of growth however did vary between cell lines. Initially the complex I cybrids grew notably faster than any of the other cell lines. Although at 72hrs growth this difference was no longer significant between themselves and their nuclear controls. The E14Tg control line appeared to grow slower than CC9.3.1 controls but was not significantly different from the complex IV cells, complex V or polymorphic control (Figure 4.7.C).

150

As with the automated counting method, imaging and quantification of the cells through the biostation also showed complex I cells had an initial higher growth rate than other cells.This increase lost significance after 72hrs. The imaging also revealed morphological differences between cell lines with complex I cybrids growing in more crowded colonies than controls and complex IV cells showing thinner independent cell growth (Figure 4.7.D). All other cell lines showed similar morphologies to controls.
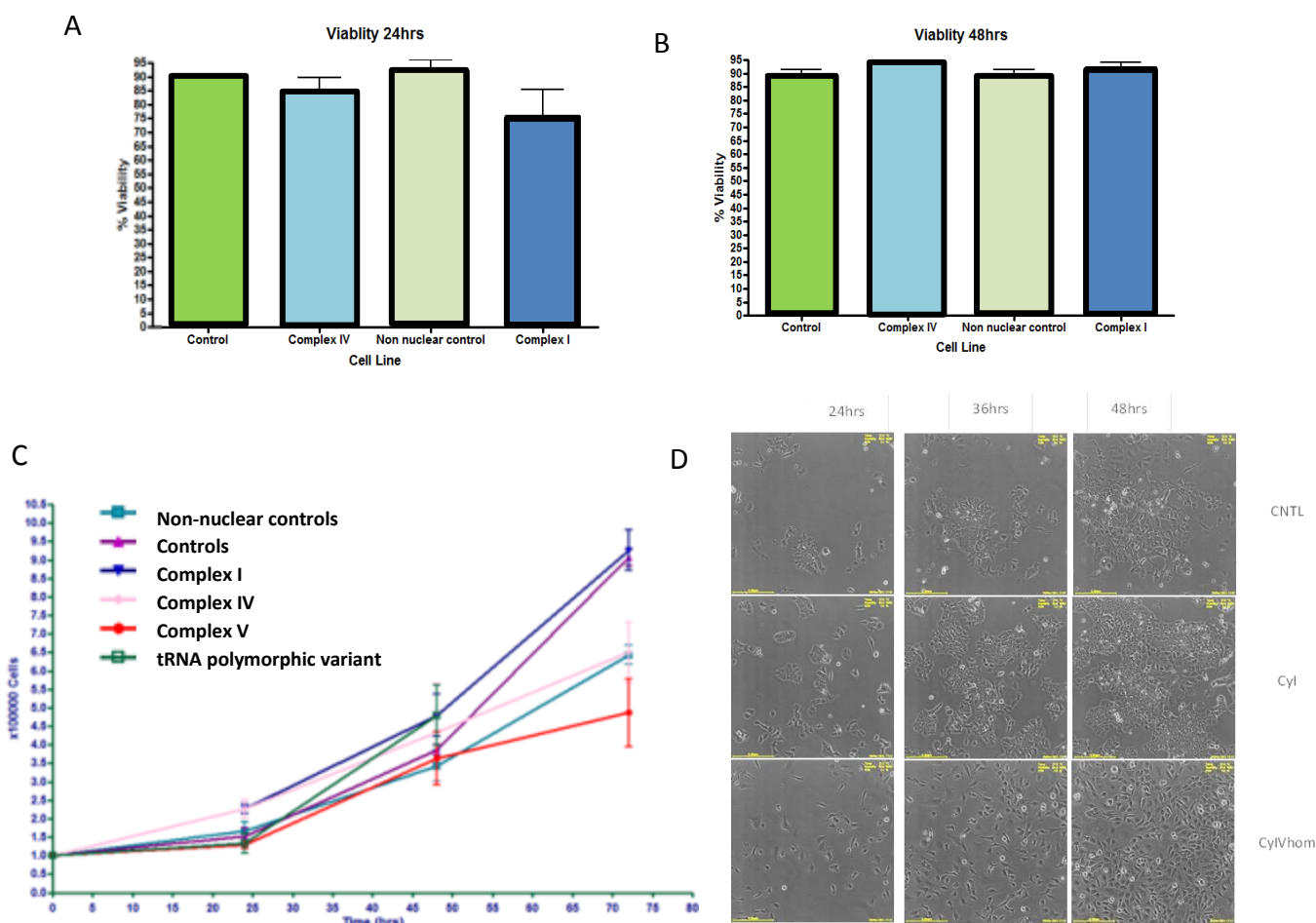
Figure 4.7. Growth analysis of cybrid cell lines

Cell showed no significant differences in viability after 24hrs (A) and 48hrs (B). The rate of growth showed some level of variation (C). Morphology of the cells varied for complex I and complex IV cell lines with complex I cells showing 'colony style growth' (white arrow) and complex IV cells showing more independent angular cell growth. All counts were performed in triplicate.

4.3.5   **Bioenergetics**

Following optimization of micro oxygraphy the decision was taken to utilize the
Seahorse extracellular flux analyser to look at bioenergetics. This 24wp system allowed
for multiple repeats of several cell lines. Studies revealed significant differences
between complex I cybrid oxygen consumption rates and controls for basal and
maximal measurements. All other cell lines showed no such significant changes. All
OCR measurements taken from the complex I cells were dramatically lower than all
other cell lines and this difference was most marked when reserve capacity was
calculated (Figure 4.8). Extracellular acidification rates (a proxy for glycolysis) were
significantly higher in the complex I cells compared to controls and complex IV cybrids
(Figure 4.9). A summary of findings can be seen in Table 4.3.
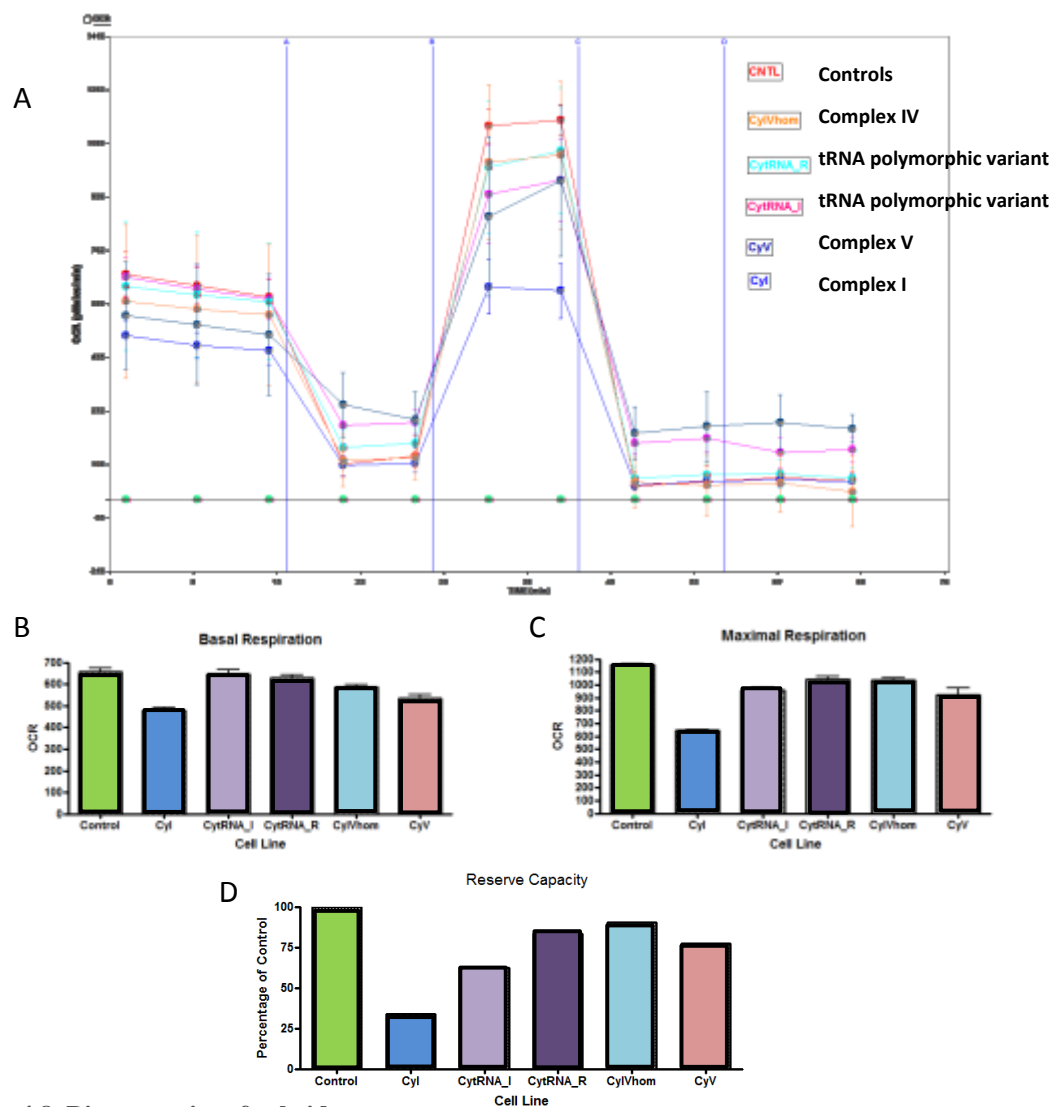
Figure 4.8. Bioenergetics of cybrids

*A/ Oxygen consumption rates generated through seahorse bioanalyser. B/ Basal Oxygen consumption
rates of all cell lines. C/ Maximal OCR after FCCP treatment D/ Reserve Capacity generated from
Maximal and basal measurements.*
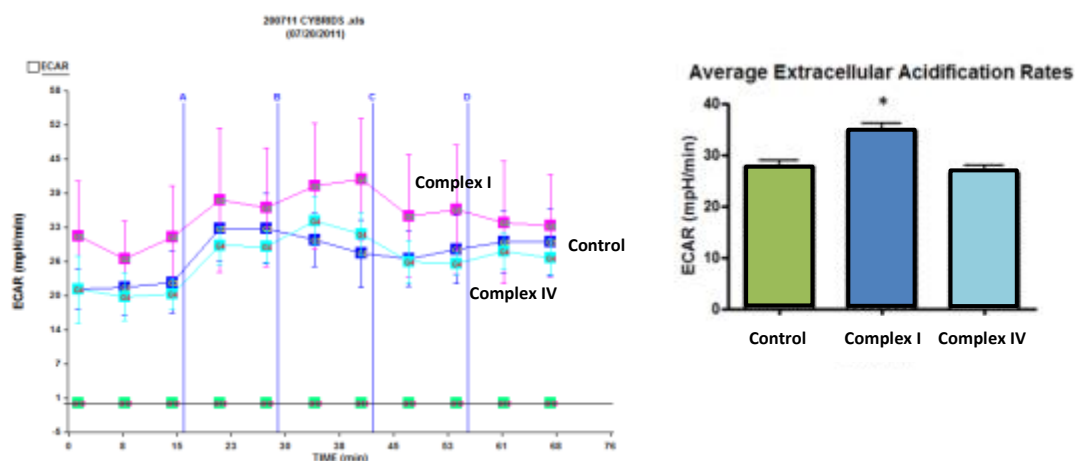
Figure 4.9. Extracellular acidification rates

Complex I cybrid cells showed significantly higher rates of extracellular acidification (pink line) compared to controls (dark blue) and complex IV cells (light blue). Average ECAR is quantified for each cell line (*P=0.032).

Collective Cybrid Cell Lines	Bioenergetic Capacity (%of controls)		
	Basal	Maximal	Spare Resp. capacity
Complex I	72.5	54.3	33.8
Complex IV	90.8	86.9	90.5
Complex V	83.2	78.7	77.5
RNA polymorphism_R	97.7	87.4	83.1
RNA polymorphism_I	98.5	82.6	62.4

Table 4.3. Summary of respiratory capacity

Table shows mean OCRs as a percentage of mean control OCR.

4.3.6   **Neuronal differentiation**

As previously identified, differentiation capacity was severely compromised in the complex I cells compared to controls. With fewer neurons generated from the cybrids and those that were showing limited arborisation (Figure 4.10).
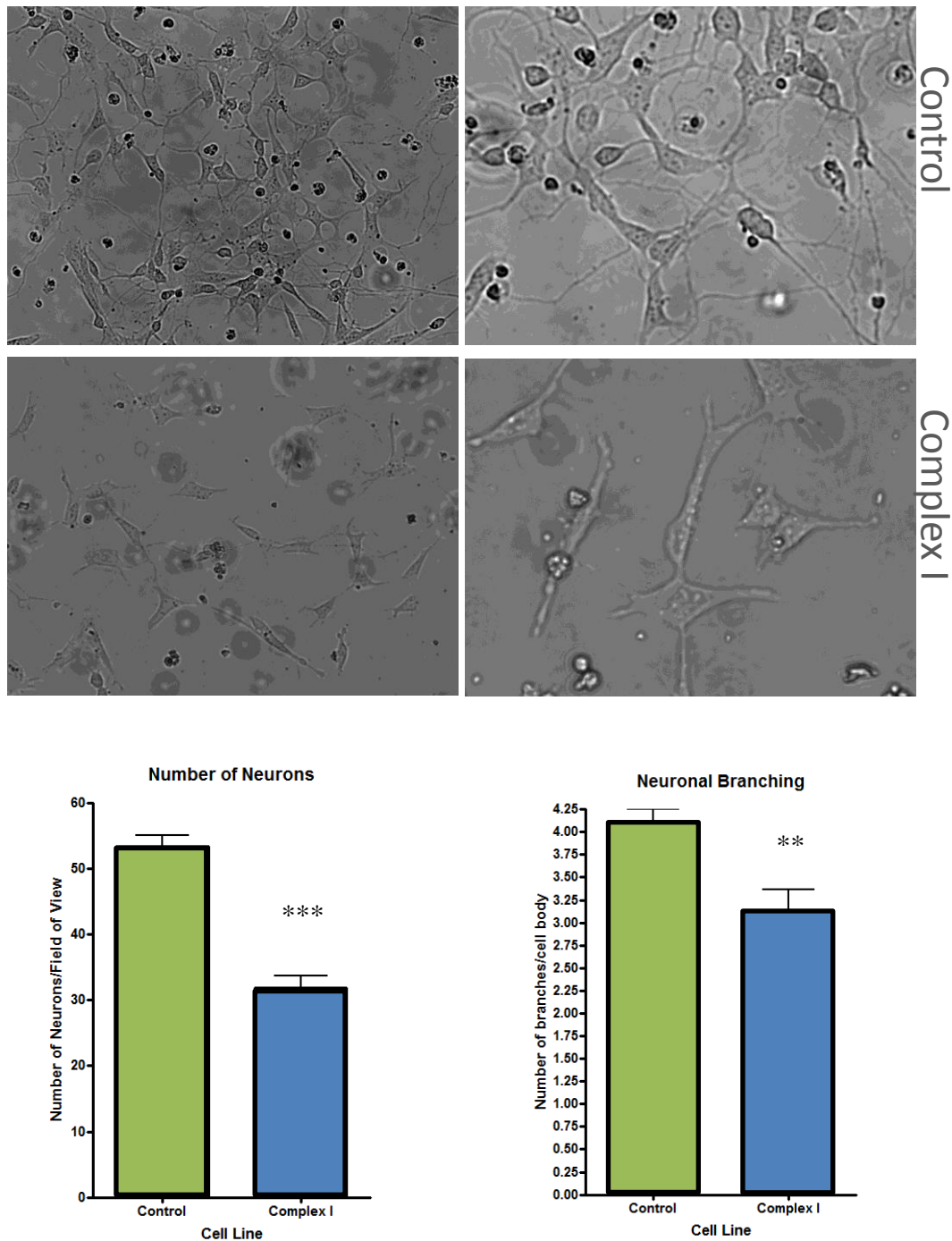
Figure 4.10. Impaired differentiation of Complex I Cybrids.

A/ Representative Images of neuronal differentiation in control cells and complex I cybrids. B/ Quantification of differentiation capabilities, n=15 images over three differentiations. (***P<0.001), (**P=0.002)

4.4 **DISCUSSION**

This chapter summarises the genetic, bioenergetic and differentiation capacity of cybrid cell lines used throughout this study. Prior work has utilised some of these cell lines and, as such, a level of description already exists from these and preliminary work following creation of the cell lines. This work and previous experiments show that oxygen consumption rates are diminished in complex I cells. This coincides with previous studies that showed a severe reduction in complex I enzymatic activity. Interestingly despite showing a smaller but still significant reduction in complex IV activity, this cybrid line did not show significant changes in OCR. The tRNA polymorphic control did not show statistically significant changes for enzymatic activity or OCR levels. Data for enzymatic activity for remaining cell lines was not available but OCR studies did not show a significant deviation from the normal range for basal, maximal or reserve capacity calculations.

The growth rates of cybrid cell lines was assessed. Interestingly the severe complex I mutant cell lines showed an initial greater rate than controls, up to around 24hrs. After this initial 'spurt' the number of cells balanced out and no significant differences were observed. Despite observing an increase in media acidification in the complex I cybrids a change in cell viability was not recorded. Growth conditions were kept the same as work carried out on the cells previously but utilised 0.1% gelatine as an adherence aid and did not utilise a feeder layer. Differentiation capacity was reduced in the complex I cells as previously reported. Both number and neuronal morphology were challenged in the complex I cybrids whereas no quantifiable difference was seen in the complex IV line. Steady state protein levels of subunits of complex I and complex IV were assessed for the two cybrid lines. Both showed a reduction in the proteins associated with their respective mutations suggesting the mutations affect both function and expression of the complexes.

The cybrid cell lines allow a unique means to study the impact of mitochondrial dysfunction. Importantly the pluripotent nature of the ES cells allowed the generation of neurons. This is particularly important considering the most prominent and disabling feature associated with mtDNA mutations is neuronal dysfunction. Furthermore

155

mitochondrial dysfunction and the accumulation of mutations and deletions within mtDNA is associated with a plethora of common neurodegenerative disorders, including PD and the ageing process itself. Studies at the cellular level such as the cybrid work make it possible to increase understanding and hopefully improve therapeutics. Given the inability to obtain neuronal material until post mortem, cell models provide invaluable insight into processes at work that lead to cellular demise, changes that are not observed in tissue samples that represent the end point of disease. Arguably early mechanistic changes offer the best possibility of therapeutically modulating cellular events to prevent catastrophic cell loss. The ES cells also enable assessment of the impact in non-differentiated and differentiated cells. A transition that may reveal important differences in the impact of bioenergetic dysfunction.

Other means to explore the impact of mtDNA mutations include the generation of transgenic mice. There are a number of limitations with these methods, firstly producing such models is problematic with previous reports showing mouse oocytes harbouring mutated mtDNA are quickly lost during oogenesis (Fan *et al.*, 2008). Mouse models also rarely recapitulate all disease symptoms and as such are limited in their relevance to human disorders. The benefit of the cybrid cell lines is complete control of the environment they are cultured in. In contrast to other cell models the cybrid lines contain mutations that are inherent and as such negate the need for administering complex inhibitors, toxins that often have a dramatic and acute effect alongside non mitochondrial effects.

Several unexpected findings arose from these studies. Notably the variable growth rates of the complex I cells, which regularly surpassed their control counterparts. Interestingly alongside increased growth, acidification of the media was notably quicker in these cells (observations of media pH). These findings could be caused by an initial switch to glycolysis over oxidative phosphorylation. Such a phenomenon has been previously described in cancer cells (Zheng, 2012). Another unexpected finding was the oxygen consumption rates of the complex IV cybrids which showed no statistical difference from control lines. The milder mutants still show around 37% complex IV enzymatic activity of the controls. Despite this notable deficiency no significant reduction in basal, maximal or reserve capacity was observed. It may be that our experimental model does not provide enough stress to truly see an effect of this

mutation. Indeed all substrates are provided in abundance within the growth media. Alternatively it may be that the ability for cells to consume oxygen is related to the severity of the mutation and these studies would suggest the threshold for this dysfunction is fairly high.

During these studies we confirmed previous reports that complex I cybrids were compromised in their ability to differentiate into neurons. The reasons for this are unclear at this point but various explanations are plausible. Firstly, it has been alluded to that neuronal differentiation may be dependent on complex I activity. A report by Papa *et al* showed a marked increase in the activity of complex I during differentiation of mouse hippocampal and glial cells (Papa *et al.*, 2004). Indeed it makes sense that increased complex I activity increases energy metabolism that can then respond to high energy demand from differentiating cells. The reduction in complex I activity in the cybrid cell lines may therefore be unable to respond to this demand and as such create fewer and less well defined neurons (limited arborisation). In line with Papa's study it would seem more likely that a reduction in proliferation of neurons rather than increased cell death accounts for the reduction of neurons observed, although the latter is possible through increased oxidative stress. This said an increase in cell death was not seen in these cells (unquantified observations). In previous complex I models Wong *et al* also showed a decreased production of neurons and glial cells when generated from Leber's hereditary optic neuropathy, LHON-NT2 cybrids, containing two of the most commonly associated LHON mutations, 11778G>A and 3460G>A (Wong *et al.*, 2002). Interestingly this report found no difference in cell morphology, expression of neural genes or membrane potential but did reveal an increase in superoxide production in differentiated neurons. Differences in findings may stem from complex specificity or indeed dependence on severity.

4.4.1   **Areas for future investigation**

The cybrids used in this study could be further characterized; importantly measurements of bioenergetics in newly derived neurons still need to be undertaken. This may be extremely important for understanding any changes seen when neurons are compared to undifferentiated cells. Further control of characterization experiments could also be a future development. For example controlling for stage of cell cycle and monitoring each

cell lines progression through stages of this cycle could ensure this variable is not affecting the results and may reveal further differences between the cybrid cell lines. Although this thesis has focused on the impact of mitochondrial dysfunction on PD pathogenesis (stemming from complex I deficiency) future developments would likely include mtDNA disorders. For example, the creation of new cybrid lines and using the existing lines that were not encompassed in this study could reveal far more about complex and mutation specific bioenergetic and morphological changes.

To continue and build upon methodologies used within this PhD with a focus on Parkinson's disease it would be extremely beneficial to generate PD cybrids, i.e. enucleated ES cells, repopulated with known PD mutations. Along these lines the incorporation of iPS cells derived from PD patient fibroblasts into similar experimental models could provide more PD specific information on how mutations impact on bioenergetics, differentiation and mitochondrial characteristics such as morphology and dynamics. Both the iPS cells and novel cybrid lines could easily be incorporated into methodologies already established for this work but could offer interesting new angles that may build upon or explain findings gained from these studies. Finally the specific generation of dopaminergic neurons instead of the mixed culture used in these studies will enable greater links to be drawn with PD pathogenesis. Although this was attempted as part of this work, newer protocols now exist that would enable greater efficiency of specific cell type generation. This said, it will be important to consider the impact the cellular milieu has upon cell function and survival.

Chapter Five

Mitochondrial Dysfunction and Autophagy

Chapter 5. Measuring the effect of mitochondrial dysfunction on the autophagy pathway in fixed cells

5.1   INTRODUCTION

5.1.1   Overview

Autophagy is a crucial, highly conserved process that functions to remove unnecessary or damaged subcellular structures; including mitochondria (reviewed in 1.6). The importance of this degradative process is highlighted when it is compromised in experimental models, autophagy knockout (KO) cell models for example, show severe phenotypes. In mouse *ATG5* or *ATG7* knockout studies, ablation of either of these key autophagy genes causes severe neurodegeneration, highlighting the importance of basal autophagy for neuronal survival (Hara *et al.*, 2006). Furthermore, several autophagy related proteins have been shown to be affected in various neurodegenerative disorders (Son *et al.*, 2012). Beclin1, for example, has been shown to be markedly reduced in Alzheimer's disease (Pickford *et al.*, 2008), LC3-II protein expression shows a marked increase in mouse models of Huntington's disease (Heng *et al.*, 2010) and several genetic mutations in Amyotrophic lateral sclerosis (ALS) disturb the autophagic process in motor neurons (Chen *et al.*, 2012).

Cellular homeostasis is crucially reliant on maintenance of mitochondrial integrity through autophagy and biogenesis. Just as a population of mitochondria rely on functional autophagic systems the same can be said of the reverse. Increasing evidence is pointing towards a regulatory role for mitochondria in the initiation of the autophagy process itself. Conditions as broad ranging as ageing, cancer and neurodegeneration imply a connection between mitochondria and autophagy, with a disruption of either associated with the pathogenesis of these disorders. Where much data implies that dysfunctional autophagy can bring about cellular demise through (amongst other routes) accumulation of damaged mitochondria, as yet no evidence discredits the more prominent role of mitochondrial dysfunction as an initiating factor. Previous cell models of mitochondrial dysfunction have revealed various alterations ranging from up regulation to a reduction in the autophagy process (Chen *et al.*, 2007a; Mader *et al.*, 2012). These changes therefore, seem highly reliant on cell type and means of inducing mitochondrial dysfunction.

Most models rely on the use of electron transport chain inhibitors or cell lines derived from mouse models with mitochondrial dysfunction. The use of Complex I and II inhibitors (rotenone and thenoyltrifluoroacetone) in Hek293 cells for example has been shown to induce autophagy and cell death, and this death can be decreased by autophagy inhibition (Abramov *et al.*, 2007). Conversely, rotenone administered to differentiated SH-SY5Y cells has been shown to inhibit autophagic flux (Mader *et al.*, 2012). Although at first glance these findings may appear contradictory the inhibition of autophagic flux may represent an initial increase of autophagy but blockage of final clearance. These discrepancies show that the use of complex inhibitors may be too crude to pick up subtle alterations in the autophagy pathway, changes which are likely to react rapidly to relatively small bioenergetic changes.

To understand further the relationship between mitochondria and autophagy in this study, the cybrid cell line model was employed (reviewed in chapter 4). This had multiple benefits as it allowed the assessment of specific mtDNA mutations, known to create severe respiratory phenotypes, against cells of the same nuclear background; whilst allowing strict control of the cells environment.

5.1.2   Stages of the pathway

To observe a dynamic event in a relatively static assay, multiple points of the autophagy initiation, induction and completion pathway were chosen (Figure 5.1 and reviewed in depth in chapter 1.6). Looking at relative levels of each of these would hopefully give a more accurate interpretation of events within the biological system.
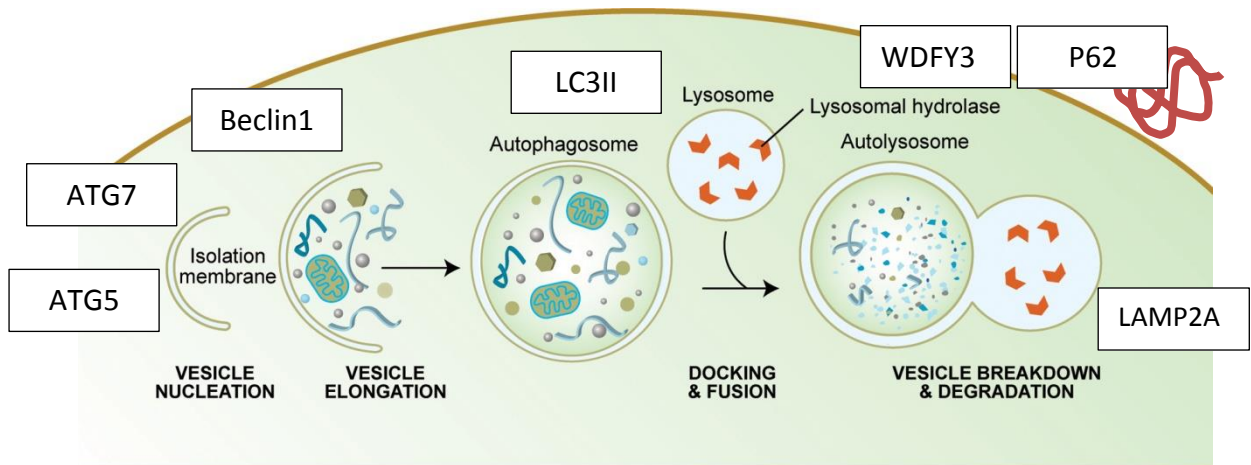
Figure 5.1. Points of autophagy pathway to be assessed.

A range of markers were used within this study to ensure all aspects of the autophagy pathway, from initiation, formation and completion were encompassed.

All of the proteins assayed have been previously studied to some extent with relation to Parkinson's disease or synucleinopathies. A 2009 study for example, revealed that Beclin1 gene transfer is able to ameliorate some neurodegenerative pathology in alpha-synuclein models of the disease. This rescue was proposed to occur through intracellular degradation of alpha-synuclein (Spencer *et al.*, 2009a). LC3 II has been investigated with relation to PD, a study in 2011 showed that properties of LC3 II were altered and levels increased in an insoluble fraction from patients with DLB (Tanji *et al.*, 2011). Furthermore rotenone treatment has been shown to up regulate LC3 expression and down regulate p62 expression (Xiong *et al.*, 2013). The adaptor protein-p62 has been shown to preferentially target alpha-synuclein inclusions and knock out experiments have revealed it is required for alpha-synuclein autophagy (Watanabe *et al.*, 2012). LC3 II accumulation may represent an increase in the autophagy pathway but equally a blockage in autophagic flux, i.e. compromised clearance of autophagosomes. P62 also known as Sequestosome-1, targets specific cargoes for autophagy and is often taken as a proxy for autophagy function as its accumulation shows direct inverse correlation with LC3 II. Finally, ATG5 is crucial for initiation of autophagy as demonstrated through knock down experiments. Recently, a functional variant within the ATG5 promoter has been described in idiopathic Parkinson's disease (iPD) and shown to significantly enhance transcriptional activities of the ATG5 gene promoter (Chen *et al.*, 2013).

To better understand the processes at work during complex I dysfunction several protocols have been developed to monitor autophagy. Importantly distinguishing specific mitophagic events proves problematic given the broad spectrum of targets the autophagy pathway is responsible for. Further complexity is encountered as mitophagic events are regulated by a number of factors including autophagy flux, autophagosome formation, maturation and degradation.

5.1.3   Aims of this study

This study aimed to analyse the levels of basal autophagy in a cell line model of complex I dysfunction. Complex I cybrids were chosen for two reasons, firstly the mutations carried within these cybrids were more severe and secondly complex I is heavily implicated in the pathogenesis of Parkinson's Disease, a neurodegenerative condition which is well evidenced to have altered autophagy and mitochondrial functioning. Importantly the mitochondrial dysfunction in these cells is not brought about by pharmacological treatment and is therefore intrinsic to the cells. Prior characterisation of these cells revealed dramatic changes in enzymatic and OXPHOS capabilities (ch4, table 4.3). The impact of this on stages along the autophagy pathway was to be explored. In doing so any alterations that were observed could be tracked to their point in the autophagy pathway and possible mechanisms for changes could be explored.

1. Optimize ICC of different autophagy markers

2. Quantify expression of autophagy markers in stem cells and neurons from complex I cybrids and their nuclear controls.
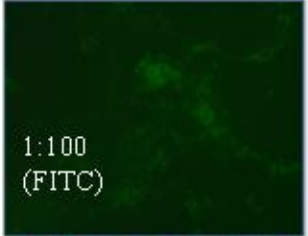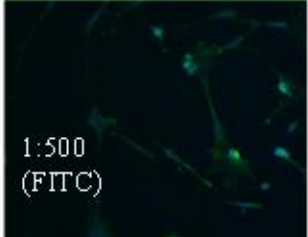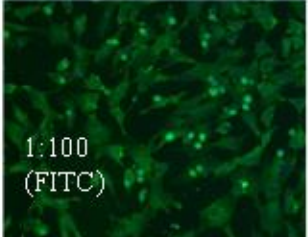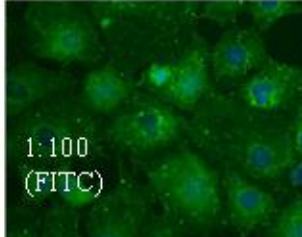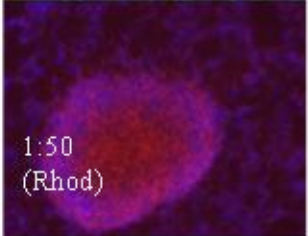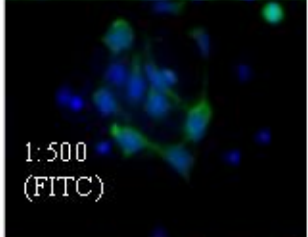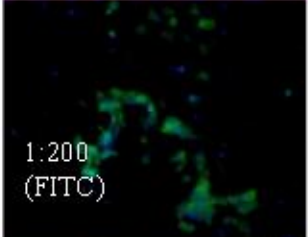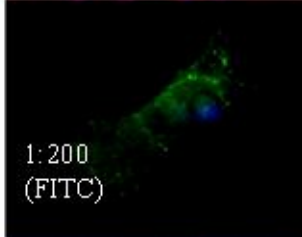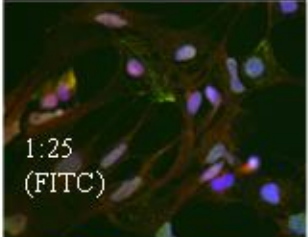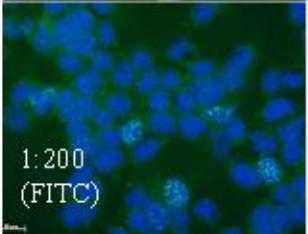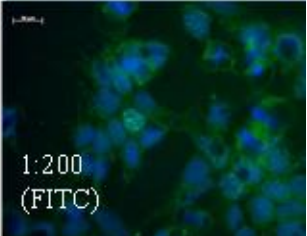
5.2   METHODS

5.2.1   Basic methodology for undifferentiated cells

Undifferentiated passage matched cells to be used in this study were thawed at least 48hrs prior to seeding to coverslips, maintained in T75s at 37°C with 5% CO_2 and allowed to reach confluency. Cells were then harvested and seeded at appropriate densities (1x10^{5}cells/well) into six well plates containing 22mm glass coverslips, pre-coated with PDL and laminin. The cells were allowed to settle and grow for 48hrs before washes with PBS and fixation in 4% PFA for 10mins, followed by a further three PBS washes. Cells were stored in their final PBS wash at 4°C until stained. Staining was carried out as per the basic immunocytochemical protocol outlined in ch2.3.6.1. For each antibody, optimal working concentrations were ascertained by testing a range of concentrations as seen in Figure 5.2. Equally, antibodies from different manufacturers often gave highly variable results. As such, selecting the most effective antibody from a range of producers was vital (Figure 5.3).

Figure 5.2. Optimization of autophagy antibodies for ICC

All antibodies used in this study were tested at a range of concentrations to gain the best results possible. Certain antibodies were deemed ineffective for this application. For example LAMP2A did not reveal positive staining where as ATG7 and WDFY3 required high concentrations that were deemed unworkable. Importantly, each stain was scrutinized under a range of magnifications as higher magnifications often revealed desirable staining patterns often missed at lower magnifications (eg rh panels of ATG5 and Beclin1). Rhodamine was used in some cases as it seemed to be brighter with certain antigens. For WDFY3 as the staining was weak, the cells were counterstained with porin to ensure correct visualization.

	Example tested concentations		Final Working Conc.
LAMP2A	1:500 (FITC)	1:100 (FITC)	Ineffective
ATG5	1:500 (FITC)	1:100 (FITC)	1:100 (FITC)
ATG7	1:100 (FITC)	1:50 (Rhod)	1:50 (Rhod)
Beclin1	1:500 (FITC)	1:200 (FITC)	1:200 (FITC)
WDFY3	1:50 (FITC)	1:25 (FITC)	1:25 (FITC)
LC3	1:500 (FITC)	1:200 (FITC)	1:200 (FITC)
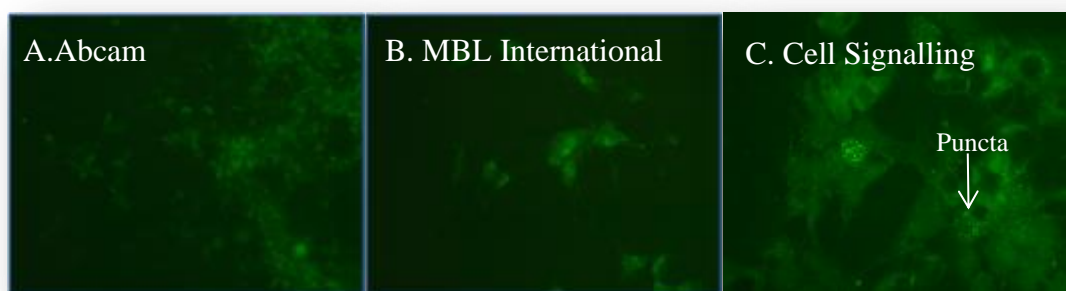
Figure 5.3. Variation between antibodies

Several different antibodies were often trialed for the same marker. LC3 for example was ineffective or weak for this application when purchased from certain companies (A and B) but displayed the desired pattern of staining, i.e. punctate, when purchased from Cell Signaling (Massachusetts) (C).

5.2.1.1   *Imaging and quantification*

All cell imaging was carried out using the Zeiss AxioImager at x40 magnification, using Axiovision version 4.8. Antibodies showed a range of staining patterns dependant on their cellular targetand so, different quantification methods were employed. For markers which showed clear punctate staining such as LC3, matlab (Mathworks, MA) was used to quantify 'dots per cell'. The automated program created by Mr. John Grady (PhD student, Mitochondrial Research Group) uses parameters such as intensity and diameter to count puncta within a cell border defined by the user (Figure 5.4). Optimum diameters were calculated using measurement tools within the software. For stains which were more diffuse in nature, densitometry was used which quantifies the intensity of any given marker, again within a user defined cell area. The numbers generated from both methodologies were then compared for different cell lines, and results for each marker were tested for significant differences using a Student T test unless otherwise stated.

Interestingly, certain markers, namely ATG5 and Beclin1 showed a combination of staining patterns. For example although their staining was not 'truly punctate' as seen with LC3, the stains did show areas within a cell of higher intensity, with densitometry these variations are not accounted for as the software generates an average intensity for the entire cell area (see Figure 5.6). For this reason both densitometry and a refined

version of the matlab program were employed, in doing so data was generated for both differences between the overall marker intensities, and any differences that may occur in the accumulation of higher intensity areas within a cell.
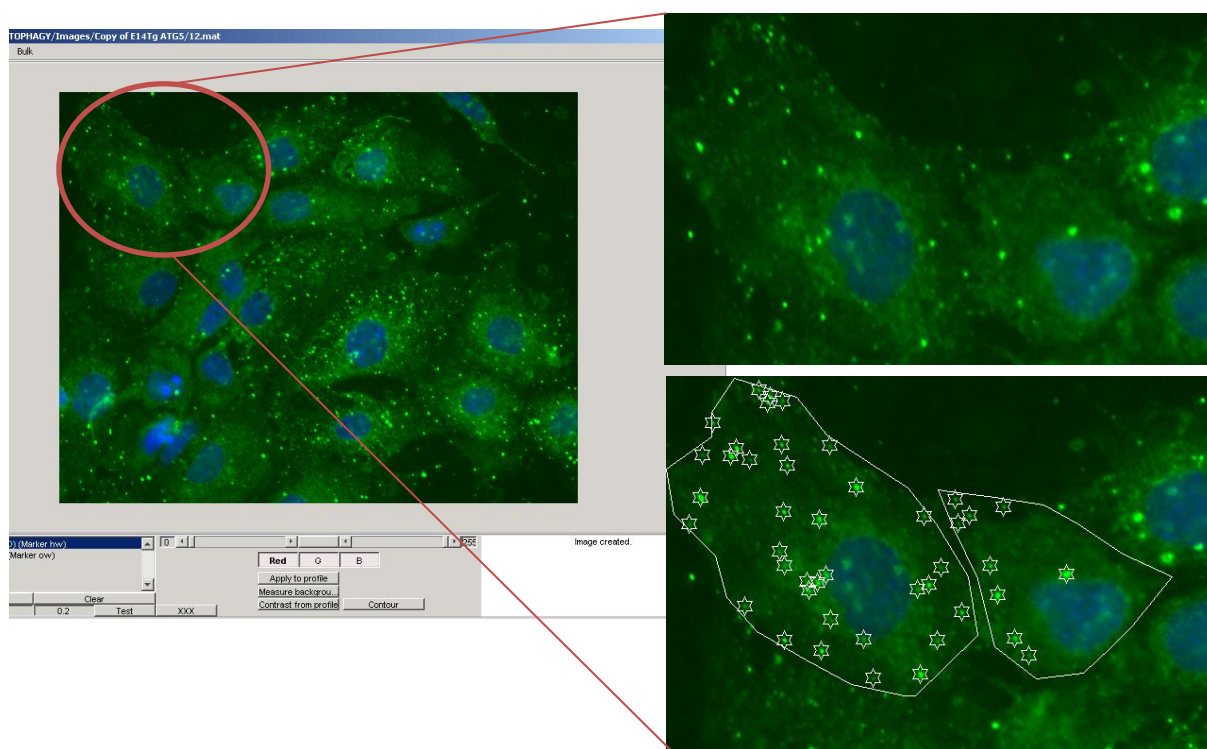
Figure 5.4. Matlab quantification of puncta

A specially designed matlab algorithm (created by Mr John Grady) was used to quantify puncta/cell. Using intensity and diameter parameters the software was able to identify punctate structures within a user defined cell border.

5.2.2   **Neuronal observations**

To look at changes in markers specifically within neuronal populations, the ES cells were differentiated as per the protocol outlined in ch2.3.3.5. On day 15 of the Bain's protocol (Bain *et al.*, 1995) neurons were gently washed with PBS, fixed with 4% PFA before three further washes in PBS. If storage was required the neurons were left in PBS at 4°C. Staining was carried out as per undifferentiated cells.

5.2.2.1 *Image capture and quantification.*

To limit bias when capturing images of neurons, the Axiovision's mosaic feature was employed. Briefly, the automatic stage was programmed to meander taking 8x8 grids of x40 magnification images. To ensure image quality throughout, points of 'focus correction' were programmed in prior to running the imaging protocol. This method generated large tiled images that could be separated into smaller tiles for quantification; by doing this the population of neurons captured was randomised. As with undifferentiated cells, differences between cell lines were analysed through student t tests if not otherwise stated. Due to the morphology of neurons, the quantification proved slightly more complicated than undifferentiated cells. As such neurons were analysed both for whole cells and cellular regions- cell bodies and processes.

5.3 RESULTS

5.3.1 Undifferentiated cells

All markers revealed differences in staining patterns between complex I cells and their passage matched controls. Three independent experiments were carried out and results combined to ensure day to day experimental variations were accounted for.

5.3.1.1 *BECLIN 1 Staining*

BECLIN 1 showed significantly lower staining intensities in complex I cybrid cells when compared with non cybrid control and cybridization controls ($P<0.0001$) as shown in Figure 5.5. Although 'true puncta' were not observed in the BECLIN1 stains, areas of increased staining intensity were seen and as such the same stained sections were analysed using the matlab program which had been modified to locate larger regions of increased staining intensities. Consistent with the observed data, these results revealed a dramatic reduction in high intensity areas (Figure 5.6 arrow). The complex I cells showed a uniformly distributed weak signal (Figure 5.6B).

Figure 5.5. Beclin 1 staining intensities

A. Average intensities of Beclin1 stains for three ES cell lines, controls, complex I mutants and tRNA polymorphic cybridization controls, revealed significant reduction in Beclin 1 positive puncta in complex I cybrid cells (p<0.0001). N=75, data collected over 3 separate experiments.
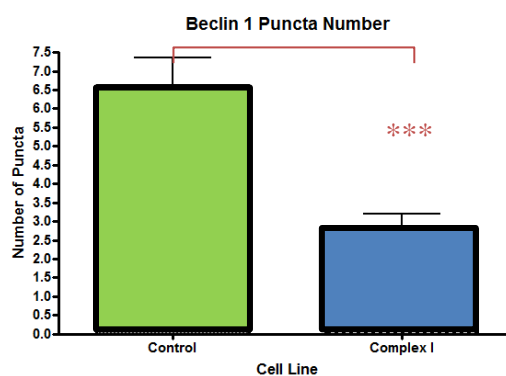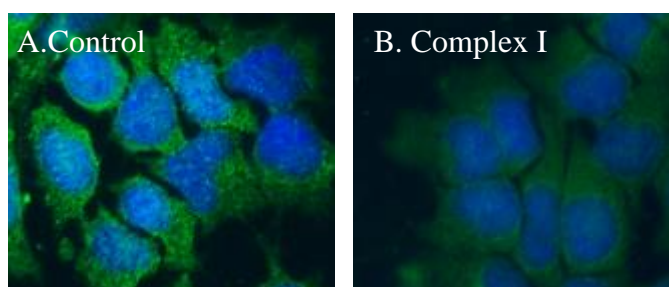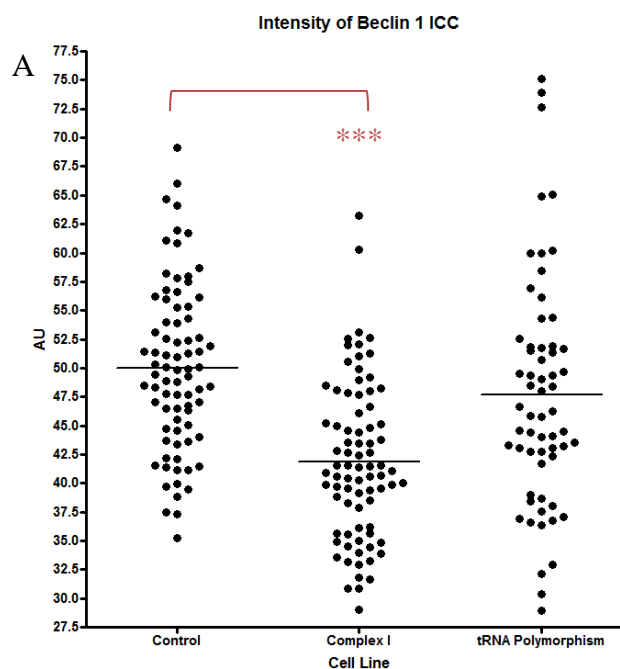
Figure 5.6. Beclin 1 areas of high intensity

Images were run through a specially designed matlab program to assess the amount of high intensity areas of staining in cells from controls and complex I cells. Controls showed a significant increase in high intensity areas (P<0.0001) compared to complex I cells, which reflected the observed results (B). N=75, data collected over 3 separate experiments.

5.3.1.2 *ATG5 Staining*

The intensity of ATG5 staining was not significantly different for any of the cell lines studied (Figure 5.7). Although a notable difference in staining patterns was observed with areas of high intensity within control cells but absent in complex I cybrids where a more uniform diffuse weak stain was seen (lower images). For this reason the modified matlab program was employed to assess for areas of higher staining intensity. These studies revealed a significant reduction in higher intensity areas within complex I cells (Figure 5.8).
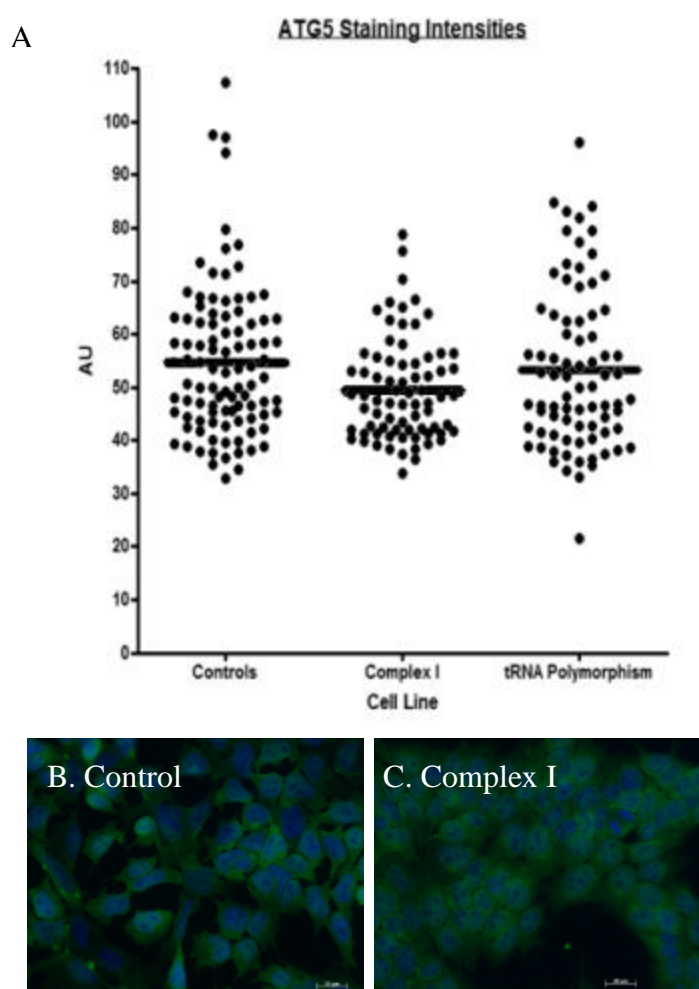
Figure 5.7. ATG5 staining intensities

A. Average intensities of ATG5 stains for three ES cell lines, controls, complex I mutants and tRNA polymorphic cybridisation controls, revealed no significant changes. Rrepresentative images of control (B) and complex I(C) cybrid ATG5 stains. N=75, data collected over 3 separate experiments.
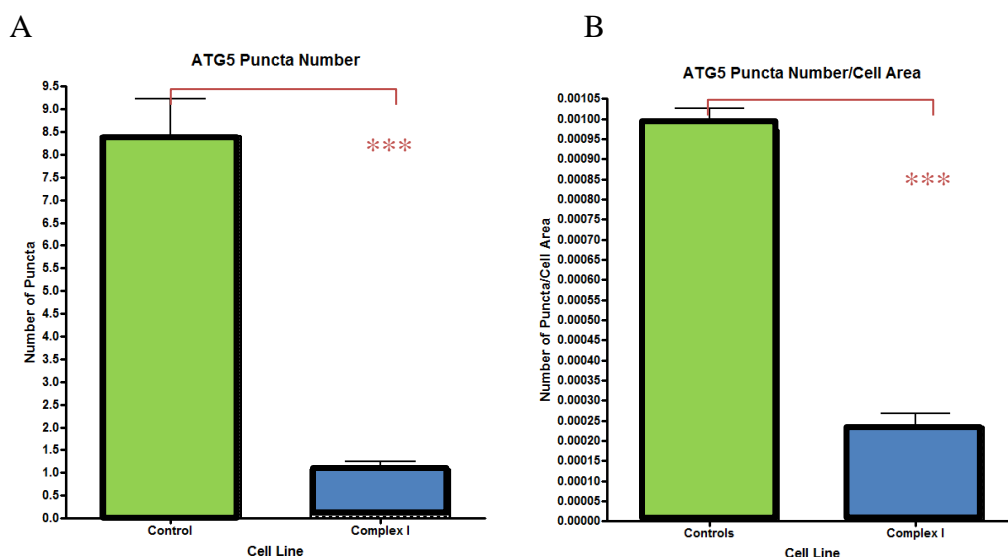
Figure 5.8. ATG5 areas of high intensity

Images were run through a specially designed matlab program to assess the amount of high intensity areas of staining in cells from controls and complex I cells. Controls showed a significant increase in high intensity areas (P<0.0001) compared to complex I cells (A), which was maintained when normalised to cell area (B). N=75, data collected over 3 separate experiments.

5.3.1.3   *LC3 Puncta Results*

LC3 staining was quantified using matlab, where the number of puncta was counted for each cell. Based on puncta numbers generated these were separated into four categories- ranging from very high (many intense puncta), through high, medium and low (uniformly distributed weak signal) shown in right hand panel (Figure 5.9. C). Analysis of the percentage of cells for each line that fell into each category was then analysed (Figure 5.9. A). Complex I cells displayed statistically lower percentages of cells in the very high or high brackets compared to all other cell lines (P<0.0001). When analysed separately from a second experiment actual puncta numbers were again statistically lower within the complex I cells (P=0.005) (Figure 5.9. B).

A

B
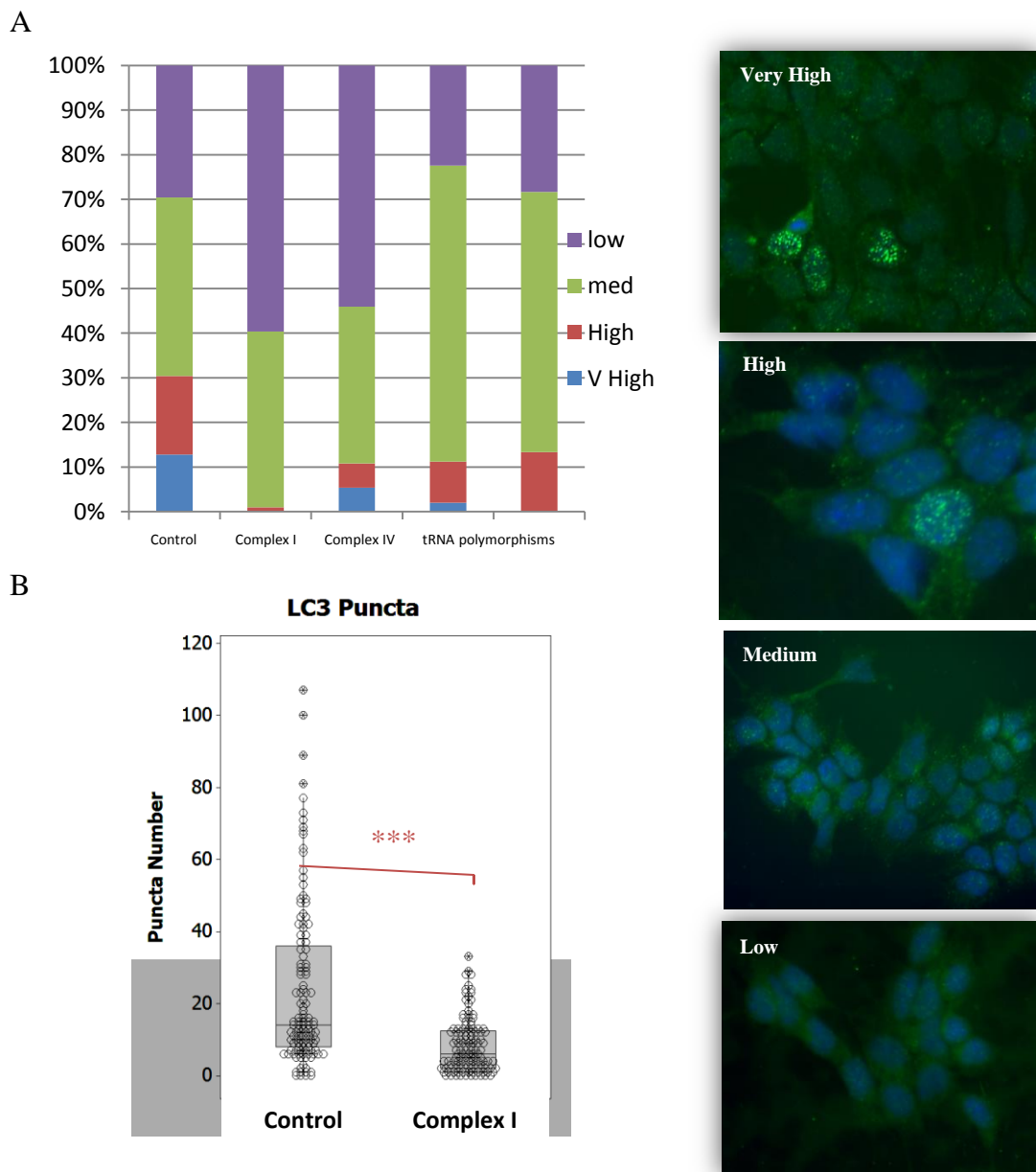
Figure 5.9. LC3 puncta stains

A. Percentages of cells falling into each puncta number category shown in rh panel. Complex I mutants showed low levels of cells with very high or high staining, with majority falling into the low bracket N=75, data collected over 3 separate experiments. B. Individual puncta counts again showed much lower numbers in complex I cells compared to controls (P<0.0001), N=100.

5.3.1.4 *LC3 staining following rapamycin treatment*

Rapamycin is a known inducer of autophagy, through its action on mTOR. To ensure the LC3 antibody was picking up LC3 puncta, its expression was induced using 24hrs of 150nM rapamycin treatment in control cell lines (Figure 5.10 top panel). An increase from medium/high expression to very high expression was observed. The same rapamycin treatment was used on the complex I cells (Figure 5.10 bottom panel). Interestingly the cells went from low to high/very high LC3 puncta expression, implying the capacity to induce autophagy was not lost in these cells; rather a reduced basal expression existed.
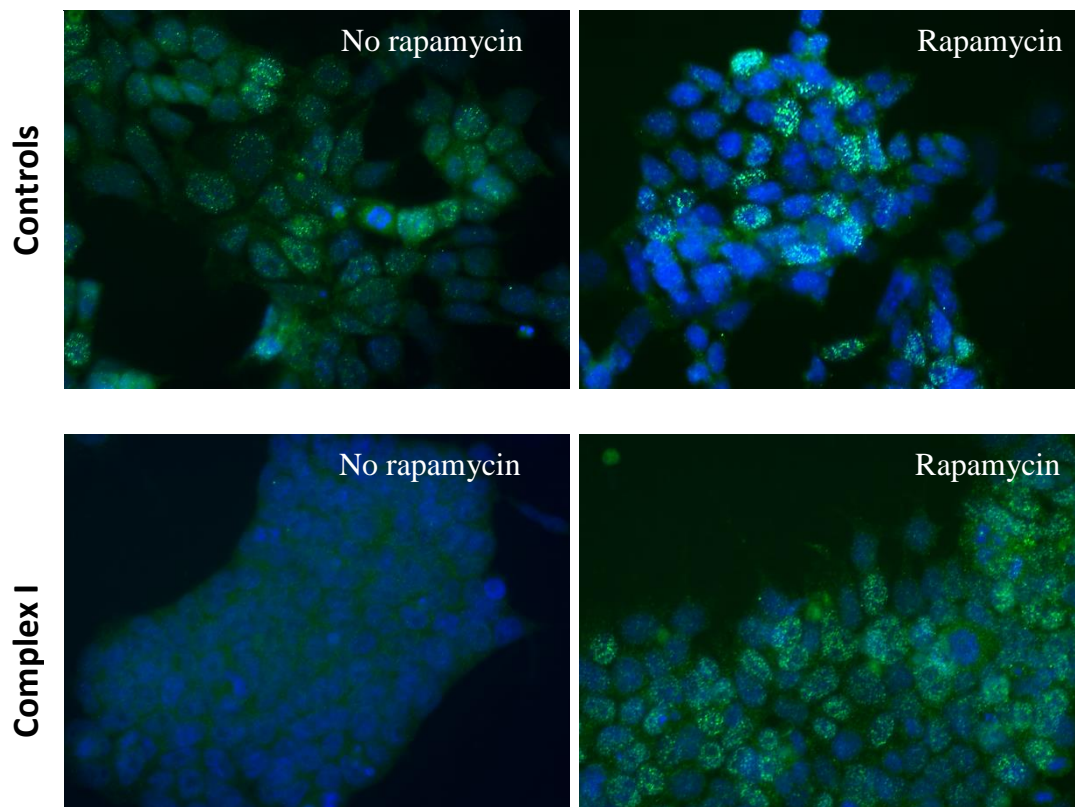
Figure 5.10. Rapamycin treatment of cells increases LC3 expression

Cells were treated for 24hrs in 150nM rapamycin, following which they were fixed and stained for LC3. An increase in LC3 expression was seen in both controls and complex I cells following rapamycin treatment (rh panels).

5.3.1.5 *Western Blots of autophagy markers*

Immunoblotting was performed on cell lysates of control and complex I cybrid undifferentiated cell lines as per methods outlined in chapter 2.4.3. Unfortunately the number of antibodies that were effective in the western blot application were limited. Despite this, three antibodies showed sufficient signal and specificity, these included, LC3, P62 and ATG12. LC3 showed a reduction in overall intensity, however it is the conversion of LC3 I to LC3 II that associates with autophagosome function, picking up LC3 I signal was difficult and LC3 II sensitivity to the immunoblotting method has previously been reported as far greater than that of LC3 I (Figure 5.11). A shows a LC3 blot demonstrating weak LC3 signal in complex I cybrids. P62 showed a dramatic increase in levels compared to control cell lines (Figure 5.11B) implying reduced autophagy. Finally ATG12 whose conjugation with ATG5 is important for vesicle expansion and completion showed a reduction in expression at around 58kDa, where we would expect to find ATG12-ATG5 heterodimer expression (Figure 5.11C).
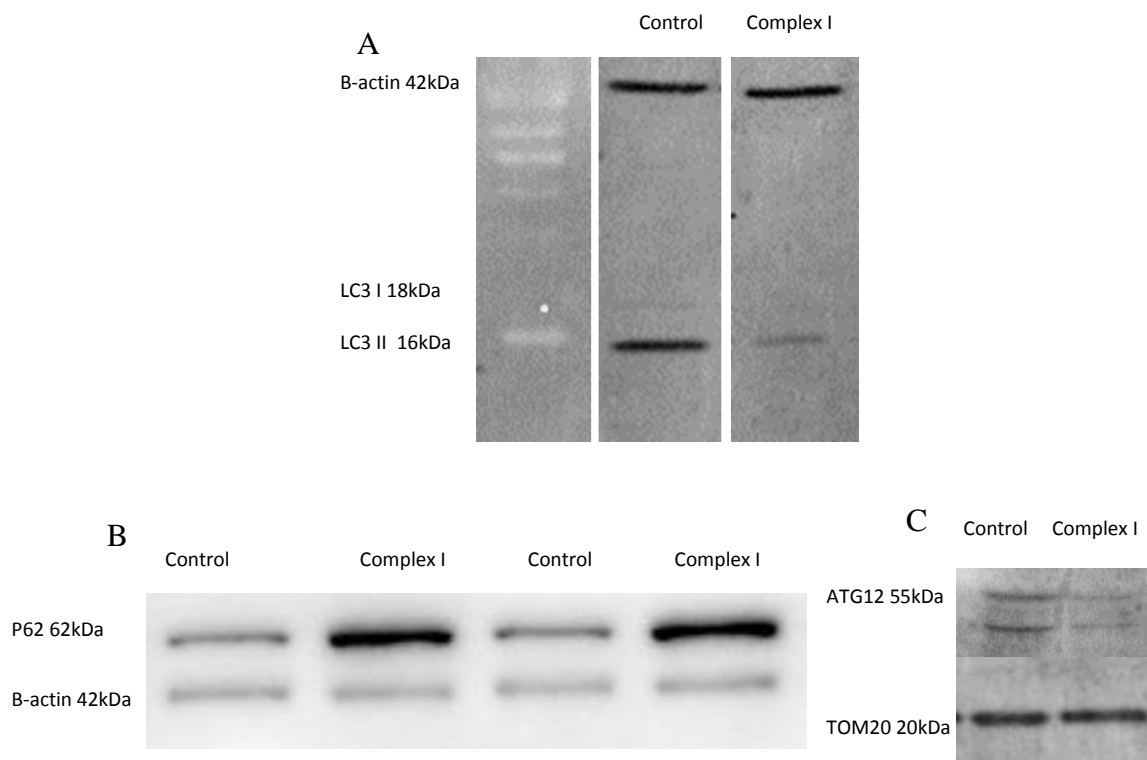
Figure 5.11. Immunoblotting of autophagy proteins

Cell lysates from control and complex I undifferentiated cybrid lines were analysed for steady state protein levels of LC3, P62 and ATG 12. LC3 and ATG12 showed a reduction in expression (A,C) whereas P62 expression was dramatically increased (B).Blots are representative images from a minimum of three experiments.

5.3.2 **Neuronal Observations**

Following differentiation and fixation at day 15, a mixed neuronal population for both control and complex I cybrid cells were stained for autophagy marker expression. Analysis of neurons proved more difficult than undifferentiated cells with cell bodies often being overexposed in order to visualise neuronal processes. Despite this, several differences were noted (Figure 5.12).

5.3.2.1 *LC3 staining*

In cell bodies intensity of staining was greater in controls than complex I cells (Figure 5.13. A), although no differences were observed in the number of puncta (Figure 5.13. B). A noticeable difference however did occur when analysing puncta in neuronal processes. The complex I cybrids displayed hardly any puncta outside their cell bodies, (Figure 5.13. C), suggesting inhibition of LC3 trafficking or aggregation in cell bodies.
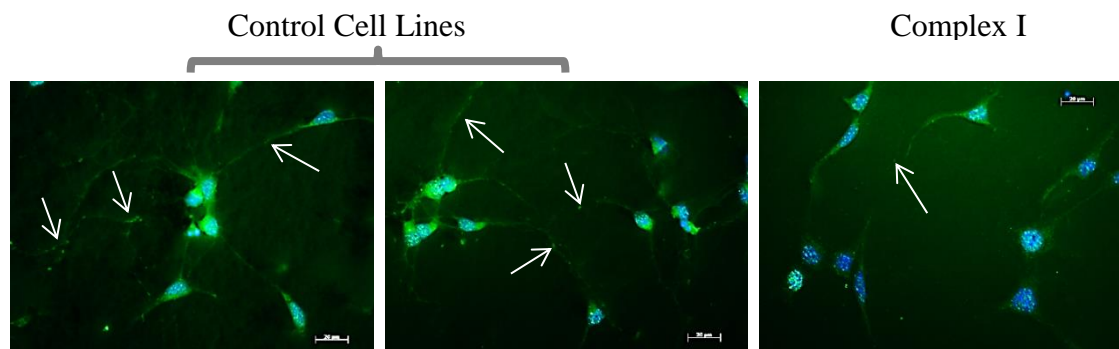
Figure 5.12. Neuronal LC3 images

Control cells showed typical patterns of staining, with puncta seen both within the cell bodies and along processes (white arrows). Complex I cells conversely did not show puncta outside cell bodies.
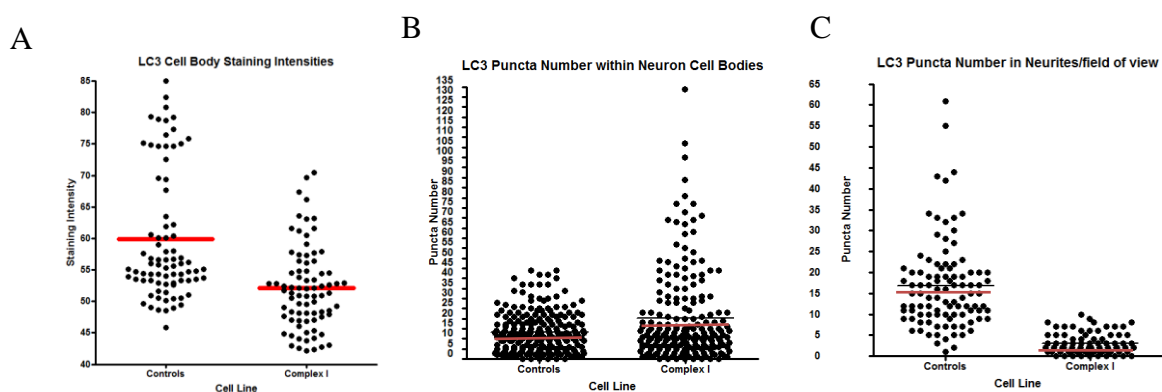
Figure 5.13. Quantification of LC3 in neurons

A. LC3 showed higher overall intensities in cell bodies of control neurons compared to complex I derived neurons (P<0.0001). B. No differences were observed however for number of puncta in cell bodies. C. Numbers of puncta observed in processes was dramatically increased in controls when compared to complex I neurons (P<0.0001). N=75 over two separate experiments.

5.3.2.2   *Neuronal ATG5 Observations*

Day 15 fixed neurons were also analysed for ATG5 expression. Complex I derived neurons had statistically higher cell body ATG5 intensities than their control counterparts (P=0.0005) (Figure 5.14. B). The patterns of staining were dramatically different between control and complex I deficient cells, with many puncta visible in processes of control neurons (white arrows) but entirely absent from complex I derived neuronal processes which displayed intense uniform cell body staining (white arrow head) (Figure 5.14. A). This phenomena was reflected in the quantification of puncta/neurite with a significantly lower number of ATG5 processes having puncta (P<0.0001) (Figure 5.14. C).
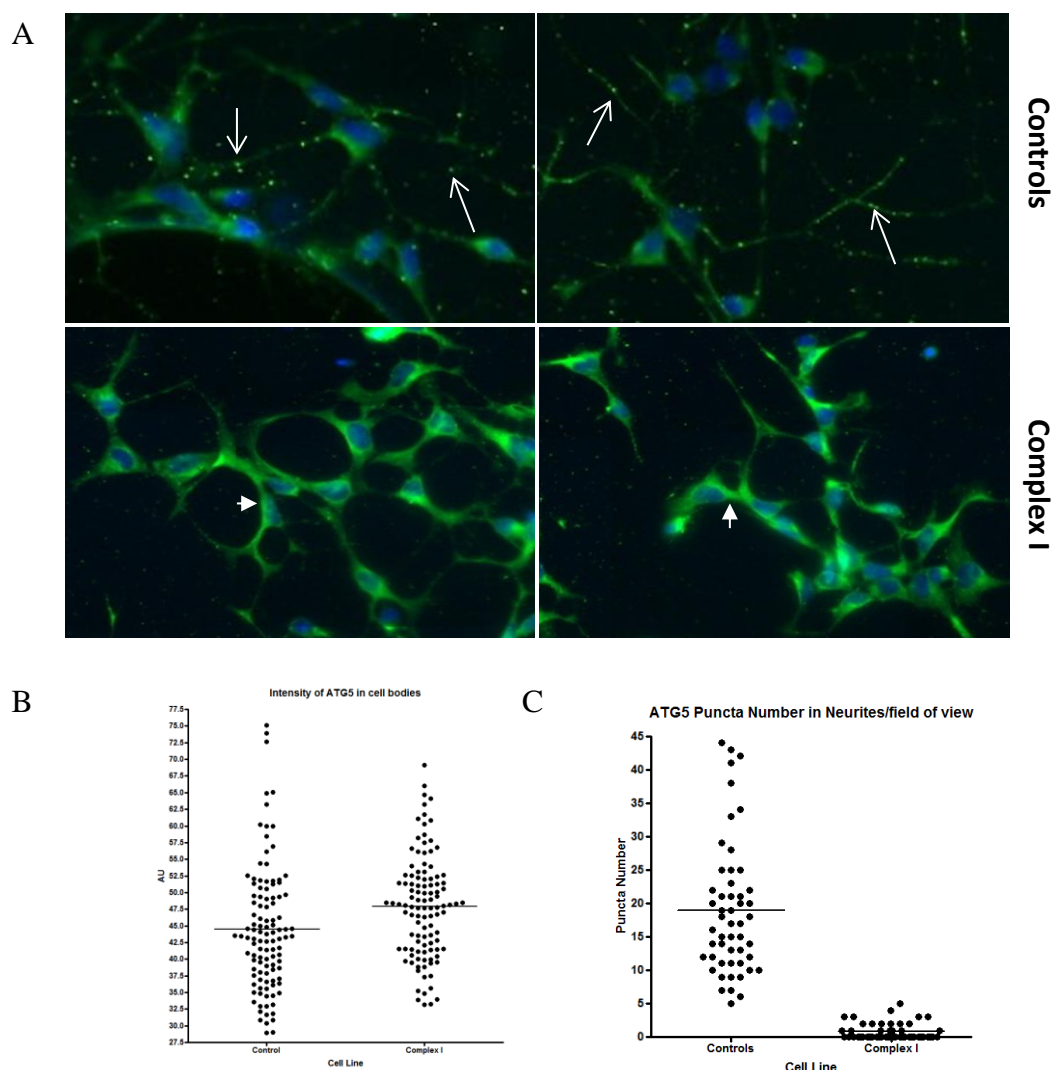
Figure 5.14. ATG5 neuronal staining

A. Representative images of ATG5 staining reveal clear differences, with Complex I cells devoid of puncta within their processes (white arrows) and accumulation of staining within the cell bodies (white arrow heads). B. Quantification of ATG5 intensities in cell bodies reveals stronger staining in complex I cells (P=0.0005) N=75 C. Puncta number was dramatically reduced in neurites of complex I cells when compared to controls (P<0.0001) N=50 over two experiments.

5.3.2.3   *Neuronal BECLIN 1 Observations*

BECLIN1 was also assayed through immunocytochemistry of control and complex I cybrid derived neurons. Staining revealed no statistically significant differences in patterns (Figure 5.15. A) or intensity of stains (Figure 5.15 .B).
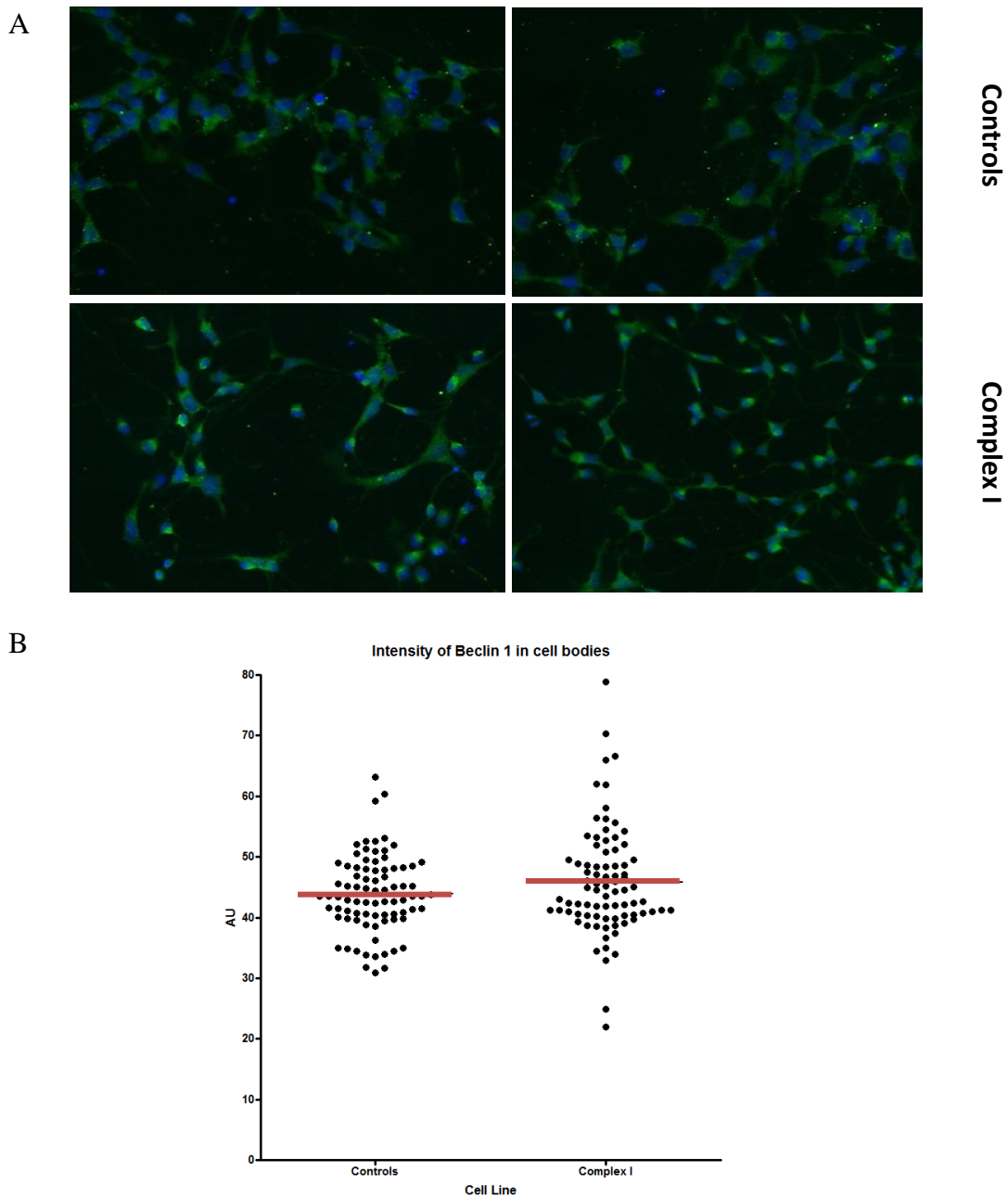
Figure 5.15. Beclin1 neuronal staining

Control and complex I derived neurons were stained for Beclin1. No differences were observed between patterns (A) or intensities of stains (B). N=60 over two experiments.

5.4   **DISCUSSION**

This chapter focused on the impact of inherent complex I dysfunction on the autophagy process in mouse embryonic stem cells. Changes were observed in both undifferentiated and newly derived neurons. It would appear complex I dysfunction compromises autophagy. In undifferentiated cells, reductions in all markers were seen; in neurons the patterns of staining were dramatically different. Given that autophagy and mitochondria are both reliant on the other in some way, it is likely that dysfunction in one will impact on the other. The interrelation between these processes has previously been investigated by other groups. Systems involved in the regulation of autophagy have been shown to be compromised with mitochondrial respiratory deficiency, be it through suppression of autophagic flux, autophagy gene expression or through stimulation of PKA activity, which recruits the ATG1-ATG13 complex to pre-autophagosomal structure (Graef and Nunnari, 2011).

This study seems to point towards a decline in autophagy in undifferentiated cells with compromised mitochondrial activity stemming from complex I dysfunction. Interestingly the same alterations in the autophagy pathway were not observed in neurons derived from the ES cells. The same dramatic reduction in autophagy markers was not observed in the cell bodies of neurons. However the abundance of puncta within neuronal processes of complex I cells was greatly diminished for both LC3 and ATG5. Why this was not the case for Beclin1 is unclear but may represent the need for further antibody optimization in the neuronal cells, alternatively, Beclin 1 may be recruited and/or transported by different mechanisms.

The literature is somewhat divided with regards to defining a single impact of mitochondrial dysfunction on the autophagy process. These findings, at least in part, are likely to stem from different model systems and assays with results varying dependant on the nature and severity of the defect. This work showed a significant decrease in markers across the autophagy pathway indicating an overall reduction in autophagy correlated with a complex I deficiency in undifferentiated cells. Certain models have also revealed a decrease in autophagy following reduced ATP levels and increased oxidative stress. In human retinal pigment epithelium cells for example, a relatively minimal decrease in ATP brings about a three times reduction in autophagic activity

(Schutt *et al.*, 2012). The use of complex I inhibitors in other studies however has shown autophagy to increase in response to the inhibition (Chen *et al.*, 2007c). Rotenone, for example, causes autophagic vacuole accumulation without efficient lysosome degradation inhibiting autophagic flux prior to inducing cell death (Mader *et al.*, 2012).

The discrepancy between some previous findings and these results may arise from the unique approach we have taken with the cybrid cell lines, but equally could represent an adaptive response with regards to CI dysfunction. Rotenone application by its nature creates an acute response and subsequently the increase in autophagy may be an adaptive response to clear dysfunction. It is plausible that this response becomes overwhelmed (through, for example, ROS accumulation) and subsequently results in blockage and decreased autophagic flux. In our model the CI dysfunction is the basal phenotype for the undifferentiated cells and as such represents a far more chronic dysfunction which may bring about different adaptions. This is likely far more relevant to an inherent disease state as it does not occur as an acute insult, rather a gradual accumulation of problems bought about through complex I dysfunction. The changes in neurons in neurodegenerative disease states or indeed ageing are clearly chronic in nature, making this model arguably more appropriate for the study of such events. In other models it may be the sudden difference from a baseline CI activity which triggers autophagic increase which is not detected in our undifferentiated cells. This may differ when a second challenge in the form of differentiation (an energy dependant process) occurs and may explain the differences between the stem cells and neurons. It must also be considered that autophagy is a highly energy consuming process which may be affected by the ATP deficit seen in these cells (Plomp *et al.*, 1989). Alternatively, a decrease in autophagy markers may represent a change in mitophagy which arises due to changes in the organelles themselves. Closer investigation with live cell analysis to differentiate large scale autophagy from mitophagy will be required to answer this.

5.4.1   **Mitochondria and Autophagy Interplay-**

The explanation for the observed results could, at this stage, be explained by several theories. Firstly, the reduction in cellular energy brought about by the mtDNA mutations may be a contributing factor in lowering basal autophagy. This decrease in

autophagy adds further burden to the cellular environment, compromising transport and mitochondrial dynamics, through physical blockage and/or energy rationing. Initiation of autophagy is energy dependant as too are degradation and biosynthesis following release of degraded cellular material. The changes observed may therefore demonstrate modulation of the autophagic process in response to the metabolic capacity of the cell. More immediately critical cellular processes may take precedence over degradative pathways at the long term cost to the cellular environment. Other studies argue that respiratory activity but not ATP is required for autophagy activity i.e. it is the process but not ATP itself which signals autophagy. This said, ATP may still be implicated through concomitant increase in acidic vesicle pH (Tabb *et al.*, 1992).

An alternative mechanism for mitochondrial mediated control of the autophagy process may exist through ROS signalling. Changes in membrane potential and complex I deficiency have been reported to induce generation of mitochondrially derived reactive oxygen species (ROS) (Abramov *et al.*, 2010). Clearly the cybrid cells display severe complex I inhibition (detailed in chapter 4.2.4). Previous studies have shown contrary to an expected decrease in membrane potential, the CI cybrids are able to maintain above that of the controls (Abramov *et al.*, 2010). These two factors were shown to dramatically increase ROS production. The role this has on autophagy must not be overlooked. It has previously been proposed that ROS generated from the mitochondria could induce autophagy through H_2O_2 production (Scherz-Shouval and Elazar, 2007) as well as superoxides (Kim and Choi, 2008). Specifically the degradation of catalase contributes to autophagy, suggesting regulation through H_2O_2 levels (Yu *et al.*, 2006). How this causes autophagy induction is as yet unclear but may occur through regulation of the activity of ATG 4 (Scherz-Shouval *et al.*, 2007) or BECLIN 1 (Chen *et al.*, 2012). Although the cells used in this study generate high levels of ROS which would imply induction of autophagy, the limited flux of ROS levels may mean this signalling pathway is quickly overwhelmed or alternatively not triggered. It would be tempting to postulate that the high ROS levels may become even greater in neurons and this accounts for the observed differences between them and undifferentiated stem cells.

A relatively recent finding, proposes dysfunctional mitochondria bring about defective autophagic clearance through altered mobilization of autophagosomes from their site of formation to action (Arduino *et al.*, 2012). The fixed cell model described in this

chapter is unable to look at what impact the observed changes have upon such dynamics but will be addressed in later chapters. Regardless of the cause of downregulated autophagy in the complex I cells the potential impact is threefold. (1) limited autophagy subsequently leads to an increase in cellular 'clutter', (2) preservation of mitochondrial integrity is compromised and (3) damaging cellular components are not removed leading to further damage and depleted pools of vital macromolecules. Looking within the differentiated neurons provided more clues regarding the impact of autophagy modulation stemming from mitochondrial complex I dysfunction. It would appear within this cell type the impaired trafficking of autophagosomes may be the impact of a mitochondrial dysfunction. To answer this more work looking at the dynamics and morphology of mitochondria alongside other cellular components; critically autophagosomes, will be needed.

5.4.2   Role in Parkinson's Disease

Changes in mitochondria and autophagy have been implicated in a range of neurodegenerative disorders. Specifically changes in complex I of the mitochondrial electron transport chain is frequently highlighted as a pathogenic factor in the development of Parkinson's Disease. Through gene studies, alterations in mitophagy have also been highlighted, for example through *PINK1* and *PARKIN*. Mutations in both these are known to cause familial forms of the disease and both these proteins have roles in signaling dysfunctional mitochondria for mitophagic removal. Looking at autophagy changes within the cybrids with complex I dysfunction is beginning to reveal how the two changes, complex I dysfunction and alterations in autophagy, may work concurrently to ultimately lead to cell death. The studies described within this chapter show that complex I dysfunction is independently able to cause changes in autophagy proteins, both in terms of expression and within the neurons, localization. Such changes may accumulate with complex I dysfunction in 'real-life' situations, indeed post mortem tissue studies of PD patients show changes in key autophagy proteins and it is known CI expression is reduced in neurons of PD patients (reviewed in ch8). The next challenge for this work will be to assess these in parallel, in a) living cells to observe dynamics and b) in human PD brain tissue samples to relate results gathered this far to the human condition. Other familial forms of Parkinson's disease have highlighted alterations in bioenergetics and autophagy. For example rare cases have been shown to

be caused by mutations in DJ1, implicated to have roles in modulation of transcription, chaperone functions and antioxidant properties (Cookson, 2003). Importantly cellular models of DJ1 KO have shown that its absence results in impaired mitochondrial respiration, dynamics and reduced basal respiration (Krebiehl *et al.*, 2010).

Interestingly the repopulation of cells depleted of mitochondria with mitochondria from PD patients is sufficient to reproduce alterations in the autophagic system, commonly seen in post mortem PD brains (Arduino *et al.*, 2012). Mutations in PARK9 (ATP13A2) cause early onset Parkinsonism, recent work has shown that this previously uncharacterized protein is localized to the intracellular acidic vesicular compartments of cultured neurons and silencing of it induces mitochondrial fragmentation (Ramonet *et al.*, 2012). ATP13A2 has also been shown to regulate mitochondrial bioenergetics through macroautophagy. Gudson *et al* showed that in ATP13A2 deficient cells mitochondrial mass and ROS production increased and autophagic flux was decreased (Gusdon *et al.*, 2012).

Modulating the autophagy pathway may well serve as a potential therapy in synucleinopathies. Through improved clearance of dysfunctional organelles as well as improving alpha-synuclein degradation. It is important to note however that simply up regulating autophagy to compensate in these disorders is likely to be insufficient. Current therapies that work by increasing autophagy are highly unspecific and as such numerous pathways are affected. Furthermore, an up regulation of autophagy is seen in some disorders so any modulation must be careful not to assist in one problem only to create another. As yet the specific molecular component of autophagy affected in these disorders is unknown. Elucidating this will be crucial in designing far more specific therapies.

5.4.3   Final Conclusions

These data show that complex I dysfunction is sufficient to bring about dramatic changes in autophagy proteins. Mitochondrial function is clearly crucial for maintenance of autophagy demonstrated by multiple experimental models whereby mitochondrial dysfunction has been shown to affect autophagy. This is possibly best demonstrated through the use of rho0 cells, where *ATG8* induction was shown to be

strictly dependent on both the presence of a carbon source and mitochondrial function (Graef and Nunnari, 2011).The implications of this bidirectional relationship are likely to be key to a range of age related disorders. Accumulation of respiratory deficient mitochondria may be tolerated to a certain level within cells, however once a certain threshold has been reached a decrease in the autophagic and mitophagic capacity of the cell occurs. This in turn may initiate a negative feedback loop that is responsible for cell loss in disease and arguably leads to cellular ageing on a broader scale. The greater implication of this work may well stretch to assisting our understanding of many more pathologies. As discussed previously, impaired autophagy has been proposed as a possible pathogenic mechanism in several neurodegenerative disorders. Moreover, as a universal quality control mechanism its role in multiple disease states may have only begun to be unravelled. As such correlating mitochondria and autophagy dysfunction may open new lines of investigation.

5.4.4   Areas for future investigation

The results gained from this project imply further investigation into the alterations of autophagy in cells with complex I dysfunction will need to continue in a more dynamic assay. Changes in mitochondrial dynamics and trafficking are likely to be key, notably within neurons. This project therefore formed the jumping board for investigations outlined in chapter 6 and 7. Investigating more subtle fluctuations of autophagy markers in response to mild to moderate stress would be interesting to see if barriers for induction of the autophagy process are altered in the complex I deficient cells. More rigorous analysis of autophagy protein levels could also be conducted through the use of autophagy inhibitors and inducers.

Chapter Six

Live Cell Studies of Mitochondria and Autophagy

Chapter 6. Mitochondrial Dynamics and Live Cybrid Cells

6.1   INTRODUCTION

6.1.1   Overview

Mitochondrial bioenergetics display a tight bidirectional relationship with mitochondrial morphology and organisation of the network. Dynamics within the network and throughout the cell are vital for mitochondrial integrity and subsequently, maintenance of the cellular environment. As such, perturbations in mitochondrial DNA that result in a reduction of energy provision, could impart their deleterious effect through not only hindering energy dependant processes but also through a secondary impact on mitochondrial dynamics.

6.1.2   Evidence for complex I impact on dynamics

Experimental evidence highlights the links that exist between maintained mitochondrial function and dynamic capabilities. Complex I, as the largest complex and entry point to the electron transport chain is likely to impart critical alterations to dynamic processes through its dysfunction. Conversely, different configurations of the mitochondrial network can effect energy provision. Sophisticated studies have demonstrated that modulation of mitochondrial dynamics can impact on bioenergetics. For example disruption of proteins involved in mitochondrial fusion, including Optic Atrophy 1 (OPA1) and the mitofusins (MFN1 or MFN2) by RNAi cause a blockage of mitochondrial fusion and result in poor cell growth and decreased cellular respiration (Chen *et al.*, 2005). Charcot-Marie-Tooth (CMT) disease is known to result from mutations in mitofusins, involved in mitochondrial fusion. Loss-of-function *MFN2* mutations lead to reduced glucose and fatty acid oxidation and mitochondrial membrane potential, whereas a *MFN2* gain-of-function mutation increases glucose oxidation and mitochondrial membrane potential (Pich *et al.*, 2005). Conversely modulating proteins involved in mitochondrial fission similarly affect bioenergetics. Using small interfering RNA (siRNA) targeting *DRP1*- a member of the Dynamin family, in HeLa cells, creates alterations in mt-network morphology which coincided with a significantly lower rate of endogenous respiration and strong reductions in mitochondrial ATP synthesis (Benard

et al., 2007). The authors suggest that the molecular machinery for ATP generation was altered in cells with decreased DRP1 and this resulted from perturbations in membrane fluidity. Previous studies have demonstrated a strong dependency of complex V activity on membrane fluidity (Aleardi et al.,2005; Ellis et al., 2005; Solaini et al., 1984). These results indicate that mitochondrial form can impact on function, however mitochondrial function can also change mitochondrial form.

Observations of how impaired bioenergetics impact on form have revealed a range of results. Rotenone, a potent complex I inhibitor causes a dose dependant decrease in complex I activity alongside a dramatic change in mt-network morphology, with an increase in mitochondrial length and branching (Benard *et al.*, 2007). Similarly in fibroblasts from patients with defined complex I deficiency caused by mutations in nuclear encoded subunits, mitochondrial morphology shows a scale of dynamic modulation seemingly correlated to level of CI dysfunction (Koopman *et al.*, 2005). Outside of these more 'extreme' complex I induced bioenergetic reductions, changing mitochondrial morphology seems a normal adaptive response to changes in energy availability. For example, stimulating respiration through nutritional modulation has been shown to cause network lengthening and increased complexity (Rossignol *et al.*, 2004).

Mitochondrial dynamics are crucial for cell health and survival, reviewed in depth in ch1.4.5. Through alterations in mitochondrial dynamics, bioenergetic dysfunction may be having a secondary impact on the cellular environment. What's more, as the two interrelate, any dysfunction is likely to be self-perpetuating. For example, a complex I dysfunction may lead to alteration of the mt-network, this in turn may further compromise bioenergetics through restriction of the molecular machinery necessary for energy production. Alternatively, a primary defect in fission or fusion may hinder bioenergetics that then cause further loss of stability of the network. Deciphering the exact molecular mechanisms that contribute to this demise will be crucial.

6.1.3   **Evidence for an impact of complex I dysfunction on autophagy**

A third contributor working in concert with mitochondrial dynamics and bioenergetics, is autophagy, or specifically with regards to mitochondria- mitophagy. Reliant on, and responsible for maintenance of morphology, dynamics and bioenergetic capacity, mitophagy is likely to play a pivotal role in this trifecta. It is possibly easy to comprehend how dysfunctional mitophagy can affect morphology, with large or damaged mitochondria not being effectively removed. Equally, how this dysfunction could alter dynamics and bioenergetics is logical, through the accumulation of compromised mitochondria which show reduced bioenergetic capacity which in turn can affect energy dependant trafficking. Less clear is how mitophagy can be affected by the form and function of mitochondria. Previous studies have shown that a drop in membrane potential and subsequent mitochondrial fission is required for mitophagy to occur (Twig *et al.*, 2008). Dynamics may also play an important role in transporting damaged mitochondria to lysosomes for degradation.

Within neurons mitochondria are largely moved along microtubules, although movement using actin filaments has been reported for smaller distances and within dendritic spines and growth cones (Saxton and Hollenbeck). The 'docking' and 'shipping' of mitochondria onto these cellular tracks is facilitated through motor proteins and a plethora of adaptor proteins such as Milton, Miro, Myosin and Dynactin. Both trafficking and fission/fusion processes rely on mitochondrial bioenergetics, and this may explain how mitophagy becomes compromised through energy deficits, as it is reliant on motility and fission/fusion events. Investigating how a process which is responsible for dealing with dysfunctional mitochondria is affected by mitochondrial dysfunction is a complicated paradox. Indeed, it may seem counter intuitive to suggest mitochondrial dysfunction may impair the very system needed to address the dysfunction, the single most powerful argument for this remains that if the system was indeed perfect, we would not see dysfunctional mitochondria, particularly in aged tissues and age related diseases. Clearly there is a point where mitophagy is not sufficient for the dysfunction it encounters. At which point the process becomes overwhelmed or unable to cope with demand may be crucial to understanding the final trigger that leads to total cellular demise and cell loss in Parkinson's disease (PD) amongst other neurodegenerative conditions.

6.1.4   **Aim of Study**

This study was designed to follow up on previous findings that suggested trafficking and dynamics may be compromised in complex I deficient stem cells and newly derived neurons, and that this may be impacting on autophagy pathways. This work aimed to characterise the morphology of the mitochondrial network within these cells and also their bioenergetic state. Following this, newly developed live cell analysis was employed to observe these dynamic events in real time and look for perturbations between complex I compromised cells and controls.

6.2   **METHODS**

6.2.1   **Network analysis**

To visualise mitochondria in undifferentiated cell lines the network was stained as per protocol in ch2.3.7.2, utilising Tetramethylrhodamine (TMRM) or mitotracker red (MTR). All cells were at least 48hrs post thaw and passage matched. Seeding densities were matched for all experiments to ensure limited variation in experimental conditions. Single plane imaging was carried out on a Zeiss AxioImager. To analyse the images a series of deconvolution steps were followed as shown in Figure 6.1. Firstly, brightness and contrast were adjusted to optimal levels; the filter then serves to simplify the images, using deconvolution to smooth the signal. Finally the binary step allows the software to identify objects as either mitochondria or not. This allowed automatic measurement of the mitochondrial network complexity, generating parameters regarding individual organelles or reticular composites. From this data two characteristics were generated- form factor, a measurement of length and degree of branching (perimeter^2/4π·area), and aspect ratio which generates data on the length based on the ratio between major and minor axes of an ellipse equivalent to the mitochondrion. These were recorded from triplicate experiments and compared for differences between complex I deficient cells and control cell lines through unpaired t tests.

6.2.2   **Membrane potential analysis**

To ascertain what impact the complex I mutation had upon membrane potential a series of imaging experiments using the cationic carbocyanine dye JC-1 were performed. Although previous work has identified the complex I cells have a higher membrane potential than controls using TMRM staining, for the sake of completeness of this project and also to have a visual output of the potential differences, it was decided to repeat these experiments using a different methodology. The unique properties of the JC1 dye enable visualisation of the membrane potential. Regions of high mitochondrial polarization are indicated by red fluorescence due to J-aggregate formation by the concentrated dye, as its accumulation is membrane potential dependant. Conversely, depolarized regions are indicated by the green fluorescence of the JC-1 monomers. Briefly cells were incubated with the membrane potential specific marker for 30 minutes at 37°C. The cells were excited by a 488nm laser and emissions were collected between 515–545nm and 575–625nm on the Nikon A1R system. Quantification of the ratio of green to red labelled organelles allowed for an estimation of the cells membrane potential. These ratios were then compared for control and complex I deficient cells.
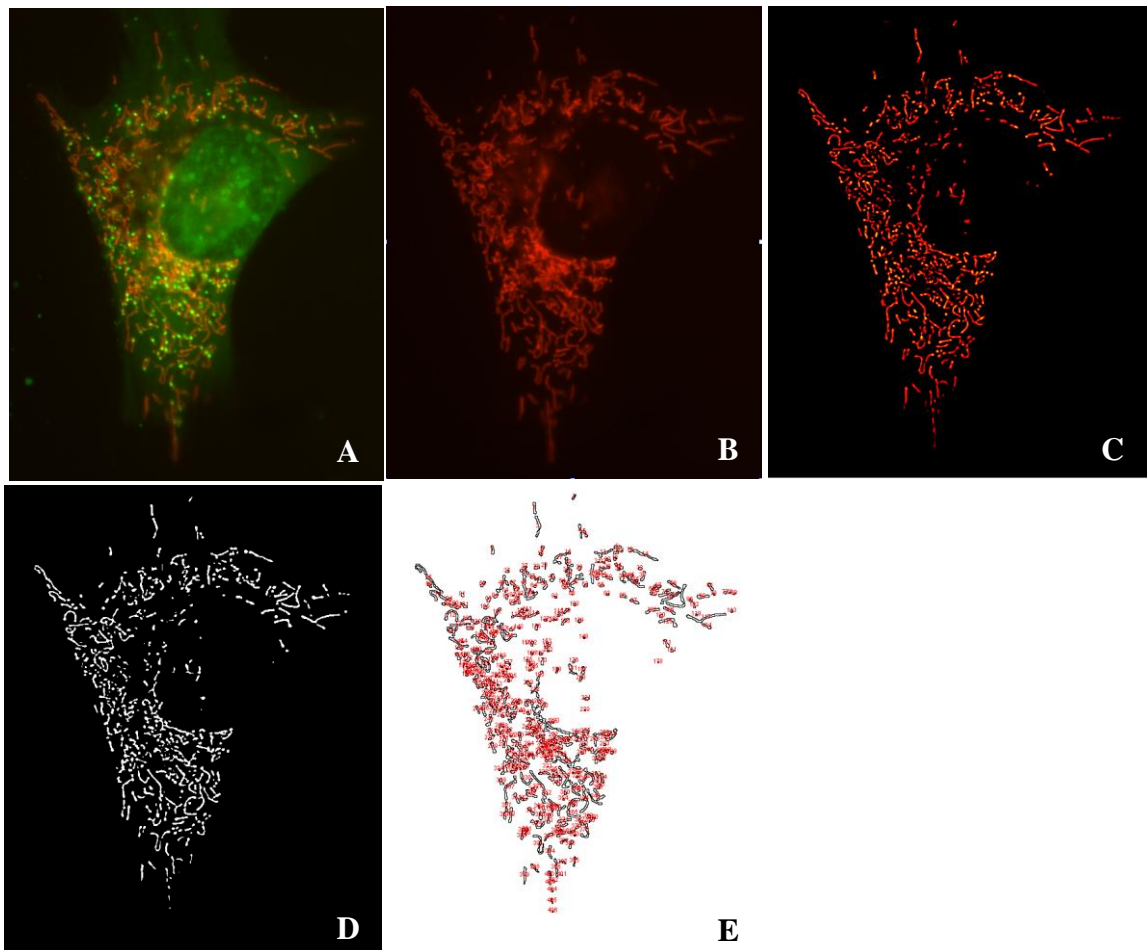
Figure 6.1. Deconvolution of the mitochondrial network

To enable automated analysis of combined pico green and TMRM images a series of deconvolution steps were followed. Original dual stained images (A) were separated into individual channels (B) a filter was then applied to simplify the image (C). The images were then converted to binary (D), outlines were mapped and individual particles measured (E).

6.2.3 Mitochondrial tracking

To look at mitochondrial dynamics within a living cell, numerous protocols were trialled (ch 3.3). Utilising the cells in their neuronal form proved advantageous as the movements of individual organelles was far easier to define, due to reduced complexity of the mitochondrial network and the thin nature of the neuronal processes. Neurons were created using the Bains protocol (Bain *et al.*, 1995) and grown on iBIDI imaging dishes. On day 15 the cells media was replaced with 1ml prewarmed media containing 5nM TMRM for 10mins at 37°C. These were then placed in a controlled environmental chamber and imaged using Total Internal Reflection Fluorescence (TIRF) microscopy. TIRF requires a high NA objective lens to produce an evanescent wave that penetrates a

short distance beyond the coverslip. TIRF enables selective excitation of fluorophores in a very limited field adjacent to the coverslip. The thinness and exponential decay of the illumination provides a very thin optical section. The technique effectively improves contrast, albeit in a limited field as fluorescent molecules outside of the field of excitation are not recorded. The technique is therefore ideal to image mitochondria moving within thin neuronal projections.

Imaging was done every second for 15 minutes. To analyse the movie files Imaris 7.6 (Bitplane) was used. This allowed the identification and mapping of individual mitochondria (using parameters such as intensity and size) before tracking them through each separate image file (Figure 6.2). Information was then generated on directionality, velocity, size and distance travelled. All parameters could then be assessed in control vs. complex I derived neurons using appropriate statistical analyses depending on data spread.

6.2.4   Autophagosome tracking

Due to the limited capacity to quantify purely 'mitophagic' events compared to general autophagy with previous ICC methods, part of these dynamic studies intended to use a combination of autophagy markers and mitochondrial stains in live cells which, at high magnification would allow us to observe mitophagic events occurring in real time. A range of mitochondrial dyes have been extensively tested in live cell models such as TMRM, TMRE, Mitotrackers, ImageIT and CellLight (Invitrogen). The ES cells are known to be a fairly sensitive cell type, despite this, both TMRM and a range of Mitotrackers were well tolerated. To monitor autophagy events, the decision was taken to use a relative new product- Cyto-ID autophagy detection kit (Enzo Bioscience). Although pre-existing products have been used in similar settings, such as Lysotracker, a lysosome marker, Cyto-ID enabled specific labelling of autophagosomes which was beneficial for this assay. Initial experiments were carried out as per manufacturer's instructions and optimized as per ch 3.4.3.

Following disappointing results using the live cell marker the decision to stably transfect the cell lines of interest with a GFP tagged LC3 was taken. This had

previously been attempted with a lipid based transfection method but proved ineffective for establishing stably transfected lines. For future experiments viral transfection was utilised, as outlined in ch 3.4.3.
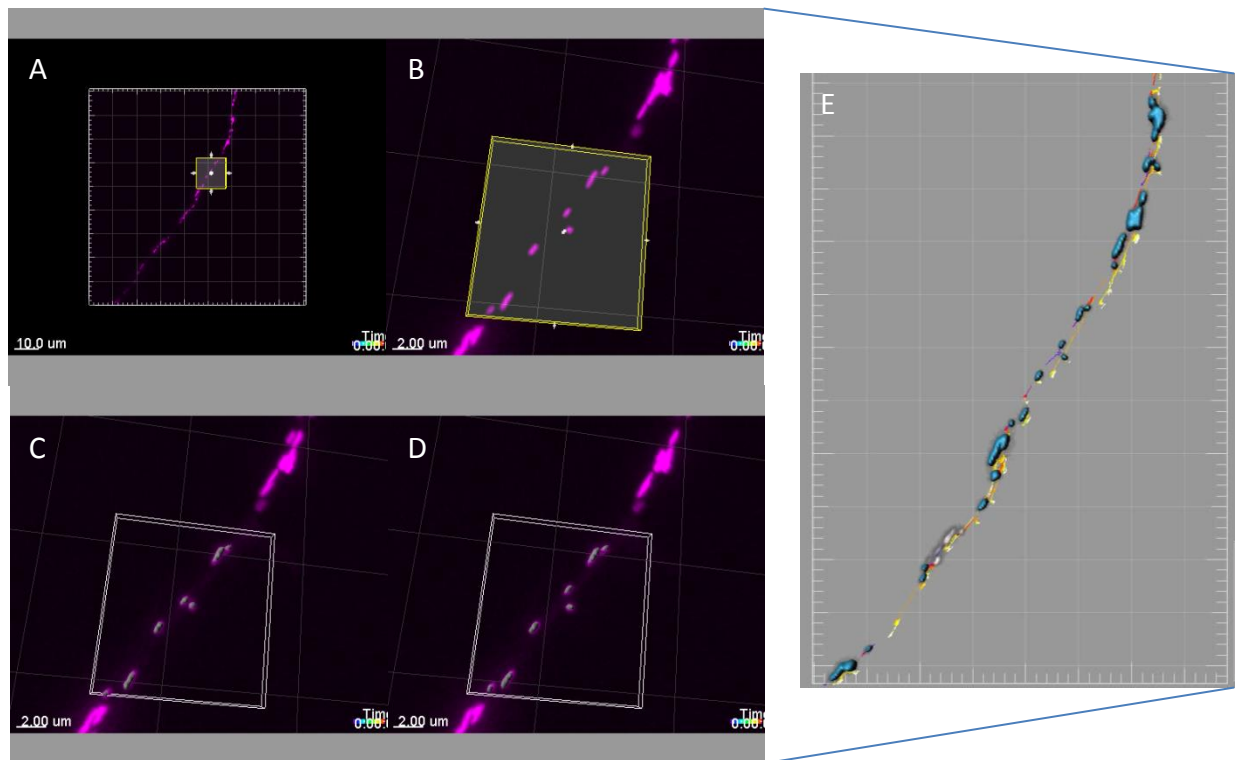
Figure 6.2. Imaris tracking methodology

To track organelles within neuronal processes, a region of interest (ROI) was defined (A-B). Using pre-determined parameters including smallest mitochondrial size and intensity, the software was able to map individual surfaces (C). Individual organelles were checked through all time frames to ensure accuracy (C-D). Tracking was the applied and data generated on track (shown as coloured lines) characteristics (E).

6.3   RESULTS

6.3.1   Network analysis

Automated analysis of the mitochondrial network revealed morphological differences between control and complex I cells (Figure 6.3). When the complexity of the network was analyzed, a significant increase in form factor measurements were calculated (P=0.005), implying a greater degree of branching of the mitochondrial network in the

complex I cybrid cells. This may occur through alteration of the fission or fusion machinery in conjunction with the complex I deficiency. Alternatively the significant increase in network complexity may represent an adaptive response to the bioenergetic deficiency observed in these cells. Interestingly, a very small proportion of cells observed during these experiments showed the complete polar morphology, i.e. complete fragmentation of the network. These cells tended to be more rounded and if observed for longer periods of time appeared to be apoptotic, i.e. rounding and detaching from the surface. The fact that the CI cybrid cells are completely devoid of cells matching the control phenotype (i.e. reticular but not as complex) suggests that the increase in network complexity may well be a survival mechanism, with any change causing collapse of the cellular environment.

6.3.2   Membrane Potential

Previous studies have displayed significant differences between complex I cybrids and controls with regards to the electrochemical gradient maintained over the mitochondrial membrane- membrane potential. Through TMRM staining and uncoupling it has been demonstrated that the transmembrane potential in complex I cells is actually maintained above that of the controls (Kirby *et al.*, 2009). To follow this, JC1 staining was utilized to visualize these differences. Our findings agreed with previous studies with a higher membrane potential in the complex I undifferentiated cells as displayed in Figure 6.4 with higher red fluorescence in the bottom panel (complex I cells).
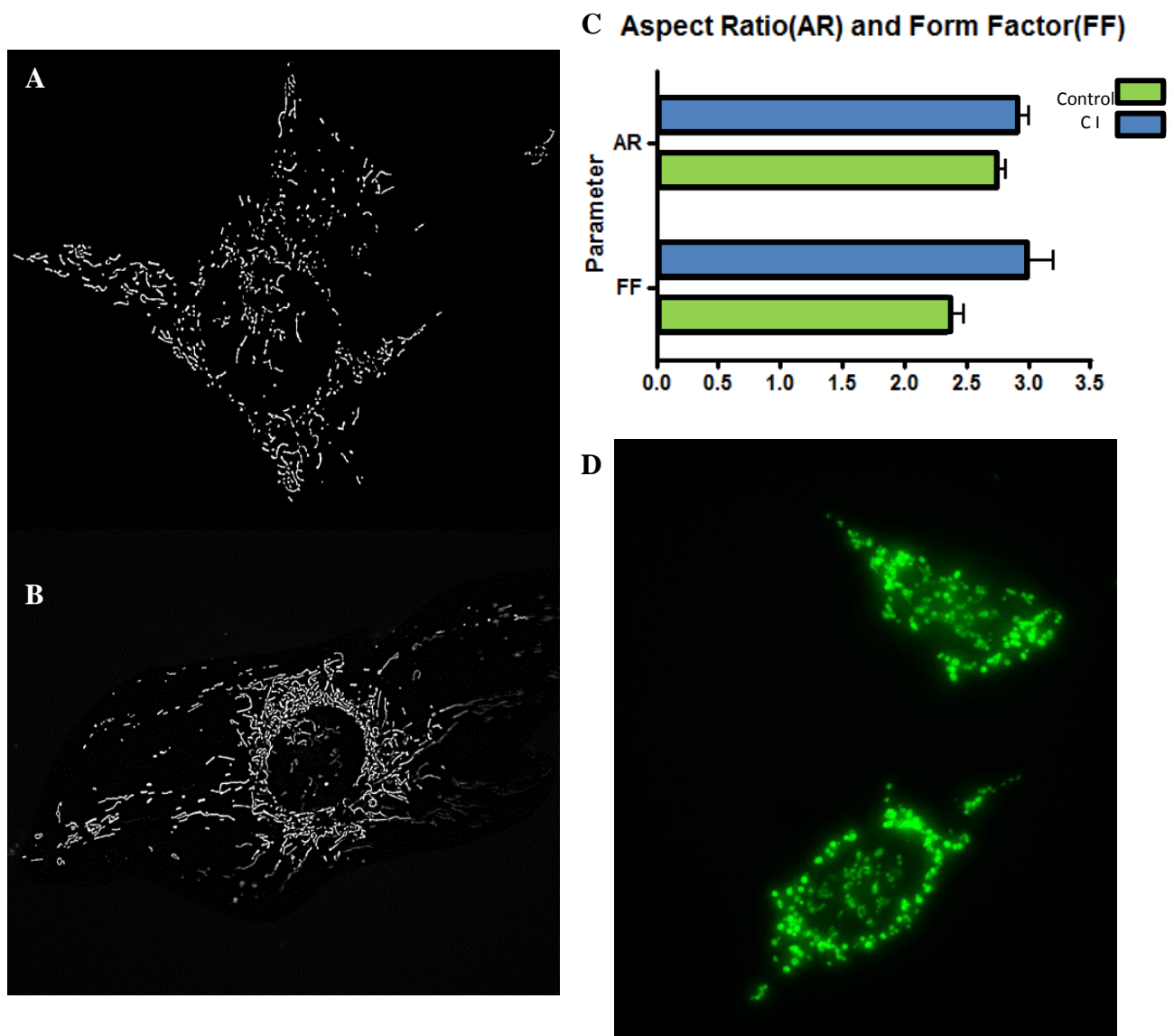
Figure 6.3. Morphology of mitochondrial network

TMRM staining was used to visualise mitochondrial networks and deconvolved to enable binary images to be generated in control cells (A) and complex I cybrid cells (B). Automated analysis was used to generate aspect ratio (AR) and form factor (FF) displaying differences in the two cell lines (C) P=0.0025, N=90 over three experiments. Although majority of the complex I cybrid cells displayed reticular networks a very distinct small group showed extreme fragmentation of the network (D).
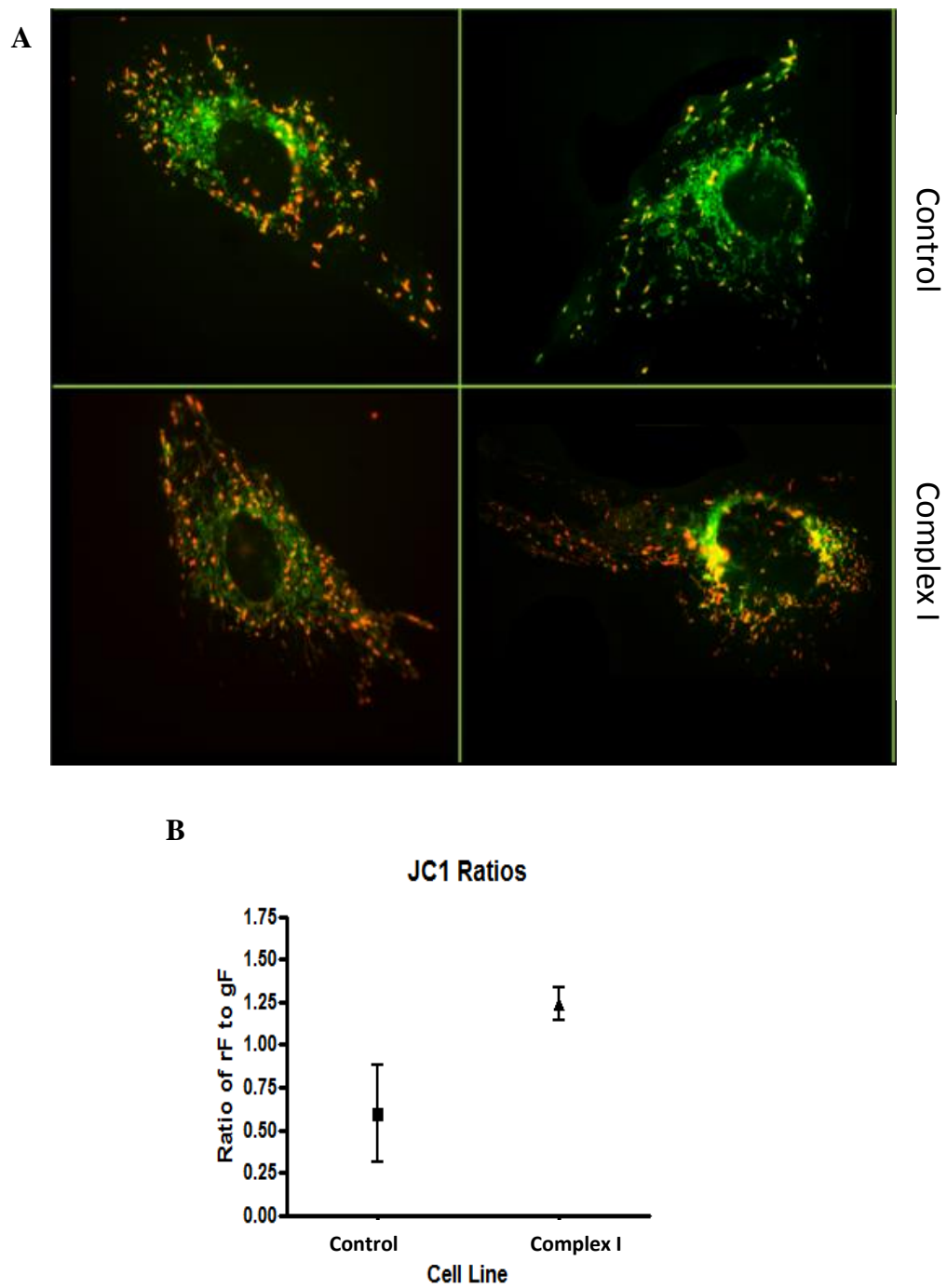
Figure 6.4. Membrane Potential

Analysis of membrane potential was achieved through JC1 staining (A) Control cells showed more green fluorescence (top panel) than their passage matched complex I cybrid counterparts (bottom panel). This difference was measured as the ratio between green and red fluorescence (B). N=100 over two experiments.

6.3.3   **Live cell studies**

To observe mitochondrial movements, a live cell assay was established which minimized the amount of user manipulation once the cells had been placed in the imaging chamber. Previous optimization had established neuronal projections were most suited to enabling visualization of individual mitochondria (ch3.3.3.1). Changes in both morphology and dynamics were seen between mitochondria within control and complex I derived neuronal populations.

6.3.3.1   *Mitochondria length*

The first observation that came from live cell imaging of mitochondria within the neuronal processes was a dramatic difference in the length of mitochondria. In complex I derived neurons the mitochondria tended to be much longer (Figure 6.5). Analysis of mitochondrial length in newly differentiated neuronal processes confirmed a significant increase in mitochondrial size in complex I cells compared to controls (P=0.0115).
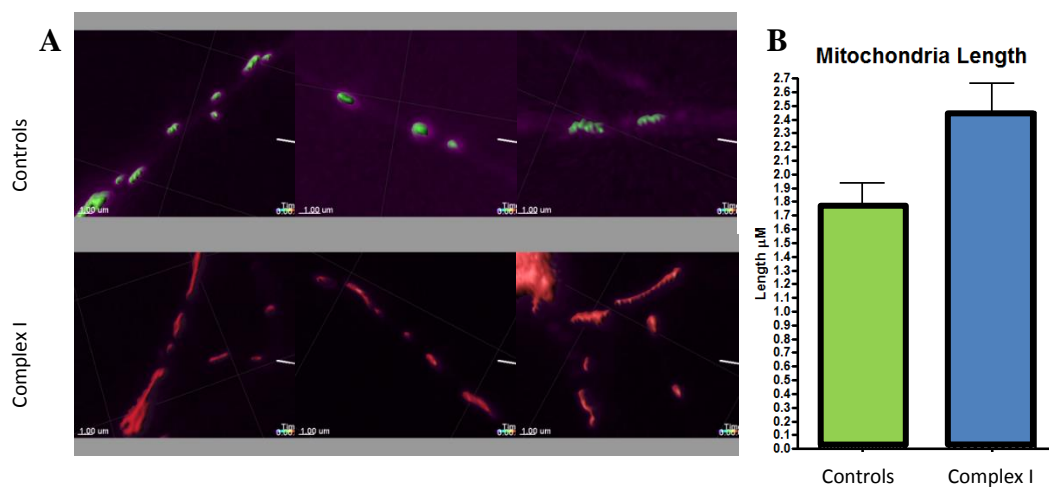
Figure 6.5. Mitochondria size in neuronal processes

The length of individual mitochondria in neuronal processes was assessed for control and complex I cybrid derived neurons in the first frames of live cell imaging experiments (A). These were quantified and compared for differences between the two cell lines (B).

6.3.3.2   *Mitochondrial movement*

The tracking of individual mitochondria revealed significant differences in how mitochondria from complex I derived neurons moved when compared to controls (Figure 6.6). The mitochondria appeared smaller in the control cells which is consistent

with the TMRM analysis in undifferentiated cells (Figure 6.3). Mitochondria that were tracked in the complex I cybrids showed reduced speed averaging 0.44µm/sec compared to 0.85µm/sec in the controls. While further analysis of the distribution of mitochondrial velocities revealed slower organelles in the complex I derived neurons (P<0.0001) shown in Figure 6.7 (A/B). Interestingly, length and displacement length (movement from point of origin) of tracks generated by mitochondria showed no difference in median length (Figure 6.7 C/D). However, analysis of the distribution of these lengths showed a greater number of longer mitochondrial tracks in the complex I derived neurons (P=0.0136). Overall, fewer mitochondria were motile within the complex I cybrid derived neurons. The tracks that were generated revealed more fusion events (when two mitochondria become one) in mitochondria of the complex I neurons than the control counterparts. Fusion events were estimated by looking at the number of individual structures in any given time frame (Figure 6.7 E). A reduction in the number of structures between two frames shows that fusion has occurred
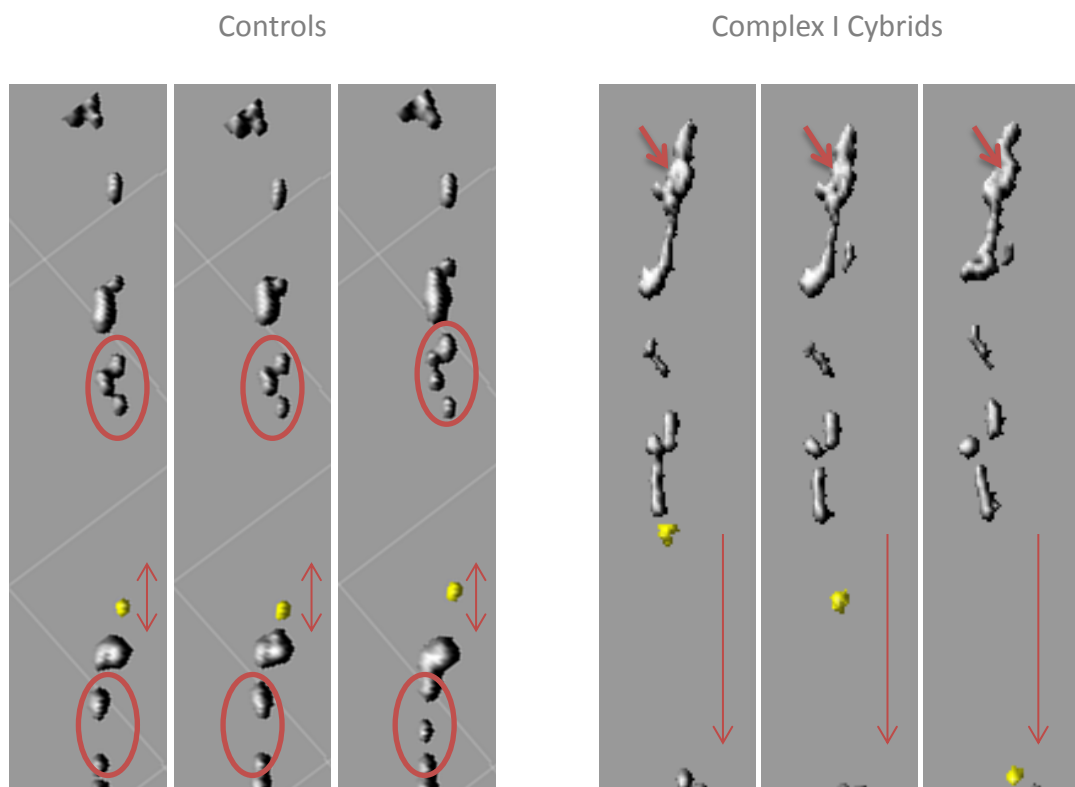
Figure 6.6. Mitochondrial movement in neuronal processes

Images show three individual points over a time lapse video showing mitochondria moving within neurons. Within control derived cells (left panel) mitochondria tended to be smaller and show small more uniform, often bidirectional movement (arrows). Mitochondria within the processes of complex I cybrid derived neurons (right panel) often formed large accumulations (large red arrow) with mitochondria that remained smaller in size travelling further and normally in one direction (thin red arrow).
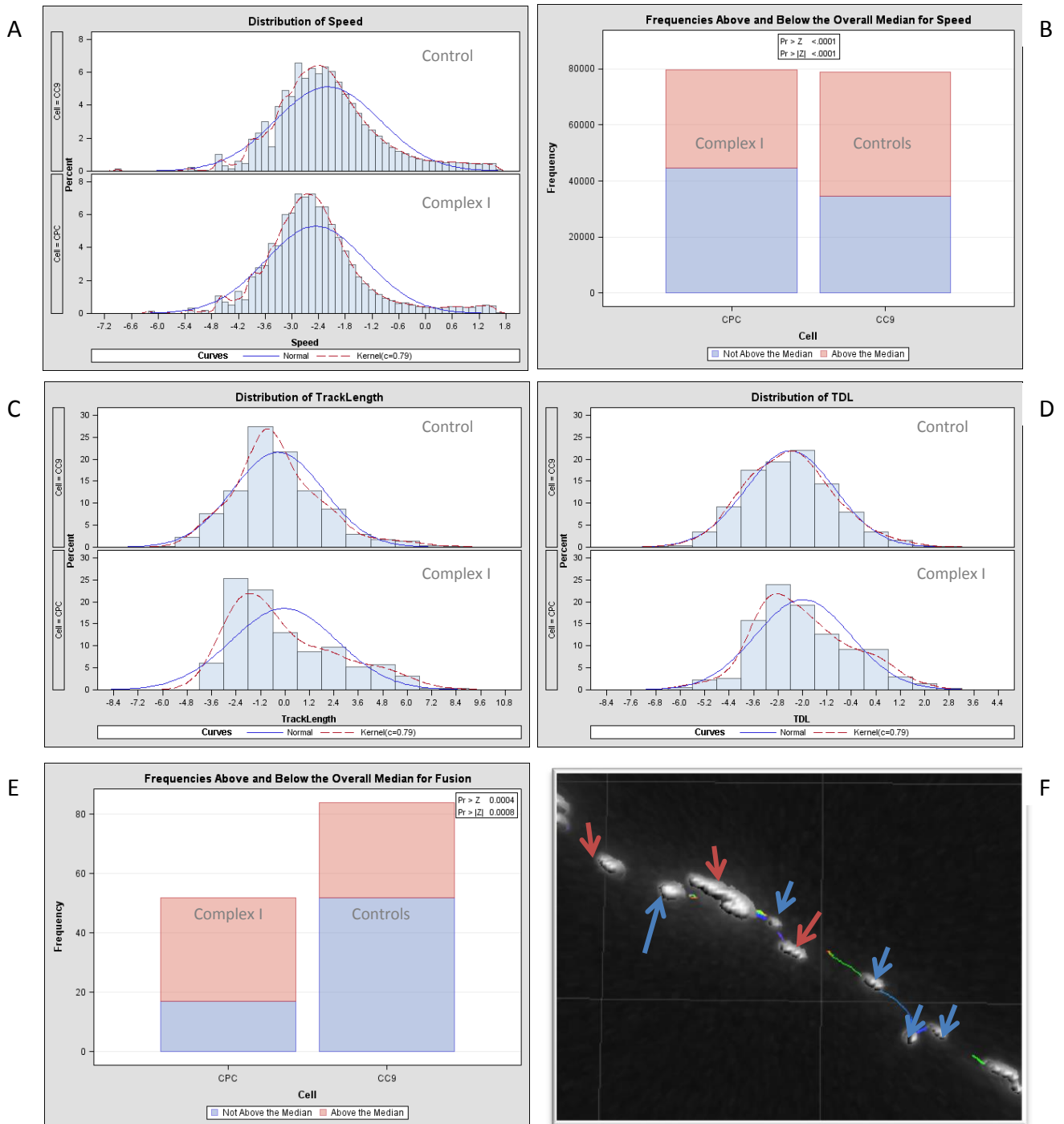
Figure 6.7. Quantification of mitochondrial movement in neuronal processes

Analysis of tracks generated from videos of mitochondria within neurons revealed difference between complex I cybrid derived cells and controls. The velocities of mitochondria in CI cells was reduced compared to controls (A) and is again clear when we look at the number of individual organelles reaching speeds above median values (B-red of blue bars). Track length (C) and track displacement length (D) showed higher values for mitochondria in complex I derived neurons, implying mitochondria that were motile, covered larger distances. Fewer mitochondria were moving in complex I derived neurons (E-height of bars) but those that were moving showed more fusion events (e- red of blue bars). F. Smaller mitochondria (blue arrows) were general more motile (as shown by coloured tracks) than larger mitochondria (red arrows).

6.3.3.3 *Autophagosome tracking*

Using the live cell autophagosome stain- Cyto-ID initially showed promising results within neurons as shown in Figure 6.8. The images show newly derived neurons, where certain characteristics that had been observed in the fixed cell ICC seemed to be observed again. For example in control cells autophagosomes seemed to extend further from the cell body compared to complex I derived neurons, although this was not quantified. Following repeat experiments however, it became clear that the neurons were clearly affected by the dye, which caused cell death (white arrow) suggested by rounding and condensation of cellular contents which caused neurons to detach from the surface of the imaging dish. The faint signal also became problematic as evident in Figure 6.8 with a strong green 'haze' due to the high level of exposure needed to see autophagosomes, this high excitation undoubtedly contributed to the toxicity of this methodology. Further optimization in undifferentiated cells also revealed cell toxicity showing it was not neuron specific (Figure 6.9).
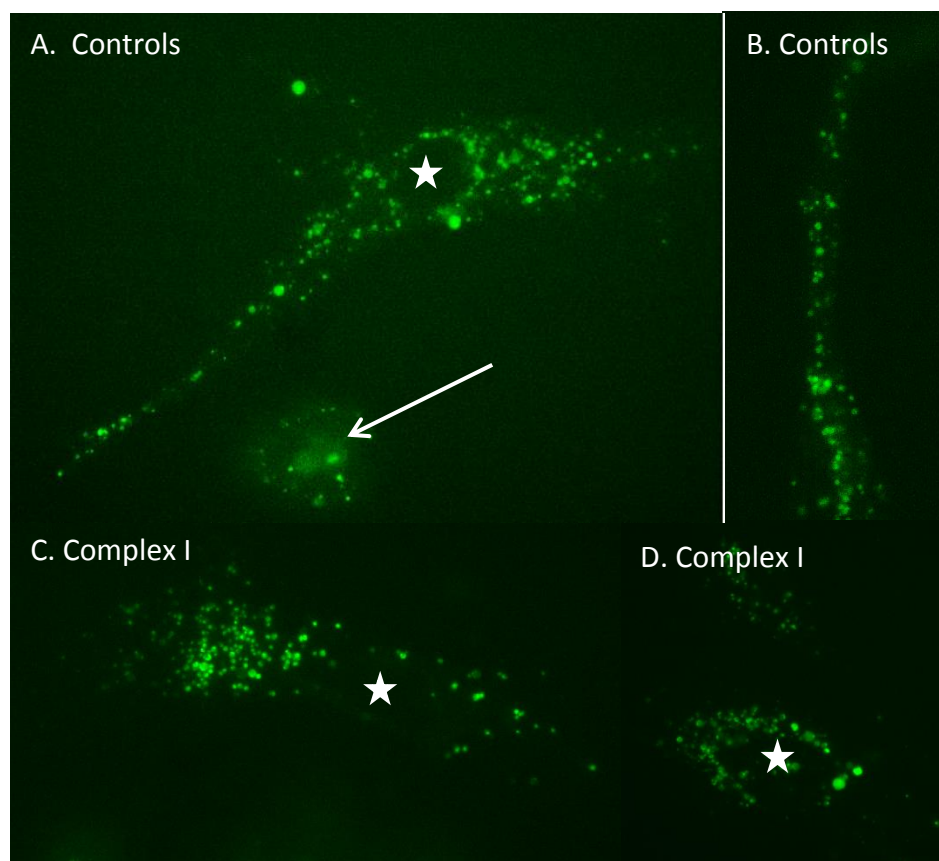
Figure 6.8. Cyto-ID Autophagosome staining in neurons

Control cells showed autophagosomes throughout the cell body and along neurites (A,B) whilst complex I derived neurons showed clustering of autophagosomes around the nucleus, which rarely extended into neurites. Unfortunately the live cell dye appeared to be toxic to the neurons as shown by increasing cell death (white arrow). White stars indicate nuclei.
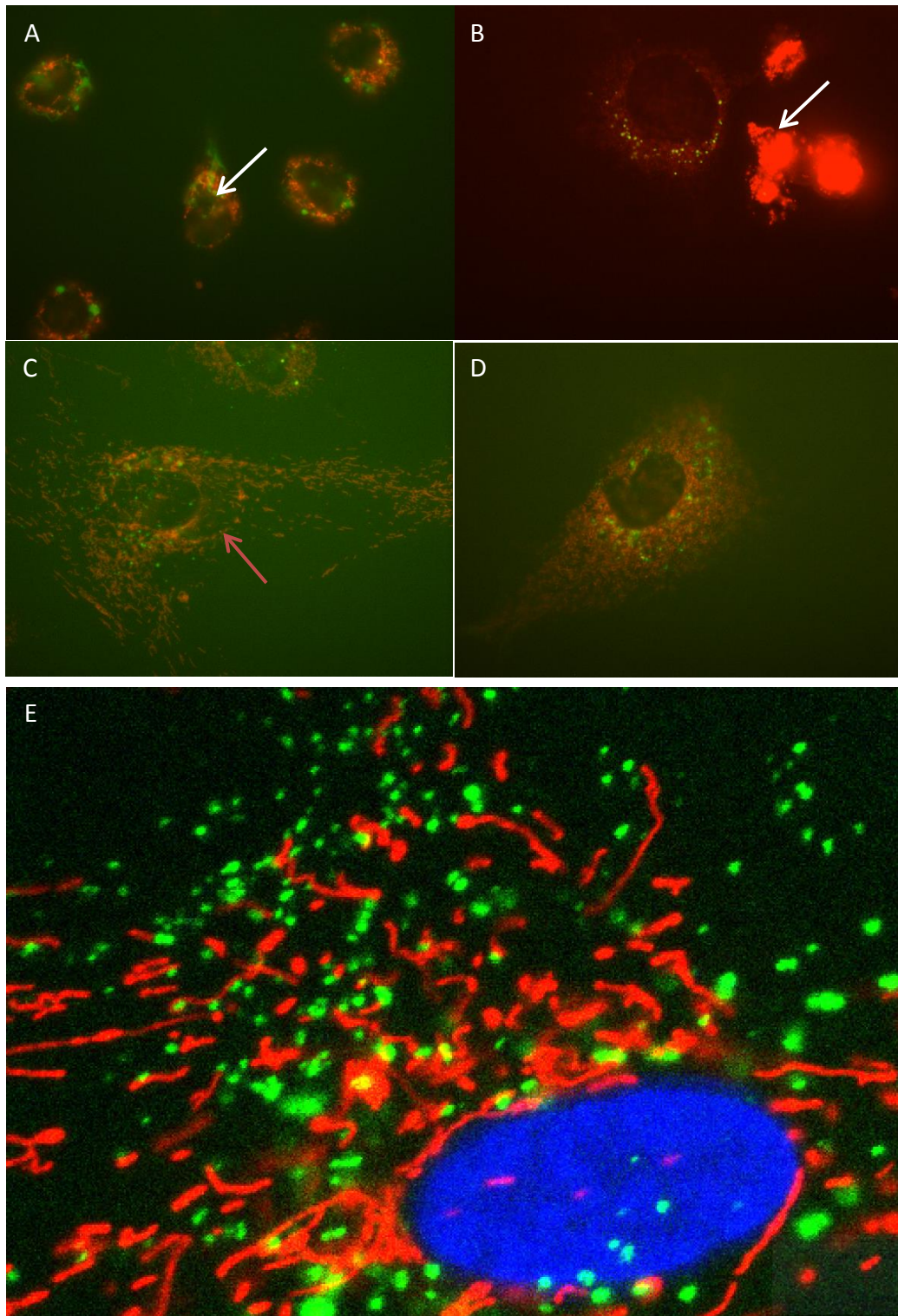
Figure 6.9. Cyto-ID toxicity in ES cells

Extended exposure to cyto-ID appeared to cause unfavourable characteristics in the cell including cell rounding (A) and cell death (B), mitochondrial fragmentation (C) and weak staining (D) The same range of concentrations worked effectively within fibroblasts (E).

6.3.3.4   *Autophagosome tracking through GFP-LC3 transfection*

Following disappointing results with Cyto-ID and the ES cells, efforts were made to transfect the cells with GFP tagged LC3. Unfortunately due to time restraints of this PhD only the Complex IV cell line was successfully transfected. This single line was therefore used to demonstrate a methodology for mitophagic assessments in the future. In line with previous morphological studies, several dynamic alterations could be assessed in this model. For example when live cells were subjected to nutrient depletion, a series of events were commonly observed, with characteristic morphological changes recorded in both mitochondria and autophagosomes. It appears under basal conditions a steady level of autophagosomes are observed alongside visible mitophagic events. Over prolonged stress a dramatic increase in autophagosomes is observed (although those that can be characterised as mitophagic decrease) in line with this an elongation of the mitochondrial network is seen. In the early stages of stress mitochondria take on typical morphologies, alongside elongations, we also observe the formation of donuts and stem loop structures (Figure 6.10). Eventually, this elongation diminishes and an increase in mitophagic events is once again observed (Figure 6.11).
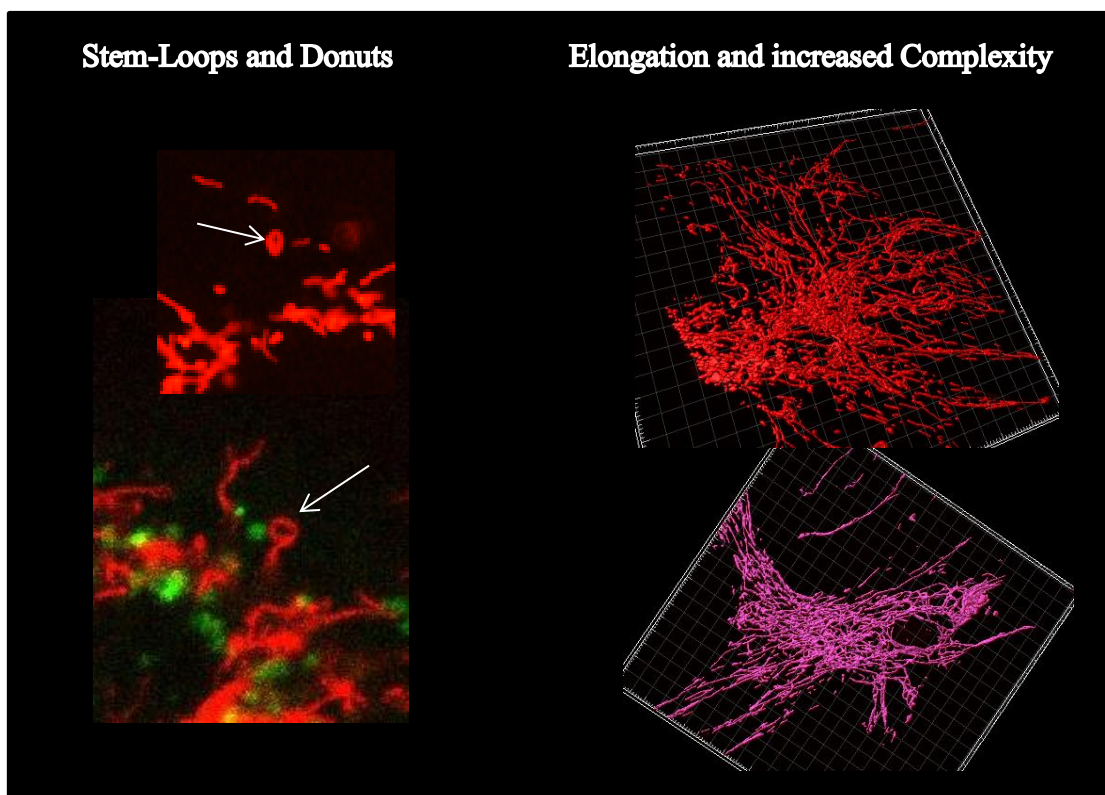
Figure 6.10. Stress induced mitochondrial morphological changes

An early response to nutrient depletion or dysfunction of energy production appears to be the formation of stem loop and donut structures (arrows) alongside the aforementioned elongation and increased complexity of mitochondrial networks.

Figure 6.11. Nutrient depletion leads to characteristic morphological changes in autophagosomes and mitochondria

Cells in media with limited glucose reveal characteristic changes over time. Under basal conditions a steady level of autophagosomes are observed alongside visible mitophagic events (arrows) (A). Over prolonged stress a dramatic increase in autophagosomes is observed (although those that can be characterised as mitophagic decrease) in line with this an elongation of the mitochondrial network is seen (B,C,D,E,F). Eventually, this elongation diminishes and an increase in mitophagic events is once again observed (G,H).
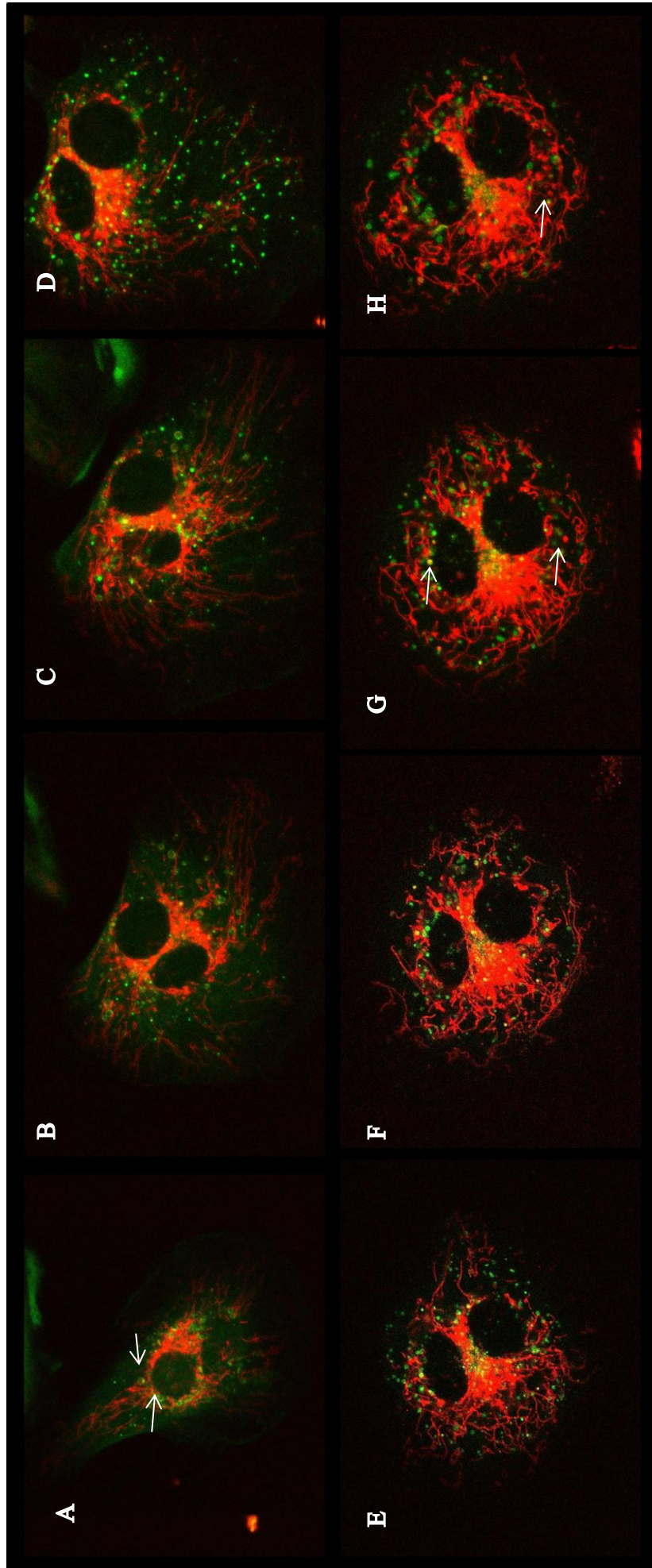
6.4   DISCUSSION

The role interplay between mitochondrial dynamics and bioenergetics has in relation to pathogenic factors in Parkinson's disease is gaining prominence. The results from the experiments outlined in this chapter reveal that cells with an inherent complex I deficiency, known to significantly reduce their bioenergetic capacity, cause changes to mitochondrial morphology, dynamics and arrangement of the mitochondrial-network.

6.4.1   Membrane potential

Morphological changes were shown to coincide with maintenance of elevated mitochondrial electrochemical membrane potential in undifferentiated cells. This increased membrane potential has been previously reported by Abramov *et al* in undifferentiated cells, astrocytes and neurons derived from the same cells used in this study (Abramov *et al.*, 2010). It remains unclear however why the complex I cells maintain their membrane potential above that of controls, although several possibilities are plausible. Clearly maintenance of the membrane potential is crucial for cell survival with loss ultimately resulting in apoptosis. This is highlighted by the fact rho0 cells that are devoid of mtDNA still maintain a small membrane potential, demonstrating that this is a priority for mitochondria.

How the complex I cells maintain such high membrane potential is also unclear. In differentiated cells Abramov *et al* revealed in response to the impaired activity of the respiratory chain, the F1F0 complex switched to ATP consumption mode which maintained the membrane potential. This switch has previously been reported following impairment of oxidative phosphorylation, where complex V reverses, hydrolysing ATP and pumping protons across the inner membrane, maintaining the membrane potential Mai *et al*, 2010). Interestingly, this reversal did not seem to occur in the undifferentiated cells which continued to maintain their membrane potential by respiratory chain activity (Abramov *et al.*, 2010). Why differentiation caused this switch is unclear although authors hypothesise that due to the low glycolytic activity of neurons, enhanced consumption of ATP may be especially harmful to this cell type. Hyperpolarised mitochondria have previously been shown to stay in the network and escape fission

(Twig *et al.*, 2008). This phenomenon may explain how increased network complexity can reduce fission events and subsequently mitophagy.

6.4.2   **Morphological changes**

Alongside an increased membrane potential the complex I cybrid cells revealed changes in mt-network morphology. Notably an increase in network complexity was revealed through form factor analysis (Figure 6.3). This phenomenon has previously been reported. Evidence from patient derived primary human fibroblasts also reveals a modulation of mitochondrial morphology alongside bioenergetic defects (Koopman *et al.*, 2005). An extended reticular network is commonly observed in fibroblasts under basal conditions. Dermal fibroblasts from patients with defined isolated complex I deficiency have been analysed with respect to mitochondrial shape, CI activity, number and ROS production. The degree of mitochondrial fragmentation seems correlated to the severity of CI mutation, with most severe complex I deficiency leading to fragmentation of the membrane; less severe cases appear to more closely resemble their control counterparts. Interestingly a proportion of the less severely affected cell lines revealed an increase in mitochondrial network complexity and length. This is supported by prior work from the same group, showing that chronic rotenone treatment of healthy fibroblasts decreased residual CI activity but increased mitochondrial branching. These phenotypes seem most similar to the complex I mt-networks we observed in this study. The reason for this isn't fully elucidated but could represent an adaptive response to bioenergetic deficiency. The gene mutations in the patient fibroblasts used in the Koopman study described above were all nuclear encoded complex I subunits, conversely the cybrids contain two mtDNA mutations, it would be interesting to see if the specific gene mutation causing complex I dysfunction affects phenotype or whether this is solely dependent on severity. Interestingly, our cybrids display far more severe complex I dysfunction than that displayed in the patient fibroblasts (7% residual activity compared to a range of 18-75% in fibroblasts) therefore it will be crucial to determine why our cells more closely resemble the less severe fibroblasts, possible explanations may include different cell types, different species or different gene mutations.

6.4.3   **Events governing morphology**

Mitochondrial fusion is known to be invaluable in times of high energy demand, the conditions within our cells may mimic high demand as the OXPHOS deficiency means the working capacity is already fully stretched and subsequently working as if under high demand. The suggested adaptive mechanism is particularly attractive when we consider the progression from 'normal' reticular networks to increased complexity to breakdown and fragmentation displayed in parallel with increasing severity of complex I dysfunction. Although the diminished CI activity seen in our cells is severe in relation to the fibroblasts described above, fragmentation of the mitochondrial network seems to precede cell death in our model and as such is not an option for this cell population. On this point, although complex I cybrids are able to survive and to some extent differentiate, this process is compromised with reduced neurons being produced from the severe CI compared to controls. This may well imply the cells have adapted to their inherent CI deficiency to survive but when challenged further, i.e. pushed to differentiate the implications of this adaption become more apparent.

Both content mixing and extended mitochondrial networks are beneficial during periods of high energy demand and as such may be employed by the CI deficient cells to boost energy generation. The idea of hyperfusion as an initial compensatory mechanism is not a new one and may also confer protective qualities. Hyperfused mitochondria may be resistant to apoptosis and mitophagy, becoming too large to engulf, also fusion acts as a means for content mixing to rescue or buffer damage. Whether the elongation of the network represents an adaption in our cells to counter energy deficits is unclear, but the reverse, inhibition of fusion is well known to cause loss of respiratory capacity (Chen *et al.*, 2005). This coincides with natural morphological differences in cells where commonly more interconnected mt-networks are found in more active cells and smaller, fragmented mitochondria tend to be more prevelant in respiratory inactive cells (Westermann, 2012). How elongation increases bioenergetic capabilities is not fully clear, however one suggested hypothesis is that fission ultimately results in population of mitochondria devoid of mtDNA required for OXPHOS, meaning they no longer contribute to ATP production. Fusion would serve to integrate these components, restoring their respiratory activity (Westermann, 2012). The observation that within our complex I cybrids membrane potential is elevated and we see an increase of network complexity, combined with previous work showing the polarised state of mitochondria

is crucial for fission/fusion events and subsequently mitophagy (Twig *et al.*, 2008) offers interesting points for consideration. A possible explanation for the autophagy alterations reported in the complex I cybrids (chapter 5) may be explained by an adaptive fusing of the mitochondrial network that minimises damage caused by the complex I deficiency, but in doing so renders the mitochondrial network unable to partake in fission and subsequent autophagic degradation.

Other reasons for network elongation may also be relevant to the morphological changes observed in our cells. Studies in senescent cells show that there is a DRP1- and FIS1-induced, and PINK1-mediated, protective mechanism, which, when compromised, could contribute to the age-related progression of common neurodegenerative disorders. This mechanism is thought to protect through resistance to oxidative stress. ROS are well documented to contribute to accumulation of mitochondrial mutations, particularly within PD; our cells may use network elongation to compensate for a high ROS environment. Indeed, when mitochondria fuse, complementation of gene products can occur rescuing deficient phenotypes (Komatsu *et al.*, 2006). Adaptive fusion of the mitochondrial network has also been shown in response to cell stressors. This stress induced hyperfusion is accompanied by increased ATP production. It is proposed that this is to allow the cells to optimize mitochondrial function to deal with the stress or challenge (Tondera *et al.*, 2009). The hyperfusion in the CI cells therefore may also be optimizing a diminished mt-network.

Previous studies have shown that affecting morphology through modulation of fission and fusion can impact on energy production in cells. DRP1 knockdown for example has been shown to have profound effects on morphology and bioenergetic capacity. The compromised cells also displayed differences in the properties of mitochondrial membranes with DRP1 siRNA cells showing increased membrane fluidity through DPH anisotropy (Benard *et al.*, 2007). Rearrangement of the mt-network on a macro scale undoubtedly alters the internal architecture of mitochondria. Cristae morphology is important for the energetic capabilities of a mitochondrion. Inner membrane morphology influences mitochondrial functioning, a process dependant on fission and fusion (Mannella, 2006).

Given the two way regulation of bioenergetics and morphology, a decline in regulation of one process or function undoubtedly impacts on the other and in a compromised system, resulting from ageing, CI deficiency, or similar insults, a vicious self-perpetuating series of events is likely to occur. The results acquired from this chapter were somewhat unexpected as much data would imply that respiratory deficiency leads to a fragmentation of the mt-network and a loss of membrane potential. This said the consistency of the data implies that this is a true finding within these cells that may be demonstrating an adaptive response novel to CI deficient cells. These data also begin to explain why despite a supposedly robust selective system for the removal of damaged mitochondria we still see evidence of mitochondrial dysfunction in neurons at all. The data collected within this project offer at least one plausible explanation for why at times the degradation of damaged mitochondria may be avoided. It is also interesting to see that cells with mitochondrial dysfunction don't automatically resign themselves to mass mitophagy or apoptosis but modulate their activity to survive. It is likely that these adaptions are not universal but dependant on the extent of bioenergetic dysfunction. For example with acute dysfunction brought about through complex inhibitors fragmentation and increased autophagy is seen, the polar opposite response is observed to chronic complex I dysfunction such as within our cybrids. To this extent the phenotypes seen in the complex I cells may represent a 'do or die' response, where the adaptations are by no means ideal but the only other option may be cell death.

6.4.4   Live cell tracking

In parallel to the single time point analysis carried out on the morphology of undifferentiated cells, live cell imaging of mitochondria in neurons revealed significant alterations on the dynamics of organelles in complex I cybrid derived neurons. Firstly the overall length of mitochondria in complex I neuronal processes was longer than those found in control counterparts. This is an interesting finding following on from the undifferentiated studies where mitochondrial complexity was also shown to be increased in the complex I cells. In complex I mutants, fewer of the mitochondria were seen to be moving with a significant decrease in the number of tracks analysed (62% of controls). Several reasons could qualify this result (Figure 6.12), for example the reduction in ATP generation within these cybrid cells may render them inefficient in energy consuming trafficking. Alternatively, or possibly in combination, the increased

size of mitochondria arguably makes them more difficult to transport, if indeed they are even recognised as 'moveable cargo'. Mitochondria that were tracked in the complex I cybrids showed reduced speed averaging 0.44µm/sec compared to 0.85µm/sec. Again this could be explained by limited energy provision or slower movement of larger organelles, indeed within these studies and previous findings, smaller organelles tended to move more often and faster.

When the length of tracks, i.e. the distance individual mitochondria covered were analysed it was found that there was no statistical difference between the median length values. However, an analysis of the histograms through the Kolmogorov-Smirnov test revealed a difference in the distribution of track lengths. A greater percentage of both track lengths and track displacement lengths within the cybrid lines were longer. Whether this represents mitochondria that maintain their motility have to function for those which have not is unclear from these studies but could be elucidated from more in-depth analysis of these individual organelles. CI induced morphological changes can have numerous effects in neurons, and dynamics rely on changes in membrane potential to act as cues and allow mechanistic reformation. Subtle changes may be even more significant in neurons when we consider directionality is strongly governed by the potential of individual organelles with 90% of high potential mitochondria moving towards the growth cone and 80% low potential moved towards the cell body (Miller and Sheetz, 2004) and potentiality is varied in dendrites and axons, highlighting clear membrane dependant functioning (Overly *et al.*, 1996). These differences are likely to be crucial for a variety of reasons, notably, transporting more energetically active mitochondria to more active areas and returning low potential mitochondria to be degraded in the cell body.
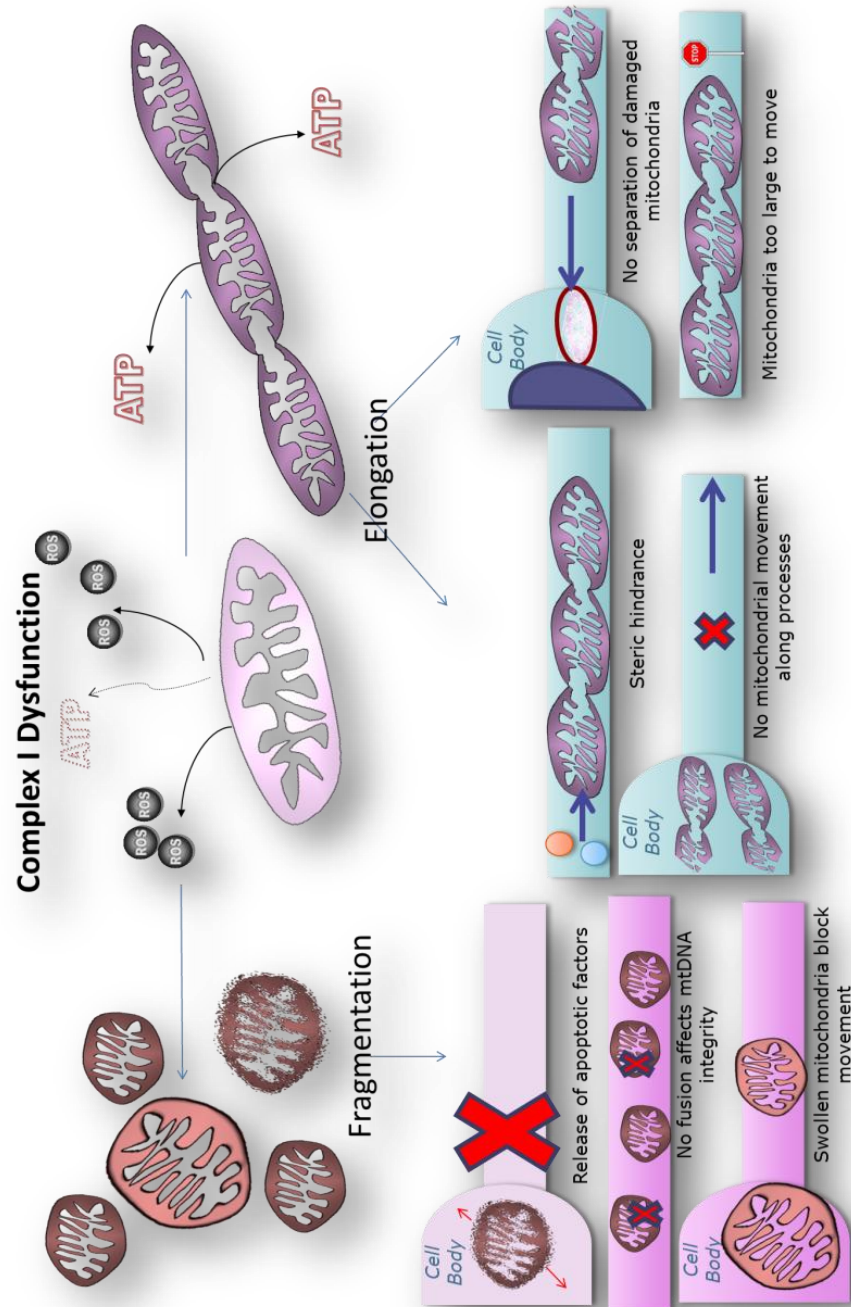
Figure 6.12. Implications of CI induced morphological differences in neurons.

Complex I dysfunction may bring about changes in mitochondrial structure and dynamics. The implications of these changes may be felt most prominently in neurons due to their reliance on mitochondrial trafficking and their post mitotic, restrictive, extended nature. If complex I dysfunction causes fragmentation and/or swelling of the mitochondrial network in neurons this may cause a blockage of axons or dendrites. Alternatively, fragmentation may lead to uncontrolled apoptotic signalling or instability of the mtDNA due to limited rescue through mitochondrial fusion. Conversely, if elongation of the network occurs mitochondria may be unable to escape the cell body and travel along processes. Their motility will be restricted due to their size and they may form physical barriers to the trafficking of other cellular components. Finally a hyperfused network may be compromised in its ability to segregate and degrade damaged mitochondria.

6.4.5   **Morphological adaptions**

Reasons for the morphological changes in response to complex I deficiency are not fully clear but may well be an adaptive response, fusion for example confers apoptotic and mitophagic resistance as well as increasing metabolic efficiency (Gomes *et al.*, 2011). Importantly previous studies have been conducted in cells following complex I inhibition through rotenone which revealed an increase in mitochondrial complexity. However cells with prolonged or severe complex I deficiency ultimately show an increase in fragmentation. As such, it is hypothesised that elongation may be a short lived adaptive response which cannot be sustained. Interestingly in our cells we observed a greater number of elongated mitochondria in the complex I cybrid derived neurites, we may postulate that this occurs as a compensatory mechanism for the inherent complex I deficiency and resulting energy reduction. This however may have very specific implications within neuronal populations (Figure 6.12). Previous studies for example have shown an increase in mitochondrial volume is associated with a drop in motility through steric hindrance (Kaasik *et al.*, 2007). This may go some way to explaining why fewer mitochondria in complex I derived neurons were moving at any given time. Furthermore, smaller mitochondria have been shown to move faster, a possible explanation for the reduction in velocity of mitochondria in the complex I derived neurons, which tended to be larger. The proportion of mitochondria that travelled further than their control counterparts are particular interesting in this study. If they are in some way compensating for slower less motile mitochondria it will be interesting to see what differs in these organelles that allows them to continue functioning effectively.

Few studies have observed complex I deficient mitochondria in living neurons. It is tempting given the preliminary findings of this work to hypothesise that network extension seen previously in complex I deficient cells also occurs in neurons derived from complex I deficient cells to counter the reduction in energy resulting from the two mutations. The differentiation capabilities of the cells are diminished, not only through the direct bioenergetic impairment brought about by the complex I dysfunction but also the indirect steric hindrance and reduced mitochondrial motility associated with the complex I mutations. It is plausible that over time, as motility is reduced, damaged mitochondria accumulate and energy demands are not met, total collapse of the cellular environment could occur, eventually leading to cell death. Interestingly, mitochondrial

mobility dysfunction in neurons with prior stress has been shown to accelerate cell death (Schon and Przedborski, 2011). The complex I dysfunction may therefore be compounded by the mitochondrial dynamic alterations it brings about.

6.4.6   Relation to Parkinson's disease

Morphological and dynamic changes in mitochondria may be key to understanding the pathogenic pathways that ultimately leads to cell loss in Parkinson's disease. Insights from familial forms of PD have highlighted a role of mitophagy (autophagic removal of mitochondria). Mutations in *PARKIN* and *PINK1*, have been shown to have a role in committing damaged mitochondria to a mitophagic fate and are the most common cause of early onset familial PD cases. It is known that both PINK1 and PARKIN can interact with the KHC/MILTON/MIRO complex. Wang *et al* showed that increasing PINK1/PARKIN expression or depolarizing mitochondria arrests mitochondrial movement (Wang *et al.*, 2011). This is achieved through phosphorylation of MIRO by PINK1 and subsequent ubiquitination by PARKIN which leads to its degradation. Halting the transport of damaged mitochondria may be necessary for the isolation and eventual degradation of the organelle through mitophagy. Mutations in these proteins may therefore assert their pathogenicity through an inability to stop and remove damaged/damaging mitochondria. The effects of this will have the greatest impact in neurons due to the complex reliance these cells have upon dynamic processes and their limited regenerative capacity. This may go some way to explaining why neuronal cell death is prominent in PD, specifically within substantia nigra populations where oxidative stress is already high and Ca^2 buffering is imperative due to the unique Ca^2 pacemaking in this cell type. In neuronal models, for example, primary neurons derived from PINK1 knockout mice as well as in human PINK1 knock-down dopaminergic neurons differentiated from mesencephalic stem cells increased ROS and reduced mitochondrial membrane potential has been observed. Interestingly in *drosophila* and mouse models it has been shown that PINK1 deficiency can impact on the function of complex I (Morais *et al.*, 2009).

Observing how mitochondria with a known complex I dysfunction such as the cybrid model, differ in their mitophagic removal, may provide insight into how these two mechanisms are related. Several other genes associated with familial PD have been

linked to mitochondrial dynamics such as LRRK2 and DJ-1 (Zhang *et al.*, 2005; Wang *et al.*, 2011; Niu *et al.*, 2012). Altered mitochondrial morphologies have previously been reported in PD cybrid cells with swollen or enlarged mitochondria clearly present in a subset of PD cells (Trimmer *et al.*, 2000). Subtle changes in mitochondrial dynamics can quickly become self-perpetuating through reductions in cellular energetics. For example, loss of MFN2 in mice has been shown to cause degeneration of dopaminergic neurons alongside motor deficits (Pham *et al.*, 2012).

A bidirectional relationship has been shown between mitochondrial organization and bioenergetics (Benard *et al.*, 2007). Indeed our data shows reduced bioenergetics (complex I mutation) affects mitochondrial organization in the neurites we observed. The convergence of several key themes rather than any individual factor, likely brings about cell loss observed in Parkinson's disease. Complex I dysfunction has been shown to be important and impacted on by mitochondrial dynamics and mitophagic removal. This study shows that complex I dysfunction alone can also cause alterations in mitochondrial dynamics suggesting a more prominent and causative role for complex I dysfunction in PD, with increases in ROS and oxidative stress secondary effects of the dysfunction.

6.4.7   **Concluding remarks**

The data produced in this project suggest bioenergetic dysfunction brought about through severe complex I mutations affects the morphology and dynamics of mitochondria. Dysfunction of electron transport chain components may exert their deleterious effects through different mechanisms, be it through decreased ATP, increased ROS production or most likely a combination of the two. A further mechanism may exist from the control of mitochondrial morphology through bioenergetics. Age related changes in the expression of mitochondrial complexes are observed in models of ageing, these may represent a preliminary challenge to the cellular environment that initiates a series of dynamic changes and may go some way to explaining why an increase in neurodegenerative conditions is observed with age.

Regardless of the timing changes in motility arise, their contribution to homeostatic loss and cell death is unquestionable and is likely to accelerate collapse of the cellular environment in concert with other direct and indirect mitochondrial factors. In line with this, groups have demonstrated that neurons with prior stress are more susceptible to changes in mitochondrial motility. Models of neurodegenerative disease already exist in which mitochondrial phenotype can be rescued by correcting motility (Cassidy-Stone *et al.*, 2008). For this reason perusing modulators of mitochondrial motility may be valuable to assist restoration of the cellular environment and ultimately prevent neurodegeneration.

6.4.8   **Limitations**

Monitoring autophagy in these cells proved problematic. The live cell marker chosen to visualise autophagosomes was trialled at a range of concentrations and shown to be effective in fibroblasts but unfortunately proved toxic at all working concentrations in the ES cells and their neuronal derivatives. This added a further step as the cells needed to be transfected in order to visualize LC3 in conjunction with a mitochondrial marker.

Studying mitochondrial function *in vivo* is difficult for obvious reasons; as such cell culture is an invaluable model to look at dynamic processes. This said the results must be interpreted with caution as different cell lines exhibit different characteristics. What more, morphological and bioenergetic changes can be brought about through modulation of the culture environment. For this reason all aforementioned experiments were carried out with strict variation control.

The development of TIRF imaging in association with IMARIS tracking (described in chapter 3) allowed for further scrutiny of the mechanisms altered in the complex I cybrid cells. This said the new technique was in very early stages of development and as such limited to semi-automatic processing as it was crucial to ensure software was effectively tracking appropriate organelle movement.

6.4.9   **Future work**

To continue this project the development of a robust mechanism to monitor mitophagy specific events is necessary. Although this work has gone someway to looking at these two processes, a more reliable and consistent method will be necessary. Following on from this it will also be valuable to look at similar assays to those described in this chapter under different conditions. Stressing the cells is likely to highlight further adaptive mechanisms in our complex I cells and may explain why a complex I dysfunction in conjunction with other cellular challenges bring about cell loss in neurodegenerative conditions. A more in-depth method for analysing fusion events would also be beneficial for this work as only inference of such events was possible in this study. As such incorporating photoactivatable dyes in combination with tracking may prove interesting. Finally assessing types of mitochondrial movement and also differences between different neuronal regions may further explain the impact complex I dysfunction has in these cells.

Chapter Seven

Morphological
Assessments in
Patient Fibroblasts

Chapter 7. Mitochondrial Dynamics and Autophagy in Patient Fibroblasts

7.1 INTRODUCTION

7.1.1 Overview

NADH: ubiquinone oxidoreductase/complex I (CI), is the largest and most complex component of the electron transport chain. As entry point to the OXPHOS system its role in initiating the electrochemical potential is key, accepting electrons from NADH and transferring them through a series of redox centers to ubiquinone. CI consists of 46 subunits, 7 of which are encoded by mtDNA. Its prominent role in the process of oxidative phosphorylation alongside an array of experimental evidence, implicate its dysfunction in numerous disorders (Sharma *et al.*, 2009), noticeably neurodegenerative conditions.

Complex I dysfunction in PD is one of the longest established, and most well evidenced pathogenic factors in the development of the disorder. Idiopathic PD for example, is characterized by a 15-30% reduction in complex I activity (Schapira *et al.*, 1990). To this end, this project was undertaken to look at parameters assessed previously in the cybrid cell lines, with respect to patients with defined complex I deficiency. The hope being, that patterns of dynamic and morphological changes within this patient group may enable us to conclude with greater certainty whether complex I dysfunction is solely responsible for the observed alterations.

7.1.2 Isolated complex I deficiency

In parallel to the role complex I dysfunction has in a range of human diseases, its dysfunction is responsible for a distinct set of disorders. Complex I deficiency is the most frequent mitochondrial defect presenting in childhood and may present itself in a variety of disorders, commonly including Leigh syndrome, leukoencephalopathy and other early-onset neurodegenerative disorders; fatal infantile lactic acidosis; hypertrophic cardiomyopathy; and exercise intolerance (Kirby *et al.*, 1999). The heterogeneity of this group of disorders results from the involvement of different nuclear and mitochondrial genes, alongside various assembly factors. Biochemical and

phenotypic analysis of patient cell lines have revealed a range of severities with regards to enzymatic and bioenergetic capacity. The exploration of morphological differences at the subcellular level in this group has also begun to highlight clues that may advance understanding of these disorders.

7.1.3   **Previous morphological exploration**

Mitochondrial morphology is dependent on a range of external and internal influences. Cellular environment, including nutrient availability, metabolic state, development and differentiation stage, cell cycle and DNA content, all impact on the form and dynamics of the organelle. The severe implications of complex I deficiency therefore unsurprisingly affect mitochondrial form and function. For this reason, several groups have analysed the impact defined complex I deficiency has upon mitochondrial number and shape. Cytopathological assessments of patient fibroblasts by Koopman *et al* has revealed significant differences in terms of form factor (mitochondrial network complexity) and mitochondrial number, the same range of variation was not seen in control cases (Koopman *et al.*, 2005). Certain patient cell lines displayed increased form factor without a significant change in mitochondrial number, implying that these cells contained elongated mitochondria. To exclude the possibility that this represented juxtaposition of organelles, transduction of patient cell lines was achieved with mito EYFP in conjunction with Fluorescence Recovery After Photobleaching (FRAP) analysis, that showed these were indeed distinct organelles.

Importantly, Koopman *et al* showed changes in morphology of patient fibroblasts are not universal, several cases displayed a decrease in form factor and/or increase in number in conjunction with relatively large reductions in complex I activity. For those patients where an elongation was observed, the CI activity reductions were more moderate. These differences appeared to segregate with severity. For this reason the group then went on to define mitochondrial complexity (the ratio of form factor to mitochondria number) which revealed two distinct groups. Class I cells, that had lower mitochondrial complexity, severe reduction of complex I activity and reduced average amounts of fully assembled complex I as given by blue native gel electrophoresis. Class II cells conversely, had greater or equivalent complexity to controls and showed higher residual complex I activity than the class I cells.

7.1.4 **Aim of study**

This study was to utilize fibroblasts from patients with confirmed, isolated complex I deficiency. Various morphological assessments would be made and compared to controls, in line with previous experiments carried out in cybrid cell lines (chapter 6). Data gathered through literature reviews and unpublished data generated previously on parameters of severity and presentation of each case through the Newcastle Mitochondrial Diagnostic Service would then be used to compare to morphological changes.

1. Analyse mitochondrial morphology.

2. Assess associations between mutation location and phenotypes.

3. Assess associations between phenotypes and severity

4. Analyse autophagosome formation with respect to control fibroblasts.

7.2   METHODS

7.2.1   Fibroblast cell lines

Cell lines utilized in this study were sourced from Newcastle Mitochondrial Diagnostic service and can be seen in Table 7.1. Two independent control lines were used alongside three mitochondrially encoded complex I mutations (2xMTND4 and one MTND5) and two nuclear encoded complex I mutations (NDUFS6 and NDUFS2). Alongside these, one nuclear encoded dynamin 2 (DNM2) mutation and two novel nuclear FBXL4 mutations were analysed. Due to the order in which experiments were conducted this chapter focuses first on CI and DNM2 mutants (highlighted below) before discussing the results generated from the two FBXL4 mutants. The discussion that follows the results considers all cell lines.

2x Control	2x CI nuclear	2x CI Mito
	DNM2	2xFBXL4
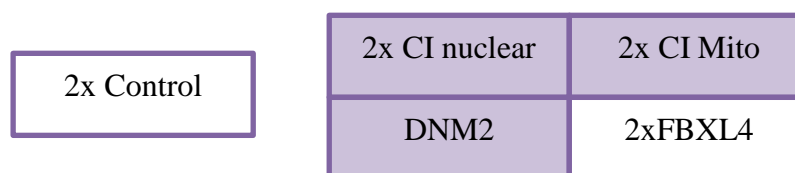
7.2.2   Complex I patient network analysis

Fibroblasts were grown in 35mm imaging dishes (iBIDI, Thistle Scientific) to 70%−80% confluency. Cells were incubated at $37^{o}C$ in the growth media described in chapter 2.5.6, with the addition of 100nM TMRM (Invitrogen) for 25mins. Cells were washed in standard media and imaging performed with a 63x oil immersion lens on the inverted Axiovert 200M (Zeiss), with shutter speeds of 200ms. Seeding densities were matched for all experiments to ensure limited variation in experimental conditions. Single plane imaging was carried out to achieve a minimum of 50 images/cell line. To analyse the images a series of deconvolution steps were followed as discussed in chapter 5.3.6. From these data, two characteristics were generated- form factor, a measurement of length and degree of branching ($perimeter^2/4\pi \cdot area$), and aspect ratio which generates data on the length based on the ratio between major and minor axes of an ellipse equivalent to the mitochondrion. These were recorded from triplicate experiments and compared for differences between each individual patient cell line and control cell lines through unpaired t tests.

Patient Fibroblast Lines (lit reference)	Characteristics		Clinical Features/ Phenotype (if known)	Mutation Load	Muscle Biochemistry		Fibroblast Biochemistry		Functional Studies		
	Mutation	Gene			CI	CI/CII	CI	CI/CII	BNPAGE	WB	ROS Production
M400-12	pGlu106GlnfsX41 (hom)	NDUFS6	severe early-onset fatal lactic acidosis (~40mmol/L) on day 4		0.022	0.125	0.240	0.196 for CII, CIII ratio of 1.211			
M304-06 (Tuppen et al., 2010) Patient 3	p.Arg118Gln; p.Met292Thr	NDUFS2	At the age of 22 months, the patient developed central hypopnoea and died.		0.021 (20%) Control range= 0.104+- 0.036.	0.313 Control range= 0.52- 0.95			Complex I assembly defect	NDUFA9 and NDUFB8 protein levels were reduced in fibroblasts of Patients	did not show any elevated levels of mitochondrial superoxides
M0607-09 (Alston et al., 2011) Patient 1	m.13514A>G	MTND5	Death at 30months	levels of 69 and 55% heteroplasmy in muscle and fibroblasts, respectively	0.044 Control range= 0.104+- 0.036	0.234 Control range= 0.58-0.90	0.055 Control range= 0.197+- 0.034	0.135 Control range= 0.58-0.90			
M034-07	m.13051G>A	MTND5		Very high	Normal complex I activity(SPEC)						Increased ROS
M0125-07	m.11777C>A	MTND4	LS; ataxia, bulbar palsy, progressive deterioration,	muscle (78%) blood (64%) and fibroblasts (52%)	0.035; controls 0.104±0. 036	0.238; normal 0.52- 0.95)	0.105; controls 0.197±0 .034	0.147; controls 0.219±0.06 7	CI-20 expression normal		increased ROS
M0828-11	heterozygous p.Arg369Trp	DNM2	Adult presentation CPEO, myopathy, centranucleomyopathy associated with 5% COX-ve fibres and multiple mtDNA deletions in muscle	mitochondrial network abnormality confirmed in cells, no other functional assays performed							

Table 7.1 Patient fibroblasts used in this study

Table shows cell lines used in the fibroblast morphological assessments and where available associated biochemical and phenotypic data.

7.2.3   **Autophagosome analysis**

Fibroblasts were once again maintained in 35mm imaging dishes (iBIDI, Thistle Scientific) to 70%–80% confluency. Cells were incubated at 37°C in standard media. On day of imaging, assay buffer and Cyto ID (both Enzo Biosciences) were prepared as per manufacturer's instructions. Cells were washed in assay buffer then incubated for 30mins in assay buffer supplemented with 1µl cytoID reagent. Cells were washed with assay buffer twice then maintained in normal growth media throughout imaging. All autophagosome imaging was carried out on the Nikon A1R confocal microscope to enable z stacks to be obtained. Optimal z stack depth was established through Niquest on the microscope and z stack numbers range between 18-30. To analyse both number and volume of autophagosomes Imaris 7.6 (Bitplane) was employed Figure 7.1. Autophagosomes were identified as structures within the software and numbers within individual cells recorded. Volumes of individual structures were also recorded and compared for controls vs. patient cell lines.
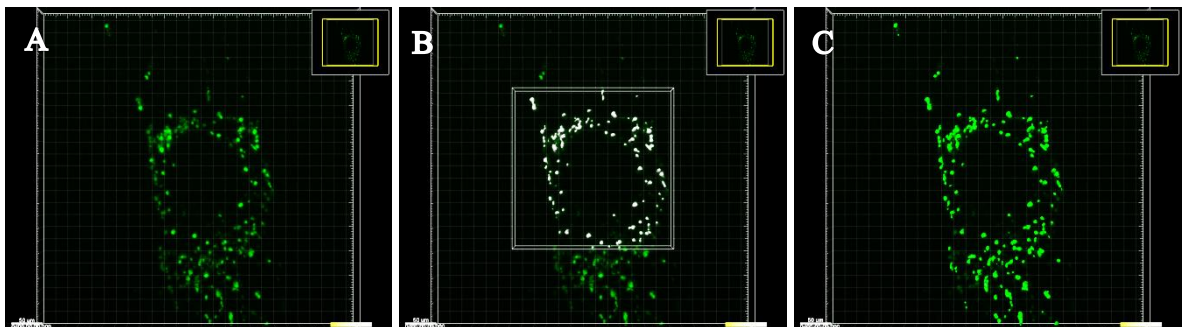
Figure 7.1. Identification and quantification of autophagosomes in fibroblasts

Cyto ID was used to stain autophagosomes in live fibroblasts. Z stack images were taken using the Nikon A1R and 3D images reconstructed (A). Regions of the cell were defined and structures of autophagosomes mapped (B). These characteristics were then applied to the entire image. Measurements of autophagosome number and volume were recorded (C).

7.2.4   **Network analysis of FBXL4 patient lines**

Alongside complex I deficient cases, two lines containing novel pathogenic mutations in the FBXL4 gene and one uncharacterized mutation in DNM2 were also analysed. In doing this morphological differences could be assessed in cases outside of complex I deficiency and parallels between the two could be analysed. Alongside mitochondrial assessments nucleoids were stained with PicoGreen for characterization.

7.3   RESULTS

7.3.1   Network analysis complex I patients

Analysis of the mitochondrial network was undertaken for two nuclear encoded complex I mutations, three mitochondrially encoded complex I mutations and a DNM2 mutant. Control cell lines routinely displayed a complex reticular mitochondrial network characteristic of healthy fibroblasts (figures 7.2 and 7.4 left panel). In contrast, all patient cell lines showed marked differences in mitochondrial shape. Initially networks were analysed based on form factor and aspect ratios. It soon became apparent however that this methodology was not suitable for the data generated from these cells. Within each patient cell line populations of different morphologies existed. For this reason network morphologies were grouped into categories based on their network complexities and mitochondrial lengths. The five groups were, 'as control', 'fragmented', fragmented and clumped', elongated throughout' and elongated with perinuclear clustering'. The results of these can be seen in Figure 7.3 and representative images are displayed in Figure 7.2 and Figure 7.4 .

Figure 7.2. Mitochondrial morphologies in patient fibroblasts (1)

Variation was observed in typical mitochondrial morphologies between cell lines. Control cell lines typically displayed extended reticular networks (LH Panel). The MTND4 line showed a combination of fragmented and clumped organelles (white arrow) and some with elongated networks (white arrow head). The DNM2 mutants showed mostly fragmented mitochondria although some perinuclear clustering was observed, an extremely similar phenotype was observed in the MTND5 cell lines (not shown).

Control M0158-12   M125-07 MTND4   M0828-11 DNM2

Control M0158-12   M125-07 MTND4   M0828-11 DNM2
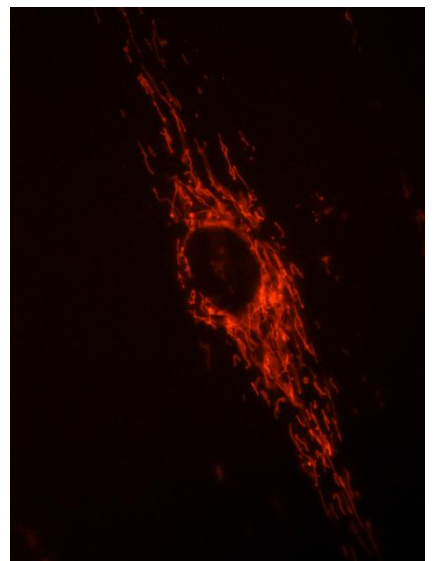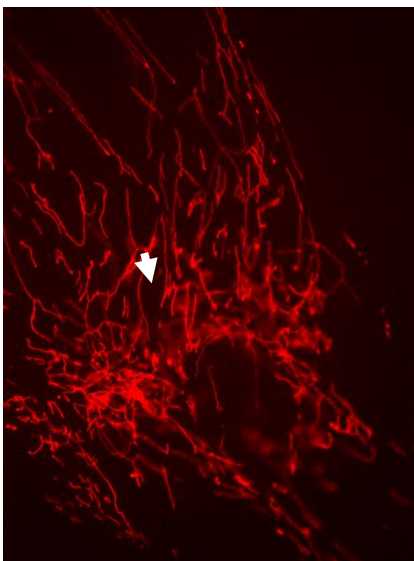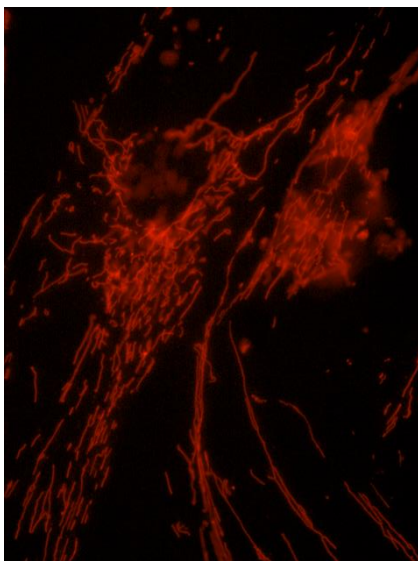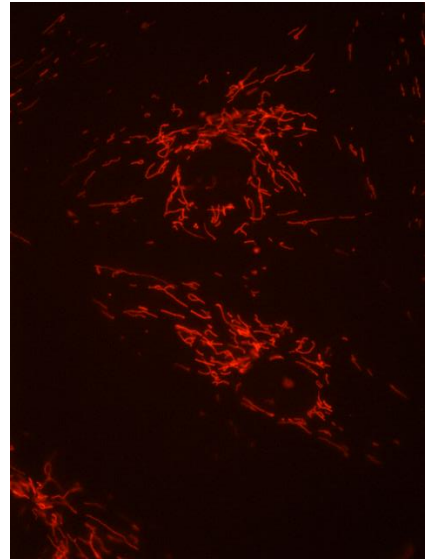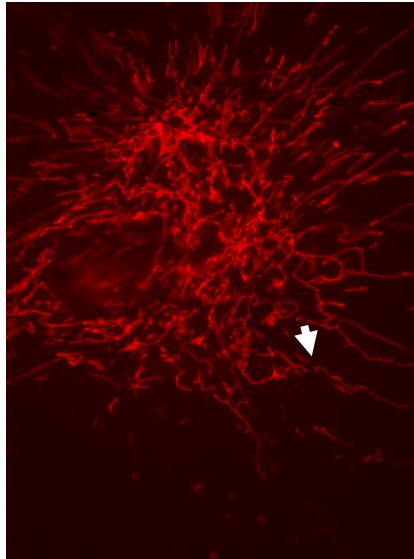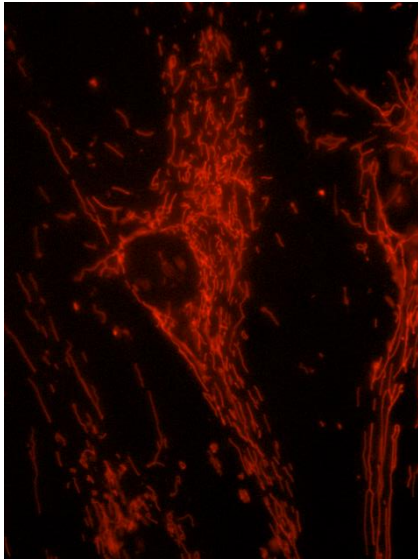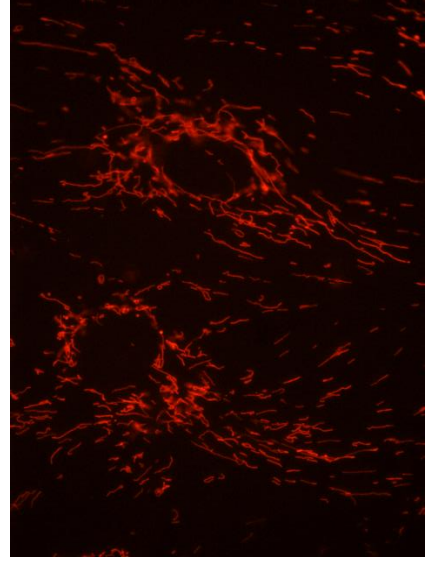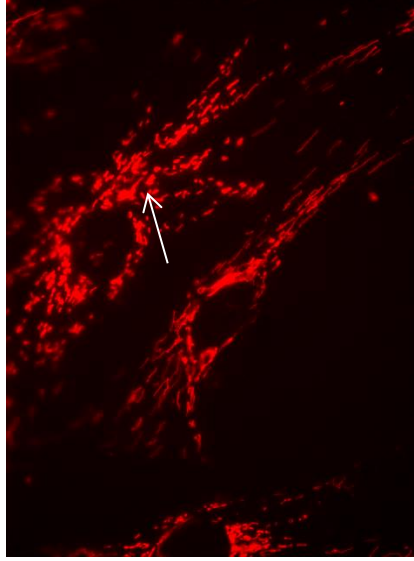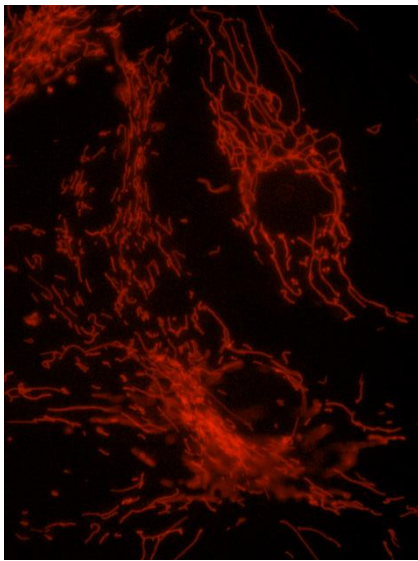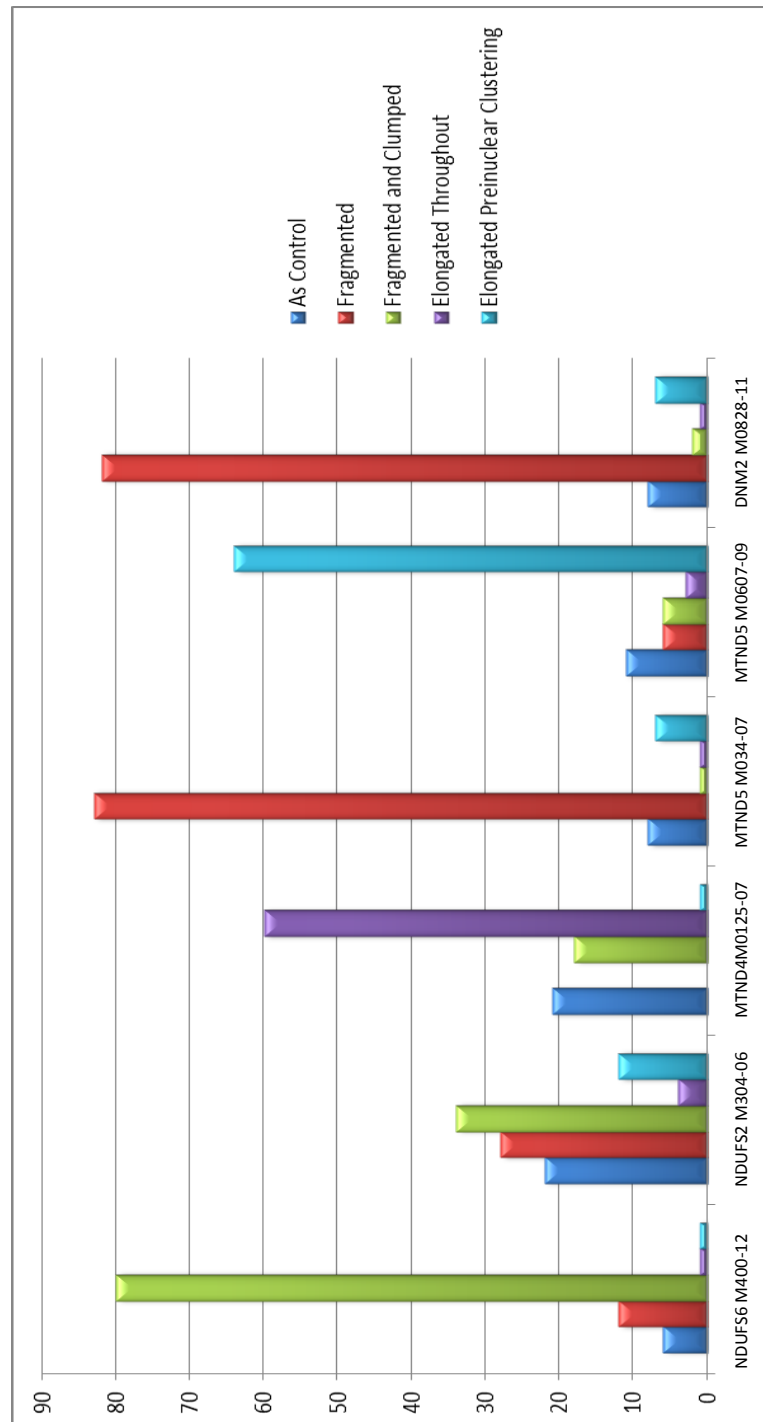
Figure 7.3. Proportions of networks falling into each predefined morphological category

Mitochondrial network morphologies were assessed in six patient cell lines and compared to controls. Groups of morphologies were often observed and as such cells within each line were allocated a group and proportions calculated as above (n=75 over three separate experiments).

Figure 7.4. Mitochondrial morphologies in patient fibroblasts (2)

Variation was observed in typical mitochondrial morphologies between cell lines. Control cell lines typically displayed extended reticular networks (LH Panel). The complex I lines NDUFS2 and NDUFS6 showed fragmented mitochondria with some of the cells clumping specifically in the perinuclear region (examples shown by dotted outlines).

Control M0158-12   M0400-12 NDUFS6   M0304-06 NDUFS2
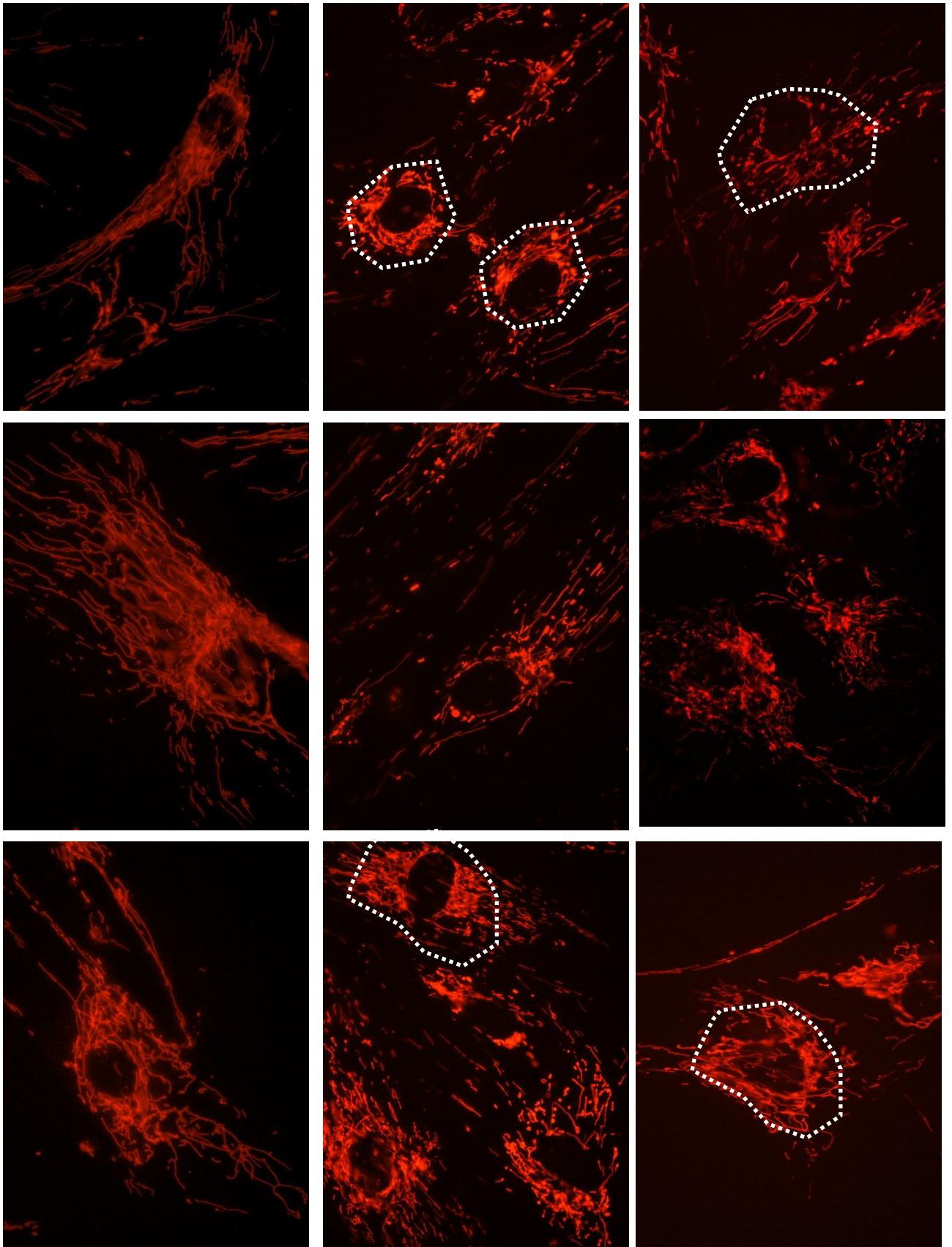
Although the data showed an array of proportions, certain patterns could be observed. Firstly, majority of cells within the DNM2 mutant showed fragmented mitochondria. This was to be expected as dynamin2 is a ubiquitously expressed large GTPase, with roles in the regulation of intracellular membrane trafficking through its crucial function in membrane fission and has been shown to be necessary for proper mitochondrial morphology and function. Interestingly, mitochondria within the MTND5 mutant showed similar phenotypes to the DNM2 mutant. No single pattern of morphological alterations was observed within the complex I deficient cells although a distinction between the nuclear encoded and two of the mitochondrially encoded lines could be seen. Both the NDUFS6 and NDUFS2 lines showed (to different extents) populations of cells that contained fragmented mitochondria. Conversely, MTND4 and MTND5 lines contained elongated mitochondrial networks with particularly the MTND5 line showing perinuclear clustering. These results may point towards mutation location specific alteration of morphologies in these cells.

Patient Fibroblast Lines (lit reference)	Characteristics		
	Mutation	Gene	Mitochondrial Morphology
M400-12	pGlu106GInfsX41 (hom)	NDUFS6	Fragmented/ Clumping
M304-06 (Tuppen *et al.*, 2010) Patient 3	p.Arg118Gln; p.Met292Thr	NDUFS2	Fragmented/ Clumping
M0607-09 (Alston *et al.*, 2011) Patient 1	m.13514A>G	MTND5	Elongated perinuclear
M034-07	m.13051G>A	MTND5	Fragmented
M0125-07	m.11777C>A	MTND4	Elongated (more variation)
M0828-11		DNM2	Fragmented

Table 7.2. Predominating mitochondrial morphology

Although variations of mitochondrial morphologies were observed in each cell line, each had a predominating phenotype.

7.3.2   **Autophagosome Quantification**

Quantification of Cyto-ID staining, which visualizes autophagosomes, was performed on five of the fibroblast cell lines. These five were selected due to time constraints and allowed the assessment of mitochondrial and nuclear encoded CI deficiencies whilst giving a variety of mitochondrial network morphologies. Significant differences were seen and are discussed below.

7.3.2.1   *Autophagosome number*

The average number of autophagosomes per cell in each cell line was quantified (Figure 7.5). Due to high variability within cellular populations only the MTND4 patient cell line was shown to be significantly higher in autophagosome number when compared to controls (P= 0.0483). NDUFS2 showed a trend towards fewer autophagosomes/cell although this was not significant (P=0.0725).
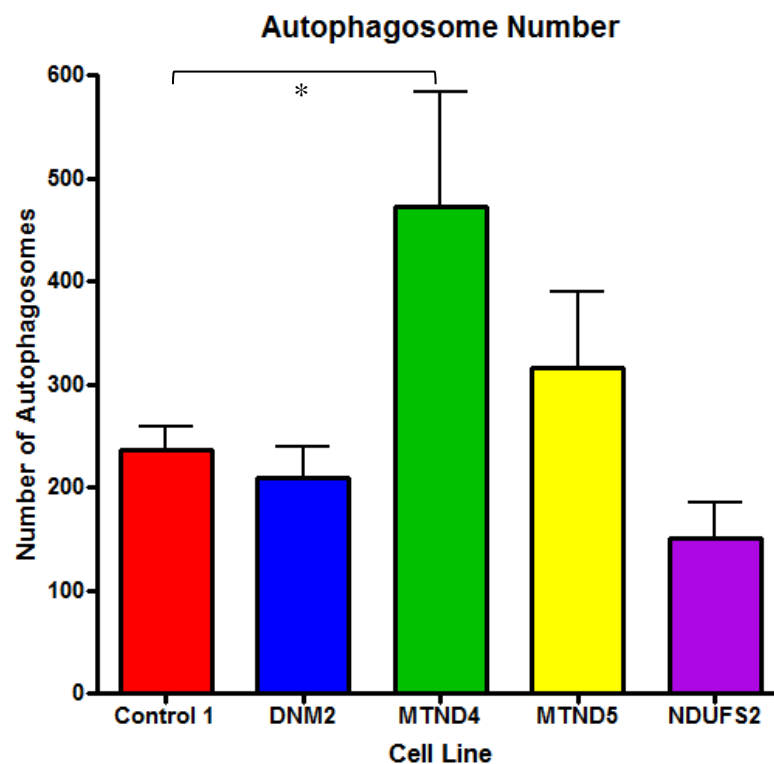
Figure 7.5. Autophagosome number in patient fibroblast lines

Only MTND4 showed a significant increase in autophagosome number compared to controls N=75 over three experiments (P=0.0483).

7.3.2.2   *Autophagosome Volume*

Analysis of autophagosome volume in patient fibroblasts revealed significant differences in all but one of the cell lines (Figure 7.6). Both MTND5 and DNM2 lines revealed far smaller autophagosomes when compared to controls (P's<0.001). NDUFS2 derived fibroblasts conversely showed larger average autophagosome volumes (P= 0.007).
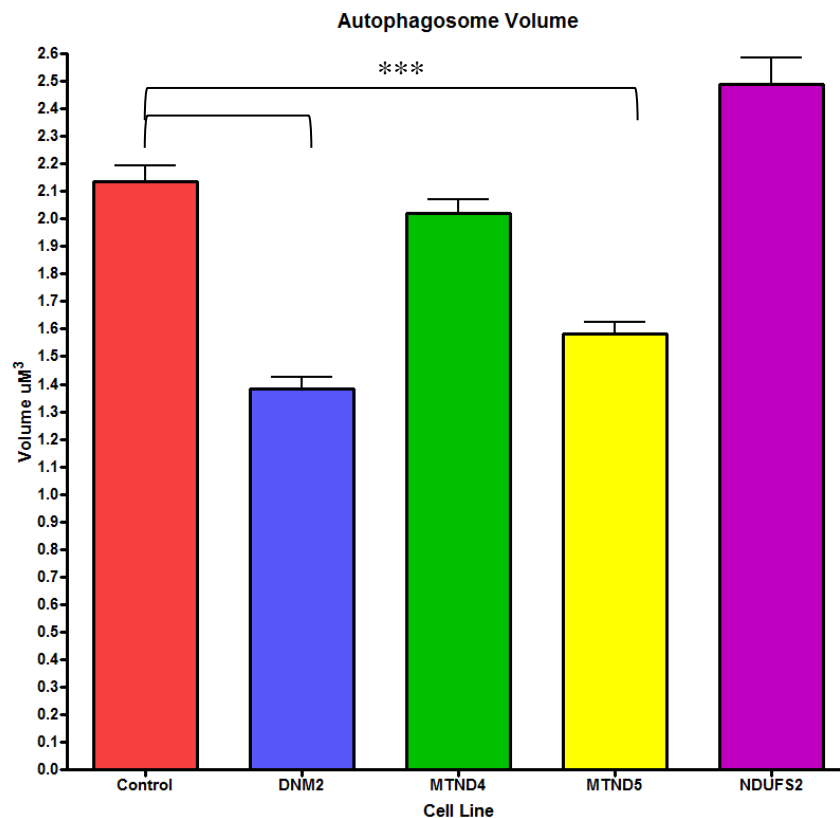
Figure 7.6. Autophagosome volume in patient fibroblast lines

All but the MTND4 line showed significant differences in autophagosome volume when compared to controls. Both DNM2 and MTND5 had smaller autophagosomes whilst those quantified in NDUFS2 were larger, N=75 over three experiments.

7.3.3   **Correlation between autophagosome and mitochondrial morphologies**

It would appear from the data collected from these five patient fibroblast cell lines that a degree of correlation occurs between mitochondrial morphologies and autophagosome formation. The DNM2 cell line and MTND5 lines showed very similar mitochondrial morphologies with the majority of mitochondrial populations falling into the fragmented category. Interestingly the similarities between these cell lines continued into autophagosome analysis. Neither showed a significant deviation from the control

autophagosome number (DNM2 P= 0.5019 and MTND5 P= 0.3314). Autophagosome volumes however were reduced in these lines. The link between these two cell lines may demonstrate that mitochondrial morphology and autophagosome formation are interrelated.

The MTND4 line was unique for two reasons. Firstly it was the only line that showed mitochondrial elongation throughout the cell. In terms of autophagosome formation, it was also unique in that a dramatic increase in autophagosome number was seen, whilst the volumes stayed the same. From these preliminary studies it would be tempting to hypothesize that fragmented mitochondrial networks are associated with changes to autophagosomal volume, potentially reflecting changes in mitophagy. Complex mt-networks in this study appear to have a larger number of 'normal' sized autophagosomes. One might suggest that this may reflect mitochondria 'protecting themselves' from autophagic degradation through fusion, the increase in autophagosomes may therefore be associated with the degradation of other intracellular components. Further studies will be necessary to see if these associations ring true in the case of other morphological alterations.

7.3.4   Correlations with severity

Unfortunately the prexisiting functional and biochemical data available for these cell lines is not sufficient to draw any conclusions with the parallels to morphology of mitochondria and autophagosomes. There appears to be a tendancy for reduced CI muscle biochemistry and fragmentation of the mitochondrial network, whilst those that retained higher functioning were those that retained greater functioning being elongated. Further cases and more indepth background from these lines will be needed.

Patient Fibroblast Lines (lit reference)	Characteristics				Morphology		Functional Studies		
	Mutation	Gene	Clinical Features/ Phenotype (if known)	Mutation Load	Mitochondria	Autophagosomes	BNPAGE	WB	ROS Production
M400-12	pGlu106GlnfsX41 (hom)	NDUFS6	severe early-onset fatal lactic acidosis (~40mmol/VL) on day 4		Fragmented/ Clumping	Not tested			
M304-06 (Tuppen et al., 2010) Patient 3	p.Arg118Gln; p.Met292Thr	NDUFS2	At the age of 22 months, the patient developed central hypopnoea and died.		Fragmented/ Clumping	Larger autophagosomes	Complex I assembly defect	NDUFA9 and NDUFB8 protein levels were reduced in fibroblasts of Patients	did not show any elevated levels of mitochondrial superoxides
M0607-09 (Alston et al., 2011) Patient 1	m.13514A>G	MTND5	Death at 30 months	levels of 69 and 55% heteroplasmy in muscle and fibroblasts, respectively	Elongated perinuclear	Not tested			
M034-07	m.13051G>A	MTND5		Very high	Fragmented	Smaller			Increased ROS
M0125-07	m.11777C>A	MTND4	LS; ataxia, bulbar palsy, progressive deterioration,	muscle (78%) blood (64%) and fibroblasts (52%)	Elongated (more variation)	Greater number	CI-20 expression normal		increased ROS
M0828-11	heterozygous p.Arg369Trp	DNM2	Adult presentation CPEO, myopathy, centranucleomyopathy associated with 5% COX-ve fibres and multiple mtDNA deletions in muscle		Fragmented	Smaller			

Table 7.3. Fibroblasts used in study with associated mitochondrial and autophagosome morphologies

7.3.5   Network analysis of FBXL4 lines

FBXL4 is an F-box protein that colocalizes with mitochondria, through whole-exome sequencing, Bonnen *et al* identified recessive nonsense and splicing mutations in FBXL4 segregating in three unrelated consanguineous kindreds in which affected children present with a fatal encephalopathy, lactic acidosis, and severe mtDNA depletion in muscle (Bonnen *et al* 2013). We looked at the morphology of mitochondria through aspect ratio and form factor, alongside nucleoid morphology. This enabled us to look at morphological alterations in patient lines without isolated complex I deficiency and further characterize how other mitochondrial defects may affect the mitochondrial network. This enabled us to assess how these pathogenic mutations affected mitochondrial networks alongside aiding characterization of these novel mutations.

Both patient cell lines harbouring the FBXL4 mutations showed a dramatic fragmentation of the mitochondrial network (Figure 7.7). Furthermore, nucleoid morphology and localization was altered (Figure 7.8). Bonnen *et al* revealed through micro-oxygraphy and protein expression studies that the FBXL4 mutants display a severe respiratory chain deficiency, loss of mitochondrial membrane potential, and a reduced expression of mitochondrial proteins. The severity of this dysfunction is in line with the patient fibroblasts from isolated complex I deficiency which also displayed mitochondrial fragmentation. Quantification of images is shown in Figure 7.9.
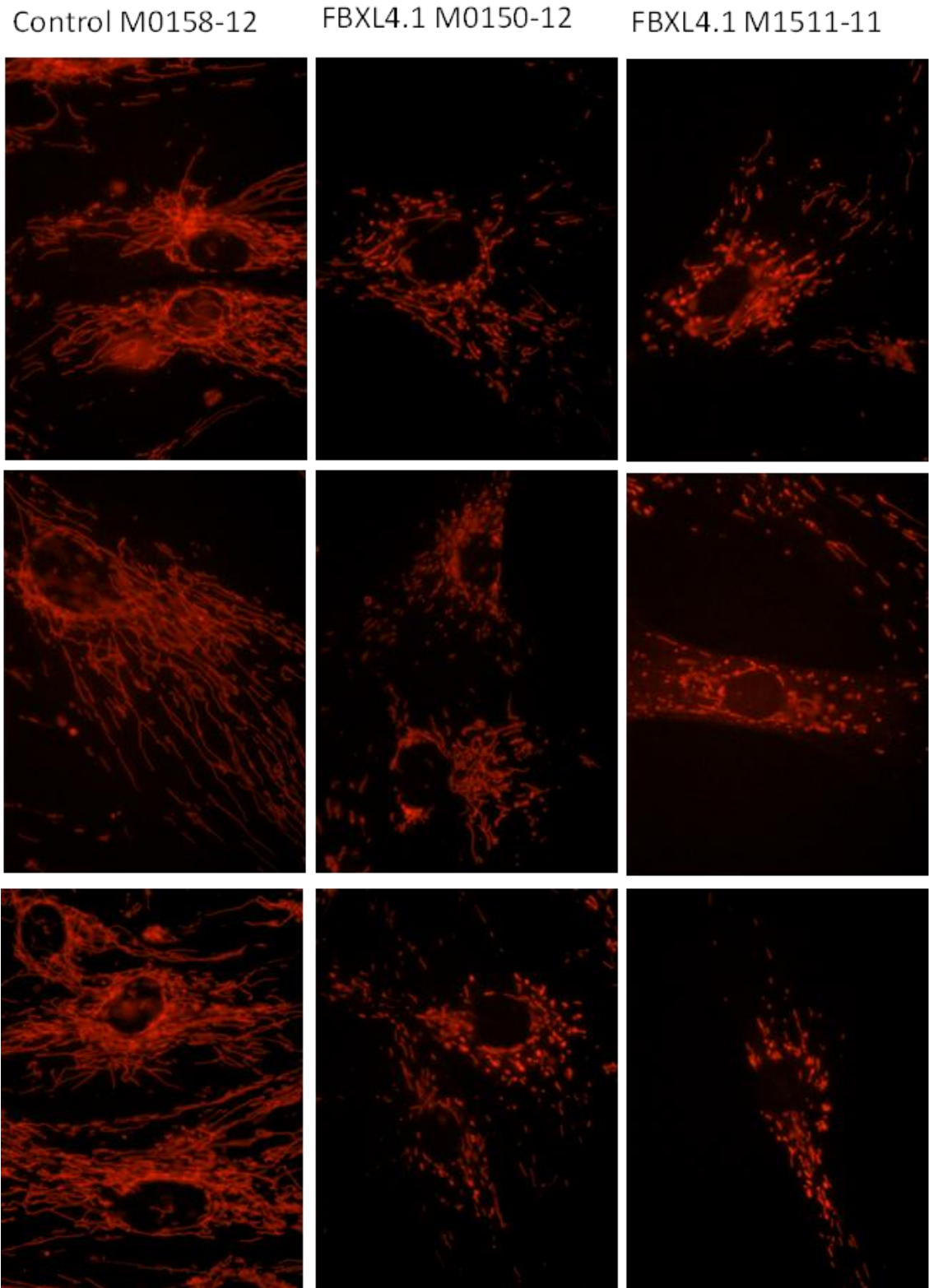
Figure 7.7. Mitochondrial Morphology in FBXL4 patient lines

Both patient cell lines harbouring the FBXL4 mutations showed a dramatic fragmentation of the mitochondrial network.
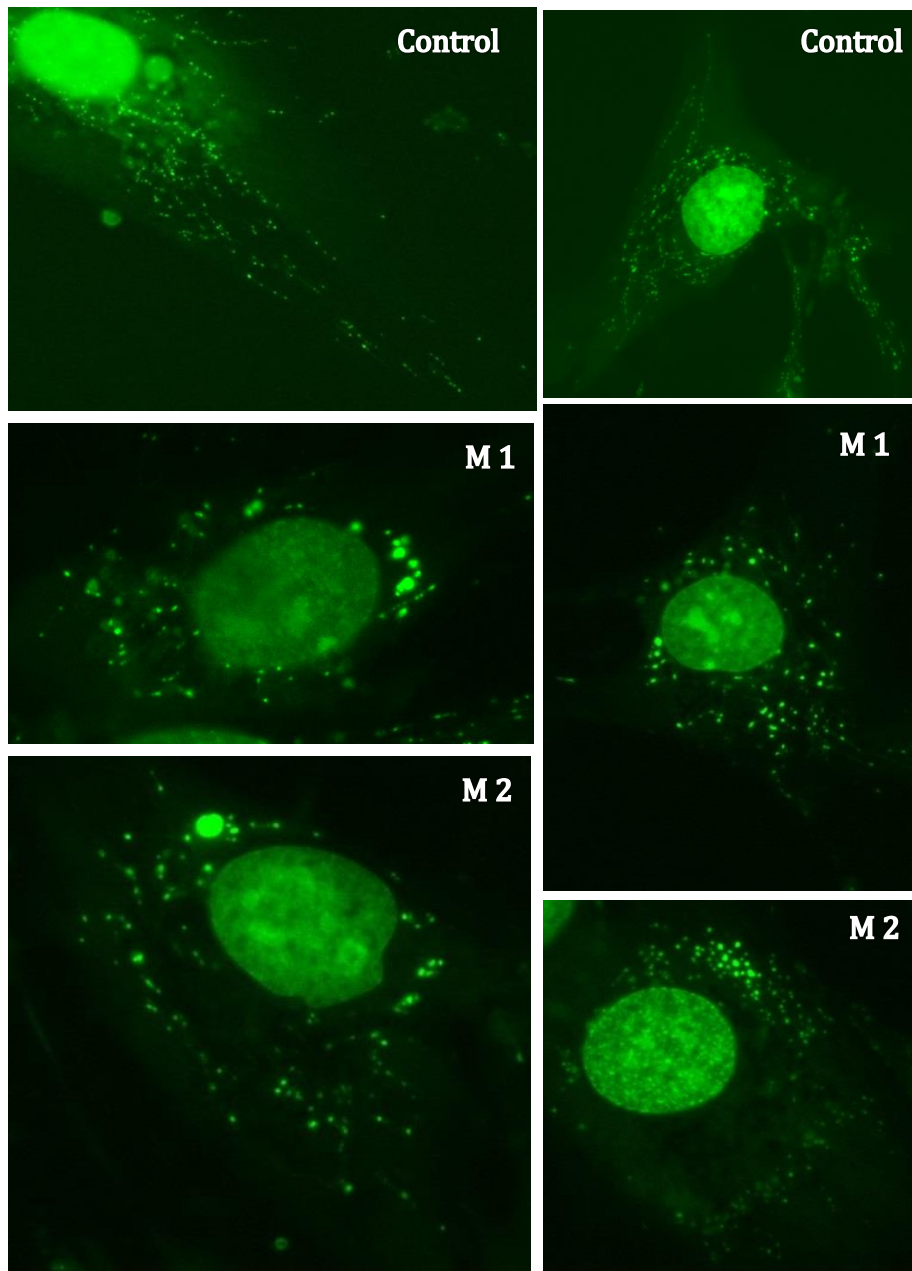
Figure 7.8 Nucleoid morphologies in FBXL4 patient lines

Nucleoids were enlarged and showed distinct perinuclear clustering in both patient cell lines(M1 and M2) compared to smaller more evenly distributed nucleoids within control cells (top panel).
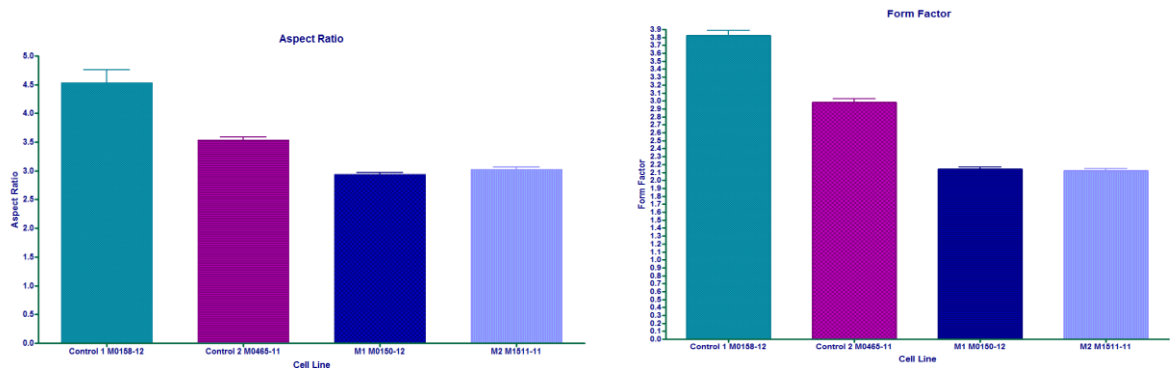
No.	P No.	M No.	Mutation	OCR	AR*	FF*	Mitochondrial Morphology	mtDNA
C1	6	M0158-12	Control		114.29	101.70	Normal	
C2	6	M0465-11	Control		85.71	98.30	Normal	Normal
M1	6	M0150-12	FBXL4		64.69	60.11	↓Branching, shortening, clumping	Perinuclear clustering, larger nucleoids
M2	6	M1511-11	FBXL4		75.46	43.45	↓Branching, shortening, clumping	Perinuclear clustering, larger nucleoids

Figure 7.9. Quantification of AR, FF and nucleoid morphologies

Aspect ratio (AR) and form factor (FF) were significantly lower in FBXL4 patient lines than controls. Control 2 (C2) was shown to have a significantly lower AR and FF than control 1 (C1), however following bioenergetic and biochemical assessments it was revealed that this cell line actually displayed a mild dysfunction and as such was not a true control. The data contained within the table therefore is likely to be a very conservative representation of the true reduction in the FBXL4 cell lines.N=100 over two experiments.

7.4   **DISCUSSION**

These studies highlight changes in mitochondrial morphologies in fibroblasts from patients with defined isolated complex I deficiency and patient fibroblasts with novel mutation in FBXL4 and DNM2. Through these experiments it is clear that severe respiratory deficiency is capable of causing *en masse* fragmentation of the mitochondrial network. Interestingly in the case of the complex I patient lines not all morphologies were disrupted in the same way. Certain cases, notably the m.13514A>G MTND5 mutant and the m.11777C>A MTND4 mutants showed elongated mitochondrial networks. Unfortunately, this study did not have a large enough sample size to correlate these differences with any certainty to severity or mutation type although it's worth noting that both these elongated phenotypes occurred in mitochondrially encoded complex I mutants. Interestingly it was only the MTND4 mutant (with its elongated network) that displayed an increase in autophagosome number. Further cases will be needed to establish if this is a true association. For certain lines that displayed fragmented mitochondria, autophagosome volume was significantly increased. Again whether this is due to the mitochondrial network in some way is unclear from these experiments alone, modulation of the mitochondrial network through pharmacological modulation and parallel assessment of autophagosome structures may go some way to answering this. Furthermore, the cause of these morphological alterations needs to be elucidated.

Clearly these findings are somewhat contradictory with regards to the ES cells in which a reduction in autophagy markers was generally observed in line with complex I mutations that resulted in increased complexity of mitochondrial networks. What is interesting is that in both fibroblasts and the ES cells the existence of a mitochondrially encoded mutation can result in increased branching of the network and elongation. This was not the case for nuclear encoded CI mutations. A line of further investigation may therefore be to assess the impact of cell to cell variation as clearly mitochondrially encoded mutations may show heteroplasmic expression which is not the case for nuclear mutations. Whether this phenomenon is responsible for the differing mitochondrial morphologies observed in these experiments is unclear. One possible explanation is where complex I dysfunction is heteroplasmic and therefore some wildtype molecules exist, it remains beneficial to the cells to attempt to 'rescue' the phenotype through fusion, thus explaining the observed mitochondrial network changes.

It has previously been speculated that CI deficient cells and the conditions resulting from this deficiency may alter mitochondrial complexity by affecting the expression or recruitment of fission or fusion proteins (Koopman *et al.*, 2007). A recent paper looking at complex I inhibition by parkinsonian neurotoxins has shown that this disruption causes an oxidative-dependent disruption of OPA1 which, amongst other roles, is responsible for maintaining cristae integrity and maintaining tight mitochondrial cristae junctions. These results show how complex I dysfunction can directly impact mitochondrial form. Although the authors note these experiments were not accompanied by mitochondrial fission but a mobilization of cytochrome *c* from cristae to the intermembrane space, in turn lowering apoptotic thresholds in these neurons (Ramonet *et al.*, 2013). Increased levels of OPA1 and DRP1 were also proposed to reflect a compensatory mechanism to enhance recycling of less functional mitochondria. Guillery in 2008 showed long OPA1 isoforms in CI deficient fibroblasts (Guillery *et al.*, 2008). Elevated MFN2 levels were also observed in two of the three patients which may represent a further compensatory mechanism by increasing fusion and complementation. An extension of the study above may well be to assess such proteins in the patient cell lines.

Another possibility that may work independently to affect mitochondrial morphology or in concert with other factors is ROS. It has previously been shown that mitochondrially derived ROS are increased in fibroblasts from patients with complex I deficiency (Luo *et al.*, 1997) and this is accompanied by induction of superoxide dismutase (Pitkanen and Robinson, 1996). In line with this, the work by Koopman *et al* showed that in the Class I patient fibroblasts (those that showed severe reduction in CI activity and reduced form factor) ROS levels were significantly higher than class II or controls implying ROS is important for mitochondrial shape through ROS production and/or antioxidant capacity (Koopman *et al.*, 2007). Interestingly in the work by Guillery described above none of the three patients showed an increase in ROS levels (Guillery *et al.*, 2008). Reasons for this may be explained by decreased levels of fully assembled CI and as such reduced sites of ROS production or an increase in antioxidants, although only one patient showed altered levels of one antioxidant (mtSOD2).

Live cell observations of mitochondrial structure and dynamics in patients with defined complex I deficiency as well as cases with mtDNA deletion and depletion contain

higher proportions of swollen mitochondrial filaments (Pham *et al.*, 2004). Furthermore these larger swollen forms showed a reduction in motility activities such as displacement, extension and retraction. In line with this, loss of mitochondrial displacement activity was also observed in cells treated with respiratory inhibitors, which parallel results from fibroblasts derived from complex I deficient patients. A further study in 2010 looked at the impact of mutations in the NDUFA1 and NDUFV1 genes. The results showed a decrease in OCR and growth rates of cells alongside delayed mitochondrial network recovery following CCCP treatment (Moran *et al.*, 2010). Unlike previous studies greater CI severity did not cause fragmentation where as one of the three patients (with defined Leigh syndrome) showed increased mitochondrial content composed of long tubular mitochondria. Although different from Koopman's findings, this report is not unique, others have also reported filamentous mitochondria despite severe complex I deficiency (Guillery *et al.*, 2008) (Hanson *et al.*, 2002). The different genetic backgrounds between cases may explain these morphological differences. Alternatively, or possibly in conjunction, compensatory mechanisms or other OXPHOS complex genes may determine the expression of the primary deficiency. Also, synergistic interactions between mtDNA and nDNA may impact CI function (Potluri *et al.*, 2009).

It has previously been suggested that there is a precedent for mtDNA mutations as a possible heritable primary cause of PD. In 1998 it was shown that within a multigenerational Parkinson's disease family Complex I dysfunction has been inherited (Swerdlow *et al.*, 1998). Cybrids generated from mtDNA from maternal descendants with PD displayed lower complex I activity, increased reactive oxygen species production and more abnormal mitochondrial morphologies, including dense lysosomal bodies, and enlarged mitochondria containing fewer cristae. These reports show that complex I dysfunction may impart its deleterious effect through morphological changes and that this can independently cause PD. In the studies described in this chapter it is clear that complex I deficiency impacts heavily on mitochondrial morphology.

Interestingly the two non complex I mutant lines also showed dramatic alterations in morphologies. This is possibly not surprising with the DNM2 mutant given its association with microtubules and cell motility which are clearly important for maintenance of the mt-network. Mutations in the FBXL4 gene are novel pathogenic

mutations and as such the impact this has on morphology was completely unknown. Further dissection of the exact cellular role of this protein will be necessary to understand how morphology is being so dramatically altered, as revealed in these studies. The F box family of proteins are involved in a plethora of cellular functions, recent studies however have shown *fbxo7* and *parkin* interact and that this protein may have an extremely prominent role in mitophagy (Burchell *et al.*, 2013). It may well be of value to explore this cellular process with regards to the FBXL4 cell lines and how this links with morphology.

Chapter Eight

Human Tissue Studies

Chapter 8. Correlating complex I deficiency and autophagy in human post mortem tissue

8.1   INTRODUCTION

8.1.1   Overview

The cell models described in previous chapters have served to look at the impact of complex I dysfunction on autophagy and mitochondrial dynamics (chapter 4,5,6). Although the relative simplicity of the cell model allows for observation of perturbations and dissection of possible mechanisms leading to the observed phenotypes, it excludes many of the contributing factors that exist in whole organisms. For this reason, to compliment the cellular data, post mortem tissue offers a means to assess changes in relative levels of protein expression, in cells contained within their true environment. To relate findings to the human condition, human upper midbrain sections were used as this area contains the substantia nigra neurons, shown to suffer the most dramatic cell loss in Parkinson's disease.

The use of human tissue has several benefits for this study. Firstly it allows the assessment of changes seen in the cell models in the disease tissue we are proposing these effects occur. Information sourced from this model therefore has the ability to refute or compliment data gained previously on potential contributors in cellular demise, specifically in the context of Parkinson's disease. Secondly, this highly relevant model means that any concerns about the artificial environment the cell culture assessments are made within, and the possible affect this has on findings, can be removed.

8.1.2   Complex I, autophagy and Parkinson's disease

The evidence implicating the dysfunction of complex I and autophagy in Parkinson's disease is compelling and covered extensively in chapter 1.7. Changes in these two factors are implicated through familial PD cases and their associated gene mutations; animal and cell models. Looking specifically in post mortem tissue, studies have shown changes to levels of immunoreactivity and localization of mitochondrial markers or autophagy related proteins discussed below.

8.1.3 **Complex I alterations in tissue from PD patients**

Several pathological observations have been reported in Parkinson's disease with regards to complex I dysfunction. In the substantia nigra of PD patients, complex I activity has been shown to be decreased (Schapira, 1993). Increased levels of carbonyls, caused by the oxidation of amino acid residues on proteins, have also been demonstrated in several catalytic subunits of complex I in PD brains suggesting excessive oxidative damage of subunits resulting in misassembly and subsequent dysfunction (Keeney *et al.*, 2006a). High levels of somatic deletions in mitochondrial DNA have been seen within the substantia nigra neurons in aged individuals and PD patients (Bender *et al.*, 2006). Furthermore this can be directly linked to decreased respiratory activity when mtDNA deletions are correlated with cytochrome-*c*-oxidase (COX) activity, increased levels of mtDNA deletions corresponded with COX deficiency. As a number of complex I subunits are encoded by the mtDNA, these deletions will directly affect this complex. Alongside this deletions may cause disruption in protein translation through removal of tRNAs.

8.1.4 **Immunohistochemical observations of autophagy**

Focusing on autophagy and post mortem analysis a 1997 ultrastructural examination by Anglade *et al* in neurons of the substantia nigra in PD patients revealed characteristics of apoptosis and autophagic degeneration (Anglade *et al.*, 1997). They suggest that even at the final stage of the disease, the dopaminergic neurons are undergoing active process of cell death. Specifically, features of autophagic degeneration including, condensation of chromatin, vaculation of the endoplasmic reticulum and lysosome-like vesicles. Interestingly, Lewy Bodies were not found in neurons displaying these charateristics, rather in apparently 'normal' neurons. Immunohistochemical observations of changes in levels of autophagy have been carried out previously with regards to other neurodegenerative disorders (Ma *et al.*, 2010). For example a broad range of disorders, including MND (Arai *et al.*, 2003) (Nakano *et al.*, 2004), tauopathies and synucleinopathies (Kuusisto *et al.*, 2001); show ubiquitin and ubiquitin related proteins such as P62 aggregate in inclusions. This is important given that P62 may link the recognition of polyubiquitinated protein aggregates to the autophagy machinery (Bjorkoy *et al.*, 2006) and is widely accepted as an inverse marker of autophagy

function. Its accumulation therefore may suggest a reduction in autophagy within these tissues.

In formalin fixed paraffin embedded temporal lobe sections of AD cases immunoreactivity and localization of common autophagy related proteins were assessed. Fewer ATG12 positive neurons were observed in cases with longer disease duration. Furthermore this marker was spatially associated with amyloid beta positive plaques. These findings were similar for Beclin1, ATG5 and LC3. Together these results suggest an increase in autophagy activation in early stages of disease but that these diminish as the disease progresses (Ma *et al.*, 2010). In synucleinopathies, a close relationship between parkin and alpha synuclein has been shown. Immunohistochemistry shows parkin epitopes are present within LBs of sporadic PD, inherited PD and DLB. Furthermore parkin shows tight intermolecular association with alpha synuclein through Fluorescence resonance energy transfer (FRET) and immunoelectron microscopy (Schlossmacher *et al.*, 2002). As the main constituents of Lewy bodies, these findings could suggest alpha synuclein accumulation is in some way sequestering Parkin; this clearly impacts on other ubiquitin targets, notably mitochondrial outer membrane proteins and subsequently the process of mitophagy.

It is clear from just the small number of citations listed above that data exists to support alterations in complex I or autophagy levels in the context of PD. Importantly, autophagy and complex I function, have not, to the knowledge of this report been assessed in relationship to each other in the PD context. This project therefore has two unique components. Firstly, a range of autophagy markers are to be studied in parallel to assess various points of the autophagy pathway. Secondly all these markers will be analysed relevant to complex I levels. This allows several questions to be addressed, firstly if and where autophagy perturbations occur in PD tissue and if this is related to mitochondrial function.

8.1.5 **Aims**

This project aimed to assess the relative levels of complex I dysfunction and a range of autophagy markers in individual substantia nigra neurons of human upper midbrain sections. A dual immunohistochemical protocol was optimized to enable visualisation of two markers in the same cells. As chromagens were not sensitive enough for this assay, and fluorescence was utilised, a vital step was the development of effective autofluorescence quenching.

1. Optimize visualisation of two markers in parallel within highly auto fluorescent samples.

2. Quantify autophagy marker levels in PD vs. control tissue

3. Define complex I deficient neurons and assess the relationship between this parameter and autophagy markers.

4. Assess neuronal density in PD vs. control tissue and look for correlations with age, autophagy markers and complex I deficiency.

8.2   METHODS

8.2.1   Post mortem tissue

All human tissue for this study was obtained from the Newcastle Brain Tissue Resource (NBTR). Consent for the use of all tissue had been given by the appropriate local research ethics committee and conforms to the UK MRC Guidelines on the use of tissue in medical research. Serial transverse formalin-fixed, paraffin-embedded sections of upper midbrain tissue were cut at a thickness of 5µm from 5 pathologically confirmed PD cases and 5 aged controls with no pathological changes (Table 8.1). Patients ranged in age from 76-85 (mean 78yo) and included 4 males and 1 female. Control subjects ranged in age from 77 to 94 (mean 85yo) and included 4 females and 1 male.

Post Mortem Tissue (upper midbrain)	Characteristics				
	Block ID	Diagnosis	Age	Sex	PM delay
19920004	Block L	PD	85	Male	95
19960124	Block J	PD	77	Male	61
19970112	Block J	PD	76	Male	39
19980012	Block J	PD	76	Female	15
19990017	Block J	PD	76	Male	85
20100150	Block O	CA	77	Male	83
20100359	Block N	CA	94	Female	15
20100685	Block N	CA	88	Female	22
20110129	Block N	CA	89	Female	34
20110272	Block N	CA	78	Female	34

Table 8.1. Upper midbrain sections used for immunohistochemical study

Tissue for this study was obtained from 5 pathologically confirmed PD cases (average 78yo) and 5 aged controls (average 85yo).

8.2.2   Staining Protocol

In order to study two proteins in the same section, a dual immunohistochemical assay was performed, staining firstly for an autophagy marker of interest (detailed in 2.3.6) followed by C120 to assess mitochondria protein levels. The staining protocol can be seen in chapter 2 and briefly consisted of deparaffinisation, rehydration, and antigen retrieval to allow access to the antigen. High temperature EDTA antigen retrieval at pressure was used for all antibodies. Following a wash in distilled water the sections were washed in phosphate buffered saline pH 7.4 (PBS) before being blocked in 1%

normal goat serum (NGS). The blocking stage reduced background staining and nonspecific binding of proteins as all primary antibodies were produced in goat. All primary antibodies were incubated for 90 minutes and following a PBS wash, appropriate secondary FITC conjugated antibodies were applied at room temperature for 60mins. A further PBS wash was carried out over five minutes before application of the complex I antibody which was incubated overnight at 4°C. Complex 1 20kDa (C120, NDUFB8) is an accessory subunit of the mitochondrial membrane respiratory chain complex 1, an NADH-ubiqiuinol oxidoreductase responsible for the transfer of electrons from NADH to the respiratory chain. Previous studies have shown C120 as a reliable marker for complex I deficiency (Keeney *et al.*, 2006a). Complex I expression and mitochondria localization can therefore be estimated from the staining pattern of the C120 antibody.

The following day, after 3 PBS washes an appropriate TRITC conjugated secondary was applied for 60mins at room temperature. A PBS wash was carried out and sections were counterstained with 2ug/ml Hoechst for 30 mins. Washes were once again carried out. Due to the overwhelming autofluorescence of the tissue type (aggravated by paraffin fixation) it was necessary to address this to obtain quantifiable results. As such all sections included the addition of a final 10 minute incubation with 70% Sudan black ETOH solution, prior to fixation. Following a final series of PBS washes sections were mounted in ProLong® Gold antifade (life technologies) which was allowed to dry fully, sealed with nail varnish and stored at -20°C until imaging.

8.2.2.1 *Imaging and quantification*

Sections were allowed to warm to room temperature to limit condensation on the slides. All imaging was carried out on the Axiovison Axioimager (Zeiss). Each time the experiment was performed a no stain control was included. Using this it was possible to set the microscope's gain and offset to a point where no staining (and as such autofluorescence) could be seen. These settings were then saved for each wavelength and used to scan each section. By doing this, any staining observed was certain to be true signal. Each section was imaged to achieve a minimum of 15 neurons for analysis for each marker/case. This gave a total of 150 neurons/marker for PD and control cases. Regions of substantia nigra neurons were first located at x10 magnification on the

brightfield channel. Once a region of interest had been found x40 images were captured for all four channels (FITC, TRITC, DAPI and Brightfield). Quantification of intensity of markers was achieved through densitometry (Axiovision). Individual neurons containing neuromelanin were identified on brightfield channels and checked to contain a nucleus on the appropriate channel. Once confirmed, outlines were traced for these individual neurons and copy and pasted onto the remaining channels to ensure the area of neuron remained the same. The intensity of each marker (autophagy marker and C120) was recorded and data was analysed as described below.

8.2.2.2   *Statistical analysis*

Several parameters were to be assessed for this project, both singularly and in conjunction with other markers. For this reason the data had to be looked at objectively for each analysis. Importantly, despite over 150 data points being collected, each single neuron was not from an independent control/PD case as such this had to be considered during analysis. Levels of each marker in relation to C120 levels were assessed for each case and then tested for statistical significance between control and PD cases. To analyse marker levels for complex I deficient neurons, these were first defined. The lowest 10% of C120 staining was established for each ATG marker and the corresponding ATG marker levels were recorded. This methodology has previously been reported in Reeve 2012 *et al*. To analyse differences, data was collated into all non-deficient vs. deficient, PD deficient vs. non deficient and control deficient vs. non deficient. Significance was assessed through Student T or Mann Whitney tests depending on the distribution of data, and defined as $P>0.05$. Each marker was also presented as a scatter graph correlated against complex I levels with PD and control cases plotted on the same axis. Importantly, as the data was assessed through a general linear model, transformation of the data was often necessary. The form this transformation took was established through a box cox transformation and is displayed below in Table 8.2. Statistical significance for the difference in gradient and intercept between control and PD cases were recorded.

Antigen	Transformation
P62	-0.25
ATG5	-0.5
Parkin	√
LC3B	-0.5
LAMP2A	-0.75
Beclin1	-0.25

Table 8.2. Box cox transformations of data

Data was transformed to allow for analysis of significance through box cox.

8.2.3   Cresyl fast violet (CFV) stain

To establish the density of nigral neurons in PD patients and aged controls, two-dimensional neuronal cell counts were performed as described previously (Lax et al., 2012). For each case, two of the 5µm sections as described in Table 8.1 were stained with CFV to allow identification of the SN neuronal population. An outline of the SN was created at low magnification (2x), followed by a meander scan which was performed at a higher magnification (40x). This enabled a measurement of absolute cell number from the entire region of interest. Cells were only counted if they contained a defined nucleus, nucleolus and neuromelanin, this excluded neuromelanin accumulations commonly observed with age and/or non-dopaminergic neurons. Cell density was then calculated from the cell counts and substantia nigra area (mm^2) and averaged for the two sections.

8.2.3.1   *Statistical analysis*

Cell densities in Parkinson's disease and control tissue were compared for differences through Student t/ Mann Whitney tests, dependent on distribution of data. Further analysis of the data was carried out in relation to patient age. From these data, PD cases where cell densities were statistically lower than controls were extracted and compared against controls and a PD case where cell density was retained.

8.3   **RESULTS**

8.3.1   **Correlation of autophagy markers to levels of complex I expression in single neurons**

Dual immunohistochemistry was performed to detect immunoreactivity of C120 and specific autophagy markers in parallel, within individual substantia nigra neurons. Neurons were sampled from 5 PD cases and 5 aged controls. Each autophagy marker stain was repeated on different days to control for variability in experimental conditions. At least 15 neurons were assessed from each case for each marker. The graphs that follow show autophagy marker densities plotted against their corresponding C120 levels in individual SN neurons (figures 1-6). Figure 1 shows a typical staining pattern in C120 deficient and non-deficient cells. All autophagy marker levels were shown to be positively correlated to C120 levels. Thus , in cells displaying lower complex I levels, there was a reduction in all autophagy markers (P<0.001) as shown in Figure 8.1.
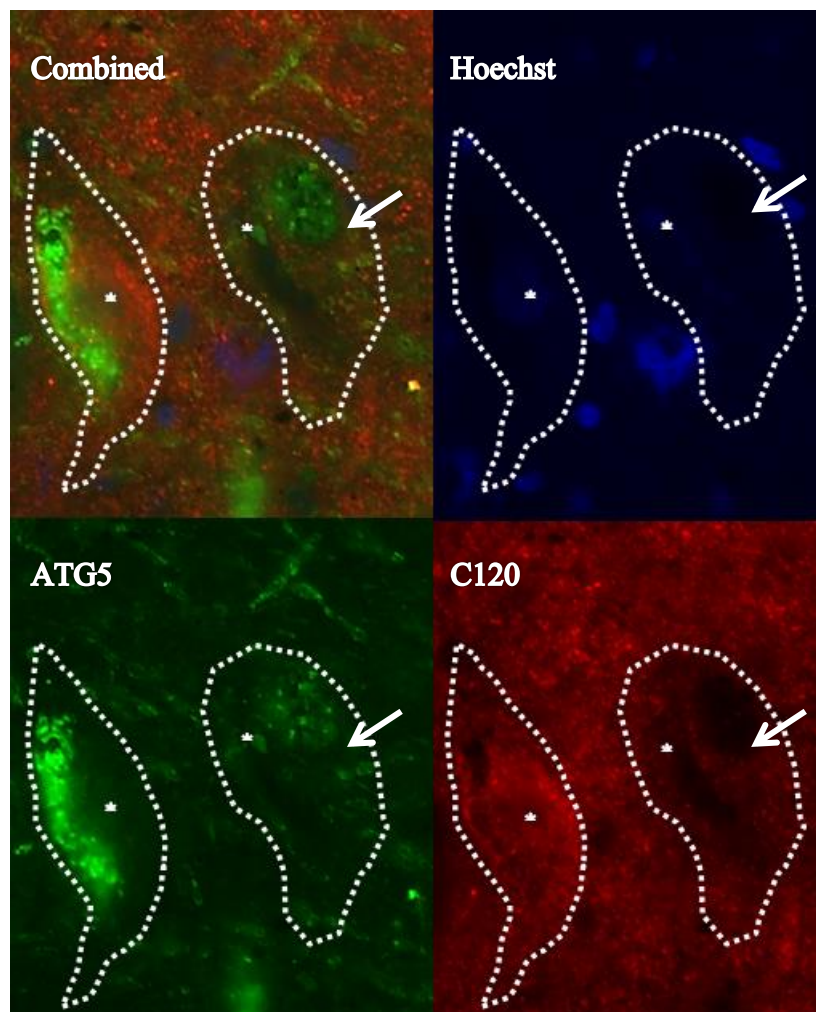
Figure 8.1. Reduced autophagy markers in C120 deficient cells.

All autophagy markers (in this case ATG5) showed reduced expression in C120 deficient cells (right hand cell shown with arrow). Small white stars denote the nuclei of the two cells.

248

P62 recognizes and tags cellular waste, which is then degraded through autophagy. These studies revealed no significant differences between the levels of P62 in neurons of PD patients and control tissue. However, when analysed against C120 levels, a strong correlation was observed (P<0.001), with lower C120 corresponding to decreased P62 levels (Figure 8.2). This is interesting in the context of previous work carried out within the Mitochondrial Research group as it would appear the accumulation of P62 to aggregates actually requires functional complex I. This has previously been shown with regards to Lewy body accumulation where Lewy Bodies are found in cells that have retained complex I function (Reeve *et al.*, 2012). Similarly, previous work by Anglade et al showed Lewy Body accumulation occurs in cells devoid of autophagic characteristics (Anglade *et al.*, 1997). Taken together these data suggest that maintained complex I function allows for Lewy body aggregation and the targeting of cellular waste through P62 in an environment where autophagy markers are not observed. This may be due to autophagy retaining its function within these cells and subsequently autophagic flux continuing at a rate that means markers are transient. Although P62 is often taken as an inverse marker of autophagy function, within these tissue studies it would appear that complex I dysfunction may add further complexity to the relationship. No significant differences were seen in the rate (gradient and intercept) between PD and control P62 accumulation (P=0.4939 and 0.0924 respectively).

All other autophagy related markers showed increases correlated to increases in C120 levels, further verifying that autophagy is decreased in complex I deficient cells (Figures 8.3-8.8). Again, no statistical significance was identified for rates of accumulation in relation to C120 levels between PD and control tissue for LC3 (gradient P=0.134, Y-Intercept P=0.7308), Parkin (gradient P=0.1403, Y-Intercept P=0.5314), ATG5 (gradient P=0.3083, Y-Intercept P=0.1199) or Beclin 1 (gradient P=0.7756, Y-Intercept P=0.4151). Interestingly a significantly different rate of LAMP2A accumulation between PD and control cases was observed (gradient P=0.0081) with greater LAMP2A immunoreactivity in SNc neurons of PD tissue with equivalent C120 levels to that of controls. Taken another way this result shows that there is statistically more LAMP2A in SNc within PD cases compared to controls. This agrees with previous ultrastructure observations where greater accumulation of lysosomes is observed in PD cases.

A

B
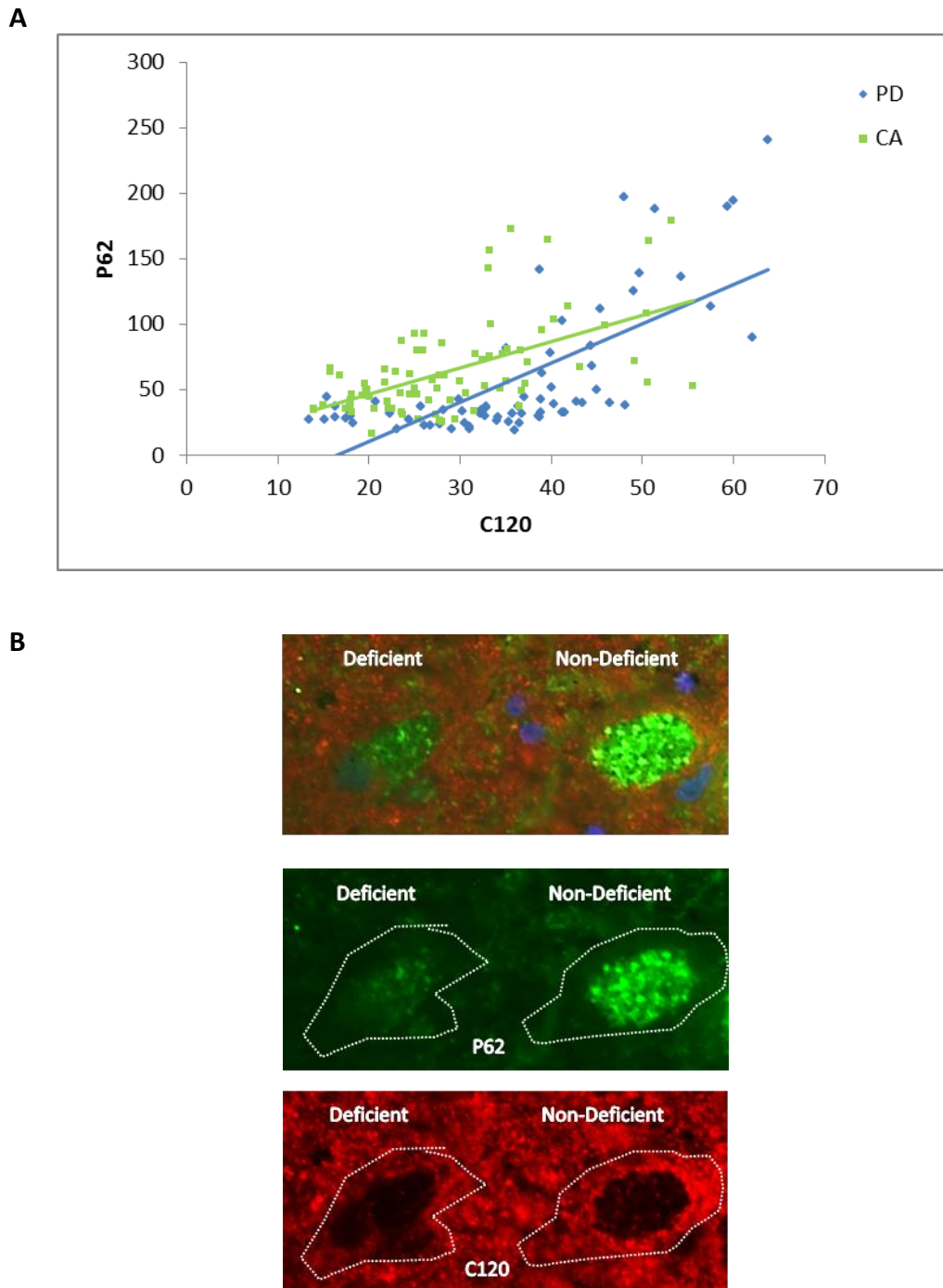
Figure 8.2. Relationship between P62 and C120 levels in PD and control tissue

A. Raw data of P62 and C120 densitometry levels in individual SN neurons (n=150). A strong positive relationship was observed between P62 and C120 accumulation in both PD and control(CA) tissue (P<0.001). The rate of P62 accumulation did not alter significantly between PD and control cases (gradient P=0.4939, Y-intercept P=0.0924).B. Example images of reduced P62 in C120 deficient neuron, Top panel shows combined P62 (green), C120 (red) and nuclear (blue) stains.

250
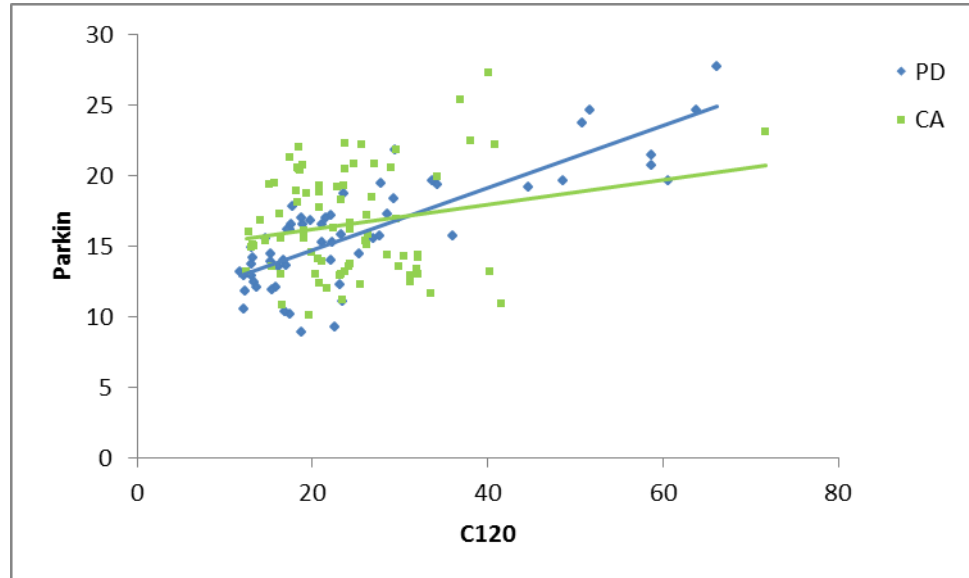
Figure 8.3. Relationship between Parkin and C120 levels in PD and control tissue

Raw data of parkin and C120 densitometry levels in individual SN neurons (n=150). A strong positive relationship was observed between parkin and C120 accumulation in both PD and control (CA) tissue (P<0.001). The rate of parkin accumulation did not alter significantly between PD and control cases (gradient P=0.1403, Y-intercept P=0.5314).
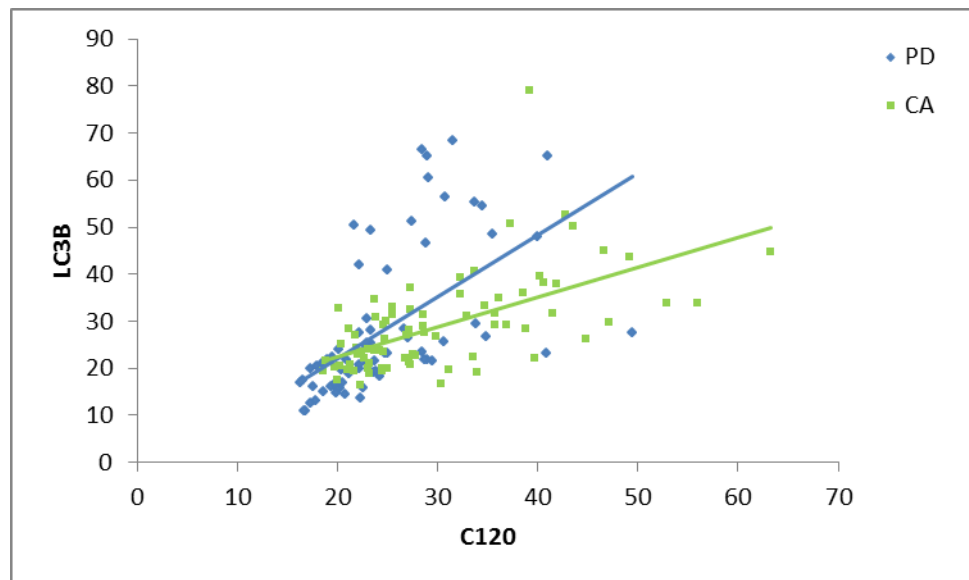
Figure 8.4. Relationship between LC3 and C120 levels in PD and control tissue

Raw data of LC3 and C120 densitometry levels in individual SN neurons (n=150). A strong positive relationship was observed between LC3 and C120 accumulation in both PD and control (CA) tissue (P<0.001). The rate of LC3 accumulation did not alter significantly between PD and control cases (gradient P=0.1364, Y-intercept P=0.7308).

251
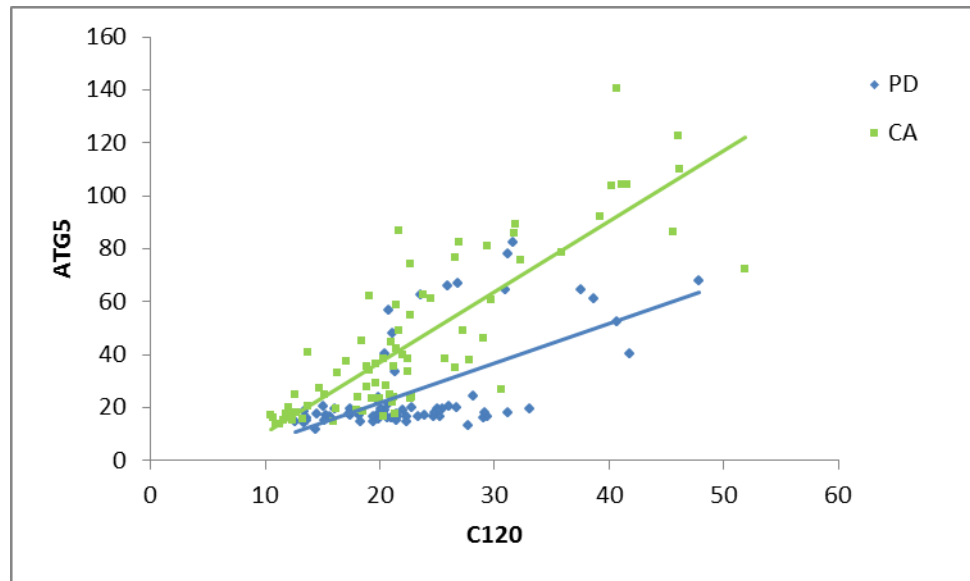
Figure 8.5. Relationship between ATG5 and C120 levels in PD and control tissue

Raw data of ATG5 and C120 densitometry levels in individual SN neurons (n=150). A strong positive relationship was observed between ATG5 and C120 accumulation in both PD and control (CA) tissue (P<0.001). The rate of ATG5 accumulation did not alter significantly between PD and control cases (gradient P=0.3083, Y-intercept P=0.1199).
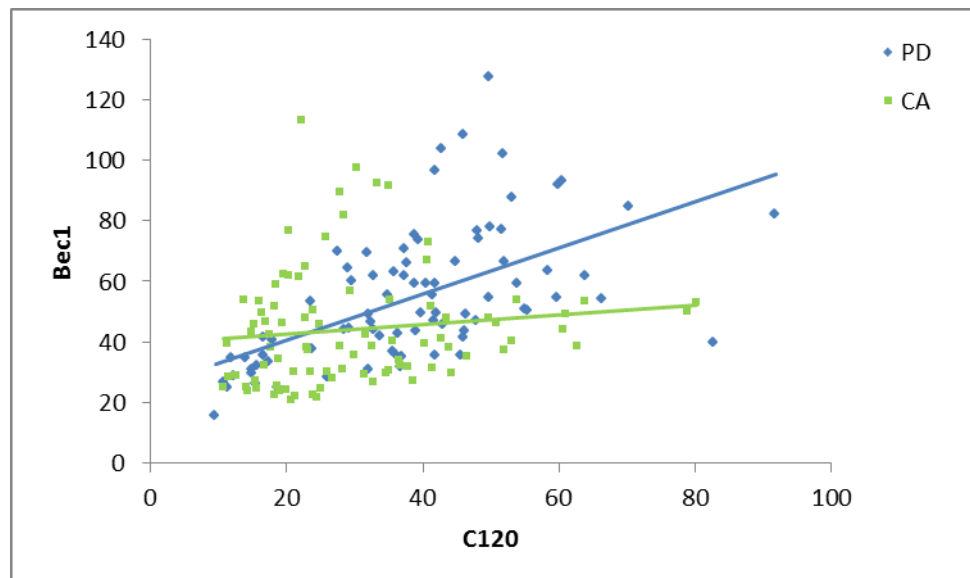
Figure 8.6. Relationship between Bec1 and C120 levels in PD and control tissue

Raw data of Bec1 and C120 densitometry levels in individual SN neurons (n=150). A strong positive relationship was observed between Bec1 and C120 accumulation in both PD and control (CA) tissue (P<0.001). The rate of Bec1 accumulation did not alter significantly between PD and control cases (gradient P=0.7756, Y-intercept P=0.4151).

Figure 8.7.Beclin 1 In C120 deficient cells

Middle image shows C120 deficient and non-deficient neurons in situ. The deficient neuron is enlarged to the left and the non-deficient is shown on the right. Nuclear (blue), C120 (red) and Beclin1 (green) staining is shown for both. C120 deficient neurons showed a reduction in Beclin 1 staining; this was not observed in C120 normal cells.
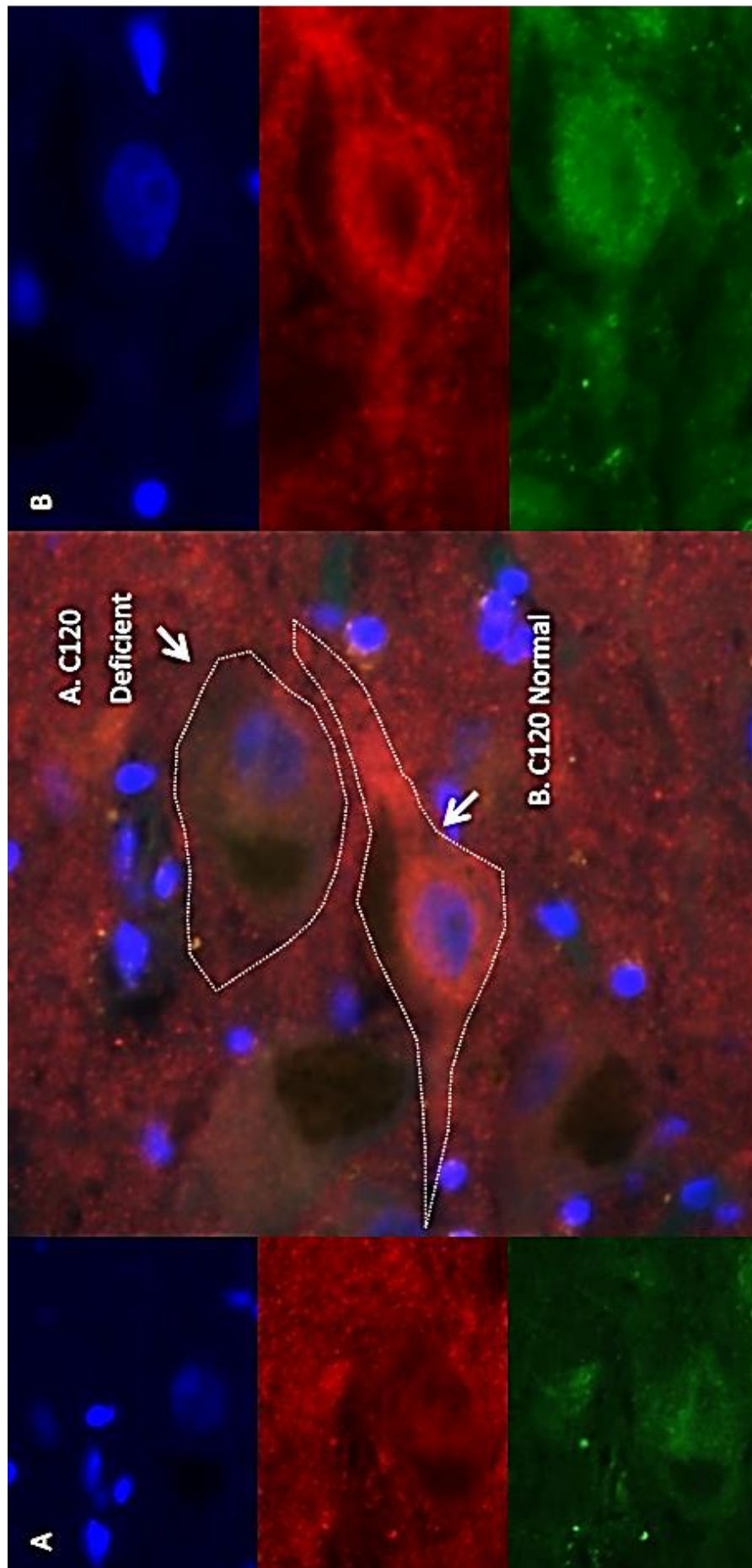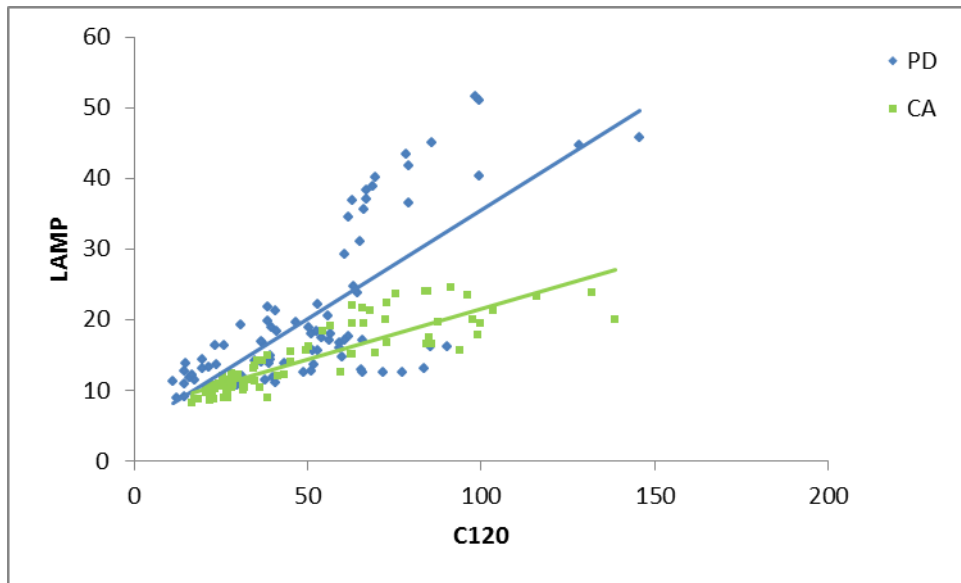
Figure 8.8. Relationship between LAMP2A and C120 levels in PD and control tissue

Raw data of Lamp and C120 densitometry levels in individual SN neurons (n=150). A strong positive relationship was observed between lamp and C120 accumulation in both PD and control tissue (P<0.001). The rate of Lamp accumulation was significantly different between PD and control cases (gradient P=0.0081), with greater LAMP2A at equivalent C120 levels in PD vs. controls.

8.3.2   **Autophagy markers in neurons defined as being complex I deficient**

The data presented previously showed a strong correlation between reduced complex I levels (C120) and reduced autophagy markers. To further analyze this complex I deficient cells were defined (deficient cells were defined as those falling into the lowest 10% of densitometry values for each marker).

C120 deficient cells for each autophagy marker were then grouped into combined (figure 8), control (figure 9), and PD (figure 10). Interestingly differences were seen for different groups in some of the markers (Table 8.3). P62 was found to not be significantly reduced in complex I deficient cells for combined data (P=0.532), controls only (P=0.1237) and PD only (P=0.2371). For combined control and PD cases (Figure 8.9) all other markers showed significant reduction in the complex I deficient cells, (Beclin 1, P<0.0001, LC3 P=0.001, Parkin P=0.0036, LAMP2A P<0.000 and ATG5 P<0.0001). Interestingly when these were divided into PD (Figure 8.11) and controls only (Figure 8.10), LC3, LAMP2A and ATG5 remained significant for both. For Beclin 1 differences between deficient and non-deficient cells was not significant in controls (P=0.1231) but was strongly significant in PD cells (P<0.0001). Similarly Parkin staining in deficient and non-deficient cells was not significant for control neurons (P=7.122) but significant within PD cells (P=0.0271).

Marker	P Values		
	Combined	Controls	PD
P62	0.0532	0.1237	0.2371
Beclin 1	<0.0001	0.1231	<0.0001
LC3	<0.0001	0.0115	0.008
Parkin	0.0036	0.7122	0.0271
LAMP2A	<0.0001	<0.0001	<0.0001
ATG5	<0.0001	<0.0001	<0.0001

Table 8.3. P values of correlation between autophagy markers and C120 levels.

All combined autophagy markers with the exception of P62 showed a strong correlation with C120 levels. When these were further divided into controls and PD tissue controls were no longer significant for Bec1 and Parkin.
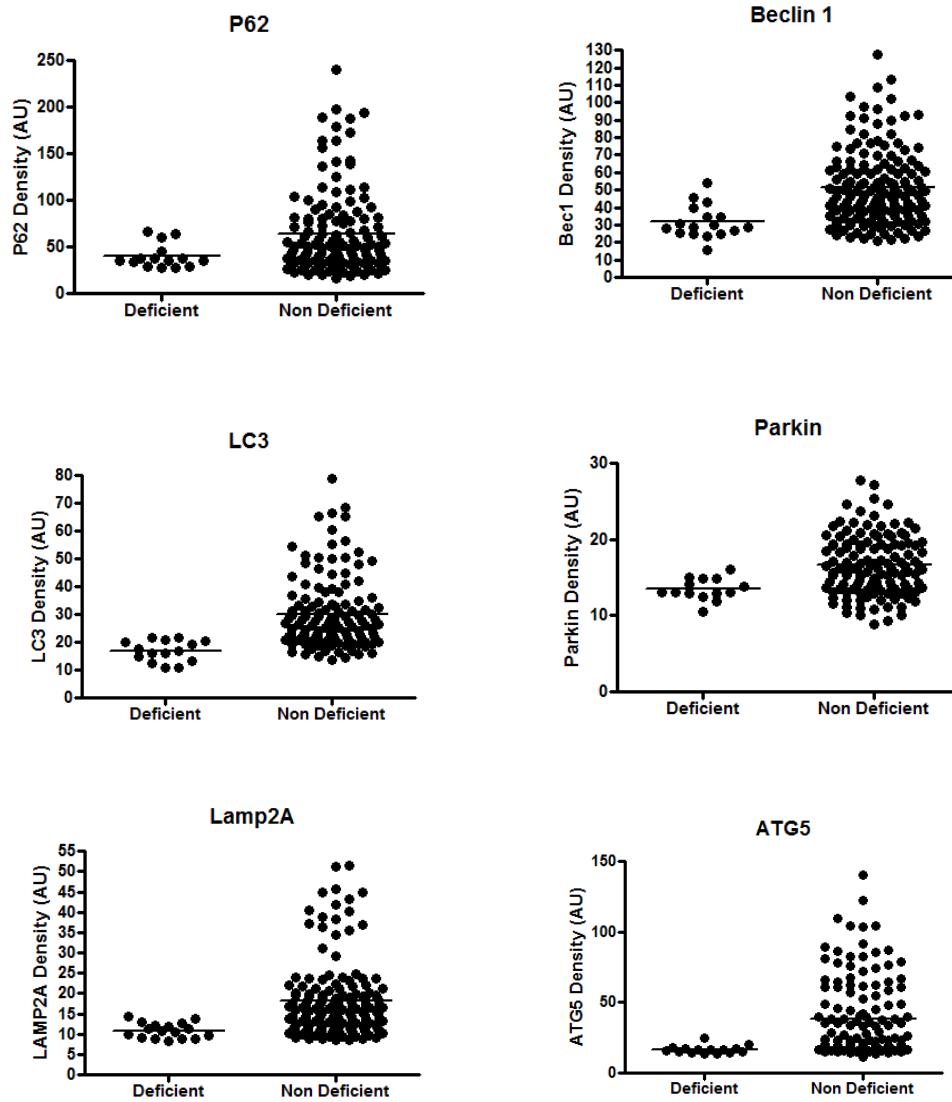
Figure 8.9. Autophagy markers in deficient and non-deficient C120 cells, combined.

All autophagy markers were significantly lower in C120 deficient cells, with the exception of P62 which still showed a strong trend.
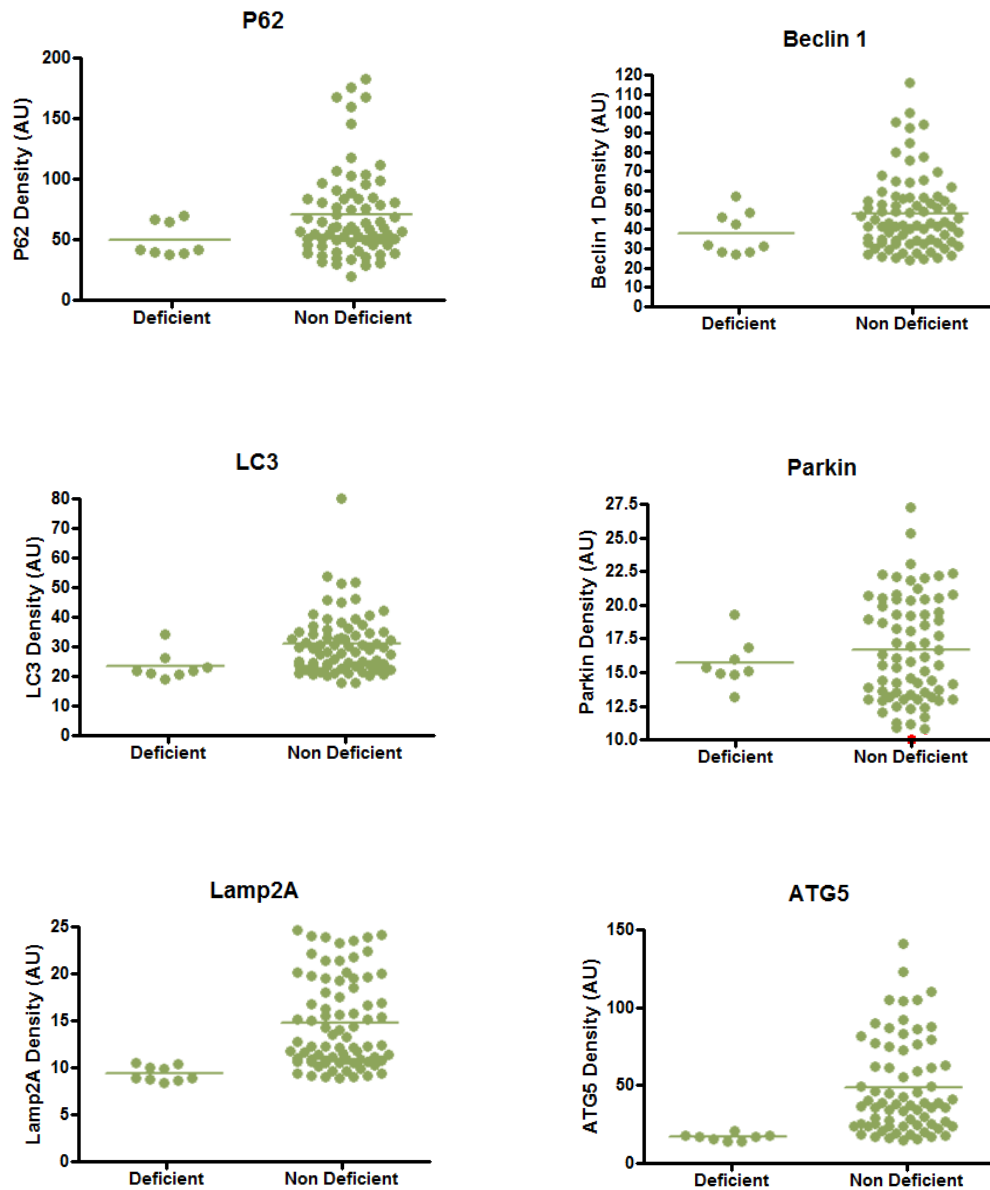
Figure 8.10. Autophagy markers in deficient and non-deficient C120 cells, controls.

LC3, LAMP2A and ATG5 were significantly lower in C120 deficient cells for control tissue. Lack of significance in other markers may represent too small n value in deficient cells category.
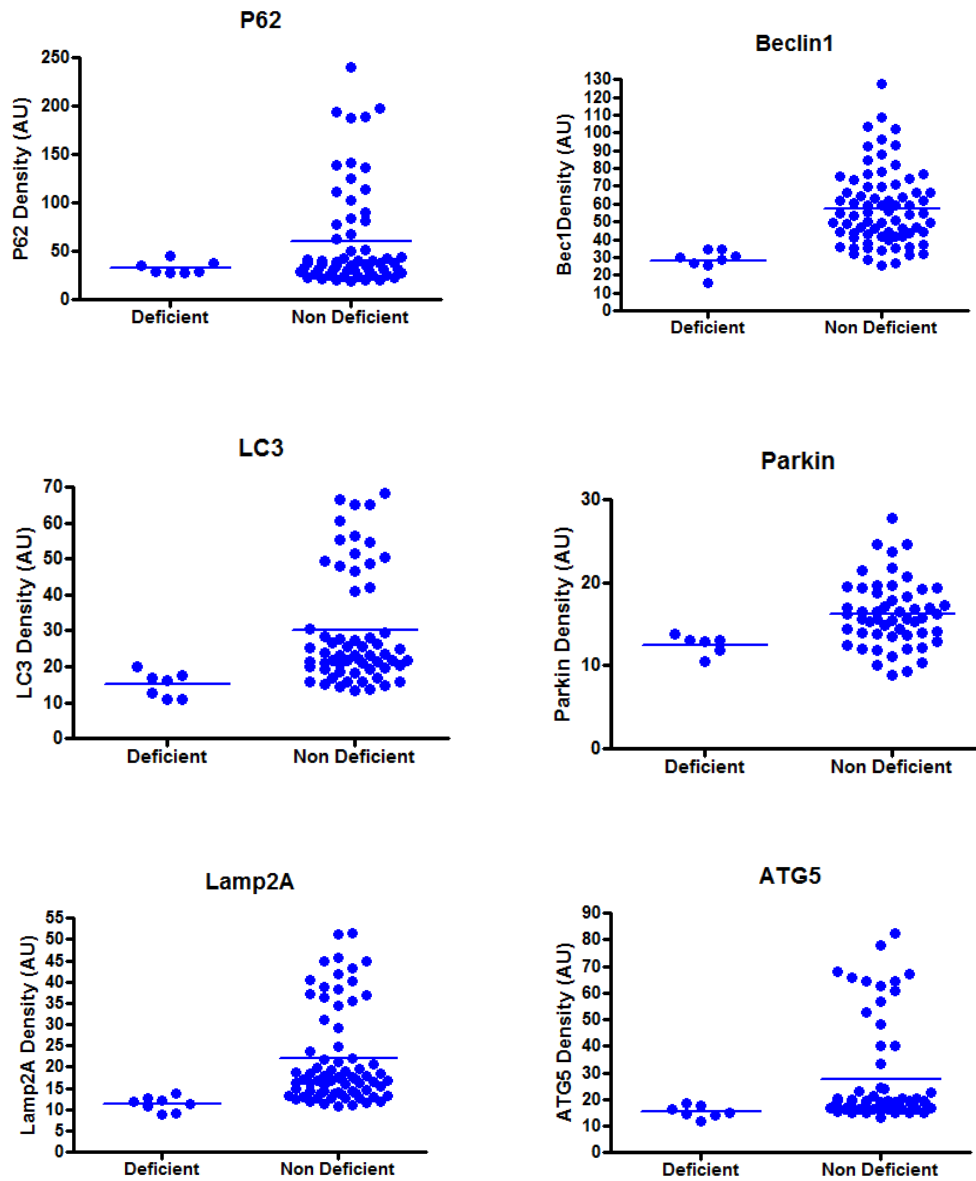
Figure 8.11. Autophagy markers in deficient and non-deficient C120 cells, PD tissue.

All autophagy markers were significantly lower in C120 deficient cells, with the exception of P62 which still showed a strong trend.

8.3.3 **Neuronal counts**

To demonstrate cell density was altered in the PD cases compared to age matched controls, and to what extent this may be impacting on the immunohistochemistry results, CFV staining was undertaken to gauge substantia nigra neuronal densities/mm^2 in each of the sections. The results of this can be seen below in Table 8.4. These neuronal density measurements were then plotted against age to see if any correlation existed in our data set (Figure 8.12). As expected the control cases displayed mild neuronal density reduction in association with increasing age. The PD cases showed far greater neuronal loss with the exception of one case- 04/92, who interestingly also lived far longer than other PD cases. With this in mind overall neuronal densities were compared for all PD cases vs. combined controls. Although a trend was observed (Figure 8.12.b) this difference was not significant (P=0.1508) until the outlier, case 04/92, was removed (Figure 8.12.C) revealing a significantly reduced overall SNc density in the remaining PD cases vs. controls (P=0.0159).

Case	Area (mm^2)	Cell count	Density	Mean
17/99	13.9	81	5.8273	5.2298
	13.6	63	4.6324	
129/11	19	154	8.1053	8.9832
	14.4	142	9.8611	
112/97	10.7	60	5.6075	5.3717
	9.93	51	5.1360	
150/10	23.4	338	14.4444	12.3955
	20.2	209	10.3465	
04/92	12.8	156	12.1875	13.1893
	13.6	193	14.1912	
685/10	19.8	219	11.0606	10.2124
	17.3	162	9.3642	
447/11	19.6	158	8.0612	9.2953
	17	179	10.5294	
12/98	16.5	87	5.2727	5.6070
	17	101	5.9412	
24/96	12.2	38	3.1148	2.6306
	7.92	17	2.1465	
272/11	26.7	238	8.9139	11.7589
	20.2	295	14.6040	

(Cresyl Violet Staining)

Table 8.4. Substantia Nigra Cell densities

Area, cell counts and densities for all tissue cases, listed in order of blinded counts. Grey bars highlight PD cases.
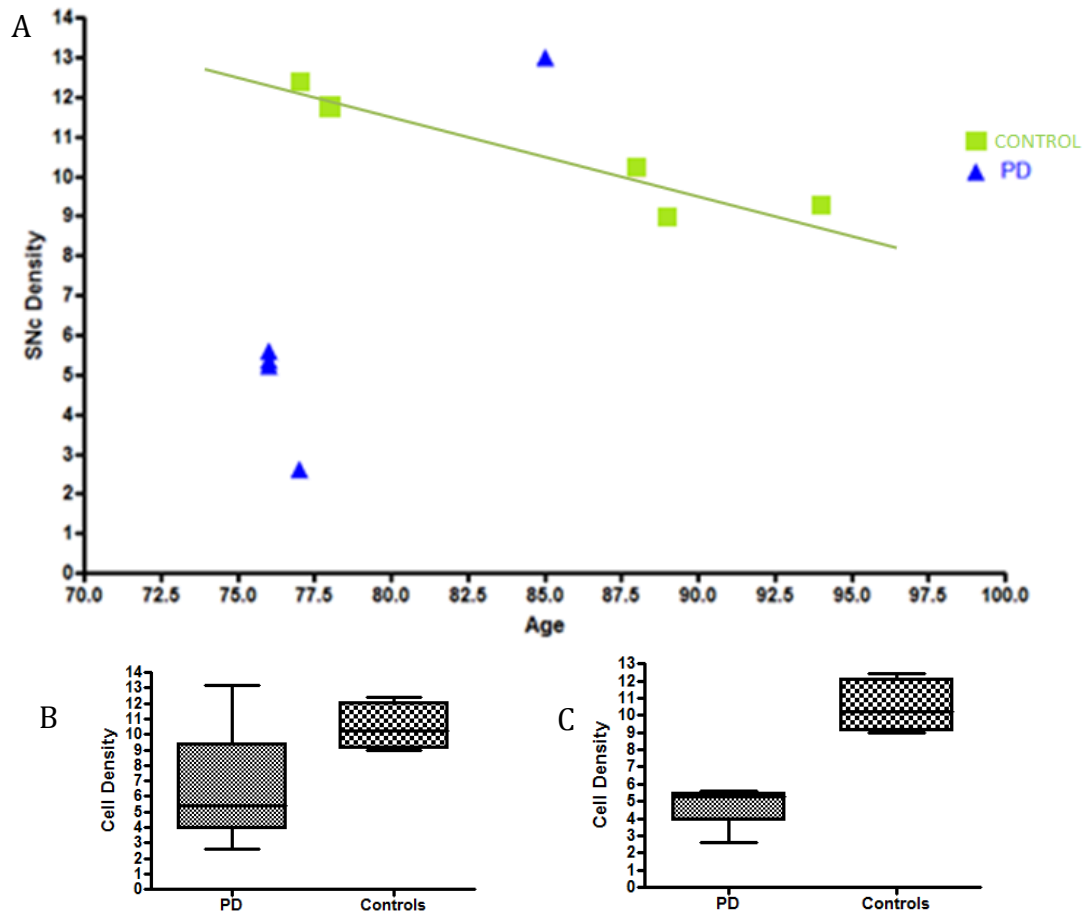
Figure 8.12. SNc Densities

A. SNc densities in relation to age for control (green) and PD cases (blue). B. Cell densities for PD and control tissue- raw data (P=0.1508) C. Cell densities for PD and control tissue- outlier removed (P=0.0159)

8.3.4 Autophagy marker evaluation following the subtraction the outlying PD case in terms of cell density

Following on from cell density studies it was deemed appropriate to further investigate the autophagy markers within the one PD case that retained its cell density. For this purpose all control cases were grouped together and compared to the outlier and remaining grouped PD cases. The results for each marker can be seen below in Figure 8.13. As shown previously, cell density was increased in controls vs. PD cases with the exception of case 04/92 which remained within the control range of densities. Interestingly, autophagy markers in this case were elevated above all other PD cases and either fell within the control range of values (such as the case for Beclin 1, Parkin and ATG5) or exceeded control values, (P62, LC3 and LAMP2A). These results would imply that retained autophagy function in this case may be aiding cell survival.
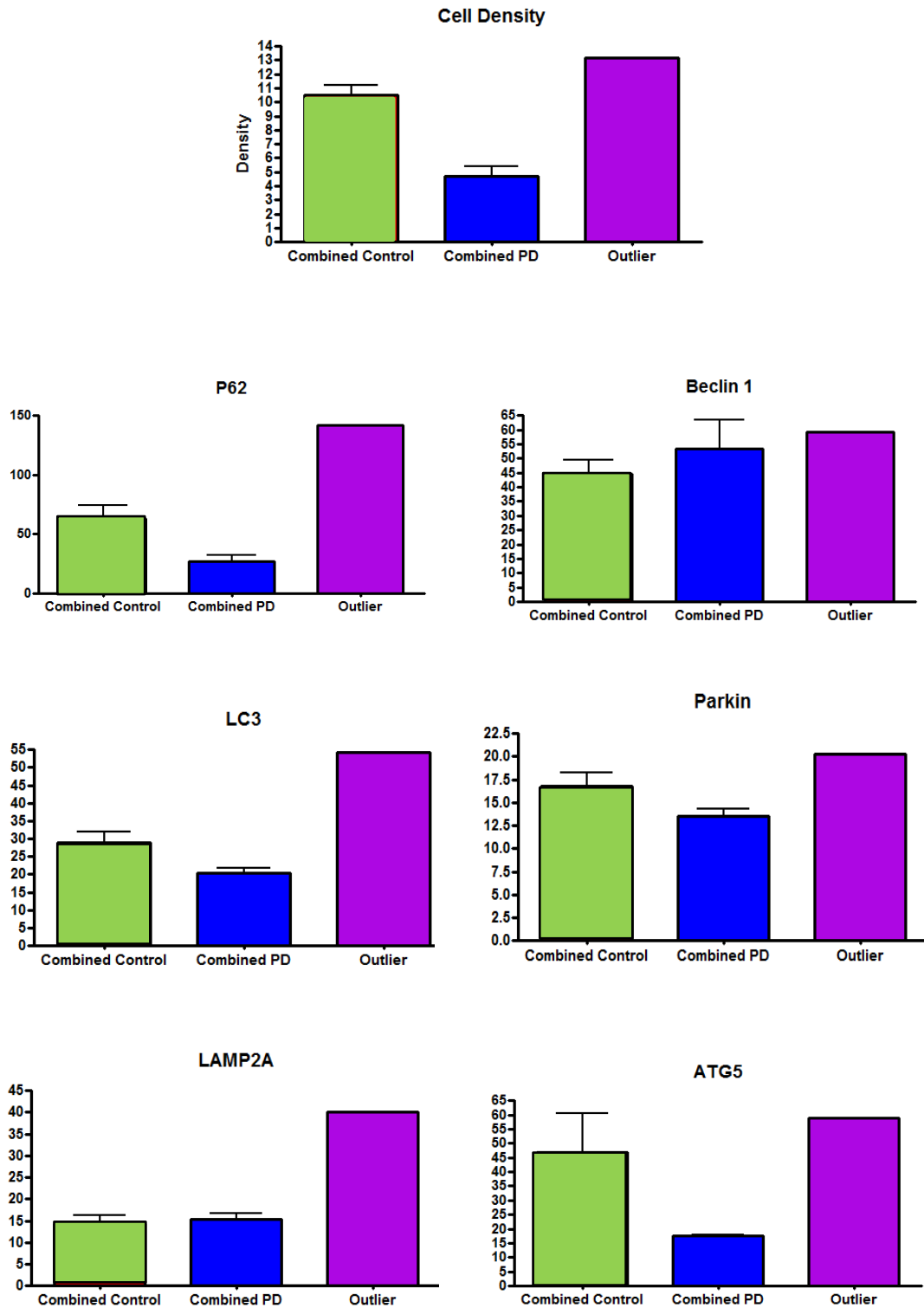
Figure 8.13. Cell densities and autophagy levels in combined controls, PD tissue and single PD outlier

The cell density of one PD case remained significantly higher than all other PD patients. For this reason time was spent analysing the autophagy markers for this case compared to remaining PD cases and controls. Within this case P62, LC3 and Lamp2A were significantly elevated above control and PD. Beclin1, Parkin and ATG5 were significantly higher than PD cases but fell within the range of control values.

261

8.3.4.1   *Impact on autophagy marker and C120 relationship*

Due to the resounding effect the individual case was having on the data, the decision was made to remove this outlier and reanalyze the data. Several marked differences were observed. Firstly box cox transformation revealed different data transformations were required prior to statistical analysis as shown in Table 8.5.

Antigen	Transformation
P62	-0.25
ATG5	-0.75
Parkin	λ
LC3B	-0.25
LAMP2A	λ
Beclin1	-0.25

Table 8.5. Box cox transformations following removal of outlier.

Following removal of case 04/92 the data was once again analysed for differences between gradients of autophagy markers between controls and the remaining PD cases. Interestingly, the accumulation of P62, Parkin and ATG5 now showed significant differences with all three displaying lower levels of immunoreactivity overall in PD cases. LAMP2A was no longer significant between the two groups suggesting the high levels of this antigen in case 04/92 were causing a skew of the trend.

Marker	P Values		-Outlier	
	Gradient	Intercept	Gradient	Intercept
P62	0.4939	0.0924	0.0009	NA
Beclin 1	0.7756	0.4151	0.6345	0.5418
LC3	0.1364	0.7308	0.1246	0.0827
Parkin	0.1403	0.5314	0.0032	NA
LAMP2A	0.0081	NA	0.1771	0.2418
ATG5	0.3083	0.1199	0.9740	0.0169

Table 8.6. P values for gradient and intercept of PD vs. control cases before and after removal of outlier

8.4   DISCUSSION

8.4.1   Summary of findings

This body of work set out to measure the expression of key autophagy related proteins in individual nigral neurons in PD patients, and correlate these to C120 levels. Most significantly and unique to this study I have shown autophagy markers are directly related to C120 expression. Specifically, a range of autophagy markers show expression levels that directly correlate to C120 expression levels i.e. low levels of C120 also display low levels of any one of the six tested autophagy markers. This is significant as upon first assessment one would expect complex I deficient cells (deemed mitochondrial deficient cells), to have their mitochondrial populations targeted for mitophagy and subsequently an increase in these markers. Clearly however,the relationship is more complex than this with C120 cells containing lower autophagy markers. This may imply that mitochondrial function is actually required for autophagic function.

These findings compliment observations in the cell models described in previous chapters. In complex I deficient cultured cells a marked reduction in LC3, Beclin 1 and ATG 5 were observed in undifferentiated stem cells. In neuronal cultures derived from these cells, differences in localization of these markers was also observed. Conversely, P62 data from the cell model showed a dramatic accumulation in the complex I deficient cells, this was not the case in these tissue studies. The rate of P62 accumulation correlated with increases in C120 levels, several experimental differences could explain this finding and other differences between tissue and cell data. Firstly, tissue observations were not performed at a level where processes could be analysed, as such data generated came largely from cell bodies excluding the possible accumulations at synapses. Previous tissue studies have shown that complex I function is required for LB accumulation (Reeve *et al.*, 2012) and LB pathology is often seen in cells devoid of autophagy markers (Anglade *et al.*, 1997). This may be relevant with relation to my P62 data, a marker which aggregates to cellular waste, the lower levels of P62 in CI deficient cells in tissue may suggest CI function is required for its accumulation as would appear is the case for the accumulation of alpha synuclein. Why this isn't observed in my cell culture studies through immunoblot may be due to the localization

of the protein, with overall levels increased but not in aggregations that would be picked up by IHC.

Interestingly when I defined cells that were deficient for autophagy markers I established some notable correlations. Firstly when all cells (PD and control) were combined with respect to deficient and non-deficient CI cells, all markers, with the exception of P62, were significantly reduced in deficient cells. The reason for no significant alterations in P62 levels may be due to a necessity for retained complex I function to mobilize P62 partnered with an accumulation of aggregates, balancing out over/under expression. When these two specifics were further divided in PD vs. control cases. P62, Beclin1 and Parkin levels in deficient cells were no longer significant in controls but retained significance in PD cases, implying that complex I deficiency and its associated autophagy reduction may be more marked in this condition.

The experiments detailed above show that in postmortem tissue samples, individual substantia nigra neurons show variable patterns of C120 and autophagy marker staining. This is reflective of the variation within a population and further highlights multiple contributing factors in the development of PD. It is important to consider that the underlying cause of these idiopathic PD cases is not known and therefore variation in the results is to be expected as it will likely stem from different initial pathogenic factors. This said markers generally fell within a control or PD range and certain noticeable differences were observed. Cell density in the PD cases was significantly reduced compared to controls. This was also shown to be correlated to age. Importantly, this experiment highlighted one PD case which was extremely different from other PD cases, with high remaining cell density that was at the upper levels of control data. When we further analysed this section with regards to C120 and autophagy marker levels, it was found that this case that retained high cell density had high levels of C120 and autophagy markers in their surviving neurons. This implies that cell density is correlated to retained complex I function and higher autophagy levels. There were few significant differences observed in this study between control and PD cases for C120 levels and autophagy markers, this may reflect the relatively small number of cases used, but it is also important to note that considerable variation between PD cases and within control cases was seen, meaning we possibly wouldn't expect to see significant differences between these two groups, which in themselves are quite diverse.

8.4.2   **Evidence for altered autophagy in PD tissue**

This study did not show dramatic changes in autophagy markers in PD vs control tissue. What was shown was that autophagy markers are lower in cells with complex I deficiency. Previous studies, however, have highlighted changes in levels of autophagy in neurodegenerative diseases; different experimental approaches are likely behind these differences. From earlier electron microscopy assessments showing characteristics of autophagic degeneration in PD patients SN neurons to specific autophagy gene ablation and expression studies revealing altered levels of key proteins correspond to altered disease phenotypes. Mice deficient for just one of the autophagy related proteins develop neurodegeneration. Deficiency in ATG7 or PD associated PARK9 cause PD like neurodegeneration *in vitro* and *vivo* (Decressac *et al.*, 2013). The reasons for changes in this crucial process are not fully clear but various reasons may offer explanation. Many etiological factors associated with PD reduce autophagic activity. Importantly, it is worth noting that a reduction in autophagy activity may not initially reveal itself through reduced levels of autophagy markers. Indeed increased LC3 staining and lysosomal accumulations are observed commonly in PD, it is therefore likely that autophagic flux is compromised in this disease.

Alpha synuclein, proposed to have a role in synaptic plasticity and the main component of intracellular inclusions in PD has been shown to induce cell toxicity at high levels. It has also been shown that alpha synuclein may interfere with autophagy mechanisms and that it can be degraded by lysosomes (Meredith *et al.*, 2002). Normal degradation of wildtype alpha synuclein occurs via chaperone mediated autophagy (CMA). Mutant forms of the protein have been shown to bind LAMP2 with higher affinity than its wildtype counterpart causing a blockage of their own and other substrates degradation by this method (Cuervo *et al.*, 2004). Work by Spencer *et al* showed that over expression of alpha synuclein in both neuronal cultures and transgenic mice led to dysfunctional autophagy and subsequent neurodegeneration. The consequence of this is a disruption in transportation to the lysosomal lumen and consequently a block in chaperone mediated autophagy. Interestingly, this could be reversed by Beclin1 (Spencer *et al.*, 2009a).

The role of alpha synuclein may extend beyond that of CMA effects, as the clearance of the protein has been shown to be mediated by macro as well as chaperone mediated autophagy (Webb *et al.*, 2003). Evidence shows mTOR was more abundant in neurons displaying alpha synuclein accumulation in DLB brains and ultra-structural analysis went on to show abnormal and increased autophagosomes. In PC12 cells (derived from a pheochromocytoma of the rat adrenal medulla) transfected with mutant alpha synuclein, treated with wortmannin an autophagy inhibitor an increase in synuclein accumulation and cell death is observed (Liu *et al.*, 2013). PD like neurodegenerative changes are also associated with excess cellular levels of alpha synuclein alongside a decline in markers of lysosomal function and retention of Transcription factor EB (TFEB) a major transcriptional regulator of autophagy lysosomal pathway. Furthermore in a rat model and human PD midbrain these changes could be reversed by TFEB overexpression (Decressac *et al.*, 2013).

Further evidence showing a role for autophagy in PD development stem from the effect certain neurotoxins, shown to invoke PD like symptoms in models of the disease, have upon the process. When animals are exposed to MPTP autophagic dysfunction is observed, associated with alterations in signal transduction pathways (Zhu *et al.*, 2007). In an MPTP mouse model of Parkinson's disease treatment with rapamycin (an autophagy stimulating antibiotic) is shown to protect against dopaminergic loss and ameliorate the loss of the dopamine metabolite DOPAC (Liu *et al.*, 2013).

Finally, lysosome dysfunction may play a key role in Parkinson's development as indicated by a susceptibility to alpha synuclein aggregation and parkinsonism in some lysosomal storage disorders (Raja *et al.*, 2007). In humans links between lysosomal storage disorders and polymorphisms in LAMP2A and PD have been drawn (Mazzulli *et al.*, 2011) (Pang *et al.*, 2012; Winder-Rhodes *et al.*, 2012). Changes in the autophagy pathway have previously been linked to advancing age. In animal models for example rat kidneys, levels of ATG7 and LC3 are down regulated. Conversely the levels of p62 and poly ubiquitin aggregates increases. Associated with swelling and disintegration of mitochondrial cristae.

8.4.3   **Autophagy is compromised in complex I deficient cells**

In this study I have shown a strong correlation between complex I deficiency and a reduction in several autophagy markers. This is interesting for several reasons. Firstly it goes against the idea that dysfunctional mitochondria are always isolated and selected for removal through autophagy. In neurodegenerative disorders, the loss of specific neuronal populations is more rapid than that seen in 'healthy' ageing. In line with this, studies of the density of SN neurons in this study showed a significant reduction in PD cases compared to aged controls. Interestingly within the PD cases one outlier that retained a high neuronal density was over a decade older at time of death than other patients. This is interesting as it implies that certain individuals with confirmed PD fair better in terms of cell loss and disease progression.

8.4.4   **Implications**

Autophagy is not simply important as a waste disposal mechanism, but rather a recycling centre which enables the cell to resupply depleted nutrients in times of starvation and to remove damaged protein and organelles. Any dysfunction therefore impacts in numerous ways, through accumulation of dysfunction, damage and reduction in the pool of available macromolecules. Other less well reported impacts may also be important. Previous work has shown key autophagy proteins to be localized to mitochondria and conversely several mitochondrial proteins have been shown to positively regulate autophagy. mTOR, the main regulator of autophagy has also been shown to respond to a number of cellular processes relating to mitochondria for example ROS and ATP levels.

The processes which initiate autophagy have begun to be elucidated from a recent increase in research into this area, although proteomic studies have still failed to show a clear signature for the autophagosomal membrane origin (Overbye *et al.*, 2007). Recent work explored the role of mitochondria in formation of the autophagosomal membrane in times of starvation (Hailey *et al.*, 2010). The work demonstrated that the outer membrane of mitochondria participates in autophagosomal biogenesis. The autophagy marker Atg5 was found to localize to puncta on the outer mitochondrial membrane which co-localised with LC3. Furthermore photo bleaching revealed that membranes of

mitochondria and autophagosomes are transiently shared. Although previous studies have interpreted this membrane sharing as mitophagy Hailey and colleagues demonstrated a diffusion barrier actually prevents delivery of mitochondrial proteins but NOT lipids. Suggesting this is not mitophagy but mitochondria contributing membranes to autophagosomes (Hailey *et al.*). Taken alongside the results of this study it could be that the decrease in mitochondrial proteins and subsequent mitochondrial dysfunction means these organelles are no longer able to contribute to the autophagosomal membrane thus explaining the observed decrease in markers of autophagy and why these damaged mitochondria are not degraded.

The true importance of autophagy may extend beyond its ability to recycle damaged cellular components but also serve as a means of transportation of mitochondria-derived factors and lipids. Autophagy has been identified as allowing the movement of lipids between disconnected cellular components. In contributing to the membrane healthy mitochondria may also play a role in lipid homeostasis. The dysfunctional autophagy seen in this study may also result in stunted transport of mitochondria derived factors and the transport of lipids, which may also contribute to cellular downfall.

8.4.5   Future work

This work will continue to assess further correlations of staining patterns and tissue characteristics utilizing more cases. Exploration of the marker levels in relation to Lewy body pathology would assist in understanding which neurons survive and how this relates to autophagy changes. This could be achieved through defining a level of immunoreactivity for each marker as a threshold and grading Lewy body pathology in neurons above and below this level. Furthermore it would be interesting to look at information about disease progression and see how this correlates with staining patterns. Analyzing length of disease and distributions of complex I and autophagy alterations may reveal a timeline of changes in the pathology of PD.

Further scrutiny of the images gathered for this work could also be valuable, for example looking at the distribution and localization of markers, possibly colocalizaiton

of autophagy markers and mitochondrial stains, for example Parkin and C120 may provide information on how specifically, mitophagy is altered in PD.

Chapter Nine

Final Discussion

Chapter 9. Final Discussion

9.1   INTRODUCTION

Parkinson's disease is the most common neurodegenerative disorder. Despite advances in understanding of the pathophysiology that leads to many of the debilitating symptoms associated with this disorder, the exact mechanism behind how and when cell loss begins to occur above that of 'normal' ageing is unclear. Mitochondrial dysfunction, notably through complex I of the respiratory chain have been strongly linked to the disorder. Evidence from familial studies further links the organelles as well as highlighting the process of mitophagy as contributing to the disease. Increasingly, research is focusing on how these processes may act alone or in concert with other factors (environment, toxic shock, genetics etc) to bring about *en masse* cellular demise. Mitochondria are irrevocably linked to autophagy through the process of mitophagy, the provision of energy and through their dynamics. The synergistic impact of complex I dysfunction and alterations to the autophagy pathway have not been investigated. The data contained in this thesis aimed to study how complex I dysfunction interacts with the process of autophagy and establish possible mechanisms for this to occur.

9.2   OVERVIEW OF FINDINGS

Through parallel studies in complex I deficient cybrid cell lines and human upper midbrain sections, this study has shown complex I deficiency is indeed associated with gross alterations to the autophagy pathway. Several findings in these two models supported one another. In individual substantia nigra neurons of the upper midbrain sections we found a direct relationship between complex I expression and autophagy markers, implying in complex I deficiency we also see a reduction of autophagy. This was also true in the ES cybrid cell lines where the complex I mutants routinely displayed far lower levels of autophagy markers through immunocytochemistry and immunoblotting. Interestingly, when differentiated into neurons levels of autophagy markers in complex I cells were altered (but not always lowered) but more striking was the impact on localization of several autophagy markers. Why we did not observe a lowered expression of these markers as seen in the tissue samples could be down to

numerous explanations. Firstly the severity of the complex I deficiency may be different within the two models, this study alone has discussed how increasing severity does not always invoke a simple linear response. For example complex I deficiency in patient fibroblasts is known in some cases to cause elongation of the mt-network followed by fragmentation. Secondly, the cells used in this study were differentiated into a mixed neuronal lineage and as such, large proportions of the observations would not have been within dopaminergic neurons. Finally, consideration must be given to the impact of the cellular milieu and also the accumulation of age related changes within the tissue which are likely to impact on results through accumulation of age related pigments such as neuromelanin and lipofusicin alongside the cross talk between numerous scaffold and assistant cell types. A marker that showed particularly interesting results in this study was P62. Immunoblot of complex I deficient cybrid cell lines showed a clear repeatable increase of P62 in complex I deficient cells. This can be explained through the accumulation of cellular aggregates tagged with this protein in these energetically compromised cell lines. Interestingly, the reverse was observed in the complex I deficient cells defined within the human upper midbrain sections. As with other markers within this experimental method, a decrease of P62 was observed in those cells with complex I deficiency. This is interesting in the context of previous work within the group where mitochondrial function is required for the accumulation of alpha synuclein into Lewy Bodies. These results may show that mitochondrial function is also required for P62 tagging and accumulation to protein aggregates. Alternatively, mitochondrial function may solely be required for Lewy body formation and the increase in P62 is a side effect of greater protein inclusions within which it is sequestered. The latter may be more tempting considering in the cell model, complex I dysfunction alone is capable of causing an increase in P62, why this is so may be P62 accumulating to oxidatively damaged cellular components as the complex I cybrids have been shown to cause an increase in ROS.

Mitochondrial dynamics were highlighted as linking complex I deficiency and changes to autophagy in the cybrid cell lines. An increase in mt-network was observed in the complex I cells compared to controls. Furthermore these static morphological changes carried through to dynamic studies in neurons derived from the cells with complex I deficiency, with larger and slower organelles observed in these neurites. These data also reflect previous observations that the complex I cybrids are associated with an increased

membrane potential. Results from this set of work imply that this may be an adaptive response to the energy deficit seen within these cells. With high membrane potential coupled with fusion of the network, an adaptation that protects from mitophagic degradation and thus explain the observed reduction in autophagic markers. Routine imaging observations in this study saw decreases in autophagosomes in parallel to increased mitochondrial network complexity in the ES cells and control fibroblasts.

Studies within cell lines derived from patients with defined complex I deficiency highlight complex I dysfunction is capable of causing mitochondrial morphological differences in fibroblast cells as well as the ES lines. Interestingly two novel mutations in mitochondrial proteins outside of complex I also revealed dramatic changes to the mitochondrial network. These alongside the nuclear encoded complex I mutations showed a fragmentation of the network. It was only within mitochondrial encoded mutants where we observed elongation of the network which is interesting considering our cybrid line where we also saw increased complexity was also mitochondrial encoded. Whether this is site of mutation, severity dependent or both will require the analysis of greater numbers of cell lines with increased biochemical data.

9.3   RELEVANCE TO PARKINSON'S DISEASE

Complex I is the target for many pharmacological reagents that are used to generate animal models of the Parkinson's Disease. This said no 'true' animal model is available that recapitulates all of the human features of the disease. Taken together, this implies that complex I dysfunction alone is not responsible for Parkinson's disease but is a factor that when combined with others can initiate the cell loss observed. These studies suggest that complex I's impact on mitochondrial dynamics through its dysfunction and the impact this then has on autophagic events within a cell may be one of the pathogenic routes through which cells are lost rapidly causing PD. This suggests that modulation of mitochondrial turnover or dynamics may represent a real therapeutic target in the disorder. Changes in these pathways may be felt with greater bias in the substantia nigra neurons of the upper midbrain for several reasons. Firstly, as a highly energy demanding area, mitochondria in their role as energy providers may be more crucial here than other areas. Furthermore, not only the functioning of mitochondria but also correct transportation will be required within these cells as areas of high bioenergetic

demand are often transient and/or distal from sites of biogenesis. Finally the link between calcium and the substantia nigra neurons highlight this region as highly vulnerable to mitochondrial dysfunction. As calcium sinks mitochondria may be crucial to these cells due to their Ca^2 pacemaking capabilities. In efficient transportation of mitochondria in this cell type therefore may be felt prior to others in response to diminished energy provision through imbalance in intracellular calcium levels. This phenomena has been seen in SH-SY5Y cells, where chronic reduction in complex I function much like that seen in Parkinson's disease and also our cybrid cell lines, show alterations in calcium signaling (Sherer *et al* 2001) that led to increased susceptibility to calcium overloading, and cell death. Furthermore, in cells transformed by mitochondria from individuals with Parkinson's disease calcium homeostasis alters, with these cells showing reduced mitochondrial calcium stores.

Alongside the aforementioned bioenergetics and homeostatic controls the impact of complex I on autophagy has been highlighted in this study and is of clear relevance in PD. A reduction in autophagy in relation to complex I dysfunction may further compromise the mitochondrial population. Alongside this its role in clearance of other cellular components, notably alpha synuclein aggregates in PD (which are known to not be able to be degraded by the UPS or CMA upon aggregation and thus rely on macroautophagy) are compromised. Modulating mitochondrial dynamics and/or the autophagy pathway may well serve as a potential therapy in Parkinson's disease. It is important to note however that simply up regulating autophagy to compensate in these disorders is likely to be insufficient given the various pathways that act prior to and downstream of autophagy. A combined approach addressing dynamics alongside autophagy may serve to alleviate cell loss better than either alone.

9.4   FINAL CONCLUSIONS

Previous work has displayed respiratory complexes show changes in activity with age (Morel *et al.*, 1995), this is most noteworthy in complex I where age related activity decrease is most prominent. Changes in complex I, are likely to have a profound impact on morphology, through changes in ATP levels (Meeusen *et al.*, 2004), lipid peroxidation and fluctuations in the production of free radicals, which are able to

damage and potentially act as signals which directly regulate mitochondrial dynamics (Koopman *et al.*, 2005). CI induced morphological changes can have numerous effects and dynamics rely on changes in membrane potential to act as cues and allow mechanistic reformation. Subtle changes may be even more significant in neurons when we consider directionality is strongly governed by the potential of individual organelles with 90% of high potential mitochondria moving towards the growth cone and 80% low potential moved towards the cell body (Miller and Sheetz, 2004), and potentiality is varied in dendrites and axons, highlighting clear membrane dependent functioning (Overly *et al.*, 1996). In parallel, morphological changes may cause physical barriers to cellular transport and affect autophagy as discussed above

Much experimental evidence points towards a more prominent role for complex I dysfunction and the associated mitochondrial morphological changes in the progression of PD. This dysfunction may occur through many routes, which may go some way to explaining the discrepancy of findings in different experimental models. Conversely, mitochondrial morphology can impact on CI and it is likely that changes in either quickly become self-perpetuating. The fact that many of the morphological effects in experimental models occur outside of basal conditions, i.e. when cells become stressed, further highlights the likeliness of a multifactorial model of PD. One challenge for future research will be deciphering complex pathways that will separate cause from effect. Distinguishing distinct morphological changes from primary mitochondrial dysfunction is difficult. Multiple conditions cause alterations in the movement and form of mitochondria and subsequently targeting dynamics may be a limited therapeutic in certain conditions.

Regardless of the timing changes in motility arise, their contribution to homeostatic loss and cell death is unquestionable and is likely to accelerate collapse of the cellular environment in concert with other direct and indirect mitochondrial factors. In line with this, groups have demonstrated that neurons with prior stress are more susceptible to changes in mitochondrial motility. Models of neurodegenerative disease already exist in which mitochondrial phenotype can be rescued by correcting motility (Cassidy-Stone *et al.*, 2008). For this reason perusing modulators of mitochondrial motility may be valuable to assist restoration of the cellular environment and ultimately prevent neurodegeneration.

References

Abramov, A.Y., Scorziello, A. and Duchen, M.R. (2007) 'Three distinct mechanisms generate oxygen free radicals in neurons and contribute to cell death during anoxia and reoxygenation', *Journal of Neuroscience*, 27(5), pp. 1129-38.

Abramov, A.Y., Smulders-Srinivasan, T.K., Kirby, D.M., Acin-Perez, R., Enriquez, J.A., Lightowlers, R.N., Duchen, M.R. and Turnbull, D.M. (2010) 'Mechanism of neurodegeneration of neurons with mitochondrial DNA mutations', *Brain*, 133(Pt 3), pp. 797-807.

Acin-Perez, R., Bayona-Bafaluy, M.P., Fernandez-Silva, P., Moreno-Loshuertos, R., Perez-Martos, A., Bruno, C., Moraes, C.T. and Enriquez, J.A. (2004) 'Respiratory complex III is required to maintain complex I in mammalian mitochondria', *Molecular Cell*, 13(6), pp. 805-15.

Adam, A.C., Bornhovd, C., Prokisch, H., Neupert, W. and Hell, K. (2006) 'The Nfs1 interacting protein Isd11 has an essential role in Fe/S cluster biogenesis in mitochondria', *EMBO Journal*, 25(1), pp. 174-83.

Albring, M., Griffith, J. and Attardi, G. (1977) 'Association of a protein structure of probable membrane derivation with HeLa cell mitochondrial DNA near its origin of replication', *Proceedings of the National Academy of Science USA*, 74(4), pp. 1348-52.

Alegre-Abarrategui, J., Christian, H., Lufino, M.M., Mutihac, R., Venda, L.L., Ansorge, O., Wade-Martins, R., Alegre-Abarrategui, J., Christian, H., Lufino, M.M.P., Mutihac, R., Venda, L.L., Ansorge, O. and Wade-Martins, R. (2009) 'LRRK2 regulates autophagic activity and localizes to specific membrane microdomains in a novel human genomic reporter cellular model', *Human Molecular Genetics*, 18(21), pp. 4022-34.

Alston, C.L., He, L.P., Morris, A.A., Hughes, I., de Goede, C., Turnbull, D.M., McFarland, R. and Taylor, R.W. (2011) 'Maternally inherited mitochondrial DNA disease in consanguineous families', *European Journal of Human Genetics*, 19(12), pp. 1226-1229.

Amati-Bonneau, P., Valentino, M.L., Reynier, P., Gallardo, M.E., Bornstein, B., Boissiere, A., Campos, Y., Rivera, H., de la Aleja, J.G., Carroccia, R., Iommarini, L., Labauge, P., Figarella-Branger, D., Marcorelles, P., Furby, A., Beauvais, K., Letournel, F., Liguori, R., La Morgia, C., Montagna, P., Liguori, M., Zanna, C., Rugolo, M., Cossarizza, A., Wissinger, B., Verny, C., Schwarzenbacher, R., Martin, M.A., Arenas, J., Ayuso, C., Garesse, R., Lenaers, G., Bonneau, D. and Carelli, V. (2008) 'OPA1 mutations induce mitochondrial DNA instability and optic atrophy 'plus' phenotypes', *Brain*, 131(Pt 2), pp. 338-51.

Anderson, S., Bankier, A.T., Barrell, B.G., de Bruijn, M.H., Coulson, A.R., Drouin, J., Eperon, I.C., Nierlich, D.P., Roe, B.A., Sanger, F., Schreier, P.H., Smith, A.J., Staden, R. and Young, I.G. (1981) 'Sequence and organization of the human mitochondrial genome', *Nature*, 290(5806), pp. 457-65.

Andersson, S.G. and Kurland, C.G. (1998) 'Reductive evolution of resident genomes', *Trends in Microbiology*, 6(7), pp. 263-8.

Anglade, P., Vyas, S., Javoy-Agid, F., Herrero, M.T., Michel, P.P., Marquez, J., Mouatt-Prigent, A., Ruberg, M., Hirsch, E.C. and Agid, Y. (1997) 'Apoptosis and autophagy in nigral neurons of patients with Parkinson's disease', *Histology & Histopathology*, 12(1), pp. 25-31.

Arai, T., Nonaka, T., Hasegawa, M., Akiyama, H., Yoshida, M., Hashizume, Y., Tsuchiya, K., Oda, T. and Ikeda, K. (2003) 'Neuronal and glial inclusions in frontotemporal dementia with or without motor neuron disease are immunopositive for p62', *Neuroscience Letters*, 342(1-2), pp. 41-4.

Arduino, D.M., Esteves, A.R., Cortes, L., Silva, D.F., Patel, B., Grazina, M., Swerdlow, R.H., Oliveira, C.R. and Cardoso, S.M. (2012) 'Mitochondrial metabolism in Parkinson's disease impairs quality control autophagy by hampering microtubule-dependent traffic', *Human Molecular Genetics*, 21(21), pp. 4680-702.

Azad, M.B., Chen, Y., Gibson, S.B., Azad, M.B., Chen, Y. and Gibson, S.B. (2009) 'Regulation of autophagy by reactive oxygen species (ROS): implications for cancer progression and treatment', *Antioxidants & Redox Signaling*, 11(4), pp. 777-90.

Baas, P.W., Black, M.M. and Banker, G.A. (1989) 'Changes in microtubule polarity orientation during the development of hippocampal neurons in culture', *Journal of Cell Biology*, 109(6 Pt 1), pp. 3085-94.

Bain, G., Kitchens, D., Yao, M., Huettner, J.E. and Gottlieb, D.I. (1995) 'Embryonic stem cells express neuronal properties in vitro', *Developmental Biology*, 168(2), pp. 342-57.

Beisker, W., Dolbeare, F. and Gray, J.W. (1987) 'An improved immunocytochemical procedure for high-sensitivity detection of incorporated bromodeoxyuridine', *Cytometry*, 8(2), pp. 235-9.

Benard, G., Bellance, N., James, D., Parrone, P., Fernandez, H., Letellier, T. and Rossignol, R. (2007) 'Mitochondrial bioenergetics and structural network organization', *Journal of Cell Science*, 120(Pt 5), pp. 838-48.

Bender, A., Krishnan, K.J., Morris, C.M., Taylor, G.A., Reeve, A.K., Perry, R.H., Jaros, E., Hersheson, J.S., Betts, J., Klopstock, T., Taylor, R.W. and Turnbull, D.M. (2006a) 'High levels of mitochondrial DNA deletions in substantia nigra neurons in aging and Parkinson disease', *Nat Genet*, 38(5), pp. 515-7.

Bhaskar, P.T. and Hay, N. (2007) 'The two TORCs and Akt', *Developmental Cell*, 12(4), pp. 487-502.

Billinton, N. and Knight, A.W. (2001) 'Seeing the wood through the trees: a review of techniques for distinguishing green fluorescent protein from endogenous autofluorescence', *Analytical Biochemistry*, 291(2), pp. 175-97.

Birky, C.W. (1994) 'Relaxed and Stringent Genomes - Why Cytoplasmic Genes Dont Obey Mendels Laws', *Journal of Heredity*, 85(5), pp. 355-365.

Bjorkoy, G., Lamark, T. and Johansen, T. (2006) 'p62/SQSTM1: a missing link between protein aggregates and the autophagy machinery', *Autophagy*, 2(2), pp. 138-9.

Bogenhagen, D. and Clayton, D.A. (1977) 'Mouse L cell mitochondrial DNA molecules are selected randomly for replication throughout the cell cycle', *Cell*, 11(4), pp. 719-27.

Bogenhagen, D.F., Rousseau, D. and Burke, S. (2008) 'The layered structure of human mitochondrial DNA nucleoids', *Journal of Biological Chemistry*, 283(6), pp. 3665-75.

Boland, B., Kumar, A., Lee, S., Platt, F.M., Wegiel, J., Yu, W.H., Nixon, R.A., Boland, B., Kumar, A., Lee, S., Platt, F.M., Wegiel, J., Yu, W.H. and Nixon, R.A. (2008) 'Autophagy induction and autophagosome clearance in neurons: relationship to autophagic pathology in Alzheimer's disease', *Journal of Neuroscience*, 28(27), pp. 6926-37.

Bonawitz, N.D., Clayton, D.A. and Shadel, G.S. (2006) 'Initiation and beyond: multiple functions of the human mitochondrial transcription machinery', *Molecular Cell*, 24(6), pp. 813-25.

Bowmaker, M., Yang, M.Y., Yasukawa, T., Reyes, A., Jacobs, H.T., Huberman, J.A. and Holt, I.J. (2003) 'Mammalian mitochondrial DNA replicates bidirectionally from an initiation zone', *Journal of Biological Chemistry*, 278(51), pp. 50961-9.

Boya, P., Gonzalez-Polo, R.A., Casares, N., Perfettini, J.L., Dessen, P., Larochette, N., Metivier, D., Meley, D., Souquere, S., Yoshimori, T., Pierron, G., Codogno, P., Kroemer, G., Boya, P., Gonzalez-Polo, R.-A., Casares, N., Perfettini, J.-L., Dessen, P., Larochette, N., Metivier, D., Meley, D., Souquere, S., Yoshimori, T., Pierron, G., Codogno, P. and Kroemer, G. (2005) 'Inhibition of macroautophagy triggers apoptosis', *Molecular & Cellular Biology*, 25(3), pp. 1025-40.

Brandt, U. (2006) 'Energy converting NADH:quinone oxidoreductase (complex I)', *Annual Review of Biochemistry*, 75, pp. 69-92.

Bua, E., Johnson, J., Herbst, A., Delong, B., McKenzie, D., Salamat, S. and Aiken, J.M. (2006) 'Mitochondrial DNA-deletion mutations accumulate intracellularly to detrimental levels in aged human skeletal muscle fibers', *Am J Hum Genet*, 79(3), pp. 469-80.

Burchell, V.S., Nelson, D.E., Sanchez-Martinez, A., Delgado-Camprubi, M., Ivatt, R.M., Pogson, J.H., Randle, S.J., Wray, S., Lewis, P.A., Houlden, H., Abramov, A.Y., Hardy, J., Wood, N.W., Whitworth, A.J., Laman, H. and Plun-Favreau, H. (2013) 'The Parkinson's disease-linked proteins Fbxo7 and Parkin interact to mediate mitophagy', *Nature Neuroscience*, 16(9), pp. 1257-U135.

Burger, G., Lang, B.F., Reith, M. and Gray, M.W. (1996) 'Genes encoding the same three subunits of respiratory complex II are present in the mitochondrial DNA of two phylogenetically distant eukaryotes', *Proceedings of the National Academy of Sciences of the United States of America*, 93(6), pp. 2328-32.

Caccamo, A., Majumder, S., Richardson, A., Strong, R. and Oddo, S. (2010) 'Molecular Interplay between Mammalian Target of Rapamycin (mTOR), Amyloid-beta, and Tau EFFECTS ON COGNITIVE IMPAIRMENTS', *Journal of Biological Chemistry*, 285(17), pp. 13107-13120.

Camara, Y., Asin-Cayuela, J., Park, C.B., Metodiev, M.D., Shi, Y., Ruzzenente, B., Kukat, C., Habermann, B., Wibom, R., Hultenby, K., Franz, T., Erdjument-Bromage, H., Tempst, P., Hallberg, B.M., Gustafsson, C.M. and Larsson, N.G. (2011) 'MTERF4 regulates translation by targeting the methyltransferase NSUN4 to the mammalian mitochondrial ribosome', *Cell Metab*, 13(5), pp. 527-39.

Cassidy-Stone, A., Chipuk, J.E., Ingerman, E., Song, C., Yoo, C., Kuwana, T., Kurth, M.J., Shaw, J.T., Hinshaw, J.E., Green, D.R. and Nunnari, J. (2008) 'Chemical inhibition of the mitochondrial division dynamin reveals its role in Bax/Bak-dependent mitochondrial outer membrane permeabilization', *Developmental Cell*, 14(2), pp. 193-204.

Chang, D.D. and Clayton, D.A. (1984) 'Precise identification of individual promoters for transcription of each strand of human mitochondrial DNA', *Cell*, 36(3), pp. 635-43.

Chen, D., Zhu, C., Wang, X., Feng, X., Pang, S., Huang, W., Hawley, R.G. and Yan, B. (2013) 'A novel and functional variant within the ATG5 gene promoter in sporadic Parkinson's disease', *Neuroscience Letters*, 538, pp. 49-53.

Chen, H., Chomyn, A. and Chan, D.C. (2005) 'Disruption of fusion results in mitochondrial heterogeneity and dysfunction', *Journal of Biological Chemistry*, 280(28), pp. 26185-92.

Chen, H., McCaffery, J.M. and Chan, D.C. (2007a) 'Mitochondrial fusion protects against neurodegeneration in the cerebellum', *Cell*, 130(3), pp. 548-62.

Chen, S., Owens, G.C., Crossin, K.L. and Edelman, D.B. (2007b) 'Serotonin stimulates mitochondrial transport in hippocampal neurons', *Molecular & Cellular Neurosciences*, 36(4), pp. 472-83.

Chen, S., Zhang, X., Song, L. and Le, W. (2012) 'Autophagy dysregulation in amyotrophic lateral sclerosis', *Brain Pathology*, 22(1), pp. 110-6.

Chen, Y., Azad, M.B. and Gibson, S.B. (2009) 'Superoxide is the major reactive oxygen species regulating autophagy', *Cell Death & Differentiation*, 16(7), pp. 1040-52.

Chen, Y., McMillan-Ward, E., Kong, J., Israels, S.J. and Gibson, S.B. (2007c) 'Mitochondrial electron-transport-chain inhibitors of complexes I and II induce autophagic cell death mediated by reactive oxygen species', *Journal of Cell Science*, 120(Pt 23), pp. 4155-66.

Cipolat, S., de Brito, O.M., Dal Zilio, B. and Scorrano, L. (2004) 'OPA1 requires mitofusin 1 to promote mitochondrial fusion', *Proceedings of the National Academy of Sciences of the United States of America*, 101(45), pp. 15927-15932.

Clancy, B. and Cauller, L.J. (1998) 'Reduction of background autofluorescence in brain sections following immersion in sodium borohydride', *Journal of Neuroscience Methods*, 83(2), pp. 97-102.

Clark, I.E., Dodson, M.W., Jiang, C., Cao, J.H., Huh, J.R., Seol, J.H., Yoo, S.J., Hay, B.A. and Guo, M. (2006) 'Drosophila pink1 is required for mitochondrial function and interacts genetically with parkin', *Nature*, 441(7097), pp. 1162-6.

Clarke, P.G. (1990) 'Developmental cell death: morphological diversity and multiple mechanisms', *Anatomy & Embryology*, 181(3), pp. 195-213.

Claros, M.G., Perea, J., Shu, Y., Samatey, F.A., Popot, J.L. and Jacq, C. (1995) 'Limitations to in vivo import of hydrophobic proteins into yeast mitochondria. The case of a cytoplasmically synthesized apocytochrome b', *European Journal of Biochemistry*, 228(3), pp. 762-71.

Clayton, D.A. (1982) 'Replication of animal mitochondrial DNA', *Cell*, 28(4), pp. 693-705.

Clayton, D.A. (1991) 'Replication and transcription of vertebrate mitochondrial DNA', *Annu Rev Cell Biol*, 7, pp. 453-78.

Clayton, D.A. (2003) 'Mitochondrial DNA replication: what we know', *IUBMB Life*, 55(4-5), pp. 213-7.

Clayton, D.A., Doda, J.N. and Friedberg, E.C. (1974) 'The absence of a pyrimidine dimer repair mechanism in mammalian mitochondria', *Proceedings of the National Academy of Science USA*, 71(7), pp. 2777-81.

Codogno, P. and Meijer, A.J. (2005) 'Autophagy and signaling: their role in cell survival and cell death', *Cell Death & Differentiation*, 12 Suppl 2, pp. 1509-18.

Cookson, M.R. (2003) 'Pathways to Parkinsonism', *Neuron*, 37(1), pp. 7-10.

Cowen, T., Haven, A.J. and Burnstock, G. (1985) 'Pontamine sky blue: a counterstain for background autofluorescence in fluorescence and immunofluorescence histochemistry', *Histochemistry*, 82(3), pp. 205-8.

Crews, L., Spencer, B., Desplats, P., Patrick, C., Paulino, A., Rockenstein, E., Hansen, L., Adame, A., Galasko, D. and Masliah, E. (2010) 'Selective molecular alterations in the autophagy pathway in patients with Lewy body disease and in models of alpha-synucleinopathy', *PLoS ONE [Electronic Resource]*, 5(2), p. e9313.

Crotzer, V.L. and Blum, J.S. (2009) 'Autophagy and its role in MHC-mediated antigen presentation', *Journal of Immunology*, 182(6), pp. 3335-41.

Cuervo, A.M., Stefanis, L., Fredenburg, R., Lansbury, P.T. and Sulzer, D. (2004a) 'Impaired degradation of mutant alpha-synuclein by chaperone-mediated autophagy', *Science*, 305(5688), pp. 1292-5.

Cummins, J.M., Wakayama, T. and Yanagimachi, R. (1997) 'Fate of microinjected sperm components in the mouse oocyte and embryo', *Zygote*, 5(4), pp. 301-308.

Dagda, R.K., Cherra, S.J., 3rd, Kulich, S.M., Tandon, A., Park, D. and Chu, C.T. (2009) 'Loss of PINK1 function promotes mitophagy through effects on oxidative stress and mitochondrial fission', *Journal of Biological Chemistry*, 284(20), pp. 13843-55.

Dairaghi, D.J., Shadel, G.S. and Clayton, D.A. (1995) 'Addition of a 29 residue carboxyl-terminal tail converts a simple HMG box-containing protein into a transcriptional activator', *Journal of Molecular Biology*, 249(1), pp. 11-28.

Darios, F., Corti, O., Lucking, C.B., Hampe, C., Muriel, M.P., Abbas, N., Gu, W.J., Hirsch, E.C., Rooney, T., Ruberg, M., Brice, A., Darios, F., Corti, O., Lucking, C.B., Hampe, C., Muriel, M.-P., Abbas, N., Gu, W.-J., Hirsch, E.C., Rooney, T., Ruberg, M. and Brice, A. (2003) 'Parkin prevents mitochondrial swelling and cytochrome c release in mitochondria-dependent cell death', *Human Molecular Genetics*, 12(5), pp. 517-26.

De Duve, C. and Wattiaux, R. (1966) 'Functions of lysosomes', *Annual Review of Physiology*, 28, pp. 435-92.

de Grey, A.D. (1997) 'A proposed refinement of the mitochondrial free radical theory of aging', *Bioessays*, 19(2), pp. 161-6.

de Souza-Pinto, N.C., Mason, P.A., Hashiguchi, K., Weissman, L., Tian, J., Guay, D., Lebel, M., Stevnsner, T.V., Rasmussen, L.J. and Bohr, V.A. (2009) 'Novel DNA mismatch-repair activity involving YB-1 in human mitochondria', *DNA Repair*, 8(6), pp. 704-19.

Decressac, M., Mattsson, B., Weikop, P., Lundblad, M., Jakobsson, J. and Bjorklund, A. (2013) 'TFEB-mediated autophagy rescues midbrain dopamine neurons from -synuclein toxicity', *Proceedings of the National Academy of Sciences of the United States of America*, 110(19), pp. E1817-26.

Dittmar, K.A., Goodenbour, J.M. and Pan, T. (2006) 'Tissue-specific differences in human transfer RNA expression', *PLoS Genetics*, 2(12), pp. 2107-2115.

Dohm, J.A., Lee, S.J., Hardwick, J.M., Hill, R.B. and Gittis, A.G. (2004) 'Cytosolic domain of the human mitochondrial fission protein Fis1 adopts a TPR fold', *Proteins-Structure Function and Genetics*, 54(1), pp. 153-156.

Dudkina, N.V., Eubel, H., Keegstra, W., Boekema, E.J. and Braun, H.-P. (2005) 'Structure of a mitochondrial supercomplex formed by respiratory-chain complexes I and III', *Proceedings of the National Academy of Sciences of the United States of America*, 102(9), pp. 3225-9.

Dyall, S.D. and Johnson, P.J. (2000) 'Origins of hydrogenosomes and mitochondria: evolution and organelle biogenesis', *Current Opinion in Microbiology*, 3(4), pp. 404-11.

Ekstrand, M.I., Terzioglu, M., Galter, D., Zhu, S., Hofstetter, C., Lindqvist, E., Thams, S., Bergstrand, A., Hansson, F.S., Trifunovic, A., Hoffer, B., Cullheim, S., Mohammed, A.H., Olson, L. and Larsson, N.G. (2007) 'Progressive parkinsonism in mice with respiratory-chain-deficient dopamine neurons', *Proceedings of the National Academy of Sciences of the United States of America*, 104(4), pp. 1325-30.

Elson, J.L., Samuels, D.C., Turnbull, D.M. and Chinnery, P.F. (2001) 'Random intracellular drift explains the clonal expansion of mitochondrial DNA mutations with age.', *American Journal of Human Genetics*, 68, pp. 802-806.

Elson, J.L., Swalwell, H., Blakely, E.L., McFarland, R., Taylor, R.W. and Turnbull, D.M. (2009) 'Pathogenic Mitochondrial tRNA Mutations - Which Mutations Are Inherited and Why?', *Human Mutation*, 30(11), pp. E984-E992.

Embley, T.M. and Martin, W. (2006) 'Eukaryotic evolution, changes and challenges', *Nature*, 440(7084), pp. 623-30.

Exner, N., Treske, B., Paquet, D., Holmstrom, K., Schiesling, C., Gispert, S., Carballo-Carbajal, I., Berg, D., Hoepken, H.-H., Gasser, T., Kruger, R., Winklhofer, K.F., Vogel, F., Reichert, A.S., Auburger, G., Kahle, P.J., Schmid, B. and Haass, C. (2007) 'Loss-of-function of human PINK1 results in mitochondrial pathology and can be rescued by parkin', *Journal of Neuroscience*, 27(45), pp. 12413-8.

Falkenberg, M., Gaspari, M., Rantanen, A., Trifunovic, A., Larsson, N.-G. and Gustafsson, C.M. (2002) 'Mitochondrial transcription factors B1 and B2 activate transcription of human mtDNA', *Nature Genetics*, 31(3), pp. 289-94.

Falkenberg, M., Larsson, N.-G. and Gustafsson, C.M. (2007) 'DNA replication and transcription in mammalian mitochondria', *Annual Review of Biochemistry*, 76, pp. 679-99.

Fan, W.W., Waymire, K.G., Narula, N., Li, P., Rocher, C., Coskun, P.E., Vannan, M.A., Narula, J., MacGregor, G.R. and Wallace, D.C. (2008) 'A mouse model of mitochondrial disease reveals germline selection against severe mtDNA mutations', *Science*, 319(5865), pp. 958-962.

Faxen, K., Gilderson, G., Adelroth, P. and Brzezinski, P. (2005) 'A mechanistic principle for proton pumping by cytochrome c oxidase', *Nature*, 437(7056), pp. 286-9.

Fimia, G.M., Di Bartolomeo, S., Piacentini, M. and Cecconi, F. (2011) 'Unleashing the Ambra1-Beclin 1 complex from dynein chains: Ulk1 sets Ambra1 free to induce autophagy', *Autophagy*, 7(1), pp. 115-7.

Fisher, R.P. and Clayton, D.A. (1988) 'Purification and characterization of human mitochondrial transcription factor 1', *Molecular & Cellular Biology*, 8(8), pp. 3496-509.

Fisher, R.P., Lisowsky, T., Parisi, M.A. and Clayton, D.A. (1992) 'DNA wrapping and bending by a mitochondrial high mobility group-like transcriptional activator protein', *Journal of Biological Chemistry*, 267(5), pp. 3358-67.

Foster, P.G., Cox, C.J. and Embley, T.M. (2009) 'The primary divisions of life: a phylogenomic approach employing composition-heterogeneous methods', *Philosophical Transactions of the Royal Society B-Biological Sciences*, 364(1527), pp. 2197-2207.

Frey, T.G. and Mannella, C.A. (2000) 'The internal structure of mitochondria', *Trends Biochem Sci*, 25(7), pp. 319-24.

Frezza, C., Cipolat, S., Martins de Brito, O., Micaroni, M., Beznoussenko, G.V., Rudka, T., Bartoli, D., Polishuck, R.S., Danial, N.N., De Strooper, B. and Scorrano, L. (2006) 'OPA1 controls apoptotic cristae remodeling independently from mitochondrial fusion', *Cell*, 126(1), pp. 177-89.

Gautier, C.A., Kitada, T. and Shen, J. (2008) 'Loss of PINK1 causes mitochondrial functional defects and increased sensitivity to oxidative stress', *Proceedings of the National Academy of Sciences of the United States of America*, 105(32), pp. 11364-9.

Geisler, S., Holmstrom, K.M., Treis, A., Skujat, D., Weber, S.S., Fiesel, F.C., Kahle, P.J. and Springer, W. (2010) 'The PINK1/Parkin-mediated mitophagy is compromised by PD-associated mutations', *Autophagy*, 6(7), pp. 871-8.

Geng, J., Klionsky, D.J., Geng, J. and Klionsky, D.J. (2008) 'The Atg8 and Atg12 ubiquitin-like conjugation systems in macroautophagy. 'Protein modifications: beyond the usual suspects' review series', *EMBO Reports*, 9(9), pp. 859-64.

Giles, R.E., Blanc, H., Cann, H.M. and Wallace, D.C. (1980) 'Maternal inheritance of human mitochondrial DNA', *Proceedings of the National Academy of Science USA*, 77(11), pp. 6715-9.

Gispert, S., Ricciardi, F., Kurz, A., Azizov, M., Hoepken, H.-H., Becker, D., Voos, W., Leuner, K., Muller, W.E., Kudin, A.P., Kunz, W.S., Zimmermann, A., Roeper, J., Wenzel, D., Jendrach, M., Garcia-Arencibia, M., Fernandez-Ruiz, J., Huber, L., Rohrer, H., Barrera, M., Reichert, A.S., Rub, U., Chen, A., Nussbaum, R.L. and Auburger, G. (2009) 'Parkinson phenotype in aged PINK1-deficient mice is accompanied by progressive mitochondrial dysfunction in absence of neurodegeneration', *PLoS ONE [Electronic Resource]*, 4(6), p. e5777.

Gomes, L.C., Di Benedetto, G. and Scorrano, L. (2011) 'During autophagy mitochondria elongate, are spared from degradation and sustain cell viability', *Nature Cell Biology*, 13(5), pp. 589-98.

Graef, M. and Nunnari, J. (2011) 'Mitochondria regulate autophagy by conserved signalling pathways', *EMBO Journal*, 30(11), pp. 2101-14.

Gray, H. and Wong, T.W. (1992) 'Purification and identification of subunit structure of the human mitochondrial DNA polymerase', *Journal of Biological Chemistry*, 267(9), pp. 5835-41.

Gray, M.W. (1992) 'The endosymbiont hypothesis revisited', *International Review of Cytology*, 141, pp. 233-357.

Greaves, L.C., Preston, S.L., Tadrous, P.J., Taylor, R.W., Barron, M.J., Oukrif, D., Leedham, S.J., Deheragoda, M., Sasieni, P., Novelli, M.R., Jankowski, J.A., Turnbull, D.M., Wright, N.A. and McDonald, S.A. (2006) 'Mitochondrial DNA mutations are established in human colonic stem cells, and mutated clones expand by crypt fission', *Proc Natl Acad Sci U S A*, 103(3), pp. 714-9.

Greene, J.C., Whitworth, A.J., Kuo, I., Andrews, L.A., Feany, M.B. and Pallanck, L.J. (2003) 'Mitochondrial pathology and apoptotic muscle degeneration in Drosophila parkin mutants', *Proceedings of the National Academy of Sciences of the United States of America*, 100(7), pp. 4078-83.

Grigorieff, N. (1999) 'Structure of the respiratory NADH:ubiquinone oxidoreductase (complex I)', *Current Opinion in Structural Biology*, 9(4), pp. 476-83.

Griparic, L., van der Wel, N.N., Orozco, I.J., Peters, P.J. and van der Bliek, A.M. (2004) 'Loss of the intermembrane space protein Mgm1/OPA1 induces swelling and localized constrictions along the lengths of mitochondria', *Journal of Biological Chemistry*, 279(18), pp. 18792-8.

Guillery, O., Malka, F., Frachon, P., Milea, D., Rojo, M. and Lombes, A. (2008) 'Modulation of mitochondrial morphology by bioenergetics defects in primary human fibroblasts', *Neuromuscular Disorders*, 18(4), pp. 319-330.

Gusdon, A.M., Zhu, J., Van Houten, B. and Chu, C.T. (2012) 'ATP13A2 regulates mitochondrial bioenergetics through macroautophagy', *Neurobiology of Disease*, 45(3), pp. 962-72.

Hagerhall, C. (1997) 'Succinate: quinone oxidoreductases. Variations on a conserved theme', *Biochimica et Biophysica Acta*, 1320(2), pp. 107-41.

Hailey, D.W., Rambold, A.S., Satpute-Krishnan, P., Mitra, K., Sougrat, R., Kim, P.K. and Lippincott-Schwartz, J. (2010) 'Mitochondria supply membranes for autophagosome biogenesis during starvation', *Cell*, 141(4), pp. 656-67.

Hanada, T., Noda, N.N., Satomi, Y., Ichimura, Y., Fujioka, Y., Takao, T., Inagaki, F. and Ohsumi, Y. (2007) 'The Atg12-Atg5 conjugate has a novel E3-like activity for protein lipidation in autophagy', *Journal of Biological Chemistry*, 282(52), pp. 37298-302.

Hanson, B.J., Capaldi, R.A., Marusich, M.F. and Sherwood, S.W. (2002) 'An immunocytochemical approach to detection of mitochondrial disorders', *Journal of Histochemistry & Cytochemistry*, 50(10), pp. 1281-1288.

Hara, T., Nakamura, K., Matsui, M., Yamamoto, A., Nakahara, Y., Suzuki-Migishima, R., Yokoyama, M., Mishima, K., Saito, I., Okano, H. and Mizushima, N. (2006a) 'Suppression of basal autophagy in neural cells causes neurodegenerative disease in mice', *Nature*, 441(7095), pp. 885-9.

Hardy, J., Lewis, P., Revesz, T., Lees, A., Paisan-Ruiz, C., Hardy, J., Lewis, P., Revesz, T., Lees, A. and Paisan-Ruiz, C. (2009) 'The genetics of Parkinson's syndromes: a critical review', *Current Opinion in Genetics & Development*, 19(3), pp. 254-65.

Harman, D. (1956) 'Ageing: a theory based on free radical and radiation chemistry.', *Journal of Gerontology*, 2, pp. 298-300.

Harman, D. (1972) 'The biologic clock: the mitochondria?', *Journal of the American Geriatric Society*, 20(4), pp. 145-147.

Harman, D. (1981) 'The aging process.', *Proceedings of the National Academy of Sciences USA*, 78(11), pp. 7124-7128.

Hauswirth, W.W. and Laipis, P.J. (1982) 'Mitochondrial DNA polymorphism in a maternal lineage of Holstein cows', *Proc Natl Acad Sci U S A*, 79(15), pp. 4686-90.

He, C. and Klionsky, D.J. (2009) 'Regulation mechanisms and signaling pathways of autophagy', *Annual Review of Genetics*, 43, pp. 67-93.

He, Y.P., Wu, J., Dressman, D.C., Iacobuzio-Donahue, C., Markowitz, S.D., Velculescu, V.E., Diaz, L.A., Kinzler, K.W., Vogelstein, B. and Papadopoulos, N. (2010) 'Heteroplasmic mitochondrial DNA mutations in normal and tumour cells', *Nature*, 464(7288), pp. 610-U175.

Heng, M.Y., Detloff, P.J., Paulson, H.L. and Albin, R.L. (2010) 'Early alterations of autophagy in Huntington disease-like mice', *Autophagy*, 6(8), pp. 1206-8.

Herrmann, J.M. and Neupert, W. (2000) 'Protein transport into mitochondria', *Current Opinion in Microbiology*, 3(2), pp. 210-4.

Hirst, J., Carroll, J., Fearnley, I.M., Shannon, R.J. and Walker, J.E. (2003) 'The nuclear encoded subunits of complex I from bovine heart mitochondria', *Biochim Biophys Acta*, 1604(3), pp. 135-50.

Hixson, J.E., Wong, T.W. and Clayton, D.A. (1986) 'Both the conserved stem-loop and divergent 5'-flanking sequences are required for initiation at the human mitochondrial origin of light-strand DNA replication', *J Biol Chem*, 261(5), pp. 2384-90.

Hofhaus, G., Weiss, H. and Leonard, K. (1991) 'Electron microscopic analysis of the peripheral and membrane parts of mitochondrial NADH dehydrogenase (complex I)', *Journal of Molecular Biology*, 221(3), pp. 1027-43.

Holt, I.J., He, J., Mao, C.-C., Boyd-Kirkup, J.D., Martinsson, P., Sembongi, H., Reyes, A. and Spelbrink, J.N. (2007) 'Mammalian mitochondrial nucleoids: organizing an independently minded genome', *Mitochondrion*, 7(5), pp. 311-21.

Holt, I.J., Lorimer, H.E. and Jacobs, H.T. (2000) 'Coupled leading- and lagging-strand synthesis of mammalian mitochondrial DNA', *Cell*, 100(5), pp. 515-24.

Hwang, J.J., Lee, S.J., Kim, T.Y., Cho, J.H., Koh, J.Y., Hwang, J.J., Lee, S.-J., Kim, T.-Y., Cho, J.-H. and Koh, J.-Y. (2008) 'Zinc and 4-hydroxy-2-nonenal mediate lysosomal membrane permeabilization induced by H2O2 in cultured hippocampal neurons', *Journal of Neuroscience*, 28(12), pp. 3114-22.

Ingman, M.a.G., U. (2006) 'mtDB: Human Mitochondrial Genome Database, a resource for population genetics and medical sciences', *Nucleic Acids Research*, 34, pp. D749-751.

Irrcher, I., Aleyasin, H., Seifert, E.L., Hewitt, S.J., Chhabra, S., Phillips, M., Lutz, A.K., Rousseaux, M.W., Bevilacqua, L., Jahani-Asl, A., Callaghan, S., Maclaurin, J.G., Winklhofer, K.F., Rizzu, P., Rippstein, P., Kim, R.H., Chen, C.X., Fon, E.A., Slack, R.S., Harper, M.E., McBride, H.M., Mak, T.W. and Park, D.S. (2010) 'Loss of the Parkinson's disease-linked gene DJ-1 perturbs mitochondrial dynamics', *Hum Mol Genet*.

Janiak, F., Dell, V.A., Abrahamson, J.K., Watson, B.S., Miller, D.L. and Johnson, A.E. (1990) 'Fluorescence Characterization of the Interaction of Various Transfer-Rna Species with Elongation Factor-Tu-Gtp - Evidence for a New Functional-Role for Elongation Factor-Tu in Protein-Biosynthesis', *Biochemistry*, 29(18), pp. 4268-4277.

Jellinger, K.A. (2009) 'Formation and development of Lewy pathology: a critical update', *J Neurol*, 256 Suppl 3, pp. 270-9.

Jin, S.M., Lazarou, M., Wang, C., Kane, L.A., Narendra, D.P. and Youle, R.J. (2010) 'Mitochondrial membrane potential regulates PINK1 import and proteolytic destabilization by PARL', *Journal of Cell Biology*, 191(5), pp. 933-42.

Jonckheere, A.I., Smeitink, J.A.M. and Rodenburg, R.J.T. (2012) 'Mitochondrial ATP synthase: architecture, function and pathology', *Journal of Inherited Metabolic Disease*, 35(2), pp. 211-25.

Jouaville, L.S., Pinton, P., Bastianutto, C., Rutter, G.A. and Rizzuto, R. (1999) 'Regulation of mitochondrial ATP synthesis by calcium: evidence for a long-term metabolic priming', *Proceedings of the National Academy of Sciences of the United States of America*, 96(24), pp. 13807-12.

Kaasik, A., Safiulina, D., Choubey, V., Kuum, M., Zharkovsky, A. and Veksler, V. (2007) 'Mitochondrial swelling impairs the transport of organelles in cerebellar granule neurons', *Journal of Biological Chemistry*, 282(45), pp. 32821-6.

Kamada, Y., Funakoshi, T., Shintani, T., Nagano, K., Ohsumi, M. and Ohsumi, Y. (2000) 'Tor-mediated induction of autophagy via an Apg1 protein kinase complex', *Journal of Cell Biology*, 150(6), pp. 1507-13.

Kanki, T., Klionsky, D.J., Kanki, T. and Klionsky, D.J. (2008) 'Mitophagy in yeast occurs through a selective mechanism', *Journal of Biological Chemistry*, 283(47), pp. 32386-93.

Karbowski, M., Arnoult, D., Chen, H., Chan, D.C., Smith, C.L. and Youle, R.J. (2004) 'Quantitation of mitochondrial dynamics by photolabeling of individual organelles shows that mitochondrial fusion is blocked during the Bax activation phase of apoptosis', *Journal of Cell Biology*, 164(4), pp. 493-9.

Keeney, P.M., Xie, J., Capaldi, R.A. and Bennett, J.P., Jr. (2006a) 'Parkinson's disease brain mitochondrial complex I has oxidatively damaged subunits and is functionally impaired and misassembled', *Journal of Neuroscience*, 26(19), pp. 5256-64.

Kerr, J.F., Wyllie, A.H. and Currie, A.R. (1972) 'Apoptosis: a basic biological phenomenon with wide-ranging implications in tissue kinetics', *Br J Cancer*, 26(4), pp. 239-57.

Kim, E.H. and Choi, K.S. (2008) 'A critical role of superoxide anion in selenite-induced mitophagic cell death', *Autophagy*, 4(1), pp. 76-8.

Kirby, D.M., Crawford, M., Cleary, M.A., Dahl, H.H.M., Dennett, X. and Thorburn, D.R. (1999) 'Respiratory chain complex I deficiency - An underdiagnosed energy generation disorder', *Neurology*, 52(6), pp. 1255-1264.

Kirby, D.M., Rennie, K.J., Smulders-Srinivasan, T.K., Acin-Perez, R., Whittington, M., Enriquez, J.A., Trevelyan, A.J., Turnbull, D.M. and Lightowlers, R.N. (2009) 'Transmitochondrial embryonic stem cells containing pathogenic mtDNA mutations are compromised in neuronal differentiation', *Cell Proliferation*, 42(4), pp. 413-24.

Kitada, T., Pisani, A., Porter, D.R., Yamaguchi, H., Tscherter, A., Martella, G., Bonsi, P., Zhang, C., Pothos, E.N. and Shen, J. (2007) 'Impaired dopamine release and synaptic plasticity in the striatum of PINK1-deficient mice', *Proceedings of the National Academy of Sciences of the United States of America*, 104(27), pp. 11441-6.

Komatsu, M., Kominami, E., Tanaka, K., Komatsu, M., Kominami, E. and Tanaka, K. (2006a) 'Autophagy and neurodegeneration', *Autophagy*, 2(4), pp. 315-7.

Komatsu, M., Waguri, S., Chiba, T., Murata, S., Iwata, J.-i., Tanida, I., Ueno, T., Koike, M., Uchiyama, Y., Kominami, E. and Tanaka, K. (2006b) 'Loss of autophagy in the central nervous system causes neurodegeneration in mice', *Nature*, 441(7095), pp. 880-4.

Komatsu, M., Waguri, S., Ueno, T., Iwata, J., Murata, S., Tanida, I., Ezaki, J., Mizushima, N., Ohsumi, Y., Uchiyama, Y., Kominami, E., Tanaka, K. and Chiba, T. (2005) 'Impairment of starvation-induced and constitutive autophagy in Atg7-deficient mice', *J Cell Biol*, 169(3), pp. 425-34.

Koopman, W.J.H., Verkaart, S., Visch, H.J., van Emst-de Vries, S., Nijtmans, L.G.J., Smeitink, J.A.M. and Willems, P.H.G.M. (2007) 'Human NADH: ubiquinone oxidoreductase deficiency: radical changes in mitochondrial morphology?', *American Journal of Physiology-Cell Physiology*, 293(1), pp. C22-C29.

Koopman, W.J.H., Visch, H.-J., Verkaart, S., van den Heuvel, L.W.P.J., Smeitink, J.A.M. and Willems, P.H.G.M. (2005) 'Mitochondrial network complexity and pathological decrease in complex I activity are tightly correlated in isolated human complex I deficiency', *American Journal of Physiology - Cell Physiology*, 289(4), pp. C881-90.

Korhonen, J.A., Gaspari, M. and Falkenberg, M. (2003) 'TWINKLE Has 5' -> 3' DNA helicase activity and is specifically stimulated by mitochondrial single-stranded DNA-binding protein', *Journal of Biological Chemistry*, 278(49), pp. 48627-32.

Korolchuk, V.I., Mansilla, A., Menzies, F.M. and Rubinsztein, D.C. (2009a) 'Autophagy inhibition compromises degradation of ubiquitin-proteasome pathway substrates', *Molecular Cell*, 33(4), pp. 517-27.

Korolchuk, V.I., Mansilla, A., Menzies, F.M. and Rubinsztein, D.C. (2009b) 'Autophagy Inhibition Compromises Degradation of Ubiquitin-Proteasome Pathway Substrates', *Molecular Cell*, 33(4), pp. 517-527.

Korolchuk, V.I., Menzies, F.M. and Rubinsztein, D.C. (2009c) 'A novel link between autophagy and the ubiquitin-proteasome system', *Autophagy*, 5(6), pp. 862-863.

Kraytsberg, Y., Kudryavtseva, E., McKee, A.C., Geula, C., Kowall, N.W. and Khrapko, K. (2006) 'Mitochondrial DNA deletions are abundant and cause functional impairment in aged human substantia nigra neurons', *Nat Genet*, 38(5), pp. 518-20.

Krebiehl, G., Ruckerbauer, S., Burbulla, L.F., Kieper, N., Maurer, B., Waak, J., Wolburg, H., Gizatullina, Z., Gellerich, F.N., Woitalla, D., Riess, O., Kahle, P.J., Proikas-Cezanne, T. and Kruger, R. (2010) 'Reduced basal autophagy and impaired mitochondrial dynamics due to loss of Parkinson's disease-associated protein DJ-1', *PLoS ONE [Electronic Resource]*, 5(2), p. e9367.

Kruse, B., Narasimhan, N. and Attardi, G. (1989) 'Termination of transcription in human mitochondria: identification and purification of a DNA binding protein factor that promotes termination', *Cell*, 58(2), pp. 391-7.

Kukat, C., Wurm, C.A., Spahr, H., Falkenberg, M., Larsson, N.G. and Jakobs, S. (2011) 'Super-resolution microscopy reveals that mammalian mitochondrial nucleoids have a uniform size and frequently contain a single copy of mtDNA', *Proceedings of the National Academy of Sciences of the United States of America*, 108(33), pp. 13534-13539.

Kuusisto, E., Salminen, A. and Alafuzoff, I. (2001) 'Ubiquitin-binding protein p62 is present in neuronal and glial inclusions in human tauopathies and synucleinopathies', *Neuroreport*, 12(10), pp. 2085-90.

Lamark, T., Kirkin, V., Dikic, I. and Johansen, T. (2009) 'NBR1 and p62 as cargo receptors for selective autophagy of ubiquitinated targets', *Cell Cycle*, 8(13), pp. 1986-90.

Lange, H., Kaut, A., Kispal, G. and Lill, R. (2000) 'A mitochondrial ferredoxin is essential for biogenesis of cellular iron-sulfur proteins', *Proceedings of the National Academy of Sciences of the United States of America*, 97(3), pp. 1050-5.

Langston, J.W., Ballard, P., Tetrud, J.W. and Irwin, I. (1983) 'Chronic Parkinsonism in humans due to a product of meperidine-analog synthesis', *Science*, 219(4587), pp. 979-80.

Lebon, S., Rodriguez, D., Bridoux, D., Zerrad, A., Rotig, A., Munnich, A., Legrand, A. and Slama, A. (2007) 'A novel mutation in the human complex I NDUFS7 subunit associated with Leigh syndrome', *Molecular Genetics & Metabolism*, 90(4), pp. 379-82.

Lee, D.Y. and Clayton, D.A. (1997) 'RNase mitochondrial RNA processing correctly cleaves a novel R loop at the mitochondrial DNA leading-strand origin of replication', *Genes Dev*, 11(5), pp. 582-92.

Lee, Y.J., Jeong, S.Y., Karbowski, M., Smith, C.L. and Youle, R.J. (2004) 'Roles of the mammalian mitochondrial fission and fusion mediators Fis1, Drp1, and Opa1 in apoptosis', *Molecular Biology of the Cell*, 15(11), pp. 5001-5011.

Legros, F., Malka, F., Frachon, P., Lombes, A. and Rojo, M. (2004) 'Organization and dynamics of human mitochondrial DNA', *Journal of Cell Science*, 117(13), pp. 2653-2662.

Levine, B. (2005) 'Eating oneself and uninvited guests: autophagy-related pathways in cellular defense', *Cell*, 120(2), pp. 159-62.

Levine, B. and Klionsky, D.J. (2004) 'Development by self-digestion: molecular mechanisms and biological functions of autophagy', *Developmental Cell*, 6(4), pp. 463-77.

Lightowlers, R.N., Chinnery, P.F., Turnbull, D.M. and Howell, N. (1997) 'Mammalian mitochondrial genetics: heredity, heteroplasmy and disease', *Trends in Genetics*, 13(11), pp. 450-5.

Lill, R. (2009) 'Function and biogenesis of iron-sulphur proteins', *Nature*, 460(7257), pp. 831-8.

Lin, W. and Kang, U.J. (2010) 'Structural determinants of PINK1 topology and dual subcellular distribution', *BMC Cell Biology*, 11, p. 90.

Liu, K., Shi, N., Sun, Y., Zhang, T. and Sun, X. (2013) 'Therapeutic effects of rapamycin on MPTP-induced Parkinsonism in mice', *Neurochemical Research*, 38(1), pp. 201-7.

Liu, S., Sawada, T., Lee, S., Yu, W., Silverio, G., Alapatt, P., Millan, I., Shen, A., Saxton, W., Kanao, T., Takahashi, R., Hattori, N., Imai, Y. and Lu, B. (2012) 'Parkinson's disease-associated kinase PINK1 regulates Miro protein level and axonal transport of mitochondria', *PLoS Genetics*, 8(3), p. e1002537.

Liu, V.W., Zhang, C. and Nagley, P. (1998) 'Mutations in mitochondrial DNA accumulate differentially in three different human tissues during ageing', *Nucleic Acids Research*, 26(5), pp. 1268-75.

Liu, X., Kim, C.N., Yang, J., Jemmerson, R. and Wang, X. (1996) 'Induction of apoptotic program in cell-free extracts: requirement for dATP and cytochrome c', *Cell*, 86(1), pp. 147-57.

Luo, X.P., Pitkanen, S., KassovskaBratinova, S., Robinson, B.H. and Lehotay, D.C. (1997) 'Excessive formation of hydroxyl radicals and aldehydic lipid peroxidation products in cultured skin fibroblasts from patients with complex I deficiency', *Journal of Clinical Investigation*, 99(12), pp. 2877-2882.

Ma, J.F., Huang, Y., Chen, S.D. and Halliday, G. (2010) 'Immunohistochemical evidence for macroautophagy in neurones and endothelial cells in Alzheimer's disease', *Neuropathology & Applied Neurobiology*, 36(4), pp. 312-9.

Maden, M. and Holder, N. (1992) 'Retinoic acid and development of the central nervous system', *Bioessays*, 14(7), pp. 431-8.

Mader, B.J., Pivtoraiko, V.N., Flippo, H.M., Klocke, B.J., Roth, K.A., Mangieri, L.R. and Shacka, J.J. (2012) 'Rotenone inhibits autophagic flux prior to inducing cell death', *Acs Chemical Neuroscience*, 3(12), pp. 1063-72.

Malicdan, M.C., Noguchi, S., Nonaka, I., Saftig, P., Nishino, I., Malicdan, M.C., Noguchi, S., Nonaka, I., Saftig, P. and Nishino, I. (2008) 'Lysosomal myopathies: an excessive build-up in autophagosomes is too much to handle', *Neuromuscular Disorders*, 18(7), pp. 521-9.

Mannella, C.A. (2006) 'Structure and dynamics of the mitochondrial inner membrane cristae', *Biochimica Et Biophysica Acta-Molecular Cell Research*, 1763(5-6), pp. 542-548.

Margulis, L. (1971a) 'The origin of plant and animal cells', *Am Sci*, 59(2), pp. 230-5.

Margulis, L. (1971b) 'Symbiosis and evolution', *Sci Am*, 225(2), pp. 48-57.

Martinet, W., Agostinis, P., Vanhoecke, B., Dewaele, M. and De Meyer, G.R.Y. (2009) 'Autophagy in disease: a double-edged sword with therapeutic potential', *Clinical Science*, 116(9), pp. 697-712.

Massey, A.C., Zhang, C. and Cuervo, A.M. (2006) 'Chaperone-mediated autophagy in aging and disease', *Current Topics in Developmental Biology*, 73, pp. 205-35.

Matsuda, N., Sato, S., Shiba, K., Okatsu, K., Saisho, K., Gautier, C.A., Sou, Y.S., Saiki, S., Kawajiri, S., Sato, F., Kimura, M., Komatsu, M., Hattori, N. and Tanaka, K. (2010) 'PINK1 stabilized by mitochondrial depolarization recruits Parkin to damaged mitochondria and activates latent Parkin for mitophagy', *Journal of Cell Biology*, 189(2), pp. 211-21.

Mattson, M.P. and Chan, S.L. (2003) 'Calcium orchestrates apoptosis', *Nature Cell Biology*, 5(12), pp. 1041-3.

Mazzulli, J.R., Xu, Y.-H., Sun, Y., Knight, A.L., McLean, P.J., Caldwell, G.A., Sidransky, E., Grabowski, G.A. and Krainc, D. (2011) 'Gaucher disease glucocerebrosidase and -synuclein form a bidirectional pathogenic loop in synucleinopathies', *Cell*, 146(1), pp. 37-52.

McCormack, J.G., Halestrap, A.P. and Denton, R.M. (1990) 'Role of calcium ions in regulation of mammalian intramitochondrial metabolism', *Physiological Reviews*, 70(2), pp. 391-425.

McFarland, R., Elson, J.L., Taylor, R.W., Howell, N. and Turnbull, D.M. (2004) 'Assigning pathogenicity to mitochondrial tRNA mutations: when 'definitely maybe' is not good enough', *Trends in Genetics*, 20(12), pp. 591-596.

Mears, J.A., Sharma, M.R., Gutell, R.R., McCook, A.S., Richardson, P.E., Caulfield, T.R., Agrawal, R.K. and Harvey, S.C. (2006) 'A structural model for the large subunit of the mammalian mitochondrial ribosome', *Journal of Molecular Biology*, 358(1), pp. 193-212.

Meeusen, S., McCaffery, J.M. and Nunnari, J. (2004) 'Mitochondrial fusion intermediates revealed in vitro', *Science*, 305(5691), pp. 1747-52.

Meredith, G.E., Totterdell, S., Petroske, E., Santa Cruz, K., Callison, R.C., Jr. and Lau, Y.S. (2002) 'Lysosomal malfunction accompanies alpha-synuclein aggregation in a progressive mouse model of Parkinson's disease', *Brain Research*, 956(1), pp. 156-65.

Mikelsaar, R. (1983) 'Human Mitochondrial Genome and the Evolution of Methionine Transfer Ribonucleic-Acids', *Journal of Theoretical Biology*, 105(2), pp. 221-232.

Miller, K.E. and Sheetz, M.P. (2004) 'Axonal mitochondrial transport and potential are correlated', *J Cell Sci*, 117(Pt 13), pp. 2791-804.

Miquel, J., Economos, A.C., Fleming, J. and Johnson, J.E., Jr. (1980) 'Mitochondrial role in cell aging', *Exp Gerontol*, 15(6), pp. 575-91.

Mitchell, P. (1961) 'Coupling of phosphorylation to electron and hydrogen transfer by a chemi-osmotic type of mechanism', *Naturwissenschaften*, 191, pp. 144-8.

Mitchell, P. (1976) 'Possible molecular mechanisms of the protonmotive function of cytochrome systems', *Journal of Theoretical Biology*, 62(2), pp. 327-67.

Mitsumoto, A. and Nakagawa, Y. (2001) 'DJ-1 is an indicator for endogenous reactive oxygen species elicited by endotoxin', *Free Radical Research*, 35(6), pp. 885-93.

Mizushima, N. (2005) 'The pleiotropic role of autophagy: from protein metabolism to bactericide', *Cell Death & Differentiation*, 12 Suppl 2, pp. 1535-41.

Montoya, J., Christianson, T., Levens, D., Rabinowitz, M. and Attardi, G. (1982) 'Identification of initiation sites for heavy-strand and light-strand transcription in human mitochondrial DNA', *Proc Natl Acad Sci U S A*, 79(23), pp. 7195-9.

Morais, V.A., Verstreken, P., Roethig, A., Smet, J., Snellinx, A., Vanbrabant, M., Haddad, D., Frezza, C., Mandemakers, W., Vogt-Weisenhorn, D., Van Coster, R., Wurst, W., Scorrano, L. and De Strooper, B. (2009) 'Parkinson's disease mutations in PINK1 result in decreased Complex I activity and deficient synaptic function', *EMBO molecular medicine*, 1(2), pp. 99-111.

Moran, M., Rivera, H., Sanchez-Arago, M., Blazquez, A., Merinero, B., Ugalde, C., Arenas, J., Cuezva, J.M. and Martin, M.A. (2010) 'Mitochondrial bioenergetics and dynamics interplay in complex I-deficient fibroblasts', *Biochimica et Biophysica Acta*, 1802(5), pp. 443-53.

Morel, F., Mazet, F., Touraille, S. and Alziari, S. (1995) 'Changes in the respiratory chain complexes activities and in the mitochondrial DNA content during ageing in D. subobscura', *Mechanisms of Ageing & Development*, 84(3), pp. 171-81.

Mortiboys, H., Thomas, K.J., Koopman, W.J.H., Klaffke, S., Abou-Sleiman, P., Olpin, S., Wood, N.W., Willems, P.H.G.M., Smeitink, J.A.M., Cookson, M.R. and Bandmann, O. (2008) 'Mitochondrial function and morphology are impaired in parkin-mutant fibroblasts', *Annals of Neurology*, 64(5), pp. 555-65.

Mosiman, V.L., Patterson, B.K., Canterero, L. and Goolsby, C.L. (1997) 'Reducing cellular autofluorescence in flow cytometry: an in situ method', *Cytometry*, 30(3), pp. 151-6.

293

Muller-Hocker, J., Seibel, P., Schneiderbanger, K. and Kadenbach, B. (1993) 'Different in situ hybridization patterns of mitochondrial DNA in cytochrome c oxidase-deficient extraocular muscle fibres in the elderly', *Virchows Archiv - A, Pathological Anatomy & Histopathology*, 422(1), pp. 7-15.

Muller, H.J. (1964) 'The Relation Of Recombination To Mutational Advance', *Mutat Res*, 106, pp. 2-9.

Munz, C. (2006) 'Autophagy and antigen presentation', *Cellular Microbiology*, 8(6), pp. 891-8.

Nair, U. and Klionsky, D.J. (2005) 'Molecular mechanisms and regulation of specific and nonspecific autophagy pathways in yeast', *Journal of Biological Chemistry*, 280(51), pp. 41785-8.

Nakano, T., Nakaso, K., Nakashima, K. and Ohama, E. (2004) 'Expression of ubiquitin-binding protein p62 in ubiquitin-immunoreactive intraneuronal inclusions in amyotrophic lateral sclerosis with dementia: analysis of five autopsy cases with broad clinicopathological spectrum', *Acta Neuropathologica*, 107(4), pp. 359-64.

Narendra, D., Tanaka, A., Suen, D.F., Youle, R.J., Narendra, D., Tanaka, A., Suen, D.-F. and Youle, R.J. (2008) 'Parkin is recruited selectively to impaired mitochondria and promotes their autophagy', *Journal of Cell Biology*, 183(5), pp. 795-803.

Narendra, D.P., Jin, S.M., Tanaka, A., Suen, D.F., Gautier, C.A., Shen, J., Cookson, M.R. and Youle, R.J. (2010) 'PINK1 is selectively stabilized on impaired mitochondria to activate Parkin', *PLoS Biol*, 8(1), p. e1000298.

Niu, J., Yu, M., Wang, C. and Xu, Z. (2012) 'Leucine-rich repeat kinase 2 disturbs mitochondrial dynamics via Dynamin-like protein', *Journal of Neurochemistry*, 122(3), pp. 650-8.

Nowikovsky, K., Reipert, S., Devenish, R.J. and Schweyen, R.J. (2007) 'Mdm38 protein depletion causes loss of mitochondrial K+/H+ exchange activity, osmotic swelling and mitophagy', *Cell Death & Differentiation*, 14(9), pp. 1647-56.

Ohta, S. (2006) 'Contribution of somatic mutations in the mitochondrial genome to the development of cancer and tolerance against anticancer drugs', *Oncogene*, 25(34), pp. 4768-4776.

Okatsu, K., Oka, T., Iguchi, M., Imamura, K., Kosako, H., Tani, N., Kimura, M., Go, E., Koyano, F., Funayama, M., Shiba-Fukushima, K., Sato, S., Shimizu, H., Fukunaga, Y., Taniguchi, H., Komatsu, M., Hattori, N., Mihara, K., Tanaka, K. and Matsuda, N. (2012) 'PINK1 autophosphorylation upon membrane potential dissipation is essential for Parkin recruitment to damaged mitochondria', *Nature communications*, 3, p. 1016.

Overbye, A., Fengsrud, M. and Seglen, P.O. (2007a) 'Proteomic analysis of membrane-associated proteins from rat liver autophagosomes', *Autophagy*, 3(4), pp. 300-22.

Overly, C.C., Rieff, H.I. and Hollenbeck, P.J. (1996) 'Organelle motility and metabolism in axons vs dendrites of cultured hippocampal neurons', *Journal of Cell Science*, 109(Pt 5), pp. 971-80.

Pakendorf, B. and Stoneking, M. (2005) 'Mitochondrial DNA and human evolution', *Annual Review of Genomics and Human Genetics*, 6, pp. 165-183.

Palade, G.E. (1953) 'An electron microscope study of the mitochondrial structure', *J Histochem Cytochem*, 1(4), pp. 188-211.

Pang, S., Chen, D., Zhang, A., Qin, X. and Yan, B. (2012) 'Genetic analysis of the LAMP-2 gene promoter in patients with sporadic Parkinson's disease', *Neuroscience Letters*, 526(1), pp. 63-7.

Papa, S. and De Rasmo, D. (2013) 'Complex I deficiencies in neurological disorders', *Trends in Molecular Medicine*, 19(1), pp. 61-9.

Papa, S., Petruzzella, V., Scacco, S., Vergari, R., Panelli, D., Tamborra, R., Corsi, P., Picciariello, M., Lambo, R., Bertini, E. and Santorelli, F.M. (2004) 'Respiratory complex I in brain development and genetic disease', *Neurochemical Research*, 29(3), pp. 547-60.

Paradkar, P.N., Zumbrennen, K.B., Paw, B.H., Ward, D.M. and Kaplan, J. (2009) 'Regulation of mitochondrial iron import through differential turnover of mitoferrin 1 and mitoferrin 2', *Molecular & Cellular Biology*, 29(4), pp. 1007-16.

Park, C.B., Asin-Cayuela, J., Camara, Y., Shi, Y., Pellegrini, M., Gaspari, M., Wibom, R., Hultenby, K., Erdjument-Bromage, H., Tempst, P., Falkenberg, M., Gustafsson, C.M. and Larsson, N.G. (2007) 'MTERF3 is a negative regulator of mammalian mtDNA transcription', *Cell*, 130(2), pp. 273-85.

Pham, A.H., Meng, S., Chu, Q.N. and Chan, D.C. (2012) 'Loss of Mfn2 results in progressive, retrograde degeneration of dopaminergic neurons in the nigrostriatal circuit', *Human Molecular Genetics*, 21(22), pp. 4817-26.

Pham, N.A., Richardson, T., Cameron, J., Chue, B. and Robinson, B.H. (2004) 'Altered mitochondrial structure and motion dynamics in living cells with energy metabolism defects revealed by real time microscope imaging', *Microscopy and Microanalysis*, 10(2), pp. 247-260.

Pham, X.H., Farge, G., Shi, Y., Gaspari, M., Gustafsson, C.M. and Falkenberg, M. (2006) 'Conserved sequence box II directs transcription termination and primer formation in mitochondria', *Journal of Biological Chemistry*, 281(34), pp. 24647-52.

Pich, S., Bach, D., Briones, P., Liesa, M., Camps, M., Testar, X., Palacin, M. and Zorzano, A. (2005) 'The Charcot-Marie-Tooth type 2A gene product, Mfn2, up-regulates fuel oxidation through expression of OXPHOS system', *Human Molecular Genetics*, 14(11), pp. 1405-15.

Pickford, F., Masliah, E., Britschgi, M., Lucin, K., Narasimhan, R., Jaeger, P.A., Small, S., Spencer, B., Rockenstein, E., Levine, B., Wyss-Coray, T., Pickford, F., Masliah, E., Britschgi, M., Lucin, K., Narasimhan, R., Jaeger, P.A., Small, S., Spencer, B., Rockenstein, E., Levine, B. and Wyss-Coray, T. (2008) 'The autophagy-related protein beclin 1 shows reduced expression in early Alzheimer disease and regulates amyloid beta accumulation in mice', *Journal of Clinical Investigation*, 118(6), pp. 2190-9.

Pitkanen, S. and Robinson, B.H. (1996) 'Mitochondrial complex I deficiency leads to increased production of superoxide radicals and induction of superoxide dismutase', *Journal of Clinical Investigation*, 98(2), pp. 345-351.

Plomp, P.J., Gordon, P.B., Meijer, A.J., Hoyvik, H. and Seglen, P.O. (1989) 'Energy dependence of different steps in the autophagic-lysosomal pathway', *Journal of Biological Chemistry*, 264(12), pp. 6699-704.

Potluri, P., Davila, A., Ruiz-Pesini, E., Mishmar, D., O'Hearn, S., Hancock, S., Simon, M., Scheffler, I.E., Wallace, D.C. and Procaccio, V. (2009) 'A novel NDUFA1 mutation leads to a progressive mitochondrial complex I-specific neurodegenerative disease', *Molecular Genetics and Metabolism*, 96(4), pp. 189-195.

Pridgeon, J.W., Olzmann, J.A., Chin, L.S., Li, L., Pridgeon, J.W., Olzmann, J.A., Chin, L.-S. and Li, L. (2007) 'PINK1 protects against oxidative stress by phosphorylating mitochondrial chaperone TRAP1', *Plos Biology*, 5(7), p. e172.

Raja, M., Azzoni, A., Giona, F., Regis, S., Grossi, S., Filocamo, M. and Sidransky, E. (2007) 'Movement and mood disorder in two brothers with Gaucher disease', *Clinical Genetics*, 72(4), pp. 357-61.

Ramonet, D., Perier, C., Recasens, A., Dehay, B., Bove, J., Costa, V., Scorrano, L. and Vila, M. (2013) 'Optic atrophy 1 mediates mitochondria remodeling and dopaminergic neurodegeneration linked to complex I deficiency', *Cell Death & Differentiation*, 20(1), pp. 77-85.

Ramonet, D., Podhajska, A., Stafa, K., Sonnay, S., Trancikova, A., Tsika, E., Pletnikova, O., Troncoso, J.C., Glauser, L. and Moore, D.J. (2012) 'PARK9-associated ATP13A2 localizes to intracellular acidic vesicles and regulates cation homeostasis and neuronal integrity', *Human Molecular Genetics*, 21(8), pp. 1725-43.

Ravikumar, B., Vacher, C., Berger, Z., Davies, J.E., Luo, S., Oroz, L.G., Scaravilli, F., Easton, D.F., Duden, R., O'Kane, C.J., Rubinsztein, D.C., Ravikumar, B., Vacher, C., Berger, Z., Davies, J.E., Luo, S., Oroz, L.G., Scaravilli, F., Easton, D.F., Duden, R., O'Kane, C.J. and Rubinsztein, D.C. (2004) 'Inhibition

of mTOR induces autophagy and reduces toxicity of polyglutamine expansions in fly and mouse models of Huntington disease', *Nature Genetics*, 36(6), pp. 585-95.

Rebelo, A.P., Dillon, L.M. and Moraes, C.T. (2011) 'Mitochondrial DNA transcription regulation and nucleoid organization', *Journal of Inherited Metabolic Disease*, 34(4), pp. 941-51.

Rebelo, A.P., Williams, S.L. and Moraes, C.T. (2009) 'In vivo methylation of mtDNA reveals the dynamics of protein-mtDNA interactions', *Nucleic Acids Research*, 37(20), pp. 6701-15.

Reeve, A.K., Park, T.K., Jaros, E., Campbell, G.R., Lax, N.Z., Hepplewhite, P.D., Krishnan, K.J., Elson, J.L., Morris, C.M., McKeith, I.G. and Turnbull, D.M. (2012a) 'Relationship Between Mitochondria and alpha-Synuclein A Study of Single Substantia Nigra Neurons', *Archives of Neurology*, 69(3), pp. 385-393.

Rehling, P., Brandner, K. and Pfanner, N. (2004) 'Mitochondrial import and the twin-pore translocase', *Nature Reviews Molecular Cell Biology*, 5(7), pp. 519-30.

Robberson, D.L. and Clayton, D.A. (1972) 'Replication of mitochondrial DNA in mouse L cells and their thymidine kinase - derivatives: displacement replication on a covalently-closed circular template', *Proceedings of the National Academy of Sciences of the United States of America*, 69(12), pp. 3810-4.

Rojo, J.V., Merino, A.M., Gonzalez, L.O. and Vizoso, F. (2002) 'Expression and clinical significance of pepsinogen C in epithelial ovarian carcinomas', *European Journal of Obstetrics Gynecology and Reproductive Biology*, 104(1), pp. 58-63.

Rossignol, R., Gilkerson, R., Aggeler, R., Yamagata, K., Remington, S.J. and Capaldi, R.A. (2004) 'Energy substrate modulates mitochondrial structure and oxidative capacity in cancer cells', *Cancer Research*, 64(3), pp. 985-93.

Rubinsztein, D.C., Gestwicki, J.E., Murphy, L.O., Klionsky, D.J., Rubinsztein, D.C., Gestwicki, J.E., Murphy, L.O. and Klionsky, D.J. (2007) 'Potential therapeutic applications of autophagy', *Nature Reviews Drug Discovery*, 6(4), pp. 304-12.

Rustin, P., Bourgeron, T., Parfait, B., Chretien, D., Munnich, A. and Rotig, A. (1997) 'Inborn errors of the Krebs cycle: a group of unusual mitochondrial diseases in human', *Biochimica et Biophysica Acta*, 1361(2), pp. 185-97.

Sacconi, S., Salviati, L., Nishigaki, Y., Walker, W.F., Hernandez-Rosa, E., Trevisson, E., Delplace, S., Desnuelle, C., Shanske, S., Hirano, M., Schon, E.A., Bonilla, E., De Vivo, D.C., DiMauro, S. and Davidson, M.M. (2008) 'A functionally dominant mitochondrial DNA mutation', *Human Molecular Genetics*, 17(12), pp. 1814-1820.

Sagan, L. (1993) 'On the origin of mitosing cells. 1967', *Journal of NIH Research*, 5(3), pp. 65-72.

Sarkar, S. and Rubinsztein, D.C. (2006) 'Inositol and IP3 levels regulate autophagy: biology and therapeutic speculations', *Autophagy*, 2(2), pp. 132-4.

Satoh, M.S., Huh, N.H., Rajewsky, M.F. and Kuroki, T. (1988) 'Enzymatic Removal of O-6-Ethylguanine from Mitochondrial-DNA in Rat-Tissues Exposed to N-Ethyl-N-Nitrosourea Invivo', *Journal of Biological Chemistry*, 263(14), pp. 6854-6856.

Saxton, W.M. and Hollenbeck, P.J. (2012) 'The axonal transport of mitochondria', *Journal of Cell Science*, 125(Pt 9), pp. 2095-104.

Schagger, H., Pfeiffer, K. (2000) 'Supercomplexes in the respiratory chains of yeast and mammalian mitochondria', *EMBO*, 19(8), pp. 1777-1783.

Schapira, A.H., Cooper, J.M., Dexter, D., Clark, J.B., Jenner, P. and Marsden, C.D. (1990a) 'Mitochondrial complex I deficiency in Parkinson's disease', *J Neurochem*, 54(3), pp. 823-7.

Scheffler, I.E. (1999) *Mitochondria*. New York: Wiley-Liss.

Scherz-Shouval, R. and Elazar, Z. (2007) 'ROS, mitochondria and the regulation of autophagy', *Trends in Cell Biology*, 17(9), pp. 422-7.

Scherz-Shouval, R., Shvets, E., Fass, E., Shorer, H., Gil, L. and Elazar, Z. (2007b) 'Reactive oxygen species are essential for autophagy and specifically regulate the activity of Atg4', *EMBO Journal*, 26(7), pp. 1749-60.

Schlossmacher, M.G., Frosch, M.P., Gai, W.P., Medina, M., Sharma, N., Forno, L., Ochiishi, T., Shimura, H., Sharon, R., Hattori, N., Langston, J.W., Mizuno, Y., Hyman, B.T., Selkoe, D.J. and Kosik, K.S. (2002) 'Parkin localizes to the Lewy bodies of Parkinson disease and dementia with Lewy bodies', *American Journal of Pathology*, 160(5), pp. 1655-67.

Schon, E.A. and Przedborski, S. (2011) 'Mitochondria: the next (neurode)generation', *Neuron*, 70(6), pp. 1033-53.

Schulz, K.L., Eckert, A., Rhein, V., Mai, S., Haase, W., Reichert, A.S., Jendrach, M., Muller, W.E. and Leuner, K. (2012) 'A new link to mitochondrial impairment in tauopathies', *Molecular Neurobiology*, 46(1), pp. 205-16.

Schutt, F., Aretz, S., Auffarth, G.U. and Kopitz, J. (2012) 'Moderately reduced ATP levels promote oxidative stress and debilitate autophagic and phagocytic capacities in human RPE cells', *Investigative Ophthalmology & Visual Science*, 53(9), pp. 5354-61.

Schwartz, M. and Vissing, J. (2002) 'Paternal inheritance of mitochondrial DNA', *N Engl J Med*, 347(8), pp. 576-80.

Schwarze, S.R., Lee, C.M., Chung, S.S., Roecker, E.B., Weindruch, R. and Aiken, J.M. (1995) 'High-Levels of Mitochondrial-DNA Deletions in Skeletal-Muscle of Old Rhesus-Monkeys', *Mechanisms of Ageing and Development*, 83(2), pp. 91-101.

Scorrano, L., Ashiya, M., Buttle, K., Weiler, S., Oakes, S.A., Mannella, C.A. and Korsmeyer, S.J. (2002) 'A distinct pathway remodels mitochondrial cristae and mobilizes cytochrome c during apoptosis', *Developmental Cell*, 2(1), pp. 55-67.

Scott, R.C., Juhasz, G. and Neufeld, T.P. (2007) 'Direct induction of autophagy by Atg1 inhibits cell growth and induces apoptotic cell death', *Current Biology*, 17(1), pp. 1-11.

Sen, K. and Beattie, D.S. (1986) 'Cytochrome b is necessary for the effective processing of core protein I and the iron-sulfur protein of complex III in the mitochondria', *Archives of Biochemistry & Biophysics*, 251(1), pp. 239-49.

Sharma, L.K., Lu, J. and Bai, Y. (2009) 'Mitochondrial respiratory complex I: structure, function and implication in human diseases', *Current Medicinal Chemistry*, 16(10), pp. 1266-77.

Sharma, M.R., Koc, E.C., Datta, P.P., Booth, T.M., Spremulli, L.L. and Agrawal, R.K. (2003) 'Structure of the mammalian mitochondrial ribosome reveals an expanded functional role for its component proteins', *Cell*, 115(1), pp. 97-108.

Shendelman, S., Jonason, A., Martinat, C., Leete, T., Abeliovich, A., Shendelman, S., Jonason, A., Martinat, C., Leete, T. and Abeliovich, A. (2004) 'DJ-1 is a redox-dependent molecular chaperone that inhibits alpha-synuclein aggregate formation', *Plos Biology*, 2(11), p. e362.

Shimizu, S., Kanaseki, T., Mizushima, N., Mizuta, T., Arakawa-Kobayashi, S., Thompson, C.B. and Tsujimoto, Y. (2004) 'Role of Bcl-2 family proteins in a non-apoptotic programmed cell death dependent on autophagy genes', *Nature Cell Biology*, 6(12), pp. 1221-8.

Smirnova, E., Griparic, L., Shurland, D.L. and van der Bliek, A.M. (2001) 'Dynamin-related protein Drp1 is required for mitochondrial division in mammalian cells', *Mol Biol Cell*, 12(8), pp. 2245-56.

Smits, P., Smeitink, J. and van den Heuvel, L. (2010) 'Mitochondrial translation and beyond: processes implicated in combined oxidative phosphorylation deficiencies', *J Biomed Biotechnol*, 2010, p. 737385.

Sologub, M., Litonin, D., Anikin, M., Mustaev, A. and Temiakov, D. (2009) 'TFB2 is a transient component of the catalytic site of the human mitochondrial RNA polymerase', *Cell*, 139(5), pp. 934-44.

Son, J.H., Shim, J.H., Kim, K.H., Ha, J.Y. and Han, J.Y. (2012) 'Neuronal autophagy and neurodegenerative diseases', *Experimental & Molecular Medicine*, 44(2), pp. 89-98.

Spencer, B., Potkar, R., Trejo, M., Rockenstein, E., Patrick, C., Gindi, R., Adame, A., Wyss-Coray, T. and Masliah, E. (2009a) 'Beclin 1 gene transfer activates autophagy and ameliorates the neurodegenerative pathology in alpha-synuclein models of Parkinson's and Lewy body diseases', *Journal of Neuroscience*, 29(43), pp. 13578-88.

Suen, D.F., Narendra, D.P., Tanaka, A., Manfredi, G. and Youle, R.J. (2010) 'Parkin overexpression selects against a deleterious mtDNA mutation in heteroplasmic cybrid cells', *Proceedings of the National Academy of Sciences of the United States of America*, 107(26), pp. 11835-40.

Sun, F., Huo, X., Zhai, Y., Wang, A., Xu, J., Su, D., Bartlam, M. and Rao, Z. (2005) 'Crystal structure of mitochondrial respiratory membrane protein complex II', *Cell*, 121(7), pp. 1043-57.

Swerdlow, R.H., Parks, J.K., Davis, J.N., 2nd, Cassarino, D.S., Trimmer, P.A., Currie, L.J., Dougherty, J., Bridges, W.S., Bennett, J.P., Jr., Wooten, G.F. and Parker, W.D. (1998) 'Matrilineal inheritance of complex I dysfunction in a multigenerational Parkinson's disease family', *Annals of Neurology*, 44(6), pp. 873-81.

Taanman, J.W. (1999) 'The mitochondrial genome: structure, transcription, translation and replication', *Biochim Biophys Acta*, 1410(2), pp. 103-23.

Tabb, J.S., Kish, P.E., Van Dyke, R. and Ueda, T. (1992) 'Glutamate transport into synaptic vesicles. Roles of membrane potential, pH gradient, and intravesicular pH', *Journal of Biological Chemistry*, 267(22), pp. 15412-8.

Takeuchi, N., Vial, L., Panvert, M., Schmitt, E., Watanabe, K., Mechulam, Y. and Blanquet, S. (2001) 'Recognition of tRNAs by methionyl-tRNA transformylase from mammalian mitochondria', *Journal of Biological Chemistry*, 276(23), pp. 20064-20068.

Tanaka, Y., Guhde, G., Suter, A., Eskelinen, E.L., Hartmann, D., Lullmann-Rauch, R., Janssen, P.M., Blanz, J., von Figura, K. and Saftig, P. (2000) 'Accumulation of autophagic vacuoles and cardiomyopathy in LAMP-2-deficient mice', *Nature*, 406(6798), pp. 902-6.

Tanji, K., Mori, F., Kakita, A., Takahashi, H. and Wakabayashi, K. (2011) 'Alteration of autophagosomal proteins (LC3, GABARAP and GATE-16) in Lewy body disease', *Neurobiology of Disease*, 43(3), pp. 690-7.

Tapper, D.P. and Clayton, D.A. (1981) 'Mechanism of replication of human mitochondrial DNA. Localization of the 5' ends of nascent daughter strands', *J Biol Chem*, 256(10), pp. 5109-15.

Temperley, R., Richter, R., Dennerlein, S., Lightowlers, R.N. and Chrzanowska-Lightowlers, Z.M. (2010) 'Hungry Codons Promote Frameshifting in Human Mitochondrial Ribosomes', *Science*, 327(5963), pp. 301-301.

Terman, A., Gustafsson, B. and Brunk, U.T. (2007) 'Autophagy, organelles and ageing', *Journal of Pathology*, 211(2), pp. 134-43.

Tolkovsky, A.M., Xue, L., Fletcher, G.C., Borutaite, V., Tolkovsky, A.M., Xue, L., Fletcher, G.C. and Borutaite, V. (2002) 'Mitochondrial disappearance from cells: a clue to the role of autophagy in programmed cell death and disease?', *Biochimie*, 84(2-3), pp. 233-40.

Tondera, D., Grandemange, S., Jourdain, A., Karbowski, M., Mattenberger, Y., Herzig, S., Da Cruz, S., Clerc, P., Raschke, I., Merkwirth, C., Ehses, S., Krause, F., Chan, D.C., Alexander, C., Bauer, C., Youle, R., Langer, T. and Martinou, J.C. (2009) 'SLP-2 is required for stress-induced mitochondrial hyperfusion', *Embo Journal*, 28(11), pp. 1589-1600.

Tong, W.-H., Jameson, G.N.L., Huynh, B.H. and Rouault, T.A. (2003) 'Subcellular compartmentalization of human Nfu, an iron-sulfur cluster scaffold protein, and its ability to assemble a [4Fe-4S] cluster', *Proceedings of the National Academy of Sciences of the United States of America*, 100(17), pp. 9762-7.

Tong, W.H. and Rouault, T. (2000) 'Distinct iron-sulfur cluster assembly complexes exist in the cytosol and mitochondria of human cells', *EMBO Journal*, 19(21), pp. 5692-700.

Trevelyan, A.J., Kirby, D.M., Smulders-Srinivasan, T.K., Nooteboom, M., Acin-Perez, R., Enriquez, J.A., Whittington, M.A., Lightowlers, R.N. and Turnbull, D.M. (2010) 'Mitochondrial DNA mutations affect calcium handling in differentiated neurons', *Brain*, 133(Pt 3), pp. 787-96.

Triepels, R.H., Hanson, B.J., van den Heuvel, L.P., Sundell, L., Marusich, M.F., Smeitink, J.A. and Capaldi, R.A. (2001a) 'Human complex I defects can be resolved by monoclonal antibody analysis into distinct subunit assembly patterns', *Journal of Biological Chemistry*, 276(12), pp. 8892-7.

Triepels, R.H., Van Den Heuvel, L.P., Trijbels, J.M. and Smeitink, J.A. (2001b) 'Respiratory chain complex I deficiency', *American Journal of Medical Genetics*, 106(1), pp. 37-45.

Trimmer, P.A., Swerdlow, R.H., Parks, J.K., Keeney, P., Bennett, J.P., Jr., Miller, S.W., Davis, R.E. and Parker, W.D., Jr. (2000) 'Abnormal mitochondrial morphology in sporadic Parkinson's and Alzheimer's disease cybrid cell lines', *Experimental Neurology*, 162(1), pp. 37-50.

Tsukihara, T., Aoyama, H., Yamashita, E., Tomizaki, T., Yamaguchi, H., Shinzawa-Itoh, K., Nakashima, R., Yaono, R. and Yoshikawa, S. (1996) 'The whole structure of the 13-subunit oxidized cytochrome c oxidase at 2.8 A', *Science*, 272(5265), pp. 1136-44.

Tuppen, H.A.L., Hogan, V.E., He, L., Blakely, E.L., Worgan, L., Al-Dosary, M., Saretzki, G., Alston, C.L., Morris, A.A., Clarke, M., Jones, S., Devlin, A.M., Mansour, S., Chrzanowska-Lightowlers, Z.M.A., Thorburn, D.R., McFarland, R. and Taylor, R.W. (2010) 'The p.M292T NDUFS2 mutation causes complex I-deficient Leigh syndrome in multiple families', *Brain*, 133, pp. 2952-2963.

Twig, G., Elorza, A., Molina, A.J.A., Mohamed, H., Wikstrom, J.D., Walzer, G., Stiles, L., Haigh, S.E., Katz, S., Las, G., Alroy, J., Wu, M., Py, B.F., Yuan, J., Deeney, J.T., Corkey, B.E. and Shirihai, O.S. (2008b) 'Fission and selective fusion govern mitochondrial segregation and elimination by autophagy', *EMBO Journal*, 27(2), pp. 433-46.

Vasseur, S., Afzal, S., Tardivel-Lacombe, J., Park, D.S., Iovanna, J.L., Mak, T.W., Vasseur, S., Afzal, S., Tardivel-Lacombe, J., Park, D.S., Iovanna, J.L. and Mak, T.W. (2009) 'DJ-1/PARK7 is an important mediator of hypoxia-induced cellular responses', *Proceedings of the National Academy of Sciences of the United States of America*, 106(4), pp. 1111-6.

Walker, J.E., Arizmendi, J.M., Dupuis, A., Fearnley, I.M., Finel, M., Medd, S.M., Pilkington, S.J., Runswick, M.J. and Skehel, J.M. (1992) 'Sequences of 20 subunits of NADH:ubiquinone oxidoreductase from bovine heart mitochondria. Application of a novel strategy for sequencing proteins using the polymerase chain reaction', *Journal of Molecular Biology*, 226(4), pp. 1051-72.

Wallace, D.C. (2007) 'Why do we still have a maternally inherited mitochondrial DNA? Insights from evolutionary medicine', *Annual Review of Biochemistry*, 76, pp. 781-821.

Wang, X., Winter, D., Ashrafi, G., Schlehe, J., Wong, Y.L., Selkoe, D., Rice, S., Steen, J., LaVoie, M.J. and Schwarz, T.L. (2011) 'PINK1 and Parkin target Miro for phosphorylation and degradation to arrest mitochondrial motility', *Cell*, 147(4), pp. 893-906.

Wanrooij, S. and Falkenberg, M. (2010) 'The human mitochondrial replication fork in health and disease', *Biochimica et Biophysica Acta*, 1797(8), pp. 1378-88.

Watanabe, Y., Tatebe, H., Taguchi, K., Endo, Y., Tokuda, T., Mizuno, T., Nakagawa, M. and Tanaka, M. (2012) 'p62/SQSTM1-dependent autophagy of Lewy body-like alpha-synuclein inclusions', *PLoS One*, 7(12), p. e52868.

Waters, J. and Smith, S.J. (2003) 'Mitochondria and release at hippocampal synapses', *Pflugers Archiv - European Journal of Physiology*, 447(3), pp. 363-70.

Watt, I.N., Montgomery, M.G., Runswick, M.J., Leslie, A.G.W. and Walker, J.E. (2010) 'Bioenergetic cost of making an adenosine triphosphate molecule in animal mitochondria', *Proceedings of the National Academy of Sciences of the United States of America*, 107(39), pp. 16823-7.

Webb, J.L., Ravikumar, B., Atkins, J., Skepper, J.N. and Rubinsztein, D.C. (2003a) 'Alpha-Synuclein is degraded by both autophagy and the proteasome', *Journal of Biological Chemistry*, 278(27), pp. 25009-13.

Welle, S., Bhatt, K., Shah, B., Needler, N., Delehanty, J.M. and Thornton, C.A. (2003) 'Reduced amount of mitochondrial DNA in aged human muscle', *Journal of Applied Physiology*, 94(4), pp. 1479-84.

Westermann, B. (2012) 'Bioenergetic role of mitochondrial fusion and fission', *Biochimica Et Biophysica Acta-Bioenergetics*, 1817(10), pp. 1833-1838.

Winder-Rhodes, S.E., Garcia-Reitbock, P., Ban, M., Evans, J.R., Jacques, T.S., Kemppinen, A., Foltynie, T., Williams-Gray, C.H., Chinnery, P.F., Hudson, G., Burn, D.J., Allcock, L.M., Sawcer, S.J., Barker, R.A. and Spillantini, M.G. (2012) 'Genetic and pathological links between Parkinson's disease and the lysosomal disorder Sanfilippo syndrome', *Movement Disorders*, 27(2), pp. 312-5.

Wong, A., Cavelier, L., Collins-Schramm, H.E., Seldin, M.F., McGrogan, M., Savontaus, M.-L. and Cortopassi, G.A. (2002) 'Differentiation-specific effects of LHON mutations introduced into neuronal NT2 cells', *Human Molecular Genetics*, 11(4), pp. 431-8.

Wood-Kaczmar, A., Gandhi, S., Yao, Z., Abramov, A.Y., Miljan, E.A., Keen, G., Stanyer, L., Hargreaves, I., Klupsch, K., Deas, E., Downward, J., Mansfield, L., Jat, P., Taylor, J., Heales, S., Duchen, M.R., Latchman, D., Tabrizi, S.J. and Wood, N.W. (2008a) 'PINK1 is necessary for long term survival and mitochondrial function in human dopaminergic neurons.[Erratum appears in PLoS ONE. 2008;3(7). doi: 10.1371/annotation/17d5aaa1-c6d8-4aad-a9a4-56b2c1220c83 Note: Abramov, Andrey S Y [corrected to Abramov, Andrey Y]], [Erratum appears in PLoS ONE. 2008;3(7). doi: 10.1371/annotation/ba489c2a-5cf2-481c-aff7-d2c8c4ecdcfa]', *PLoS ONE [Electronic Resource]*, 3(6), p. e2455.

Xiong, N., Xiong, J., Jia, M., Liu, L., Zhang, X., Chen, Z., Huang, J., Zhang, Z., Hou, L., Luo, Z., Ghoorah, D., Lin, Z. and Wang, T. (2013) 'The role of autophagy in Parkinson's disease: rotenone-based modeling', *Behavioral & Brain Functions [Electronic Resource]: BBF*, 9, p. 13.

Xu, B. and Clayton, D.A. (1992) 'Assignment of a yeast protein necessary for mitochondrial transcription initiation', *Nucleic Acids Research*, 20(5), pp. 1053-9.

Xu, B. and Clayton, D.A. (1995) 'A persistent RNA-DNA hybrid is formed during transcription at a phylogenetically conserved mitochondrial DNA sequence', *Molecular & Cellular Biology*, 15(1), pp. 580-9.

Yakubovskaya, E., Chen, Z., Carrodeguas, J.A., Kisker, C. and Bogenhagen, D.F. (2006) 'Functional human mitochondrial DNA polymerase gamma forms a heterotrimer', *Journal of Biological Chemistry*, 281(1), pp. 374-82.

Yamamoto, M., Suzuki, S.O. and Himeno, M. (2010) 'The effects of dynein inhibition on the autophagic pathway in glioma cells', *Neuropathology*, 30(1), pp. 1-6.

Yang, D., Oyaizu, Y., Oyaizu, H., Olsen, G.J. and Woese, C.R. (1985) 'Mitochondrial origins', *Proceedings of the National Academy of Sciences of the United States of America*, 82(13), pp. 4443-7.

Yang, Y., Ouyang, Y., Yang, L., Beal, M.F., McQuibban, A., Vogel, H. and Lu, B. (2008) 'Pink1 regulates mitochondrial dynamics through interaction with the fission/fusion machinery.[Erratum appears in Proc Natl Acad Sci U S A. 2008 Nov 11;105(45):17585]', *Proceedings of the National Academy of Sciences of the United States of America*, 105(19), pp. 7070-5.

Yang, Z., Huang, J., Geng, J., Nair, U., Klionsky, D.J., Yang, Z., Huang, J., Geng, J., Nair, U. and Klionsky, D.J. (2006) 'Atg22 recycles amino acids to link the degradative and recycling functions of autophagy', *Molecular Biology of the Cell*, 17(12), pp. 5094-104.

Yasukawa, T., Reyes, A., Cluett, T.J., Yang, M.Y., Bowmaker, M., Jacobs, H.T. and Holt, I.J. (2006) 'Replication of vertebrate mitochondrial DNA entails transient ribonucleotide incorporation throughout the lagging strand', *EMBO Journal*, 25(22), pp. 5358-71.

Ye, H., Cande, C., Stephanou, N.C., Jiang, S., Gurbuxani, S., Larochette, N., Daugas, E., Garrido, C., Kroemer, G. and Wu, H. (2002) 'DNA binding is required for the apoptogenic action of apoptosis inducing factor', *Nature Structural Biology*, 9(9), pp. 680-4.

Yen, W.L., Klionsky, D.J., Yen, W.-L. and Klionsky, D.J. (2008) 'How to live long and prosper: autophagy, mitochondria, and aging', *Physiology*, 23, pp. 248-62.

Yu, L., Wan, F., Dutta, S., Welsh, S., Liu, Z., Freundt, E., Baehrecke, E.H. and Lenardo, M. (2006) 'Autophagic programmed cell death by selective catalase degradation', *Proceedings of the National Academy of Sciences of the United States of America*, 103(13), pp. 4952-7.

Zeng, M. and Zhou, J.-N. (2008) 'Roles of autophagy and mTOR signaling in neuronal differentiation of mouse neuroblastoma cells', *Cellular Signalling*, 20(4), pp. 659-65.

Zhang, L., Shimoji, M., Thomas, B., Moore, D.J., Yu, S.-W., Marupudi, N.I., Torp, R., Torgner, I.A., Ottersen, O.P., Dawson, T.M. and Dawson, V.L. (2005) 'Mitochondrial localization of the Parkinson's disease related protein DJ-1: implications for pathogenesis', *Human Molecular Genetics*, 14(14), pp. 2063-73.

Zheng, J. (2012) 'Energy metabolism of cancer: Glycolysis versus oxidative phosphorylation (Review)', *Oncology Letters*, 4(6), pp. 1151-1157.

Zhu, J.H., Horbinski, C., Guo, F., Watkins, S., Uchiyama, Y., Chu, C.T., Zhu, J.-H., Horbinski, C., Guo, F., Watkins, S., Uchiyama, Y. and Chu, C.T. (2007) 'Regulation of autophagy by extracellular signal-regulated protein kinases during 1-methyl-4-phenylpyridinium-induced cell death', *American Journal of Pathology*, 170(1), pp. 75-86.

Zickermann, V., Kerscher, S., Zwicker, K., Tocilescu, M.A., Radermacher, M. and Brandt, U. (2009) 'Architecture of complex I and its implications for electron transfer and proton pumping', *Biochimica et Biophysica Acta*, 1787(6), pp. 574-83.

Zollo, O., Tiranti, V. and Sondheimer, N. (2012) 'Transcriptional requirements of the distal heavy-strand promoter of mtDNA', *Proceedings of the National Academy of Sciences of the United States of America*, 109(17), pp. 6508-12.